Exploring combinatorial microRNA therapy for chronic wound healing

MARA ALEXANDRA POP

Imperial College London, Department of Bioengineering

Thesis submitted in partial fulfilment of the requirements for the degree of Doctor of Philosophy

Abstract

Wound healing is a highly orchestrated process involving the coordinated action of many cell types, growth factors, cytokines and small regulatory RNAs, such as microRNAs (miRNAs). These small RNA molecules become expressed in a spatiotemporal pattern to fine-tune signalling pathways coordinating tissue repair. Recently, miRNA dysregulation has been linked to impaired healing, including the formation and progression of diabetic foot ulcers (DFUs), a type of chronic wound associated with diabetes. While most of the interest has gone into the role of individual miRNAs in DFUs, research into the combinatorial role of dysregulated miRNAs remains limited. Complicating factors, such as dosage-dependent effects of miRNAs and current stochastic delivery methods, can make it challenging to study combinatorial miRNA effects.

This project addressed some of these understudied limiting elements to explore how combinatorial miRNA dysregulation can contribute to impaired healing in DFUs. First, a set of differentially expressed miRNAs between DFU-derived fibroblasts and healthy fibroblasts was identified and, using bioinformatics, the biological impact of their dysregulation was explored in delaying wound healing. Next, three miRNAs were chosen from this dataset and their individual and combinatorial effects was investigated in primary skin cells isolated from amputated human limbs. Lastly, a novel *in vitro* engineering-based approach for miRNA delivery was used for studying incremental dosage effects of specific differentially expressed miRNAs. Altogether, these findings opened opportunities for investigating dose-dependent effects of miRNA combinations for the treatment of DFUs, yet not addressed by current research.

Declaration of Originality

I, Mara Alexandra Pop, hereby declare that the work presented in this thesis is entirely my own. Anything that is not has been referenced, cited or acknowledged accordingly.

Copyright Declaration

The copyright of this thesis rests with the author. Unless otherwise indicated, its contents are licensed under a Creative Commons Attribution-Non Commercial-No Derivatives 4.0 International Licence (CC BY-NC-ND).Under this licence, you may copy and redistribute the material in any medium or format on the condition that; you credit the author, do not use it for commercial purposes and do not distribute modified versions of the work. When reusing or sharing this work, ensure you make the licence terms clear to others by naming the licence and linking to the licence text. Please seek permission from the copyright holder for uses of this work that are not included in this licence or permitted under UK Copyright Law.

Acknowledgements

First of all, I would like to express my sincere gratitude to my supervisor Dr Ben Almquist, for his continuous guidance, support and optimism over the last four years.

I would also like to thank all the present and past members of the Almquist group for making the lab environment a great place to work in; all the members of the Higgins group for sharing their lab equipment with me, and in particular Sharad Patel for his advice on cell culture; and lastly all the members of the Kozlov Lab for making the office a great place. You have all been great friends.

I would also like to show appreciation to Dr Christoph Knappich for helping with providing amputated tissue samples from patients, Svitlana Kurinna for gifting our lab the tarmiR29 plasmid and the NAVAN team including Sergio, Ryan and Martin for their helpful advice on the nanostraw delivery platform.

Further, I would like to recognise the staff at the Facility for Imaging by Light Microscopy including Stephen and David and the technicians in the Bioengineering department Joel, Beth, Miguel, Kosta and Christina for looking after the labs and equipment so well to ensure everything worked smoothly.

I would further like to acknowledge the funding sponsors including EPSRC, Diabetes UK, the Rosetrees Trust and the Royal Society without which this project would not have been possible.

Lastly, I would like to thank my husband Matthew and my parents for their unconditional support and encouraging words throughout my PhD. Thank you for always being there for me.

TABLE OF CONTENTS

List of figures ……..12

List of tables ……34

Abbreviations ……37

1. Introduction and motivation of the thesis 39

1.1. Chronic wounds represent a major burden on society and healthcare systems 39

1.2. Wound healing is a complex and dynamic process 40

1.3. In chronic wounds the process of wound healing becomes impaired 44

1.4. In diabetes the process of wound healing is impaired 46

1.5. Treatments for chronic wounds are vast, but with limited success 48

1.6. Motivating hypothesis for PhD research 49

1.7. MicroRNAs play important roles in skin and wound healing and can become dysregulated in chronic wounds 51

1.8. MicroRNAs are a subset of epigenetic mechanisms 54

1.8.1. Long noncoding RNAs 56

1.8.2. Circular RNAs 56

1.8.3. Short interfering RNAs 57

1.9. MicroRNAs are endogenous epigenetic regulators 58

1.10. MicroRNA biogenesis involves a complex mechanism 60

1.11. MicroRNAs fine-tune a myriad of target genes 65

1.12. MicroRNAs exert different degrees of repression on targets 69

1.13. MicroRNAs cooperate at the pathway level 72

1.14. MicroRNA exhibit target selectivity 74

1.15. Aims of project 77

2. Investigating microRNA dysregulation in diabetic foot ulcer fibroblasts 79

2.1. Bioinformatics analysis to determine differentially expressed miRNAs in DFU fibroblasts vs nondiabetic healthy fibroblasts 79
2.2. Investigating the biological impact of the DE miRNAs 87
2.3. Investigating miRNA clusters amongst the DE miRNAs 94
2.4. Finding miRNAs that work together by targeting common pathways 99
2.5. Supplementary data 112
2.5.1. R script to analyse DE miRNAs using the NanoStringDiff vignette 112
3. Isolation and characterisation of primary skin cells 114
3.1. Isolation of primary skin cells from amputated human lower limb tissues 114
3.2. Characterisation of the isolated primary fibroblasts 125
3.2.1. Growth rate and doubling times 125
3.2.2. Response to growth factor stimulation 128
3.3. Methods 130
3.3.1. H&E staining of skin samples 130
3.3.2. Obtaining the growth curve of fibroblasts 130
3.3.3. Generating the Presto Blue calibration curve with fibroblasts 130
3.3.4. Growth factor stimulation of fibroblast populations 130
3.3.5. Immunostaining of fibroblast populations with collagen I and vimentin 131
3.3.6. Statistical analysis and graph generation 131
3.4. Supplementary data 132
3.4.1. Donor demography 132
3.4.2. Mycoplasma testing 133
3.4.3. Immunostaining of fibroblasts cell populations with collagen I and vimentin for the negative control 135
3.4.4. Protocol for culturing primary fibroblasts 136
3.4.5. Protocol for culturing primary keratinocytes 138

3.4.6. Protocol for H&E staining of skin samples 139

4. Testing the differentially expressed miRNAs for cooperative effects *in vitro* 140

4.1. Purchase and characterisation of the miRNA mimics 140

4.2. Liposomal-based transfection of miRNA mimics into primary dermal fibroblasts 143

4.3. Transfection of miRNA mimics into fibroblasts to check for synergy 149

4.4. Testing for synergy at the pathway level 151

4.5. Exploring the individual role of miRNAs 156

4.6. Exploring the role of miR-181a 164

4.7. Investigating dosage-dependent effects of miRNAs via lipofectamine RNAiMAX 171

4.8. Methods 178

4.8.1. Testing the integrity and size of the miRNA mimics or small RNAs extracted via the miRVana microRNA kit 178

4.8.2. Protocol for miRNA mimics or inhibitors transfection via lipofectamine RNAiMAX 180

4.8.3. Transfection of dy547 miR mimic into primary dermal fibroblasts 181

4.8.4. Transfection of miR mimic positive control into primary dermal fibroblasts 181

4.8.5. Transfection of siRNAs into primary dermal fibroblasts 182

4.8.6. Performing reverse transcription on mRNA 183

4.8.7. Running Taqman-qPCR on cDNA synthesised from mRNA 184

4.8.8. Checking integrity of large RNA extracted via Purelink Microscale RNA kit or miRVana miRNA isolation kit on nondenaturing agarose gels 186

4.8.9. Checking qPCR amplification efficiency of cDNA synthesised from mRNA or miRNAs 187

4.8.10. Extracting total RNA via the miRVana miRNA isolation kit 187

4.8.11. Running RT on microRNAs 189

4.8.12. Running qPCR on microRNAs 191

4.8.13. Over-expression of miRNAs after transfection of miR mimics (synergy protocol) 192

4.8.14. Effect of scramble miR mimic on cell proliferation..... 192

4.8.15. Testing synergy of miRNAs at functional level (proliferation assays) 192

4.8.16. Testing synergy of miRNAs at gene level 193

4.8.17. Dual behaviour of miR-181a on proliferative ability of fibroblast populations 193

4.8.18. Effect on fibroblast proliferation after transfection of miRNA inhibitors 193

4.8.19. Expression of miRs-181a & -27a and KRAS & PTEN following transfection of miRNA inhibitors..... 194

4.8.20. Testing the effect of Ly294002 on fibroblast proliferation 194

4.8.21. Effect of miR-181a mimic and Ly294002 treatment on fibroblast proliferation 195

4.8.22. PTEN and RPS6KB1 expression after miR-181a mimic transfection..... 195

4.8.23. Preparation of cell lysate for RPPA (6-well format)..... 195

4.8.24. Expression of miR-181a and KRAS &PTEN after transfection of miR-181a mimic at 10-100nM..... 197

4.8.25. Effect of miR-181a or miR-27a mimic on fibroblast proliferation at 10-100nM 197

4.8.26. Effect of miR-181a mimic on HUVEC proliferation at 10-100nM..... 198

4.9. Supplementary data..... 199

4.9.1. Effect of cell density on transfection efficiency of dy547-miR mimic via lipofectamine RNAiMAX 199

4.9.2. Checking integrity of large total RNA extracted via Purelink microscale RNA kit or miRVana miRNA isolation kit on nondenaturing agarose gels..... 200

4.9.3. Checking integrity of small RNA extracted via miRVana miRNA isolation kit on 15% polyacrylamide urea gels 201
4.9.4. Checking qPCR amplification efficiency of cDNA synthesised from mRNA 202
4.9.5. Checking amplification efficiency of cDNA synthesised from miRNAs..... 203
4.9.6. Transfection of siRNAs into primary dermal fibroblasts..... 203
4.9.7. RNU44 is a suitable normalisation gene for miRNAs 204
4.9.8. ACTB is a suitable normalisation gene for mRNAs 205
4.9.9. Effect of scramble miR mimic on cell proliferation..... 206
4.9.10. Primer sequences for genes used for qPCR on mRNAs..... 206
5. Nanostraw-electroporation platform for delivery of microRNAs into primary dermal fibroblasts 208
5.1. Mechanism of delivery 208
5.2. Protocol for microRNA delivery 210
5.3. Testing fibroblasts viability on the NS membrane..... 215
5.4. Testing fibroblasts viability on the NS membrane after electroporation..... 216
5.5. Testing cell membrane permeabilisation following electroporation..... 218
5.6. Delivering fluorescently-tagged miRNAs into fibroblasts 219
5.7. Delivering functional miRNAs/siRNAs into fibroblasts..... 220
5.8. Ratiometric delivery of miRNA mimics at increasing concentrations into fibroblasts 222
5.9. Exploring dosage effects of miR-181a on fibroblast behaviour..... 225
5.10. Delivering miRNA inhibitors into fibroblasts 227
5.11. Methods 232
5.11.1. Testing fibroblast viability on the NS membrane 232
5.11.2. Testing the cell viability of fibroblasts on the NS membrane after electroporation 232

5.11.3. Testing the cell membrane permeabilisation on the NS membrane 232
5.11.4. Delivering fluorescently-tagged miRNAs into the fibroblasts 233
5.11.5. Delivering functional miRNAs into fibroblasts 233
5.11.6. Delivering siRNAs into fibroblasts 234
5.11.7. Ratiometric delivery of miRNA mimics into fibroblasts at increasing concentrations 234
5.11.8. Delivering miR-181a mimic at increasing concentrations for KRAS qPCR 234
5.11.9. Delivering miR-181a mimic into fibroblasts for proliferation assays 235
5.11.10. Ratiometric delivery of miRNA inhibitors into fibroblasts via NS 235
5.11.11. Delivering antimiR-29 into fibroblasts via NS 236
5.11.12. Delivering GFP plasmid into primary fibroblasts via NS 237
5.12. Supplementary data 238
5.12.1. Fabrication of nanostraw membrane 238
5.12.2. Delivering miR-29 inhibitor into fibroblasts via NS 239
5.12.3. pmaxGFP plasmid delivery into primary fibroblasts via NS-mediated electroporation 241
6. Nanostraw-mediated delivery of microRNAs into primary keratinocytes 242
6.1. Primary keratinocytes are hard-to-transfect cells 243
6.2. NS-mediated delivery of miRNAs into keratinocytes in suspension (3 centrifugation protocol) 245
6.3. NS-mediated delivery of miRNAs into adherent KC 249
6.4. Improving KC viability on the NS membrane 254
6.5. Methods 259
6.5.1. KC subculture protocol 259
6.5.2. Staining protocol for monitoring cell viability and checking uptake of fluorescently–tagged miRNA into KC 259

6.5.3. Monitoring cell viability of adherent KC on NS membrane 259
6.5.4. Delivering Cy3-tagged miRNA into adherent primary KC via NS 260
6.5.5. Delivering Cy3-tagged miRNA into primary KC via lipofectamine RNAiMAX 260
6.5.6. Plasma treatment protocol 260
6.6. Supplementary data 262
6.6.1. Stimulation of primary keratinocytes with FGF-7 262
7. Main thesis conclusions and general discussion 263
7.1. Future studies 270
8. References 272
9. Appendix 293
9.1. List of chemicals and materials used 293
9.2. Permission to re-publish or modify images from third parties 298

List of figures

Figure 1: Chronic diabetic foot ulcer. Image reproduced from [9] with permission from the rights holder, Elsevier 39

Figure 2: Wound healing consists of a complex spatially and temporally coordinated interplay between various cell types, growth factors and cytokines in which the body attempts to repair itself after injury. Image reproduced with permission from [12], Copyright Massachusetts Medical Society 40

Figure 3: Wound healing consists of distinct, yet overlapping phases starting from homeostasis occurring minutes after injury in which a blood clot gets formed to stop the bleeding; inflammation involving clearing of debri and microbes in the wound bed; proliferation and re-epithelialisation involving formation of granulation tissue and skin re-growth; and remodelling of the newly formed scar tissue. Image reproduced from [19] under Creative Commons Attribution Licence. Copyright 2019 desJardins-Park, Mascharak, Chinta, Wan and Longaker 43

Figure 4: Dysregulated miRNA levels in the chronic wound bed (shown in red) progressively mute cell signalling to impair cell proliferation, migration and survival. Restoring normal levels of dysregulated miRNAs in the wound bed – via miRNA mimics or inhibitors - can temporarily manipulate the disrupted signalling pathways to drive wound healing. This, in turn, can help develop a miRNA-based therapy for the treatment of DFUs. Image modified with permission from [51]. Copyright 2004, Springer Nature 50

Figure 5: epigenetic changes encompass three major subcategories, including DNA methylation, histone modifications and noncoding RNA-driven gene silencing. Epigenetic modifications change gene expression without altering the DNA sequence by affecting the accessibility of the proteins to the DNA or by altering DNA conformation 54

Figure 6: Epigenetic modifications alter gene expression by changing the phenotype without a change in genotype. They affect the extent to which DNA wraps itself around the histones to yield a transcriptionally active or inactive chromatin. A) DNA methylation causes gene silencing following methylation of cytosine and guanine islands (CpG) residues, located in the gene promoter region; B) Histone modifications drive gene activation or silencing depending on the number and type of modifications occurring on

its tails, such as methylation (Me), acetylation (Ac), phosphorylation (P) or ubiquitination (Ub). Image of histone tail modifications is for illustrative purposes only and does not represent the specific modifications that occur on each tail. Figure created in BioRender.com and exported under a paid subscription. 55
Figure 7: siRNAs have extensive complementarity to the 3'UTR, causing cleavage of the target mRNA in the middle. This, in turn, leads to significant gene knockdown. Figure created with BioRender.com and exported under a paid subscription. 58
Figure 8: miRNA genes can be either isolated or clustered (A), and are located either in intergenic (B) or intragenic regions, where they can reside in an intron of a gene (C) or exon of a gene (D). Pink rectangles in C) and D) represent exons. Image created with BioRender.com and exported under a paid subscription. 59
Figure 9: the majority of miRNAs is generated via the canonical pathway, involving the action of Drosha and Dicer. Processing of miRNAs starts in the nucleus, where Drosha and DGCR8 cleave the pri-miRNA into a much shorter pre-miRNA that gets exported into the cytoplasm by Exportin 5. Here, Dicer cleaves the stem-loop to produce a miRNA duplex that gets recognised and bound by Argonaute proteins part of the RISC. Once loaded into RISC miRNAs bind to 3'UTR of target mRNAs to suppress gene expression either by promoting degradation of the mRNA or inhibiting translation. Image created in BioRender.com and exported under a paid subscription. 62
Figure 10: the structure of a typical human protein coding mRNA consists of a 5' methylated cap, followed by a 5' untranslated region (UTR), a coding sequence and 3' untranslated region (UTR), ultimately ending with a polyA tail at the 3'end. Image created with BioRender.com and exported under a paid subscription. 62
Figure 11: MiRNA dysregulation can occur because of a multitude of factors, including epigenetic or genomic changes, altered function of miRNA processing machinery or altered transcription factor activity. Image reproduced from [112] with permission from Elsevier 64
Figure 12: miRNAs recognise their target genes using a 7bp seed region at their 5'end that perfectly matches the 3'UTR sequence on the mRNA, while the rest of the miRNA displays only partial complementarity. Image reprinted from [115] with permission from Elsevier. 65

Figure 13: miRNA binding sites are preferentially located near the ends of the 3'UTR (B) for a more effective repression (A). Image reproduced from [115] with permission from Elsevier 66
Figure 14: miRNAs are fine-tuners of gene expression, repressing hundreds of targets at the mRNA and protein level in a mild manner that rarely exceed a fourfold change. Image reproduced with permission from [120]. Copyright 2008, Springer Nature 67
Figure 15: the repertoire of target genes of miRNAs is mostly unaffected by cell type. Following transfection of miR-124 or miR-155 into three different cell types the majority of targets remain the same across the different cell types, with few targets displaying differential repression. Image reproduced from [125] with permission from Elsevier 68
Figure 16: 3'UTR of mRNAs contain four main types of canonical seed-matches sites (8mer, 7mer-m8, 7mer-A1 and 6mer) that match the 5' end of a miRNA. Image created in BioRender.com and exported under a paid subscription. 69
Figure 17: efficacy of repression varies for target genes depending on the type of seed-matched sites they contain, namely 43%, 25%, 19% and 7% repression for 8mer, 7mer-m8, 7mer-A1 and 6mer sites, respectively. Image reproduced from [115] with permission from Elsevier 70
Figure 18: multiple seed matched sites contribute multiplicatively to repression, typical of independent and non-cooperative behaviour. For instance, the observed repression from two 7mer sites is higher than the one observed from a single 7mer site. Image reproduced from [115] with permission from Elsevier 71
Figure 19: distance contraints between miRNA-binding sites for different miRNAs dictate whether miRNAs exhibit cooperative behaviour or not. MiRs-106b, -93 and -25 suppress the target gene BMPR2 only when the distance between the three seed sites is reduced to ~35nt within each other (BMPR2-Super). Image reproduced from [130] with permission from Oxford University Press 72
Figure 20: miRs-126, -26a and -21 jointly regulate signalling downstream of the Receptor Tyrosine Kinases (RTK), such as PI3K/AKT and RAF/MAPK signalling pathways. By targeting inhibitors of this pathway the miRNAs act as signal amplifiers, leading to a general upregulation of RTK signalling, in turn driving growth and angiogenesis. Image

modified with permission from [133]. Copyright 2010 Springer Nature. Image created in BioRender.com and exported under a paid subscription. 73
Figure 21: a pull-down assay after miR-34a over-expression shows that not all direct targets (red) are also down-regulated (blue), despite miR-34a binding to the target genes. This points towards target selectivity by miRNAs. Image reproduced from [136] under a Creative Commons License 75
Figure 22: miRNAs repress target genes in a non-linear manner and can act as switches or fine-tuners depending on the mRNA concentration. At low mRNA concentrations miRNAs can immediately degrade the target gene leading to low protein levels. At increasing mRNA concentrations the target mRNAs start to accumulate and gradually titrate away the pool of miRNAs, eventually escaping miRNA repression. Image modified with permission from [138]. Copyright 2011, Springer Nature 77
Figure 23: the authors identify DE miRNAs and mRNAs between DFU-derived fibroblasts (DFUF) and nondiabetic foot fibroblasts (NDFF) and link them to cellular functions known to be disrupted in DFUs, such as proliferation, migration and differentiation... 80
Figure 24: the authors identify 21 DE miRNAs DFUF and NDFF (A) and pair four of these to dysregulated target genes from the same cells to generate miRNA-mRNA networks implicated in disrupting normal cellular processes including cell proliferation, movement or cell differentiation (B). Image taken from [141] and reproduced with permission of the rights holder, John Wiley and Sons 81
Figure 25: NanoStringDiff identifies 39 DE miRNAs in DFUF vs NDFF amongst which 97% are upregulated, while 3% are downregulated (A), whereas the original paper identifies 21 DE miRNAs amongst which 52% are upregulated and 48% are downregulated (B). 86
Figure 26: top 5 molecular and cellular functions the target genes of the 39 DE miRNAs are enriched in include cellular movement, proliferation, survival and development. All functions have a Benjamini-Hochberg corrected p-value < 0.05 90
Figure 27: genomic mapping of the miRNA-coding genes of the DE miRNAs from the NanoStringDiff dataset shows the miRNA-coding genes are scattered across many chromosomes and display enrichment in chromosome 14 and chromosome X 96
Figure 28: the Dlk1-Dio3 chromosomal region (14q32) contains maternally and paternally expressed genes and holds the largest cluster of miRNAs comprising 54 human miRNAs.

Seven of the DE miRNAs from the NanoStringDiff analysis (shown in red) were mapped to this chromosomal region, suggesting it might be implicated in the pathogenesis of DFUF. Image created in BioRender.com and exported under a paid subscription 97
Figure 29: DE miRNAs from the NanoStringDiff dataset are predicted to target many signalling components of the enriched PI3K/AKT signalling pathway, showing how miRNAs can potentially work together at the pathway level to control signal transduction. Image created in Path Designer in IPA. 100
Figure 30: DE miRNAs from the NanoStringDiff dataset are predicted to target many signalling components of the enriched EGF signalling pathway, showing how miRNAs can potentially work together at the pathway level to control signal transduction. Image created in Path Designer in IPA. 101
Figure 31: DE miRNAs from the NanoStringDiff dataset are predicted to target many signalling components of the enriched IGF-1 signalling pathway, showing how miRNAs can potentially work together at the pathway level to control signal transduction. Image created in Path Designer in IPA. 102
Figure 32: DE miRNAs from the NanoStringDiff dataset are predicted to target many signalling components of the enriched ERK/MAPK signalling pathway, showing how miRNAs can potentially work together at the pathway level to control signal transduction. Image created in Path Designer in IPA. 103
Figure 33: miRNA-mRNA networks between 7 of the DE miRNAs from the NanoStringDiff analysis (miRs-145, -143, -16, -27a, -503, -30c and -181a) show strong target sharing, with many genes being targeted by multiple miRNAs. Image created in Path Designer in IPA. 104
Figure 34: PPI network between the proteins targeted by 7 of the DE miRNAs from the NanoStringDiff dataset (miRs-145, -143, -16, -27a, -503, -30c and -181a) shows very strong interactions, implying the proteins are involved in regulating a common function 106
Figure 35: miRs-181a, -27a and -30a from the NanoStringDiff dataset are predicted to commonly target the MAPK-ERK signalling pathway and the PI3K-AKT signalling pathway, implying they might cooperate at the pathway level to jointly control signal transduction along these pathways 108

Figure 36: skin consists of three layers (epidermis, dermis and fat) with many structures embedded throughout, such as sweat glands, hair follicles, sebaceous glands, blood vessels and nerves. 114
Figure 37: representative images of amputated human biological tissues used for isolation of primary skin cells. The tissues are nondiabetic non-ulcerated, diabetic ulcerated or diabetic non-ulcerated 117
Figure 38: skin pieces cut from amputated limbs are kept in strong antibiotic solutions prior to being subjected to dispase digestion to isolate the epidermis from the dermis or being embedded in OCT for cryosectioning 118
Figure 39: after dispase separates the dermis from the epidermis primary fibroblasts and keratinocytes are isolated via enzymatic digestion involving collagenase I and trypsin-EDTA, respectively. Scale bars are 200 μm. 119
Figure 40: the dermis consists of papillary dermis, reticular dermis and Dermal White Adipose Tissue (DWAT) and contains distinct fibroblast subpopulations including papillary, reticular, dermal papilla and dermal sheath fibroblasts. These fibroblast populations can be morphologically and physiologically distinct, exhibiting different rates of growth, cellular markers and cytokine secretion, and play distinct roles during homeostasis and wound healing. Abbreviations: DS (dermal sheath), DP (dermal papilla), APM (arrector piri muscle). Image reprinted from [176] and reproduced under a Creative Commons CC-BY Licence 121
Figure 41: H&E stained skin from a nondiabetic bottom foot amputated tissue clearly shows the epidermis, papillary dermis and reticular dermis and identifies the structural differences between these. The papillary dermis contains more cells (blue dots) and thinner collagen fibres than the reticular dermis which is mainly acellular and contains dense collagen fibres. For H&E staining 16 μm thick sections were cut with the cryostat from the frozen skin tissue embedded in OCT and adsorbed onto SuperFrost glass slides. Skin sections were visualised with the light microscope. Scale bar: 100 μm 122
Figure 42: immunostaining of the isolated fibroblast populations shows the cells express both vimentin (red) and collagen I (green), markers of fibroblasts. The nuclear staining (blue) overlays with the collagen I/vimentin staining in all cells, confirming the cell culture is 'clean'. Incubation with primary antibodies against vimentin (raised in chicken, 1:200)

and against collagen I (raised in rabbit, 1:400) occurred in 5% goat serum in PBS overnight at 4°C. Incubation with secondary antibodies included goat anti-chicken 633 (1:200) and goat anti-rabbit 488 (1:200) in PBS for 1h at room temperature in the dark. Cells incubated with the secondary antibodies only served as the negative control. 124

Figure 43: the isolated fibroblasts (nondiabetic) display the characteristic sigmoidal growth curve in culture consisting of the lag phase, log phase and plateau. To obtain the growth curve nondiabetic fibroblasts were seeded at 1,600 cells/well in a 96-well plate in full DMEM medium. Each day the cells were trypsinised from one column on the well plate at a time and their cell number was counted with the haemocytometer. Nonlinear regression was used to fit the sigmoidal curve to the data points. Data points are plotted as mean ± SD. N=2, n=6/donor. 125

Figure 44: the isolated fibroblasts (nondiabetic) have a doubling time ~2.5 days that gets maintained across many passages. To obtain the doubling time the cells were seeded at 8,000 cells/cm^2 in culture flasks and their number counted when they reached 90-95% confluency. Data is plotted as mean ± SD. N=3 127

Figure 45: (Top) Presto Blue measures proliferation in a linear manner. To obtain the standard curve 1:2 serial dilutions of fibroblasts were generated in a range of 625-10,000 cells/well in a 96-well plate, followed by incubation with Presto Blue (1:10 dilution) for 1h at 37°C. Data points are plotted as mean ± SD; (Bottom) PDGF-BB stimulation in a concentration range of 20-100 ng/mL has a dosage-dependent proliferative effect on nondiabetic fibroblast populations cells as measured via Presto Blue 48h post-stimulation. Prior to stimulation with PDGF-BB cells were serum-starved in 0.1% FBS for 24h. Box & whiskers plot span min to max. Analysis of statistical significance was performed via one-way ANOVA, followed by posthoc Dunnett's multiple comparisons test. **** $p<0.0001$. N=4, n=8/donor 129

Figure 46: all fibroblast populations tested for mycoplasma contamination by PCR are negative as all DNA bands align with the negative controls and not the positive control. Bands were detected by agarose gel electrophoresis. For PCR 3-4 day old supernatant from 90% confluent T75 flasks was collected from various donors. 134

Figure 47: the negative control used during the immunostaining of the fibroblasts shows no sign of vimentin or collagen I expression, hence confirming the positive signal observed

in the immunostained fibroblasts containing the primary and secondary antibodies is true 135
Figure 48: miRNA mimics and inhibitors augment or attenuate the effect of endogenous miRNAs. Steps 1&2 describe the formation of mature miRNA duplexes after the pre-miRNA is exported into the cytoplasm. Once miRNA duplexes are loaded into RISC, the inactive strand becomes cleaved resulting in the formation of programmed RISC (step 3). This binds to the 3'UTR of a target mRNA (step 4) to suppress gene expression (step 5). MiRNA mimics of mature miRNAs increase the expression level of miRNAs to further downregulate protein levels (Step 4.1). MiRNA inhibitors bind to the endogenous miRNAs and prevent them from binding to the target mRNAs, thus upregulating protein levels (Step 5.2). Figure created with BioRender.com and exported under a paid subscription..... 141
Figure 49: denaturing 15% polyacrylamide gel shows mature miRNA mimics of miR-181a, -27a, -30a and scramble miRNA create two distinct bands of ~25nt and ~40nt and confirms they are not denatured as seen by the lack of smeared appearance. To detect the RNA bands the gel was stained with Sybr Gold. 143
Figure 50: liposomal-based transfection of cargo relies on the endosomal pathway, starting with uptake of liposome-RNA complexes (1) into the cytoplasm via endocytosis (2), followed by escape of cargo from the endosomes (3) to associate with RISC (5) or co-localisation with lysosomes (4). Image modified from [179] with permission of the rights holder, The Company of Biologists 145
Figure 51: dy547-labelled miRNA (red) transfected into primary dermal fibroblasts via lipofectamine RNAiMAX at 10-30 nM shows successful uptake 24h post-transfection (left). Close-up images display punctate uptake of the cargo consistent with liposomal-based delivery methods (top right); negative control involving fibroblasts without dy547-labelled miRNA shows no sign of autofluorescence (bottom right). Blue dye denotes the nuclear staining Hoechst 33342..... 146
Figure 52: Transfection of positive miR mimic against GAPDH via lipofectamine RNAiMAX at 100 nM into primary dermal fibroblasts causes large suppression of GAPDH gene expression 48h post-transfection, confirming liposomal-based delivery of miRNAs works efficiently. The fold change in GAPDH gene expression was determined using the $2^{-\Delta\Delta CT}$

method. Data points show mean ± SD. Analysis of statistical significance was performed via one-way ANOVA, followed by Tukey's multiple comparisons test. **** p<0.0001. N=1, n=3 148
Figure 53: individual and combined transfection of miR-181a, -27a, -30a mimics into primary dermal nondiabetic fibroblasts via lipofectamine RNAiMAX at 300nM final concentration shows large over-expression 48h later. No statistical difference is observed between the individual and the combined transfection, confirming that miRNAs become expressed to a similar amount even when delivered in combination. For the individual transfections the functional miRNAs (100 nM) were spiked with scramble miRNA mimic (200 nM) to ensure the same total amount of miRNA mimic was transfected in each condition. Bars denote mean ± SD. Statistical analysis to determine significance over cells transfected with scramble miRNA was done via one-way ANOVA, followed by posthoc Tukey's multiple comparisons test. N=2, n=3/donor. 150
Figure 54: Taqman-qPCR measurements of the endogenous levels of miR-181a, -27a and -30a show that miR-181a is very lowly expressed, followed by miR-30a and miR-27a which shows the highest endogenous expression in primary dermal nondiabetic fibroblasts. Expression values were calculated relative to expression of RNU44. Bars denote mean ± SD. N=2 151
Figure 55: to test for synergy miRNA mimics of miR-181a, -27a and -30a were transfected into primary dermal nondiabetic fibroblasts via lipofectamine RNAiMAX at 300nM final concentration individually, pairwise and in triple combination. Over-expression of each of the miRNAs has a biological effect on cell proliferation, however they show no sign of synergy. Proliferation was measured 5 days post-transfection via Presto Blue. Bars denote mean ± SD. For analysis of statistical significance one-way ANOVA was used, followed by posthoc Dunnett's multiple comparisons test. *** p<0.001, **** p<0.0001. N=3, n=9/donor 152
Figure 56: KRAS becomes repressed by varying amounts following individual transfection of miRs-181a (52 ±3%), -27a (25±5%), -30a (18±7%) or in triple combination (48±4%), however no sign of synergy is observed. Fold change values are normalised to scramble miR mimic showing a fold change of -1. MiRNA mimics were transfected via lipofectamine RNAiMAX at 300 nM and KRAS expression was measured via Taqman-qPCR 48h post-

transfection. Data points denote mean ± SD. Analysis of statistical significance was performed via one-way ANOVA, followed by posthoc Tukey's multiple comparisons test. * p<0.05, *** p<0.001, **** p<0.0001. N=2, n=3/donor 154
Figure 57: IRS1 becomes repressed moderately after individual transfection of miRs-181a (12±4%), -27a (5±7%), -30a (18±6%) or in triple combination (29±5%), however no sign of synergy is observed. Fold change values are normalised to scramble miR mimic showing a fold change of -1. MiRNA mimics were transfected via lipofectamine RNAiMAX at 300 nM and IRS1 expression was measured via Taqman-qPCR 48h post-transfection. Data points denote mean ± SD. Analysis of statistical significance was performed via one-way ANOVA, followed by posthoc Tukey's multiple comparisons test. * p<0.05, *** p<0.001, **** p<0.0001, ns means p>0.05. N=2, n=3/donor 156
Figure 58: miR-181a exhibits dual behaviour between nondiabetic and diabetic fibroblasts, increasing proliferation in nondiabetic fibroblasts, but decreasing proliferation in diabetic ulcerated and diabetic non-ulcerated fibroblasts. MiR-27a has a suppressive effect on proliferation in all three sets of fibroblast populations. MiRNA mimics were transfected into the fibroblasts via lipofectamine RNAiMAX at 100 nM and proliferation was measured 5 days post-transfection via Presto Blue. Bars denote mean ± SD. Analysis of statistical significance was performed via one-way ANOVA, followed by posthoc Tukey's multiple comparisons test. **p<0.01,**** p<0.0001. N=3, n=9/donor for each set of fibroblast populations 158
Figure 59: miR-181a is upregulated in diabetic fibroblasts compared to nondiabetic fibroblasts, whereas miR-27a shows no statistical difference. However, due to the high variability of expression amongst the populations, further donors are required to validate these observations and be able to draw a definitive conclusion on the difference in endogenous expression of these two miRNAs in diabetic vs nondiabetic fibroblasts. Bars denote mean ± SD and data points represent relative expression to RNU44. Statistical analysis to determine significance was performed via two-tailed unpaired t-test. *p<0.05, N=3.... 159
Figure 60: transfection of miR-181a inhibitor at 100 nM via lipofectamine RNAiMAX shows a trend of suppression on primary dermal nondiabetic fibroblasts, while inhibition of miR-27a exerts a proliferative effect. Proliferation was measured 5 days post-transfection via Presto Blue. Box and whisker plots span min to max. Statistical analysis was performed

via one-way ANOVA, followed by posthoc Tukey's multiple comparisons test. ****p<0.0001. N=3, n=3/donor 162
Figure 61: transfection of miR-181a inhibitor at 100 nM via lipofectamine RNAiMAX seems to exhibit a trend of stimulatory effect on diabetic non-ulcerated fibroblasts, while inhibition of miR-27a exerts a proliferative effect. Proliferation was measured 5 days post-transfection via Presto Blue. Box and whisker plots span min to max. Statistical analysis was performed via one-way ANOVA, followed by posthoc Tukey's multiple comparisons test. ****p<0.0001. N=3, n=3/donor 162
Figure 62: Taqman-qPCR confirms that transfection of miRNA inhibitors into nondiabetic fibroblasts at 100 nM via lipofectamine RNAiMAX represses expression of miR-181a or miR-27a 48h later. Data points denote mean ± SD. Statistical analysis was performed via two-tailed unpaired t-test. ****p<0.0001. N=2, n=3/donor 163
Figure 63: the PI3K/AKT signalling pathway plays key roles in regulating survival, proliferation, cell motility and protein production. Image reproduced from [193] with permission of the rights holder, Elsevier 165
Figure 64: treatment with Ly294002, a potent PI3K inhibitor, at 50 μM in 10% FBS for different lengths of time (24h or 72h) causes a large suppressive effect on nondiabetic fibroblast proliferation 3 days later, illustrating the important role PI3K/AKT signalling plays in controlling cell proliferation. Untreated fibroblasts or fibroblasts kept in DMEM supplemented with DMSO in the same ratio as for Ly294002 dilution (1:1000) served as the control to rule out any toxic effect DMSO alone might have on cell proliferation. Bars denote mean ± SD. Statistical analysis was done via one-way ANOVA, followed by posthoc Tukey's multiple comparisons test. ****p<0.0001, n=15 166
Figure 65: over-expression of miR-181a exerts its proliferative effects on nondiabetic fibroblasts through the PI3K/AKT signalling pathway as blocking this pathway via Ly294002 treatment abolishes the stimulatory effect miR-181a has on fibroblasts. Cells were transfected with 100 nM miR-181a mimic or scramble miR mimic in the presence or absence of Ly294002 for 5 days, followed by measuring proliferation via Presto Blue. Box and whisker plots show min to max. Statistical analysis was done via one-way ANOVA, followed by posthoc Tukey's multiple comparisons test. *p<0.05, **p<0.01, ****p<0.0001. N=3, n=9/donor 167

Figure 66: miR-181a over-expression causes upregulation of PTEN and downregulation of RPS6KB1 48h post-transfection of miR-181a mimic into primary nondiabetic fibroblasts, suggesting that the PI3K/AKT signalling pathway is becoming activated through other nodes. MiR-181a mimic was transfected at 100nM via lipofectamine RNAiMAX. Fold changes were calculated relative to scramble miR mimic displaying a fold change of 1 or -1, respectively. Data points denote mean ± SD. Statistical analysis was performed via two-tailed unpaired t-test. ***p<0.001, ****p<0.0001. N=2, n=3/donor 168

Figure 67: inhibiting miR-181a expression via transfection of 100nM antimiR-181a using lipofectamine RNAiMAX causes KRAS to no longer to be downregulated and PTEN no longer to be upregulated 48h post-transfection, displaying opposite effects to those of miR-181a mimic. Data points denote mean ± SD. Statistical analysis was performed via unpaired two-tailed t-test, ns means p>0.05. n=3 169

Figure 68: RPPA allows high throughput detection of expression levels and activation status of signalling proteins. It consists of spotting cell lysates from multiple samples on arrays that get probed with one antibody at a time, followed by scanning the spotted slides to generate data reports. Image reproduced from [199] under the terms and conditions of the Creative Commons Attribution License 170

Figure 69: lipofectamine RNAiMAX cannot control the amount of miR-181a delivered into primary dermal fibroblasts as transfection of miR-181a mimic at 10-100nM causes similar levels of miR-181a overexpression at all concentrations of mimic 48h post-transfection (p=0.5186). The fold change in miR-181a expression was calculated relative to fibroblasts transfected with 100 nM scramble miR mimic. Box and whisker plots span min to max. Statistical analysis was performed via one-way ANOVA. N=3, n=3/donor 171

Figure 70: 48h post-transfection of miR-181a mimic into primary dermal fibroblasts via lipofectamine RNAiMAX KRAS and PTEN become suppressed and upregulated, respectively by the same amount at all concentrations of miR-181a mimic transfected (p=0.0743 for KRAS and p=0.3199 for PTEN). This reinforced that lipofectamine RNAiMAX cannot control the dosage of miRNA delivered. Bars show mean ± SD. Statistical analysis was performed via one-way ANOVA. N=3, n=3/donor 172

Figure 71: transfection of miR-181a mimic at 10-100 nM via lipofectamine RNAiMAX into nondiabetic dermal fibroblasts increases cell proliferation at all concentrations of miR-

181a mimic tested, showing no differential behaviour. Proliferation was measured 5 days post transfection via Presto Blue and the fold change was determined relative to fibroblasts transfected with scramble miR mimic at 10-100 nM, respectively. Box and whisker plots span min and max. Statistical analysis was performed via one-way ANOVA, followed by posthoc Tukey's multiple comparisons test. **p<0.01, ****p<0.0001. N=2, n=9/donor 173

Figure 72: transfection of miR-27a mimic at 10-100 nM via lipofectamine RNAiMAX into nondiabetic dermal fibroblasts causes suppression of cell proliferation at all concentrations of miR-27a mimic tested, exhibiting no differential behaviour in between these concentrations. Proliferation was measured 5 days post transfection via Presto Blue and the fold change was determined relative to fibroblasts transfected with scramble miR mimic at 10-100 nM, respectively. Box and whisker plots span min and max. Statistical analysis was performed via one-way ANOVA, followed by posthoc Tukey's multiple comparisons test. **p<0.01, ****p<0.0001. N=2, n=9/donor 173

Figure 73: transfection of miR-181a mimic at 10-100 nM via lipofectamine RNAiMAX into HUVEC increases cell proliferation at all concentrations of miR-181a mimic tested, showing no differential effects. Proliferation was measured 5 days post transfection via Presto Blue and the fold change was determined relative to HUVEC transfected with scramble miR mimic at 10-100 nM, respectively. Box and whisker plots span min and max. Statistical analysis was performed via one-way ANOVA, followed by posthoc Tukey's multiple comparisons test. **p<0.01, ****p<0.0001. N=2, n=9/donor 174

Figure 74: MiRNAs have different functional doses for different target genes causing dose-dependent mRNA target selection. I believe that the trend of gene knockdown at increasing miRNA concentrations most likely follows a Gaussian trend. Functional dose is defined as a narrow range of miRNA concentration that causes maximal target suppression beyond which the particular mRNA is no longer a viable target 175

Figure 75: transfection of let-7a-7f plasmid into Huh7 cells via lipofectamine 2000 causes different amounts of repression of its target genes cMYC and CCND1 at the different concentrations tested. Image reproduced from [200] with permission of the rights holder, Taylor & Francis 176

Figure 76: miRNA combinations can trigger different effects at varying relative concentrations of miRNA by changing the sets of genes targeted, in turn activating different cellular pathways leading to different cellular behaviour. Image modified from [201] with permission of the rights holder, Elsevier 176
Figure 77: xylene cyanol and bromopheol blue are tracking dyes used in loading gels that aid to keep a visual track over how far down the gel DNA or RNA has migrated. Image shows a loaded pre-cast 15% denaturing urea polyacrylamide gel in XCell SureLock mini cells after having run for 80 min at 180V and 10mA in constant voltage mode 179
Figure 78: typical amplification curve observed after a qPCR run. The CT threshold for gene expression was chosen in the linear region of the amplification curve (note the log scale on the y-axis) between 0.1-0.2 185
Figure 79: native 1% agarose gels with loaded RNA samples before the run started (left) and after it finished (right). Gel was run at 90V for 80 min. 186
Figure 80: transfection of dy547-labelled scramble miRNA (red) into primary dermal fibroblasts occurs across all densities of cells tested. No notable difference in transfection efficiency is observed, showing that cells can be seeded at any of these densities for experiments. The scramble miRNA was transfected at 10-30 nM via lipofectamine RNAiMAX and cells were visualised 24h post transfection. Blue denotes the nuclear stain Hoechst 33342. 199
Figure 81: both RNA extraction methods yield good quality of total RNA as seen by the presence of the 28S rRNA band (5.0 kb) and 18S rRNA band (1.9 kb) on 1% native agarose gels. The microRNA miRVana kit displays a further band 5S rRNA (120nt) as it allows for extraction of small RNAs <200nt as opposed to the Purelink RNA kit which extracts only large RNA. The bands are not very sharp and the ratio of 28S:18S doesn't seem to be 2:1, but this might have been caused by the fact that the RNA samples were run on a native (non-denaturing) agarose gel which is known to cause less sharp bands. 200
Figure 82: the observed RNA bands on 15% polyacrylamide urea gels from the test samples correspond to the expected bands of 5.8s rRNA, 5s rRNA and tRNA, confirming that the miRVana miRNA isolation kit extracts small RNA successfully. There is no sign of band smearing in any of the samples, signifying that the extracted small RNA is intact and not degraded 201

Figure 83: amplification efficiency of all genes tested is ~100%, which means that reverse transcription of large RNA and PCR amplification work adequately. This further implies that the $2^{-\Delta\Delta CT}$ method can be reliably used to determine changes in gene expression following transfection of miRNAs. To obtain the amplification curves total RNA extracted from a confluent T75 flask of nondiabetic fibroblasts was serially diluted 1:2 in a range of 22.5-720 ng RNA/RT reaction and reverse transcribed into cDNA. Following qPCR with the various primers of interest the average CT values vs log10 of (ng total RNA/RT reaction) was plotted and linear regression analysis was used to obtain the value of the gradient. This, in turn, was used to determine the amplification efficiency..... 202
Figure 84: amplification efficiency of RNU44 is ~100%, indicating that reverse transcription and amplification of cDNA from miRNAs is adequate. This means this protocol can be reliably used for qPCR experiments involving changes in miRNA expression. 203
Figure 85: transfection of 25 nM siRNA against CAV1 into primary dermal fibroblasts via lipofectamine RNAiMAX yields a significant gene knockdown 48h post transfection with similar suppression values to the miRNA mimic positive control against GAPDH. This confirms that this transfection method works very well at delivering miRNAs into primary fibroblasts. Data points denote mean ± SD. Analysis of statistical significance was performed via unpaired two-tailed t-test. $p<0.001$, n=3 203
Figure 86: transfection of scramble miRNA mimic at 10-300 nM via lipofectamine RNAiMAX does not seem to have any effect on the proliferation of primary dermal nondiabetic fibroblasts when compared to untreated cells. This implies the scramble miRNA is neither toxic for fibroblasts nor has a biological effect on fibroblast behaviour and as such it is suitable to be used as a control miRNA mimic. Proliferation was measured 5 days post transfection via Presto Blue and compared to untreated fibroblasts. Statistical analysis to determine significance was calculated via one-way ANOVA, p=0.2107. N=2, n=9/donor 206
Figure 87: (Left) schematic representation of field localisation at the tip of the NS due to the tight interface between the cells and the NS. Image reprinted with permission from [203]. Copyright 2013 American Chemical Society; (Right) Scanning electron microscope image of the NS membrane with protruding NS - courtesy of Mr Ryan Swoboda, NAVAN . 209

Figure 88: NS wells before seeding cells (in Petri dish) and after seeding cells (in 24-well plate). The NS wells fit in a 24-well plate that can be placed in the incubator or centrifuged. Pink colour denotes DMEM medium 210
Figure 89: (top) schematic representation of the cell cap containing the NS well and the cargo droplet; (bottom) the cell cap is placed in the NAV100 device for electroporation. The NAV100 allows adjustment of parameters including pulse width and frequency..... 211
Figure 90: set-up of the nanostraw-electroporation system showing the NAV100 device connected to the power supply and the oscilloscope/picoscope 212
Figure 91: typical electrical signal recorded on the picoscope during electroporation. The signal displayed a square wave of 200 μs duration (top) occurring at intervals of 25 ms 213
Figure 92: the picoscope records the voltage across the cell cap (ΔV). Due to a 1 ohm resistor placed in series with the cell cap the voltage drop across the cell cap corresponds to the electrical current passing through the cell cap. BNC output represents the output of the NAV100 device..... 214
Figure 93: (left) fibroblasts seeded on the NS membrane overnight show high cell viability; (right) fibroblasts seeded on the NS membrane overnight, trypsinised and re-seeded into well plates display high cell viability and normal cell morphology the following day, thus confirming the NS membrane is not toxic to the cells. Green denotes viable cells, red denotes dead cells 215
Figure 94: electroporation of fibroblasts at various voltages (15-25V) and durations (1 electroporation of 40 sec and 3 electroporations of 40 sec each at 3 min intervals) shows that 25V, three electroporations kills the cells. Cells were stained on the NS membrane with Live/Dead stain 3h post electroporation. Green denotes live cells, red denotes dead cells. All scale bars denote 300 μm 217
Figure 95: set-up used for all deliveries of biomolecules into primary dermal fibroblasts involved 3 electroporations of 40 sec each at 3 min intervals 217
Figure 96: uptake of propidium iodide (PI, red) - a cell impermeant fluorescent DNA intercalator - into fibroblasts confirms cell membrane poration is taking place during electroporation at 20V. The minimal uptake of propidium iodide in the absence of electroporation further confirms that the presence of the electric field is necessary for

efficient delivery. PI (0.1 mg/mL) was present in the cargo droplet in the cells cap. Cells were stained with Cell Tracker Green – a cell permeable dye that stains viable cells green – on the NS membrane. All scale bars denote 150 μm 219
Figure 97: NS-mediated delivery of Cy3-tagged scramble miRNA (red) into primary dermal fibroblasts revealed efficient uptake and homogenous distribution of miRNA throughout the cytoplasm 24h post delivery. This confirmed the nanostraw-electroporation system enables direct intracellular access without relying on endosomal pathways for cargo uptake. The negative control denotes fibroblast cells in culture without Cy3-tagged scramble miRNA delivered and shows there is no autofluorescence in the Cy3 channel. Blue denotes the nuclear stain Hoechst 33342. 220
Figure 98: NS-mediated delivery of miRNA mimic positive control against GAPDH shows efficient suppression of GAPDH at all concentrations tested (75% gene suppression) 48h post delivery. This confirms that NS-mediated delivery of miRNAs into primary dermal fibroblasts is highly efficient. Bars denote mean ± SD. Statistical analysis to determine significance was done via one-way ANOVA, followed by posthoc Tukey's multiple comparisons test. ****p<0.0001. n=4 221
Figure 99: NS-mediated delivery of siRNA against CAV1 into nondiabetic fibroblasts shows efficient gene knockdown (75% gene suppression) 48h post delivery, confirming the nanostraw-electroporation delivery system works efficiently at delivering small RNAs into fibroblasts. Bars denote mean ± SD. Statistical analysis was performed via two-tailed unpaired t-test, ****p<0.0001. n=3 222
Figure 100: NS-mediated ratiometric delivery of miR-181a and miR-27a mimics at 5 μg final concentration into primary nondiabetic fibroblasts reveals a linear increase in miRNA over-expression with increasing miRNA mimic concentrations 48h post delivery, confirming the nanostraw-electroporation platform can deliver miRNAs in a dosage-controlled manner. R^2 values were obtained by linear regression analysis. N=2, n=4/donor 223
Figure 101: NS-mediated delivery of miR-181a mimic at increasing concentrations (0.5-4.5 μg) causes knockdown of KRAS at all three concentrations 48h post delivery. The level of suppression reaches a plateau at 4.5 μg of miR-181a mimic, showing no signs of dosage-dependent suppression in the tested range. Data points denote mean ± SD. Statistical

analysis was performed via one-way ANOVA, followed by posthoc Sidak's multiple comparisons test. **p=0.0015, ***p=0.0002, ****p<0.0001. N=2, n=2-3/donor..... 225
Figure 102: NS-mediated delivery of miR-181a mimic at increasing concentrations (0.5-4.5 μg) into primary nondiabetic fibroblasts shows a trend of increasing proliferation with increasing concentration of miR-181a mimic. Graph shows the fold change in proliferation over 4 days post delivery normalised to fibroblasts to which 5 μg of scramble miR mimic was delivered. Box and whisker plots span min to max. Statistical analysis to determine significance was done via pairwise two-tailed unpaired t-tests vs scramble miR samples. *p<0.05. N=3, n=2-3/donor 226
Figure 103: NS-mediated delivery of miR-181a and miR-27a inhibitors at 5 μg final concentration into nondiabetic fibroblasts shows a trend of increasing miR-181a suppression with increasing antimiR-181a concentrations, but not for miR-27a 48h post delivery. Box plots span min to max. Statistical analysis was performed via one-way ANOVA, followed by posthoc Tukey's multiple comparisons test. **p<0.01, ***p<0.001, ****p<0.0001. N=2, n=3-4/donor 227
Figure 104: representation of the workings of tarmiR29 plasmid - in the presence of scramble miR endogenous miR-29 can suppress Renilla activity (top), but this gets sequestered by presence of antimiR-29, causing de-repression of Renilla activity (bottom). Abbreviations: MRE stands for miRNA response element. 229
Figure 105: NS-mediated delivery of antimiR-29 at increasing concentrations into primary nondiabetic fibroblasts causes de-repression of Renilla activity 48h post transfection of the tarmiR29 plasmid at all concentrations of antimiR-29 tested, however no miRNA dosage-dependent de-repression of luciferase activity is observed. The tarmiR29 plasmid harbours binding sites for miR-29 and codes for the luciferases Firefly (control luciferase) and Renilla (reporter luciferase). In the presence of scramble miR endogenous miR-29 can suppress Renilla activity, but this gets sequestered by presence of antimiR-29, causing derepression of Renilla activity. Box and whisker plots span min to max. Statistical analysis was performed via pairwise two-tailed unpaired t-tests. p<0.05. N=3, n=2-3/donor..... 230
Figure 106: Fabrication starts with commercially available track-etched polycarbonate membranes (shown in grey) that are in a range of pore sizes. First, an alumina coating of

10-30nm thickness (shown in blue) is deposited on all surfaces of the membrane (top, bottom and inside of pores) using atomic layer deposition to create a uniform coating. The deposited alumina creates the nanostraw bodies within the interiors of the pores. Next, the alumina on the top surface is removed using reactive ion etching (RIE) to expose the polymer underneath. Finally, oxygen RIE is used to expose the nanostraws by selectively etching the polymer until the desired height of nanostraws is obtained (1-2 μm). Image reprinted with permission from [210]. Copyright 2012 American Chemical Society. 238

Figure 107: NS-mediated delivery of Cy3-tagged scramble miRNA (red) into primary nondiabetic fibroblasts is successful as measured 24h post delivery, confirming that delivery of Cy3-anti29-294 is most likely efficient as well. Blue denotes the nuclear stain Hoechst 33342 239

Figure 108: Firefly raw luminescence values in primary nondiabetic fibroblasts remain similar across all experimental conditions (p=0.0806) following delivery of antimiR-29 and scramble miR, confirming that Firefly is a reliable control. Statistical analysis was performed via one-way ANOVA. N=3, n=2-3/donor 240

Figure 109: NS-mediated delivery of pmaxGFP plasmid (green) into primary nondiabetic fibroblasts shows poor expression of GFP 72h later, confirming that the NS geometry used for delivery of small RNAs (1.2-1.5 μm height and 100 nm diameter) may perhaps not be adequate for delivery of large cargos. Blue denotes the nuclear stain Hoechst 33342 241

Figure 110: the epidermis consists of 4-5 different layers depending on the skin region, starting from the stratum basale closest to the dermis to stratum corneum at the skin surface. Each of the layers contains keratinocytes with different morphology, cellular composition and function. Other cell types, such as melanocytes or Merkel cells are also present in the epidermis. 243

Figure 111: basal primary keratinocytes from human breast tissue in culture imaged with the light microscope. Small eye-shaped keratinocytes denote proliferating cells, large fried egg-shaped denote differentiated keratinocytes. These cells were used for characterising the nanostraw-electroporation platform for miRNA delivery into this hard-to-transfect cell type. 244

Figure 112: set-up of the '3 centrifugation' protocol for miRNA delivery into primary KC in suspension. First, KC are detached from the cell culture flasks and seeded into NS wells placed in a 24-well plate. Next, the NS wells are centrifuged to ensure the cells come in close contact with the nanostraws and the miRNAs are delivered via NS-mediated electroporation. After delivery the NS wells are returned to the incubator briefly to allow the cells to recover, followed by detaching the KC from the NS membrane and re-seeding them into 96-well plates for functional assays. Image created in BioRender.com and exported under a paid subscription. 245
Figure 113: KC display healthy morphology (left) and high cell viability (right) 24h after extensive manipulation that involved two treatments with TryplE and three centrifugations over short periods of time, confirming the '3-centrifugation' protocol should be suitable for NS-mediated miRNA delivery. Green denotes viable cells, red denotes dead cells 246
Figure 114: representative microscopy images of KC the day after NS-mediated electroporation at 15V and 20V reveals higher KC viability is maintained at 15V, suggesting 15V should be used for NS-mediated delivery of miRNAs into primary KC. Green denotes viable cells, blue denotes cell nuclei. Scale bars denote 150 μm..... 247
Figure 115: NS-mediated delivery of Cy3-tagged scramble miRNA (red) into primary KC via the '3 centrifugation' protocol shows no sign of cargo uptake 24h later, suggesting pore formation in the plasma membrane is not successful using this protocol. Blue denotes the nuclear stain Hoechst 33342 248
Figure 116: (top) primary KC cultured in uncoated 96-well plates are still able to adhere to the plastic surface and display high cell viability (green) 24h after seeding; (bottom) furthermore the cells are also able to proliferate well over 4 days, suggesting primary KC should be able to survive on the uncoated NS membrane. Uncoated denotes lack of coating matrix, normally used during routine subculture of KC. Bottom images were taken at 5x magnification. 250
Figure 117: primary KC seeded on uncoated NS membrane display very low cell viability 24h after seeding, suggesting the NS membrane is unable to allow KC to adhere to it. Blue denotes KC nuclei, green denotes viable cells. Scale bar denotes 300 μm 251

Figure 118: plasma treated surfaces display more 'wetting', as indicated by a lower contact angle of the water droplet relative to the surface. Plasma membrane introduces oxygen-containing functional groups onto surfaces, turning hydrophobic surfaces into hydrophilic ones..... 252
Figure 119: plasma treating the NS membrane with oxygen makes the membrane more hydrophilic as confirmed by the perfect wetting of the water droplet (left) compared to the dome-shaped water droplet on the untreated NS membrane (right)..... 252
Figure 120: primary KC seeded on plasma treated NS membrane display significantly higher cell viability 24h later than on untreated NS membrane. Blue denotes KC nuclei, green denotes viable cells. Scale bar denotes 300 μm..... 253
Figure 121: (left) NS-mediated delivery of Cy3-tagged scramble miRNA (red) into primary KC shows highly efficient and homogenous uptake of miRNA 24h after delivery; (right) in contrast liposomal-based delivery of the same miRNA into primary KC leads to much poorer uptake confined to the nuclei, reinforcing the known difficulty of transfecting primary KC with liposomal-based methods. Blue denotes KC nuclei following staining with Hoechst 33342..... 254
Figure 122: NS membranes with 'expanded pores' reveal a flat surface containing pores (left) that are not extending outwards (right), but have the same chemical surface modification. Nanostraws are depicted in blue, etched polycarbonate surface is depicted in grey. Image reprinted with permission from [210]. Copyright 2012 American Chemical Society..... 255
Figure 123: primary KC seeded on NS membrane with expanded pores exhibit ~100% cell viability 24h after seeding, both on the hydrophobic membrane (left) or hydrophilic membrane that was pre-treated with oxygen plasma (right). The NS membrane with expanded pores lacks the extended NS, but still underwent the same chemical surface modification as the usual NS membrane. Green denotes viable KC. Scale bars denote 300 μm 255
Figure 124: coating the NS membrane with CM after plasma treatment does not seem to improve KC viability over uncoated membrane, possibly due to the inability of the CM to stick to the NS membrane. Image was taken 24h after KC were seeded into the NS wells. Green denotes viable KC, blue denotes KC nuclei. Scale bar denotes 300 μm.... 256

Figure 125: pre-coating the NS membrane with 10% FBS for 1-3h prior to seeding the primary KC improves cell viability dramatically the following day (top). However, this is not sustainable long-term as cell viability starts declining over the next several days (bottom), suggesting that coating the NS membrane with FBS is beneficial only short term. Green denotes viable KC, blue denotes KC nuclei. Images represent different NS wells. All scale bars denote 300 μm 258
Figure 126: FGF-7 has a large stimulatory effect on basal primary KC that leads to ~50% increase in proliferation after 2 days of stimulation with FGF-7 compared to unstimulated cells. Box and whisker plots span min to max. Statistical analysis was performed via one-way ANOVA, followed by posthoc Tukey's multiple comparisons. ****p<0.0001, n=9 262
Figure 127: screenshot of permission to re-use figure in the thesis 299
Figure 128: screenshot of permission to re-use figure in the thesis 300
Figure 129: screenshot of permission to re-use figure in the thesis 300
Figure 130: screenshot of permission to re-use image in the thesis 301

List of tables

Table 1: the raw miRNA counts from the dataset from the paper are written in the format specified in the NanoStringDiff vignette and served as input data into the NanoStringDiff R code. Each row corresponds to one miRNA gene being profiled starting with positive controls, negative controls and housekeeping genes followed by the endogenous genes; each column corresponds to a different sample (patient) being analysed for each category; namely n=3 control samples corresponding to NDFF and n=3 treatment samples corresponding to DFUF 84

Table 2: NanoStringDiff identifies 39 DE miRNAs between DFUF and NDFF, amongst which 38 are upregulated and 1 downregulated in DFUF compared to NDFF. LogFC is log2(DFUF/NDFF), lr represents the likelihood ratio test statistic, pvalue represents the p-value and qvalue represents the Benjamini-Hochberg adjusted p-value 86

Table 3: only 8 miRNAs are identified as being DE by both methods of analysis with NanoStringDiff identifying 31 additional DE miRNAs not identified in the paper 87

Table 4: the top 5 canonical pathways the target genes of the 39 DE miRNAs are enriched in (top of table) include cancer signalling. Interestingly, other enriched canonical pathways include growth factor signalling and signalling involved in cell proliferation and survival. All pathways have a Benjamini-Hochberg (B-H) corrected p-value < 0.05 89

Table 5: according to DAVID and String analysis the target genes of the 39 DE miRNAs are enriched in cancer signalling and signal transduction important for cellular pathways controlling cell proliferation and survival, such as PI3K-Akt or Ras signalling 91

Table 6: according to DAVID and String analysis the 39 DE miRNAs are enriched in biological processes involving response to stimuli, signal transduction and cell proliferation (top section); molecular functions involving binding of receptors, cytokines or GFs (middle section) and cellular components involving plasma membrane and cell surface (bottom section) 92

Table 7: genomic mapping shows the exact location the miRNA genes of the DE miRNAs from the NanoStringDiff analysis are mapped to on the chromosomes. This includes the band and the chromosome name 96

Table 8: Seven of the DE miRNAs from the NanoStringDiff dataset (miRs-145, -143, -16, -27a, -503, -30c and -181a) are enriched in pathways cancer signalling and signalling pathways important for cell growth and proliferation, such as PI3-Akt or MAPK signalling pathway. 107
Table 9: Seven of the DE miRNAs from the NanoStringDiff dataset (miRs-145, -143, -16, -27a, -503, -30c and -181a) are enriched in processes involving cellular movement, growth and proliferation as well as response to stimuli. 107
Table 10: demography of the amputated tissue samples shows that most of the donors are male and elderly. Mean age: 62±10 years. Some of the information is missing. 132
Table 11: miRNA mimics of miR-181a, -27a, -30a were bought from Dharmacon together with negative and positive miR mimic controls. MiRNA mimics are double-stranded oligonucleotides designed to mimic the function of endogenous mature miRNAs to facilitate gain-of-function studies. 142
Table 12: miR-181a and miR-27a work as tumour suppressors or oncogenes depending on the genes they target, cell type and disease state such that it becomes difficult to predict the effects of a miRNA in vitro 153
Table 13: miRs-181a, -27a and -30a have different types of canonical sites on the 3'UTR of KRAS, which could be responsible for the difference in KRAS repression efficiency observed after over-expression of the miRNAs according to the Targetscan Human database Version 7.2 on human KRAS ENST00000256078.4 155
Table 14: miRNA inhibitors against miR-181a and miR-27a were purchased from Dharmacon for loss-of-function studies. The hairpin inhibitor negative control allows to normalise for any effects caused by scramble miRNA inhibitor alone 160
Table 15: protocol used for transfection of miRNA mimics or inhibitors via lipofectamine RNAiMAX 180
Table 16: first step in reverse transcription of mRNAs involves annealing the oligodT primers 183
Table 17: second step in reverse transcription of mRNAs involves synthesis of cDNA 183
Table 18: the mix added to each well in the PCR plate includes primers, mastermix and water, followed by addition of cDNA later on 184

Table 19: qPCR on mRNA consists of three steps involving activation of the polymerase, followed by amplification over 40 cycles 184
Table 20: the mastermix for running qPCR on microRNAs contains dNTPs, reverse transcriptase, reverse transcription buffer, RNAse inhibitor and water 189
Table 21: reverse transcription of microRNAs involves three holding steps at various temperatures for different periods of time 189
Table 22: the mastermix for running qPCR on microRNAs consists of Taqman probes, cDNA, mastermix and water 191
Table 23: qPCR runs on microRNAs consist of polymerase activation, followed by cDNA amplification over 40 cycles 191
Table 24: RNU44 is a suitable normalisation gene for qPCR on miRNAs as expression of RNU44 does not change significantly following transfection of functional miRNA mimics compared to fibroblasts containing scramble miR mimic only (FC ~1). The fold changes were calculated by computing the average of the 2^{-CT} values of RNU44 across 3 samples from each condition (i.e. column in table) and dividing it by the average value of the samples containing 300nM scramble miR mimic. 204
Table 25: ACTB is a suitable normalisation gene for qPCR on mRNAs as expression of ACTB does not change significantly following transfection of functional miRNA mimics compared to fibroblasts containing scramble miR mimic only (FC~1). The fold changes were calculated by computing the average of the 2^{-CT} values of ACTB across 3 samples from each condition (i.e. column in table) and dividing it by the average value of the samples containing 300nM scramble miR mimic 205
Table 26: gene name, accession number, sense and anti-sense primers for the genes that were used for qPCR in the PhD project 206
Table 27: gene name, accession number and anchor nucleotide for the housekeeping genes that were used for qPCR in the PhD project. As the sense and anti-sense primer sequences are proprietary information of Primerdesign only the anchor nucleotide can be published 207
Table 28: permission to re-publish or modify figures from journals has been requested and granted 298

Abbreviations

ABAM	Antibiotic Antimycotic solution
CM	Coating matrix
CT	Cycle Threshold
DE	Differentially expressed
DFU	Diabetic Foot Ulcer
DFUF	Diabetic Foot Ulcer Fibroblasts
DMEM	Dulbecco's Modified Eagle Medium
DMSO	Dimethyl Sulfoxide
DTI	Defined Trypsin Inhibitor
ECM	Extracellular Matrix
EDGS	Epilife Defined Growth Supplement
EGF	Epidermal Growth Factor
ELISA	Enzyme-Linked Immunoabsorbant Assay
EMT	Epithelial Mesenchymal Transition
FBS	Fetal Bovine Serum
FC	Fold change
FGF	Fibroblast Growth Factor
GF	Growth Factor
GO	Gene Ontology
H&E	Hematoxylin & Eosin
HUVEC	Human Umbilical Vein Endothelial Cells
IGF-1	Insulin-like Growth Factor 1
IPA	Ingenuity Pathway Analysis
IRS1	Insulin Receptor Substrate 1
KC	Keratinocytes
KEGG	Kyoto Encyclopedia Of Genes And Genomes

KRAS	Kirsten Rat Sarcoma 2 Viral Oncogene Homolog
miR(NA)	microRNA
MMP	Matrix Metalloproteinases
mRNA	Messenger RNA
N	Number of biological replicates (e.g. donors)
n	Number of technical replicates
NDFF	Nondiabetic Foot Fibroblasts
NS	Nanostraws
OCT	Optimal Cutting Temperature Compound
ORF	Open Reading Frame
PBS	Phosphate Buffered Saline
PCR	Polymerase Chain Reaction
PDGF	Platelet Derived Growth Factor
PFA	Paraformaldehyde
PI	Propidium Iodide
PPI	Protein-Protein Interaction Network
PTEN	Phosphatase and Tensin Homolog
qPCR	Quantitative Polymerase Chain Reaction
RISC	RNA-Induced Silencing Complex
RPPA	Reverse Phase Protein Array
RT	Reverse Transcription
SDS	Sodium Dodecyl Sulfate
siRNA	Silencing RNA
TBE	Tris-borate-EDTA
TC	Tissue Culture
TU	Transcription Unit
TGFβ	Transforming Growth Factor Beta
UTR	Untranslated Region
VEGF	Vascular Endothelial Growth Factor

1. Introduction and motivation of the thesis

1.1. Chronic wounds represent a major burden on society and healthcare systems

Chronic skin wounds, such as pressure, diabetic or venous ulcers have a large impact on societies around the world [1]. In the UK they affect an estimated 1-2 % of the adult population with prevalence amongst elderly people over 65 being as high as 5% [2]. These devastating wounds have an enormous detrimental impact on the quality of life of the affected individuals, leading to increased depression and anxiety, loss of mobility and social isolation [3–5].

Focusing on diabetic foot ulcers (DFUs) alone, these devastating wounds account for 15-25 % of leg ulcers, affecting 1 in 4 diabetics throughout their lifetime [6,7] (Figure 1). In the UK it is estimated that DFUs affect 2.5% of people with diabetes at any time, corresponding to about 60,000 people with foot ulcers across the UK [3]. These wounds significantly increase the risk of lower limb amputation as high as 23-fold compared to non-diabetics, with 85% of amputations being preceded by DFUs [3,5]. In fact it is estimated that once a foot ulcer develops, up to 28% of cases may result in some form of amputation [3], reaching a rate as high as 135 amputations a week in people with diabetes in England alone (Diabetes UK statistics, 2014). Furthermore even if the DFU heals, recurrence rates of DFUs are as high as 66% [8].



Figure 1: Chronic diabetic foot ulcer. Image reproduced from [9] with permission from the rights holder, Elsevier

DFUs and DFU-related amputations are further associated with elevated levels of mortality, with a 5-year mortality rate of 44% observed within 5 years after developing a diabetic foot

ulcer and as high as 70% for patients undergoing a major first amputation. Surprisingly, the 5-year survival rates of patients with DFUs were found to be much lower than patients suffering from common cancers, such as breast and prostate cancer (57% vs 83% and 80%, respectively) [3].

In addition, DFUs and DFU-related amputations represent a heavy burden on the healthcare system, costing the NHS £660 million every year accounting for every £1 in £150 of direct spending [3]. With an increasing frequency of diabetes in the UK (1.9 million in 1998, 3.7 million diabetics in 2018) and prevalence of diabetic amputations together with an ageing population, the number of DFUs and amputations are only expected to increase without any further advances for treatment.

1.2. Wound healing is a complex and dynamic process

Wound healing is a highly complex, spatially and temporally coordinated process in which the body attempts to repair itself after injury and involves the action of many cell types, growth factors and cytokines [10] (Figure 2). Normal wound healing consists of four sequential, yet overlapping phases: homeostasis, inflammation, proliferation and remodelling ultimately resulting in the formation of a scar [11] (Figure 3).

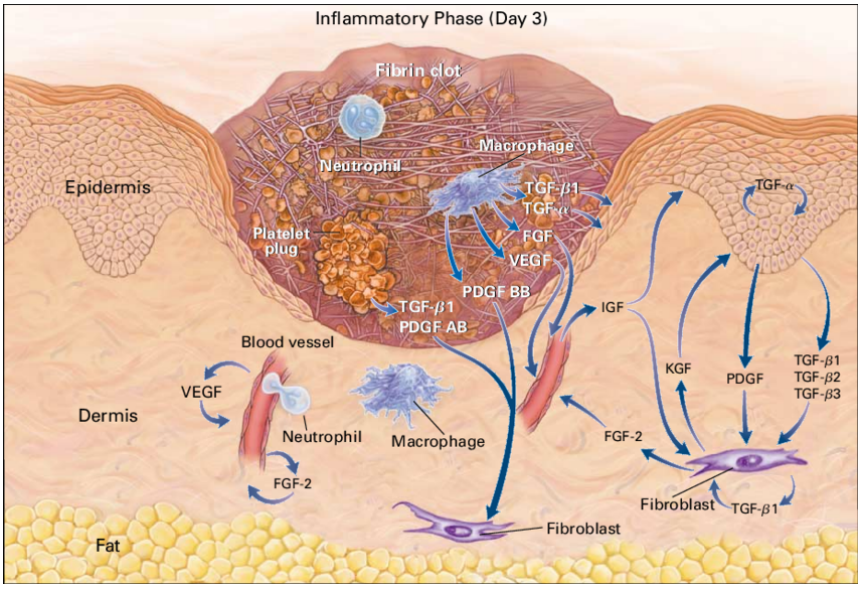


Figure 2: Wound healing consists of a complex spatially and temporally coordinated interplay between various cell types, growth factors and cytokines in which the body attempts to repair itself after injury. Image reproduced with permission from [12], Copyright Massachusetts Medical Society

Homeostasis is the first phase of wound healing and begins immediately after injury. Platelets are the first cells to arrive at the wound site and form a clot to stop the bleeding. They start to release inflammatory factors, cytokines and growth factors, such as TGF-β and PDGF-AB into the blood to recruit inflammatory cells and fibroblasts to the wound site. Meanwhile, fibrin and fibronectin cross-link in the wound bed to form a plug that fills up the wound site to prevent further blood loss, as well as traps proteins and allows platelets to adhere to. This plug also functions as a matrix for wound cells to migrate across and proliferate and represents the main structural support for the wound until it gets later replaced by granulation tissue and eventually by collagen. Following a short period of vasoconstriction, vasodilation occurs mediated by the action of prostaglandins and histamine allowing the blood vessels to become porous and facilitate the entry of inflammatory cells into the wound site from the bloodstream.

Inflammatory phase starts with the arrival of polymorphonuclear neutrophils to the wound site. These cells arrive here within one hour of wounding and become the predominant cells in the wound for the first two days after injury, phagocytosing debri, killing bacteria and breaking down damaged tissue. They become replaced by monocytes that mature into macrophages once in the wound site. Macrophages continue with clearing debri, including neutrophils and the fibrin clot, produce matrix metallo proteinases (MMPs) to break down damaged matrix, as well as secrete growth factors such as PDGF-BB, TGF-β1 and VEGF to push the healing process into the proliferative phase by stimulating migration and proliferation of fibroblasts, keratinocytes and endothelial cells into the wound site. Macrophages remain in the wound site for about 5-7 days and are essential for wound healing.

Proliferative phase begins before the inflammatory phase is over (day 5) and involves neovascularisation (a process known as angiogenesis), formation of granulation tissue and re-epithelialisation. Two to three days after wounding fibroblasts from adjacent uninjured tissue start to enter the wound site and proliferate, degrading the fibrin clot by producing various MMPs and laying down granulation tissue - a provisional extracellular matrix - consisting mainly of type-III collagen, a weaker form of collagen. Concurrently with fibroblast proliferation endothelial cells start migrating into the wound area to form new blood vessels that supply the active wound cells with oxygen and nutrients. Endothelial cells are attracted

to the wound area chemotactically by growth factors produced by inflammatory cells, keratinocytes and fibroblasts including FGF-2 and VEGF and also directly by acute tissue hypoxia. The latter stimulates production of HIF (Hypoxia-inducible factor), an endothelial transcription factor that activates VEGF production. During this phase of healing mature intradermal adipocytes further repopulate the skin wound and are necessary for fibroblast recruitment and deposition of ECM, as shown by genetic and pharmacological inhibition of mature adipocyte formation in mouse wound healing models [13].

At the same time re-epithelialisation starts to take place in which basal keratinocytes (KC) from the wound margins start to migrate together across the matrix as a sheet - known as the epithelial tongue- to form a new epithelium and close the breached barrier. This process is driven by lack of contact inhibition between cells and can begin as early as a few hours after wounding. Activation of the KC is marked by changes in the cytoskeleton and cell surface receptors, such as induction of K6, K16 and K17 keratins, needed for re-epithelialisation [14]. Before they begin migrating, KC at the wound edge must first loosen the adhesion to each other and to the basement membrane via disassembly of their desmosomes and hemidesmosomes, respectively. This release allows the KC to enter the wound bed and migrate over the freshly deposited granulation tissue. Migrating KC form actin filaments and pseudopodia, which attach the cells to the ECM and pull them along the matrix. KC continue to migrate across the wound bed until the cells from both wound edges meet in the middle, at which point they stop migrating due to contact inhibition. In the meantime, keratinocytes at the wound edges continue to proliferate to provide more cells for migration, a process driven by EGF and TGF-α produced by macrophages and keratinocytes. In hairy skin the hair follicle bulge stem cells are further recruited to the wounded epidermis to generate short-lived transit amplifying cells that repopulate the epidermis after injury [15]. A cross-talk between fibroblasts and keratinocytes further takes place in which fibroblasts secrete FGF-7 to stimulate keratinocyte proliferation, with keratinocytes in turn producing TGF-β1/2/3 to stimulate fibroblast proliferation, collagen deposition and differentiation into myofibroblasts (Figure 2).

Myofibroblasts, the primary ECM-secreting cells during wound healing, express α-smooth muscle actin and pull the edges of the wound together by pulling on the ECM. Contraction

usually commences a week after injury allowing the wound to significantly reduce in size. At these later stages of wound healing myofibroblasts further start to be driven towards an ECM-degrading senescent phenotype by the matricellular protein CCN1 to prevent excessive fibrosis [16]. The contraction stage finishes as myofibroblasts stop contracting and commit apoptosis, followed by a breakdown of the provisional matrix which signals the onset of the maturation stage of wound healing.

Remodeling phase represents the last stage of wound healing and involves replacing the disorganised type-III collagen fibres deposited during the proliferation stage with the stronger type-I collagen fibres in a cross-linked and aligned fashion to provide more strength. By this stage, most of the newly laid blood vessels have undergone apoptosis and the wound area develops into an acellular and avascular scar tissue. As the tissue remodels the tensile strength of the wound increases, reaching up to 80% of pre-injured strength. This stage of wound healing can last anything from weeks to a year to fully complete depending on the type and size of the wound. The majority of (large) wounds will follow this process to heal, however superficial wounds as well as wounds in fetal skin have been shown to heal through regeneration in a scarless manner [17]. Interestingly, wounds were further found to heal faster in hair-bearing areas (i.e. scalp) than those in non-hairy areas (i.e. palms), thus illustrating the important, and perhaps somewhat undermined, role the hair follicle plays in wound healing [18].

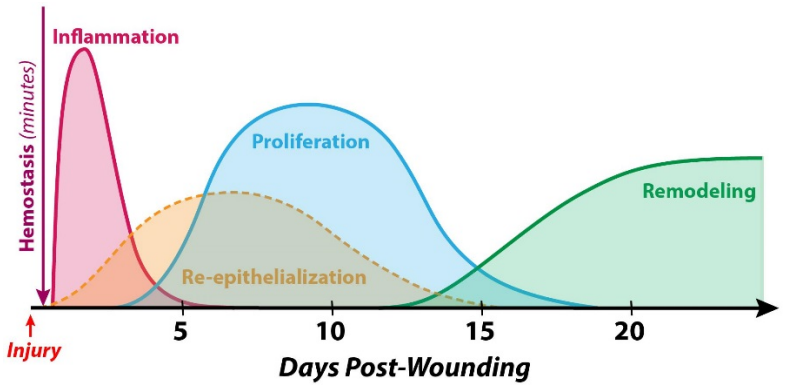


Figure 3: Wound healing consists of distinct, yet overlapping phases starting from homeostasis occurring minutes after injury in which a blood clot gets formed to stop the bleeding; inflammation involving clearing of debri and microbes in the wound bed; proliferation and re-epithelialisation involving formation of granulation tissue and skin re-growth; and remodelling of the newly formed scar tissue. Image reproduced from [19] under Creative Commons Attribution Licence. Copyright 2019 desJardins-Park, Mascharak, Chinta, Wan and Longaker

1.3. In chronic wounds the process of wound healing becomes impaired

Although wound healing occurs in a timely and orderly fashion, any deviation from the normal process can lead to abnormal healing; this can be either under-healing, such as a chronic wound or over-healing, such as a keloid or hypertrophic scar. Chronic wounds do not progress through the standard course of healing and take a considerably long time to heal or may not heal at all due to stalling early on in the process of wound healing, being unable to proceed to the proliferative phase.

There are several main local and systemic factors that can contribute to the development of chronic wounds, some of which include inadequate blood supply caused by damage to the peripheral vasculature (diabetes), local pressure (pressure ulcers) or fibrosis and microvascular cuffing (venous ulcers) resulting in ischaemia, and in extreme cases to gangrene. Local tissue hypoxia can prevent nutrients and oxygen from getting to the wound site to support healing. In the case of DFUs, approximately half of patients further suffer from neuropathy leading to partial or complete loss of sensation in the foot or leg, causing patients to be unaware of any wound developing until it has reached a reasonable size and most likely has already become infected. Many times infection reaches deep as far as into the bone causing osteomyelitis at which point it can become very difficult and challenging to treat the wound, often ending in amputation of the limb.

Chronic wounds are often found to display many abnormalities at the tissue and cellular level compared to acute healing wounds [20,21] some of which include infection and biofilm formation [22], persistent low-grade inflammation preventing healing from progressing to the proliferative phase [23], hyperproliferative but non-migratory keratinocytes at the wound edge preventing re-epithelialisation [24,25], senescent fibroblasts with diminished migratory capacity that switch from an ECM synthesising to a degrading phenotype [26], impaired angiogenesis rendering an oxygen-poor wound environment, elevated levels and activity of MMPs that continually degrade the newly laid ECM [27], decreased levels of growth factors [28] and dimished response to growth factor stimulation [29,30], as well as dysregulations at the molecular level, including changes in gene expression and epigenetic changes [31]. For instance, biopsies from non-healing venous leg ulcers displayed over 60 differentially expressed genes compared to healing

venous ulcers at the epidermal wound edge and in the dermal wound bed, with significant differences related to processes involved in tissue repair, epidermal structural integrity, differentiation, hyperproliferation and transcription factors [32]. Regarding growth factor signalling, for example EGF signalling was found to be dysregulated in chronic wounds. EGF directly stimulates keratinocyte migration and proliferation during re-epithelialisation and has not only been found in decreased levels in chronic wounds [28], but keratinocytes from chronic wounds were shown to display internalisation of the EGF receptor into the cytoplasm as opposed to membrane localisation in normal epidermis [33]. This prevented EGF from binding to the receptors at the membrane surface and activating the downstream pathway.

In the case of DFUs, fibroblasts isolated from these wounds have been shown to produce thinner ECM than nondiabetic foot fibroblasts (NDFF), a phenomenon typical of DFUs [34]. Furthermore these DFU-derived fibroblasts were found to stimulate endothelial sprouting by 3.7-fold less than NDFF and in a 3D skin model, induce hyperproliferation of healthy keratinocytes seeded on the surface compared to NDFF (47% more proliferative), as well as impair re-epithelialisation in a wounded 3D skin model (36% wound closure vs 100% wound closure over 72h post-wounding compared to NDFF). These findings further show how deep the impact of abnormal behaviour of fibroblasts can be on inducing a diseased phenotype in otherwise healthy cells, perpetuating the chronicity of the wound.

Altogether, these changes provide a degradative environment incapable of nurturing wound resolution causing the chronic wound to remain in a 'frozen-like' state.

1.4. In diabetes the process of wound healing is impaired

Many times DFU do not heal because of intrinsic disruptions in the wound healing capabilities of the diabetic cells. Diabetes is a metabolic disease caused by persistent high levels of glucose in the blood, either due to the inability of the pancreas to produce insulin (type I diabetes – T1D) or due to insulin insensitivity (type II diabetes - T2D). If left untreated for long periods of time, diabetes can cause vast damage to cells by enhancing the production of oxidative stressors leading to increased oxidative stress [35], a phenomenon known as hyperglycaemia-induced damage [a].

Such damage caused to endothelial cells is vastly known in diabetes, with this disease inducing micro-vascular and macro-vascular damage by inhibiting production of vasodilators, such as nitric oxide, increasing activity of vasoconstrictors such as endothelin-I and leading to overproduction of extracellular matrix, which causes capillary occlusion. However, endothelial cells are only one of the cell type that are affected by diabetes as keratinocytes, fibroblasts and macrophages have also been shown to be victims of chronic high glucose levels.

For example, dermal fibroblasts from diabetic db/db mice (a mouse model of leptin deficiency) were found to exhibit a 75% reduction in migration, as well as a 7-fold impairment in VEGF production compared to wild-type fibroblasts *in vitro* [36]. This behaviour was also recapitulated in adult type I diabetic patient skin fibroblasts that exhibited lower basal VEGF production compared to age-matched nondiabetic fibroblasts, with very little VEGF production after stimulation with hypoxia or insulin. PKCδ levels were also found to be upregulated in T1D fibroblasts which induced impaired p-Akt phosphorylation in response to insulin stimulation, in turn impairing migration and delaying wound healing *in vivo* [37]. Similarly, biopsies from human diabetic skin were revealed to lack expression of IGF-1 in the basal layer of epidermis compared to nondiabetic skin, contributing to diminished keratinocyte proliferation and delayed re-epithelialisation during diabetic wound healing [38].

[a] Interestingly, diabetes-induced damages can result in permanent damage to the cells, even when returned to a normal glycaemic environment, a process known as hyperglycaemic memory, such that these cells continue to exhibit abnormalities when cultured *in vitro* at early passages.

Additionally, macrophages were found to have an impaired ability to phagocytise in diabetic mice and display reduced capability to clear apoptotic cells at the wound site, in turn prolonging the inflammatory phase and impairing commencement of the proliferation phase [39]. Interestingly, diabetic wounds in mice furthermore displayed metabolic changes which associated with delayed skin wound healing [40]. Label-free two photon microscopy of full-thickness diabetic wound edges in mice showed a significantly lower optical redox ratio – a measure of the relative rates of glucose catabolism to oxidative phosphorylation- than nondiabetic controls at day 10 post-wounding [41]. This was consistent with hyperproliferative and non-migratory keratinocytes, typically found at nonhealing edges of many chronic wounds. Similarly, wound iron levels were found to be significantly reduced during diabetic wound healing, corresponding to impaired macrophage polarization, delayed ECM deposition and impaired wound healing [42,43]. Lastly, diabetic skin and DFUs were shown to display a significant reduction in microbiome diversity compared to healthy nondiabetic skin, illustrating the important role microbial composition of skin has on wound healing [44].

Altogether, these changes make diabetic wounds intrinsically difficult to heal.

1.5. Treatments for chronic wounds are vast, but with limited success

Treatments that have been tried for chronic wounds are vast ranging from mechanical-based approaches, such as negative pressure therapy, electrical stimulation or offloading orthotics and cellular-based approaches, including tissue-engineered skin substitutes and stem cell therapies to biologics, comprising growth factor therapy or nucleic acid therapy and small-molecule drugs, such as prostaglandins, Wnt/β-catenin inhibitors and glucocorticoid inhibitors. However, despite many promising ongoing pre-clinical studies, no single therapy has yielded widespread clinical success so far [45], with approximately one third of DFU patients still being unable to heal and requiring some sort of amputation [3].

In the case of DFUs, for instance, PDGF-BB (Regranex Gel, Smith and Nephew) is the only FDA approved therapy for the treatment of neuropathic diabetic foot ulcers with an area smaller or equal to 5 cm^2. [46] Regranex (becaplermin) uses a carboxymethylcellulose gel as vehicle for delivery, a high viscosity and non-toxic compound that allows sustained delivery of active proteins [47]. Its efficacy in humans when applied topically at 30 μg or 100 μg becaplermin per 1g of gel for 20 weeks revealed controversial results, however with some clinical studies suggesting a rate of complete healing twice as high compared to patients receiving a placebo gel or good ulcer care alone, while others showing no significant difference between the groups [48]. This, perhaps is of no surprise as DFU fibroblasts were previously shown to respond very poorly to growth factor stimulation compared to NDFFs, including PDGF-AB (7.5 vs 16.3-fold change in proliferation) and IGF-1 (1.7 vs 5-fold change in proliferation) indicating that these cells display intrinsic molecular and biological changes that prevent them from responding to treatments [49]. Furthermore, even in the case of successful ulcer closure Regranex comes with a "Black Box" warning as prolonged use (more than 3 tubes) has been associated with increased risk of cancer metastasis [50] likely due to the high concentration of PDGF-BB required to have a physiological effect, illustrating the urgent need to develop a successful treatment yet.

1.6. Motivating hypothesis for PhD research

Failure of DFU cells to respond to GF stimulation, together with their poor ability to migrate, proliferate and secrete adequate levels of growth factors and cytokines, suggests the cell signalling pathways controlling these cellular processes are disrupted in the DFU cells. This can lead to incorrect flow of information along the signalling pathways making cells unable to perceive and correctly respond to the wound microenvironment. Such errors in signalling interactions, in turn, affect the signal transduction leading to incorrect processing of cellular information and ultimately initiating the wrong cellular process, such as increased production of proteases or decreased secretion of ECM.

We hypothesise, in the case of DFUs this disruption might be partially caused by dysregulated levels of miRNAs, small regulatory RNAs that scramble the cell signalling networks to progressively mute cell signalling, driving impaired wound healing (Figure 4). Furthermore, we postulate these dysregulated miRNAs cooperate as synergistic networks to delay processes important for tissue repair, an aspect currently unexplored in chronic wounds.

As such, we are interested in studying how dysregulated miRNAs in the wound bed affect the cell signalling pathways important for wound healing. In particular, we are interested in understanding miRNA dysregulation in fibroblasts due to the crucial role they play in wound healing and the deep impact their abnormal behaviour has on preventing timely wound closure. This, in turn, could help develop a potential miRNA-based therapy aimed at temporarily restoring balanced levels of miRNAs - via miRNA mimics or inhibitors - to rewire the disrupted cell signalling pathways in DFU-derived fribroblasts and drive wound resolution.

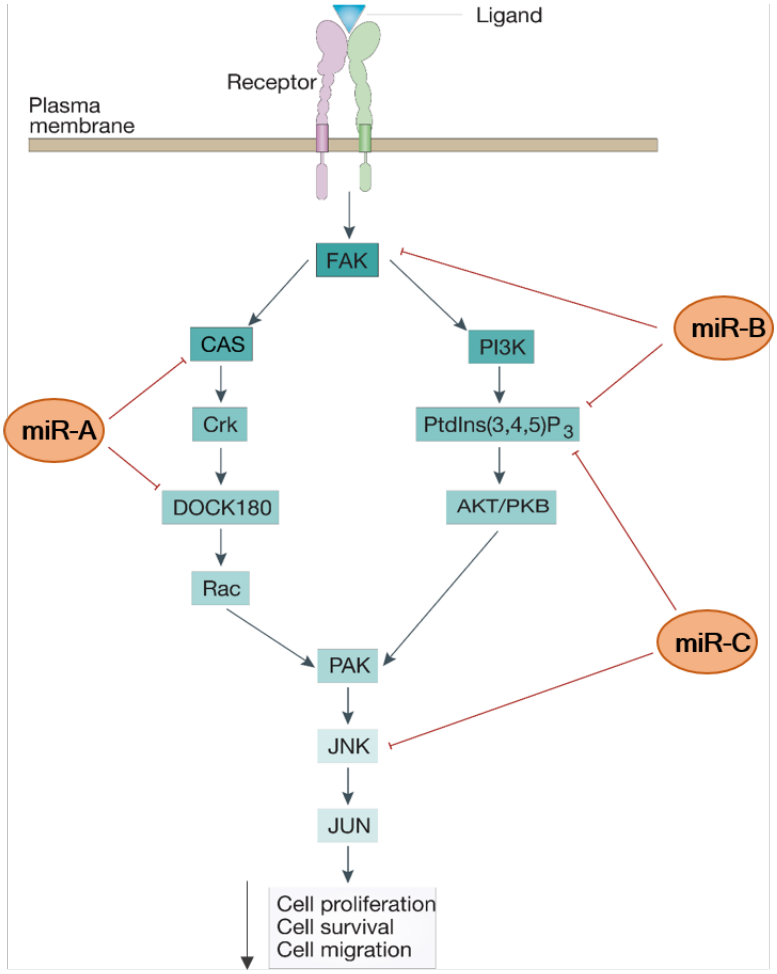


Figure 4: Dysregulated miRNA levels in the chronic wound bed (shown in red) progressively mute cell signalling to impair cell proliferation, migration and survival. Restoring normal levels of dysregulated miRNAs in the wound bed - via miRNA mimics or inhibitors - can temporarily manipulate the disrupted signalling pathways to drive wound healing. This, in turn, can help develop a miRNA-based therapy for the treatment of DFUs. Image modified with permission from [51]. Copyright 2004, Springer Nature

1.7. MicroRNAs play important roles in skin and wound healing and can become dysregulated in chronic wounds

MicroRNAs (miRNAs) are small noncoding endogenous RNAs (20-25bp long) involved in regulating gene expression at the post-transcriptional level by binding to and degrading target mRNAs and/or inhibiting their translation into proteins. MiRNAs are expressed in a spatiotemporal pattern that varies with tissue and cell type and regulate a variety of cellular processes from differentiation and proliferation to apoptosis [52–54], playing particularly significant roles in conferring robustness to systems during developmental transitions [55]. Their vast importance in gene regulation is best supported by the fact that a) miRNAs are conserved across many species [56], b) they are highly abundant with some miRNAs expressed as highly as 50,000 copies per cell [57], c) the majority of protein-coding genes are miRNA targets [58] and d) dysregulation of miRNAs is found in many diseases.

Recently, miRNAs have been increasingly shown to play important roles in wound healing, coordinating key processes such as inflammation, angiogenesis, proliferation and remodelling of the wound [59], while their dysregulation has been linked to abnormal healing and chronic wound formation [59–61].

The important role of miRNAs in skin was first shown from studies involving deletion of Dicer, an essential enzyme for producing mature miRNAs. Newborn mice carrying epidermal-specific Dicer deletion displayed stunted and abnormal growth of hair follicles lacking stem cell markers, as well as hyperproliferation and abnormal organisation of the epidermis [62,63]. Interestingly, different skin lineages were shown to express differential miRNAs. Murine epidermis for instance preferentially expressed the miR-200 family (a, b and c), miR-141, miR-429 and miR-19/miR-20 family (comprising miR-19b, miR-20, miR-17-5p and miR-93), while others such as the miR-199 family (a and b) were exclusively expressed in hair follicles [64], supporting diverse roles for miRNAs in the development or maintenance of skin and its appendages. One such example is miR-203 that is highly expressed in the epidermis and is involved in skin morphogenesis. This miRNA acts as a switch between keratinocyte differentiation and proliferation in adult epidermis by directly repressing p63 in the suprabasal layers [65]. The transcription factor p63 maintains keratinocyte proliferation and is strongly expressed in the basal layer. Under the influence of miR-203 it becomes heavily

repressed in the suprabasal layers leading to reduced keratinocyte proliferation and thus promoting differentiation into stratified epithelia. This miRNA, however was found to be highly upregulated in the epidermis from edges of chronic venous ulcers contributing to hyperproliferation of keratinocytes [66].

Other miRNAs are involved in coordinating keratinocyte migration, such as miR-31 that is induced by TGF-β1 and TGF-β2 in wound edge keratinocytes during the inflammatory and proliferative phase of wound healing [67]. In an ex vivo wound healing model over-expression of this miRNA increased the proliferation and migration of keratinocytes partially via directly targeting the EMP-1 protein contributing to re-epithelialisation, suggesting that up-regulation of this miRNA might be a promising target for driving re-epithelialisation in chronic wounds. Some miRNAs, however can have opposing effects on re-epithelisation, such as miR-198 that directly targets and inhibits pro-migratory proteins PLAU and LAMC2 in keratinocytes, impairing their migration. This miRNA was found to be persistently expressed in skin biopsies from wound edges of non-healing DFUs compared to epidermis of acute wounds following a failed switch to silence this miRNA upon wounding, in turn delaying re-epithelialisation [68].

The vast involvement of miRNAs in coordinating tissue repair was further illustrated in a study investigating the miRNA profile during formation of granulation tissue. Here, the authors identified 54 miRNAs that changed expression more than two-fold at day 7 post-wounding compared to normal skin in a mouse wound model [69]. Amongst these miR-21 was up-regulated 3.1-fold which was shown to be important for driving early wound contraction and collagen deposition under the influence of TGF-β1. This miRNA was further shown to promote re-epithelialisation during wound healing by inducing keratinocyte migration via targeting TIAM1 and TIMP3 [70], an inhibitor of MMPs. Interestingly, miR-21 was found to be upregulated in non-healing venous ulcers, together with miR-16, -20a, -106a, -130a and -203, where it targeted EGR3 (Early growth response protein 3) and LepR (Leptin receptor) contributing to impaired granulation tissue formation, delayed re-epithelialisation and prolonged inflammation in a rat acute wound healing model [71].

Likewise, miRNAs were shown to regulate angiogenic processes during wound healing. The important implication of miRNAs in angiogenesis was first demonstrated in Dicer deficient

mice which showed lethal embryonic developmental defects and impairments in blood vessel formation together with altered expression of critical angiogenic regulators including VEGF and the genes of its receptors KDR and FLT-1 [72]. In humans, endothelial cells siRNA-mediated knockdown of Dicer inhibited cell proliferation and migration and reduced cord formation *in vitro*, reinforcing that miRNAs are essential for normal endothelial cell function [73].

MiR-126, for instance is an endothelial specific miRNA that regulates angiogenesis and maintains vascular integrity in vivo. Deletion of this miRNA in mice caused defects in endothelial cells proliferation, migration and blood vessel formation leading to leaky vessels, haemorrhaging and partial embryonic lethality [74]. MiR-126 exerts its pro-angiogenic actions by repressing Spred-1, an intracellular inhibitor of RAS/MAP kinase signalling downstream of FGF and VEGF - potent inducers of angiogenesis – in turn augmenting the angiogenic signaling.

Other miRNAs, however can have anti-angiogenic effects, such as miR-92a that is highly expressed in human endothelial cells, was shown to block angiogenesis *in vitro* and *in vivo* by targeting several proangiogenic proteins, including Integrin alpha-5 [75]. In mouse models of limb ischemia and myocardial infarction where expression of this miRNA was significantly increased, systemic inhibition of miR-92a led to enhanced blood vessel growth and functional recovery of the damaged tissue, suggesting a therapeutic benefit for treating ischemic diseases and ulcers. Furthermore in the context of diabetes, increased levels of miR-503 were found in plasma and muscles of amputated ischemic limbs from diabetic patients, contributing to diabetes-associated vascular complications [76]. Under high glucose conditions *in vitro* this miRNA was found to inhibit endothelial cell proliferation, migration and network formation via direct targeting of cell-cycle genes CCNE1 (Cyclin E1) and cdc25A (Cell division cycle 25A), further reinforcing the wide implication miRNA dysregulation can have on impairing normal wound healing.

1.8. MicroRNAs are a subset of epigenetic mechanisms

MiRNAs are a subcategory of an epigenetic modification known as noncoding RNA-driven gene silencing (Figure 5). Epigenetic modifications, unlike genetic modifications that alter the DNA sequence, cause changes in gene expression by affecting the accessibility of proteins to the DNA or by altering DNA conformation, i.e. a change in phenotype without a change in genotype (Figure 6). These modifications occur naturally and can be stable being passed on through multiple generations of cell divisions. There are three major mechanisms that are known to contribute to epigenetic changes, consisting of DNA methylation, histone modifications and noncoding RNA-driven gene silencing. These systems are highly interdependent and work in concert with each other to coordinate gene expression [b], including during normal wound healing [77].

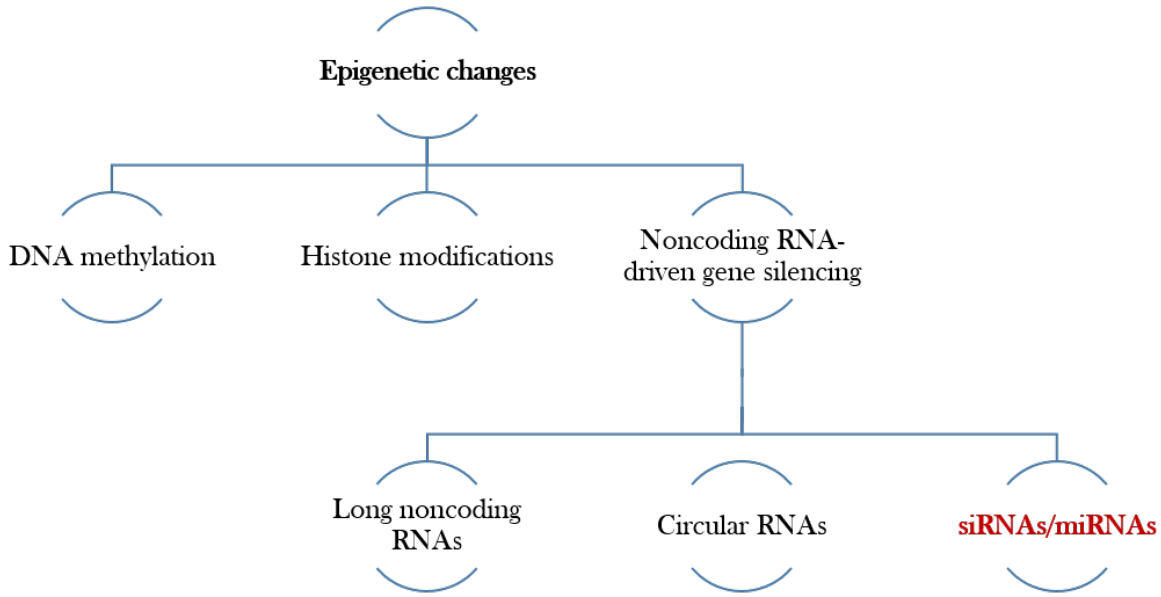


Figure 5: epigenetic changes encompass three major subcategories, including DNA methylation, histone modifications and noncoding RNA-driven gene silencing. Epigenetic modifications change gene expression without altering the DNA sequence by affecting the accessibility of the proteins to the DNA or by altering DNA conformation

[b] DNA methylation, histone modifications and noncoding RNAs, such as miRNAs do not work as separate entities, but instead have evolved at the genome-wide level to 'communicate' in order to coordinate gene transcription. For instance, a functional complementation exists between DNA methylation and miRNA-mediated gene regulation with genes being either preferentially regulated by promoter DNA methylation at the transcriptional level or miRNAs at the post-transcriptional level, but not both [222]. Similarly, DNA methylation and histone modifications 'communicate' to coordinate transcription [223] with miRNAs mediating the cross-talk between these two mechanisms, hence suggesting a tight interplay between these three systems to allow the 'right' gene expression at the 'right' time [224].

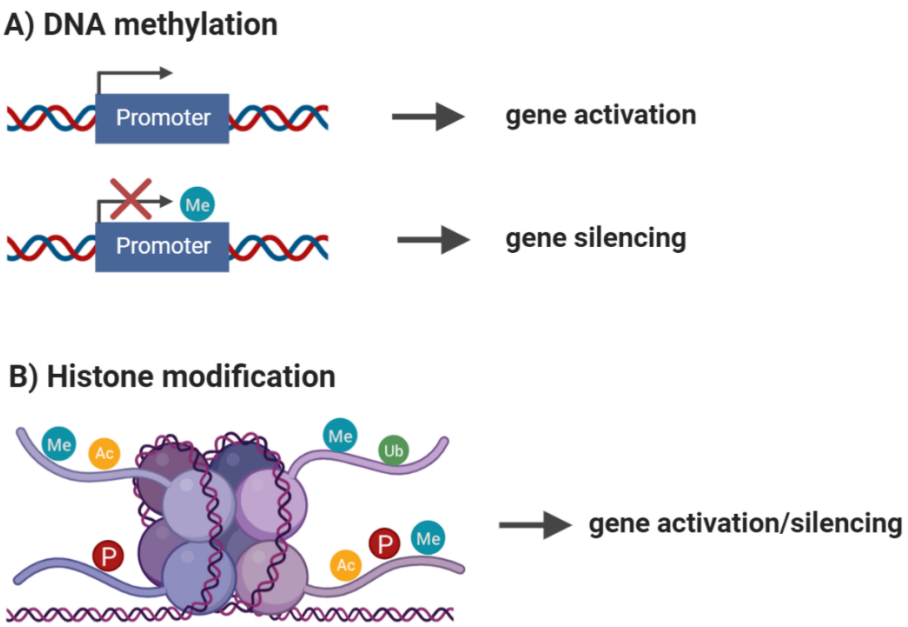


Figure 6: Epigenetic modifications alter gene expression by changing the phenotype without a change in genotype. They affect the extent to which DNA wraps itself around the histones to yield a transcriptionally active or inactive chromatin. A) DNA methylation causes gene silencing following methylation of cytosine and guanine islands (CpG) residues, located in the gene promoter region; B) Histone modifications drive gene activation or silencing depending on the number and type of modifications occurring on its tails, such as methylation (Me), acetylation (Ac), phosphorylation (P) or ubiquitination (Ub). Image of histone tail modifications is for illustrative purposes only and does not represent the specific modifications that occur on each tail. Figure created in BioRender.com and exported under a paid subscription.

While DNA methylation and histone modifications (Figure 6) are some of the most widely known and extensively characterised epigenetic modifications, being described as early as 1970s, the idea that noncoding RNAs could exert regulatory roles is still relatively new.

Noncoding RNAs constitute 98% of the transcriptome, with the remaining 2% being translated into proteins. For a long time the purpose of these transcripts that do not code for proteins was unknown being regarded as 'junk' or 'transcriptional noise'. However, vast amount of evidence has meanwhile shown these noncoding RNA molecules can indeed be functional, capable of modulating gene expression at the transcriptional and post-transcriptional level [78]. In fact, the importance of these noncoding transcripts in biology is perhaps best supported by the strong positive correlation between the complexity of an organism and the size of noncoding, rather than protein-coding genome [79].

Noncoding RNAs (ncRNAs) encompass a large variety of RNAs, some of which are constitutively expressed and play a housekeeping role (i.e. ribosomal RNA and transfer

RNA), while others are spatiotemporally expressed and play a regulatory role (i.e. miRNAs, long noncoding RNAs). Regulatory RNAs further encompasses two classes of RNAs: ncRNAs less than 30 nucleotides in length are classified as short RNAs (i.e. microRNAs, siRNAs and piwiRNAs), while those longer than 200 nucleotides are regarded as long RNAs (i.e. long noncoding RNAs and circular RNAs). Early pioneering work by Andrew Fire and Craig Mello in the late 1990s first showed that RNA can have regulatory roles when they discovered that small RNAs can silence gene expression in C. elegans. This process is now known as RNA interference (RNAi) which refers to the ability of short double stranded RNAs, such as siRNAs and miRNAs to silence gene expression at the post-transcriptional level by destroying target messenger RNA (mRNA) molecules [80]. In animals the process of RNAi is particularly important during development especially during morphogenesis regulating processes like cell differentiation and self-renewal.

1.8.1. Long noncoding RNAs

Long noncoding RNAs (lncRNAs) are poorly conserved, endogenous noncoding RNAs with a length >200 bp that do not encode proteins. Gene expression profiling has shown that lncRNAs display lower expression patterns than protein-coding genes, display tissue-specific expression patterns and are predominantly located in the chromatin and nucleus [81]. They are usually transcribed from different sites of the genome and are classified into different subtypes depending on the genomic location relative to the protein-coding genes [82]. Their well-defined secondary structure allows them to further interact with DNA, RNA and proteins making them highly versatile molecules that exert profound regulatory functions on the genome. For instance, they have been shown to be involved in chromatin modification, direct transcriptional regulation, gene silencing through producing endogenous siRNAs, modulation of miRNA regulation and post-translational regulation of protein activity [83].

1.8.2. Circular RNAs

Circular RNAs (circRNAs) are a novel class of non-coding RNAs that only recently have been associated with epigenetic regulation. They are produced by alternative splicing of pre-mRNAs via a process known as 'backsplicing', where an upstream splice acceptor is joined to a downstream splice donor in a covalent link to form a closed loop that lacks polyadenylated and capped tails [84]. CircRNAs are conserved being found across many species from fruit fly

to mouse and human [85], demonstrating cell-type specific and dynamic expression levels [86], particularly during embryonic development [87]. They are predominantly cytoplasmic and highly stable being often expressed at low levels, but in some cases being considerably more abundant than their associated linear transcripts [88]. Although the regulatory function of the vast majority of circRNAs still remains to be elucidated, some circRNAs were shown to work as miRNA sponges with one of the most notable examples being CIRS-7. This circRNA is derived from the CDR1 antisense script, being highly expressed in the mammalian brain and contains more than 60 conserved binding sites for miR-7, being able to bind up to 20,000 miR-7 molecules per cell [85]. In this way it can act as a competitive inhibitor of miR-7, titrating the available pool of miR-7 molecules away from their targets. Interestingly, this circular sponge cannot be cleaved by miR-7 or its associated Ago2 protein as it lacks complementarity to this miRNA beyond the 12th nucleotide, however it can be cleaved by miR-671 [89], indicating perhaps the existence of a 'miRNA storage' inside cells, ready to release a 'load' of miRNAs when required without the need of de novo production of miRNAs.

1.8.3. Short interfering RNAs

Short interfering RNAs (siRNAs) are processed from long double stranded (ds) RNA that is usually exogenous, coming from a virus or other foreign genetic material or being artificially introduced into the cell in laboratory conditions, with the exception of some endogenous siRNAs that are generated from long noncoding RNAs. Once it enters the cells the dsRNA is recognised and cleaved by the ribonuclease protein Dicer into shorter double stranded fragments 20-25bp long with a 2-nucleotide overhang at their 3' end known as siRNAs. These fragments are then loaded into the active RNA-Induced Silencing Complex (RISC) where they get separated into single strands. Loading occurs asymmetrically such that protein Argonaute 2 (Ago2) part of the RISC complex recognises and binds the thermodynamically relatively unstable 5' end of the RNA duplex (the "guide strand"), while the more stable 3' terminus (the "passenger strand") will become degraded. RISC will now bind to a target mRNA based on complementary base-pairing to trigger endonucleolytical cleavage in the middle of the siRNA-mRNA duplex between the nucleotides pairing to residues 10 and 11 of the siRNA [90] (Figure 7). The base-pairing complementarity between the guide strand and the mRNA is

perfect, making siRNAs highly specific to their target mRNAs, although some nontargeting side-effects can occur.

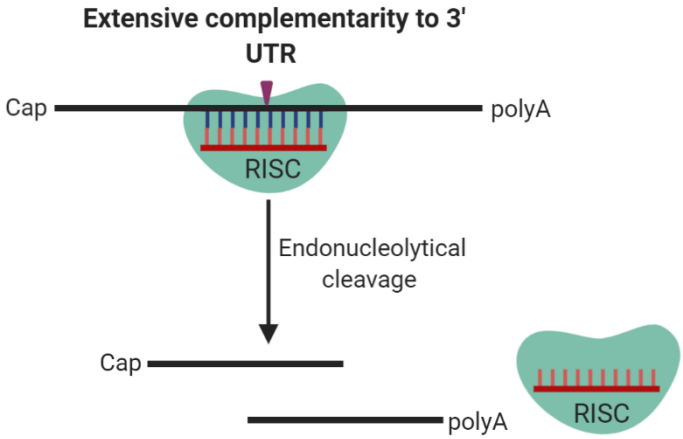


Figure 7: siRNAs have extensive complementarity to the 3'UTR, causing cleavage of the target mRNA in the middle. This, in turn, leads to significant gene knockdown. Figure created with BioRender.com and exported under a paid subscription.

1.9. MicroRNAs are endogenous epigenetic regulators

MicroRNAs (miRNAs), unlike siRNAs are endogenous and encoded throughout the genome constituting about 1-2% of genes in worms, flies and mammals. MiRNA genes can be found either between independent transcription units (intergenic) or within a transcription unit (intragenic) where they can reside either in an intron of a protein-coding or noncoding gene (intronic) or an exon of a noncoding gene (exonic) (Figure 8B, C and D, respectively). Originally it was believed that most miRNAs lie in intergenic regions (i.e. in their own transcription unit), but over time this number has been gradually growing with studies showing that ~50% of known mammalian miRNAs are associated with known transcription units (TUs) that can be mapped to a known coding or noncoding gene [91]. Amongst these the vast majority of miRNA genes were found to reside in intronic regions of hosting TUs, both protein-coding and noncoding RNAs with only a small percentage of genes residing within the exons of hosting TUs (80% intronic vs 20% exonic, respectively) [92]. Whereas intergenic miRNAs are expressed by their own promoter, miRNA and host genes expression profiles from human microarray data showed a strong positive correlation between intronic miRNAs and their host genes, suggesting that miRNAs are transcribed in parallel with their host

transcripts [91,93]. This is because many times intronic miRNAs share the promoter of the host gene and thus are generated from a common precursor transcript, although it has been noted that miRNA promoters can sometimes be distinct from the promoters of the host genes [94].

Furthermore, miRNA genes can be often found in close proximity to each other (rather than scattered independently) forming a polycistronic transcription unit [95] (Figure 8A). Such clustered miRNAs usually have very similar expression profiles, suggesting that they are co-transcribed and processed from a single common transcriptional unit. Microarray expression profiling of 175 miRNAs from 24 human organs revealed that proximally paired miRNA genes that are within <50 kb of each other are generally co-expressed, suggesting this distance to be the upper bound for a majority of polycistronic transcripts to commonly regulate clustered miRNAs [93]. Simultaneous transcription of miRNAs further has an evolutionary advantage as miRNAs from the same cluster were shown to have the tendency to target overlapping sets of genes to achieve greater cooperative repression [96]. MiRNA clusters usually host two or three miRNAs, however larger clusters also exist such as the miR-17-92 cluster on chromosome 13 that consists of six miRNAs precursors (mir-17, 18a, 19a, 20a, 19b-1, and 92a-1). In fact, in humans the largest miRNA gene cluster is found on chromosome 19q13.41 and harbours 46 tandemly repeated miRNAs genes over a ~100kb long region [97]. These miRNA genes are highly related to each other and have been found to be predominantly expressed in the placenta, contributing to placental-maternal signalling [98].

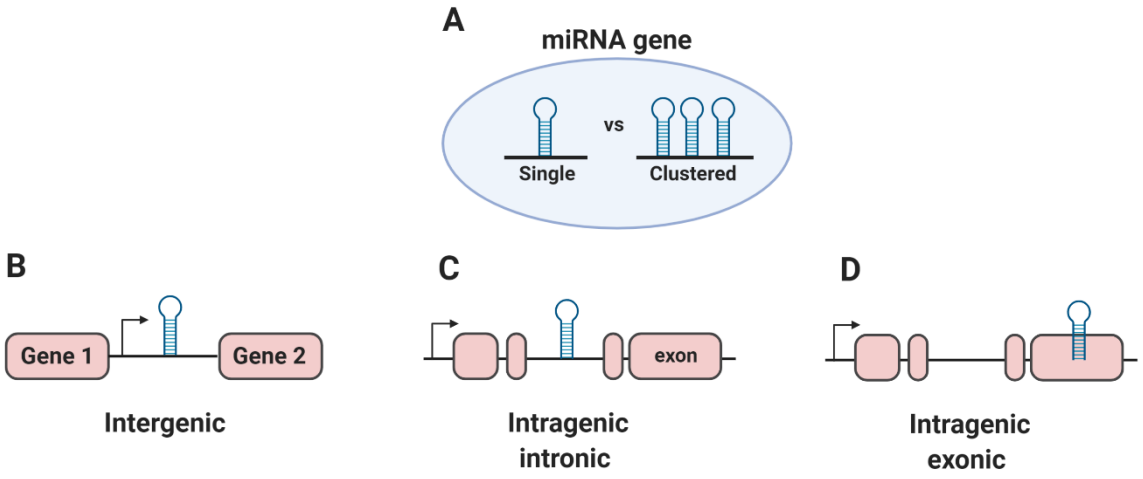


Figure 8: miRNA genes can be either isolated or clustered (A), and are located either in intergenic (B) or intragenic regions, where they can reside in an intron of a gene (C) or exon of a gene (D). Pink rectangles in C) and D) represent exons. Image created with BioRender.com and exported under a paid subscription.

1.10. MicroRNA biogenesis involves a complex mechanism

The majority of miRNAs are generated from miRNA coding genes via the canonical synthesis pathway involving the action of two RNAse III proteins, Drosha and Dicer (Figure 9). In the canonical synthesis pathway the miRNA gene is transcribed by RNA polymerase II into an 1,000 bp long RNA fragment containing a hairpin structure known as pri-miRNA. This gets then processed by the two nuclear proteins, Drosha and DGCR8 that associate to form a microprocessor complex, into a 70 bp long hairpin known as pre-miRNA[c]. The pre-miRNA is then exported out of the nucleus into the cytoplasm by Exportin 5 where the maturation process begins. Here the endoribonuclease Dicer recognises and cleaves the stem-loop to produce a 22 bp long duplex with a 2-nucleotide overhang at the 3' end. The miRNA duplex is then recognised and bound by the RISC complex containing the Argonaute (AGO2) proteins where it will undergo strand separation similar to siRNAs to generate the guide and the passenger strand based on the relative thermodynamic stability of the two ends of the small RNA duplex. Similar to siRNA loading, the strand with the relatively unstable 5' terminus is typically selected as the guide strand [99,100]. In addition to thermodynamic stability of the duplex, in humans AGO proteins also preferentially select for guide strands that start with a U at nucleotide position 1 [101]. While the passenger strand is degraded quickly following strand selection, the guide strand will now direct the RISC complex to the target mRNA where it will bind the 3'UTR of target mRNA via complementary base pairing. Once bound to the mRNA the AGO proteins recruit factors that inhibit the expression of the target mRNAs via two mechanisms: triggering deadenylation of the polyA tail by fostering the activity of deanylases such as CCR4-NOT to stimulate mRNA decay in P-bodies, cytoplasmic domains involved in mRNA turnover; or preventing translation into protein either at the initiation step by inhibiting the eukaryotic initiation factor 4E (EIF4E) or at the elongation step by causing ribosome stalling or ribosome 'drop-off'.

The fact that miRNAs bind to the 3'UTR of mRNAs is not 'by chance' as this region of mRNAs was found to play crucial roles in post-transcriptional regulation of genes by influencing the

[c] For intronic miRNAs this step occurs after the transcript has been incorporated into the spliceosome, but before intron excision [92], contrary to the common belief that the microprocessor complex cleaves the pri-miRNA from excised introns after the splicing reaction has occurred to ensure miRNA and protein biogenesis from the same primary transcript.

localisation, stability, export and translational efficacy of an mRNA (Figure 10). It can do so due to the presence of its many regulatory elements, such as miRNA binding sites, AU-rich elements or the polyA tail that affect the spatial and temporal expression of an mRNA [102]. Although miRNA targeting can also occur in 5′ UTRs and ORFs, this is less frequent and effective than 3′ UTR targeting as silencing complexes, such as RISC bound to these regions would get displaced by the translation machinery as it translocates along the ORF from the cap-binding complex at the 5′ end to the stop codon at the 3′ end [103]. To confer appreciable repression RISC must remain associated with the target site for longer periods of time – thus being subjected to ribosome interference - as opposed to perfectly complementary sites to artificial siRNAs that may not need to remain associated as they result in catalytic cleavage.

Although the majority of miRNAs are generated via the canonical pathway, other non-canonical pathways of miRNA biogenesis have been identified that do not involve the action of Drosha or Dicer or require additional machinery for efficient processing [104]. Drosha independent miRNAs, for example are spliced directly from introns of larger transcriptional units such as pre-mRNAs by the spliceosome (rather than being cleaved by Drosha) before being exported into the cytoplasm and processed by the usual mechanisms. These miRNAs are known as 'Mirtrons' and have originally been thought to occur only in C. elegans and Drosophila, but some mirtrons have now been found in mammals, such as mir-877 and mir-1224 that were conserved [105]. Dicer independent miRNAs, such as pre-miR-451 can directly incorporate into Ago2 to generate mature miR-451 without the involvement of Dicer while other miRNAs, such as let-7 require the action of terminal uridylyl transferases (TUTases) for efficient processing by Dicer. These non-canonical pathways, however are responsible for the biogenesis of only 1% of conserved miRNAs in vertebrates while the poorly conserved miRNAs are often low in abundance.

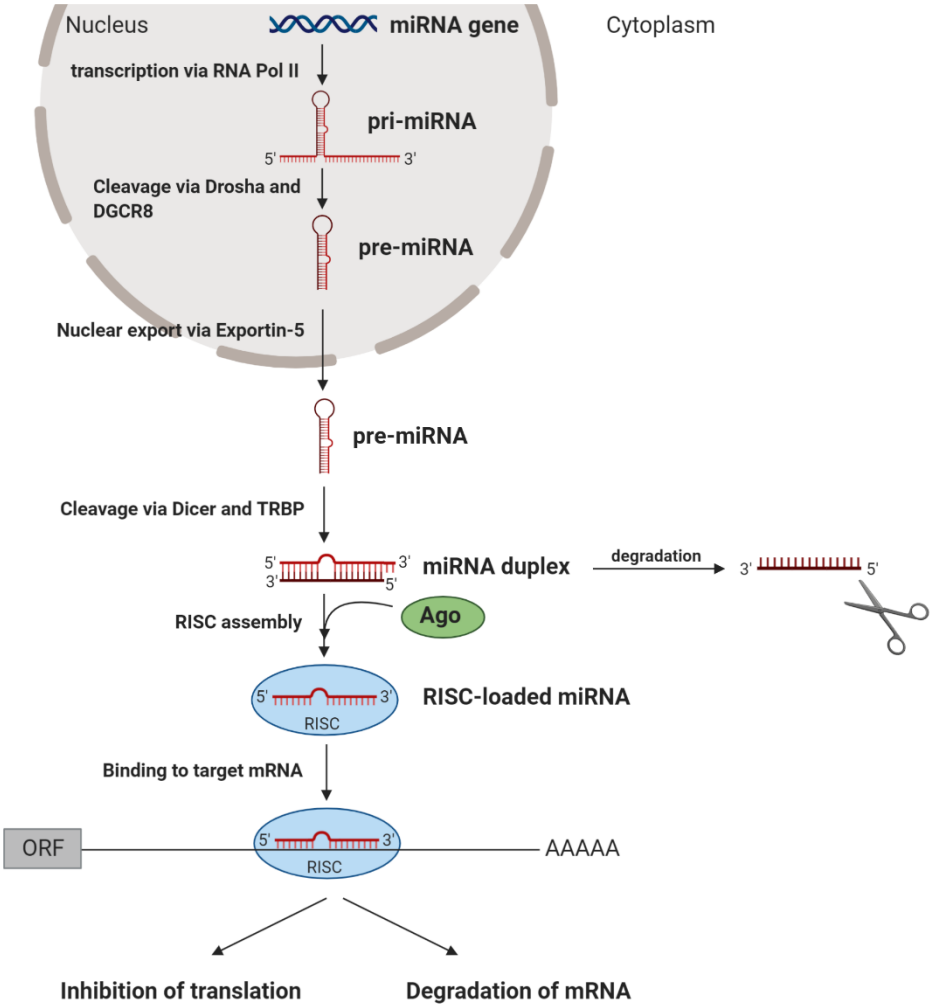


Figure 9: the majority of miRNAs is generated via the canonical pathway, involving the action of Drosha and Dicer. Processing of miRNAs starts in the nucleus, where Drosha and DGCR8 cleave the pri-miRNA into a much shorter pre-miRNA that gets exported into the cytoplasm by Exportin 5. Here, Dicer cleaves the stem-loop to produce a miRNA duplex that gets recognised and bound by Argonaute proteins part of the RISC. Once loaded into RISC miRNAs bind to 3'UTR of target mRNAs to suppress gene expression either by promoting degradation of the mRNA or inhibiting translation. Image created in BioRender.com and exported under a paid subscription.

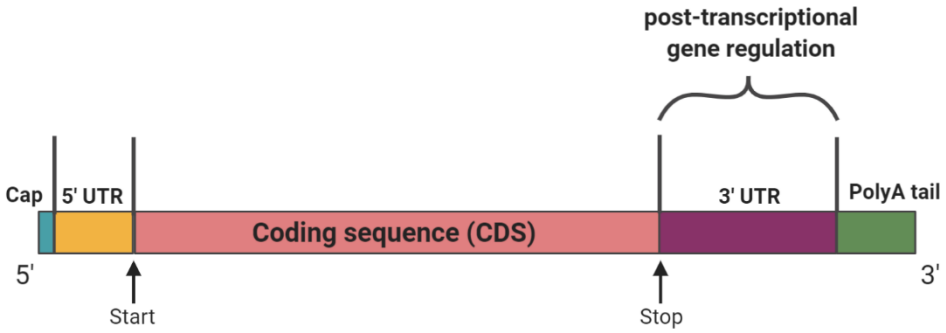


Figure 10: the structure of a typical human protein coding mRNA consists of a 5' methylated cap, followed by a 5' untranslated region (UTR), a coding sequence and 3' untranslated region (UTR), ultimately ending with a polyA tail at the 3'end. Image created with BioRender.com and exported under a paid subscription.

However, despite the biogenesis of miRNAs being under robust control, it can easily be seen how errors occurring at any point along this pathway can result in incorrect miRNA production or processing and, ultimately, abnormal miRNA expression, such as in DFUs (Figure 11). Such alterations [106] include:

- **Chromosomal abnormalities** can cause altered miRNA expression as miRNAs genes are often located in regions of the genome that are deleted. A study mapping 186 human miRNA genes found that more than half were located at fragile sites of the genome (chromosomal regions that are susceptible to gaps or breaks) or common breakpoint regions (locations on a chromosome where DNA might get deleted, inverted or swapped around) [107], illustrating how changes in chromosomal integrity can profoundly affect miRNA expression.

- **Defects in the miRNA biogenesis machinery**, such as Drosha or Dicer enzymes can lead to abnormal miRNA expression levels by impairing mature miRNA production. For example, one study found that Dicer was downregulated by more than two-fold in streptotozin-induced diabetic rats compared to nondiabetic rats in unwounded skin [108]. Furthermore, Dicer gene expression exhibited different patterns between diabetic and nondiabetic wounds following injury. In the nondiabetic rats, wounding was followed by a sharp decrease in Dicer expression at day 2, while in diabetic rats Dicer expression remained unchanged until day 7 in which a boost of Dicer expression occurred.

- **Epigenetic changes**, such as altered DNA methylation or histone modification can target the promoters of miRNA genes. In fact, genomic sequence studies revealed that approximately half of miRNA genes are associated with CpG islands, being potential targets for DNA methylation [109]. In the context of diabetic wound healing the miR-200b promoter, for instance was found to be hypo-methylated in human vascular endothelial cells when exposed to high glucose conditions mimicking diabetic hyperglycaemia, as well as in endothelial tissue from chronic diabetic wounds [110]. MiR-200b is a critical angiomiR whose downregulation is required to promote angiogenesis by driving endothelial cell migration and inducing expression of crucial

pro-angiogenic genes such as Ets-1, VEGFR2 and MMP-1 [111]. Hypomethylation resulted in increased levels of miR-200b leading to endothelial cell dysfunction *in vitro*, including impaired Matrigel tube formation, lower nitric oxide production and down-regulated VEGF expression, illustrating how abnormal epigenetic changes can impair angiogenesis and, in turn, wound healing.

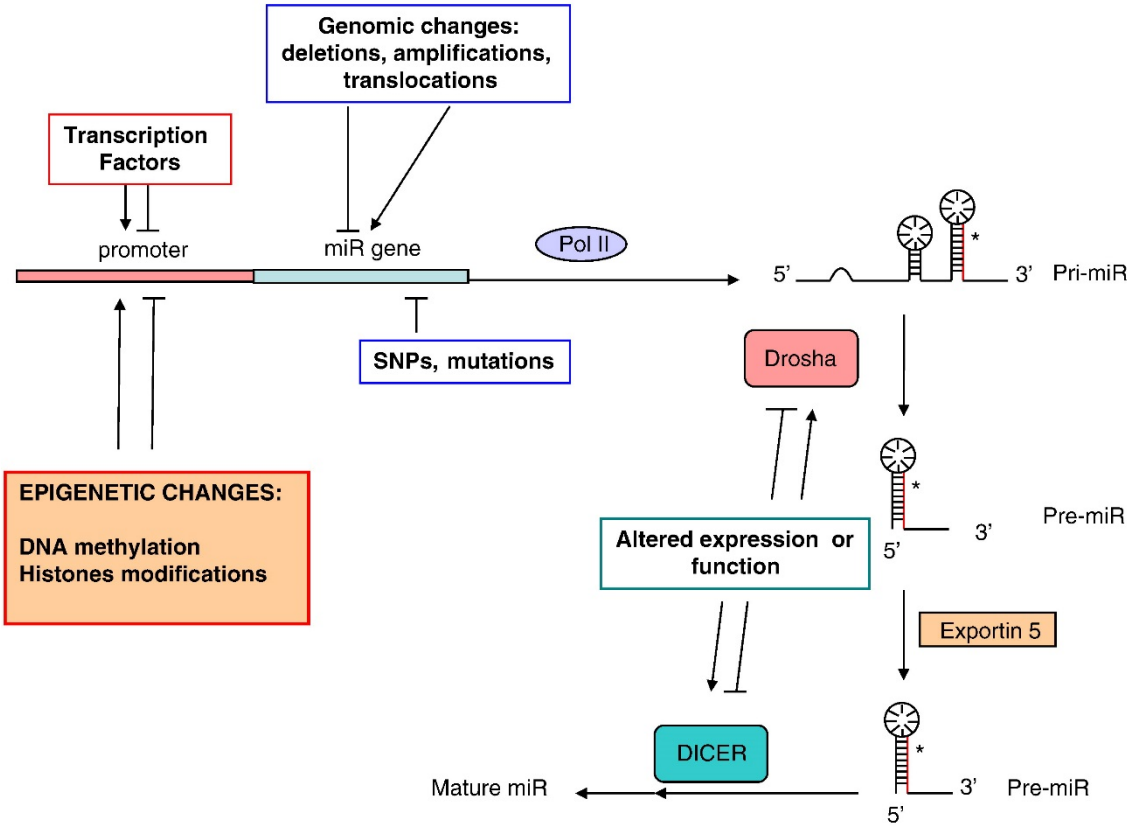


Figure 11: MiRNA dysregulation can occur because of a multitude of factors, including epigenetic or genomic changes, altered function of miRNA processing machinery or altered transcription factor activity. Image reproduced from [112] with permission from Elsevier

1.11. MicroRNAs fine-tune a myriad of target genes

MiRNAs recognise target mRNAs using a 7bp long 'seed' region (nucleotides 2-8) at their 5' end that perfectly matches the complementary 3'UTR of the mRNA strand with the rest of the miRNA exhibiting only partial complementarity to the mRNA (Figure 12). The 5' region of miRNAs, in particular seed positions 2-8, is crucial for target recognition and miRNA function, and is the most conserved region of metazoan miRNAs [113]. Experiments in Drosophila flies involving introducing single nucleotide changes at different positions along the miRNA-binding site confirmed that target repression was not affected by a mismatch at positions 1, 9 or 10, but any mismatch in positions 2-8 strongly reduced the magnitude of target downregulation [114].

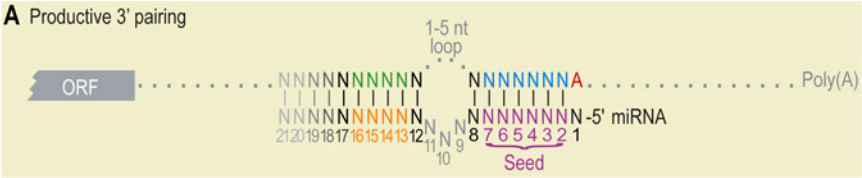


Figure 12: miRNAs recognise their target genes using a 7bp seed region at their 5'end that perfectly matches the 3'UTR sequence on the mRNA, while the rest of the miRNA displays only partial complementarity. Image reprinted from [115] with permission from Elsevier.

Although the seed region is crucial for target recognition, downstream nucleotides such as positions 13-16 can also contribute to base pairing with the target genes particularly when matching in the seed region is suboptimal [115]. Interestingly, despite 3'UTRs of mRNAs being very long compared to a miRNA (average length of a human mRNA 3'UTR is 1470 bp [116]) miRNA-binding sites were shown not to be randomly distributed throughout the 3'UTR. In fact, they were found to be preferentially located in close vicinity to the stop codon and the polyA sites, with the exception of the first ~15-20 bases of the 3'UTR [115,117] (Figure 13B). The short stretch of ~15-20 nucleotides void of miRNA target sites at the beginning of the 3'UTR was shown to be necessary to ensure the RISC silencing complex does not get too close to the ribosomes, which otherwise would strip it off the mRNA preventing re-association until the ribosome detached from the target mRNA.

This preferential residing near both ends of the 3'UTR was shown to be necessary for effective repression as miRNA binding sites residing in the quartiles near the ORF or polyA tail were found to be more functional than those residing in the two central quartiles of the 3'UTR,

particularly for longer 3'UTRs (Figure 13A) [115]. Avoiding the centre of 3'UTRs could be explained by the fact that the interior of 3'UTRs is prone to fold into secondary structures and hence might not be accessible to the RISC complex, than at the beginning and end where it assumes a more open structure. When looking at miRNA target positioning it was shown that miRNA seeds were preferentially positioned in highly accessible regions that have open structures and are thus more accessible to RISC binding [118]. This was found to be the case in human, mouse, fly and worm, suggesting that preferential positioning of miRNA target sites in regions of high accessibility is a conserved feature in genomes.

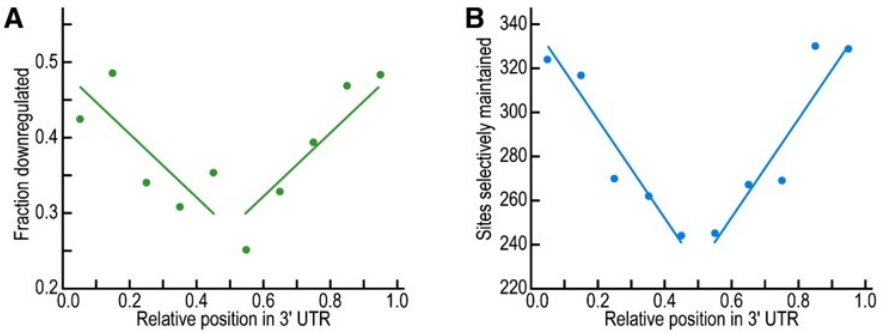


Figure 13: miRNA binding sites are preferentially located near the ends of the 3'UTR (B) for a more effective repression (A). Image reproduced from [115] with permission from Elsevier

Due to incomplete complementarity between the miRNA and the target mRNA, a single miRNA can target many different genes - as opposed to siRNAs that have one specific target (with very few off-target effects) – and the same gene can be targeted by many different miRNAs [d]. A microarray study looking at mRNA expression profiles showed that over-expressing miR-124 or miR-1 into HeLa cells caused mostly mild (less than two fold) downregulation of hundreds of mRNAs, of which many were direct targets [119]. Similar effects were observed when measuring the impact of individual miRNA on protein output using SILAC-based proteomic experiments: exogenous miR-1 or miR-155 expression in HeLa cells caused hundreds of direct target genes to be translationally repressed in a modest manner

[d] Interestingly, genome-level studies have found that genes have evolved to 'control' their 3'UTR length to allow for fewer or more miRNA binding sites and thus how many miRNAs they are targeted by. For instance, functional genes that are spatially or temporally expressed were shown to have a longer 3'UTR to include more distinct miRNA-bindings sites and allow stringent regulation by miRNAs. Housekeeping genes, on the other hand whose expression is constitutively maintained across tissues, tended to have fewer regulatory miRNAs and have evolved to have shorter 3'UTRs to avoid miRNA regulation [225].

with the fold change of repression rarely exceeding fourfold [120]. Analogous findings were obtained for the endogenous miR-223 in mouse neutrophils [121].

Coupling the proteomic data with microarray data further revealed that most targets are repressed at both the mRNA and the translational level, with the fold changes of mRNA and proteins for the same gene showing a strong positive correlation, predominantly for targets with stronger complementarity to the seed region of the miRNA (Figure 14). This result, in turn, posed the question on the sequence of events that occurs during miRNA-mediated silencing, namely does mRNA decay or translational repression come first? Given that translational repression and mRNA destabilisation are sometimes coupled, i.e. translational repression triggering mRNA destabilisation [122], for a long time it was believed that translational depression was the cause of miRNA-mediated gene silencing. This observation was supported by studies in Drosophila flies and zebrafish on the effects of miRNAs which concluded that mRNA degradation is triggered as a secondary consequence [123]. However, these results were contradicted by studies done in mammalian cells. Here, ribosome profiling in HeLa cells and mouse neutrophils measuring the overall effects on protein production following miRNA over-expression confirmed that lowered mRNA levels accounted for most (>84%) of the decreased protein production with only a small minority of genes being translationally repressed with little or no change at the mRNA level [124].

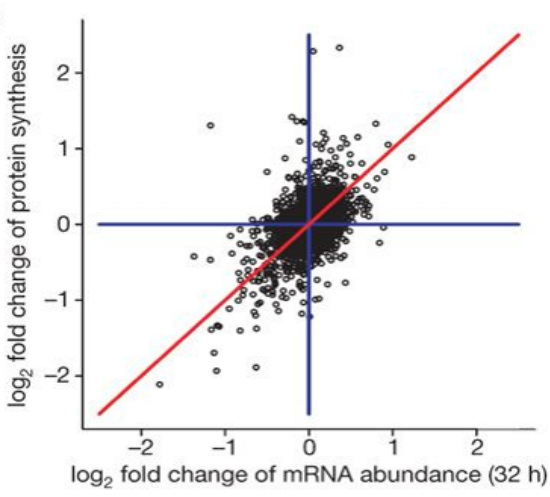


Figure 14: miRNAs are fine-tuners of gene expression, repressing hundreds of targets at the mRNA and protein level in a mild manner that rarely exceed a fourfold change. Image reproduced with permission from [120]. Copyright 2008, Springer Nature

Furthermore, despite miRNAs having hundreds of targets, global analyses of the effects of different cellular contexts on miRNA targeting found that most miRNA-target interactions are unaffected by cell type [125]. mRNA-seq analysis following transfection of miR-124 or miR-155 into three different cell lines (HeLa, HEK293 and Huh7) showed that, although the repression of some targets differed between the cell lines, miRNA-mediated repression remained remarkably consistent for the majority of targets in the different cell types (Figure 15). Interestingly, some of the observed differential repression - 10% of the target repertoire when comparing any two cell types - was found to be due to alternative 3′ UTR isoforms generated through alternative cleavage and polyadenylation (APA). APA changed the length of the 3′ UTR, shortening or lengthening it, in turn influencing the inclusion and placement of miRNA-binding sites within more or less favourable contexts and ultimately repression efficacy.

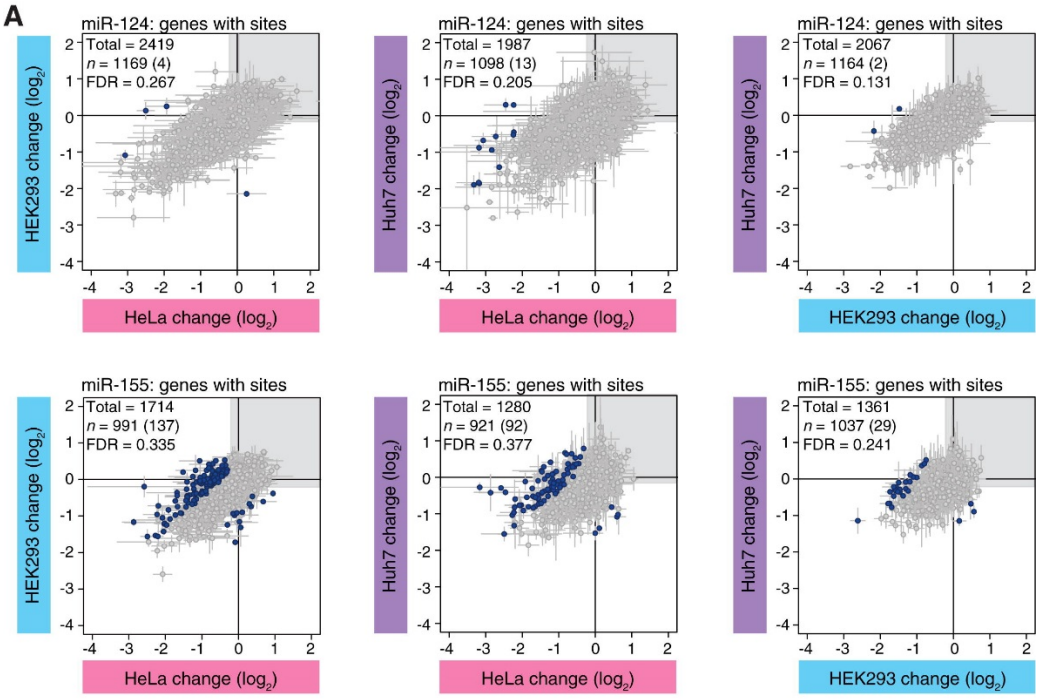


Figure 15: the repertoire of target genes of miRNAs is mostly unaffected by cell type. Following transfection of miR-124 or miR-155 into three different cell types the majority of targets remain the same across the different cell types, with few targets displaying differential repression. Image reproduced from [125] with permission from Elsevier

Collectively, these findings suggested that a) mammalian miRNAs act predominantly at the mRNA level to inhibit gene expression by destabilising the target mRNAs, b) mRNA targets are mostly unaffected by cell type and c) for most interactions miRNAs act as rheostats making small-scale adjustments to fine-tune protein output. This fine-tuning effect miRNAs since led

to these small key players being described as the 'micromanagers' of gene expression with each miRNA binding site on the 3' UTR acting as an adjustable resistor or a rheostat [126]. This comparison seems appropriate because miRNAs act to decrease gene expression, similar to a resistor that is placed in a circuit causes the current to decrease, but does not eliminate its flow.

1.12. MicroRNAs exert different degrees of repression on targets

To control the degree of complementarity – and thus the amount of repression exerted by miRNAs - target mRNAs have evolved over time to follow certain patterns of miRNA seed-matched sites on their 3'UTR, some of which became conserved across species. So far, four main types of seed-matched sites on the 3' UTR of mRNAs have been found to be selectively conserved across species [127]: the *6mer site* that perfectly matches the 6-nt miRNA seed; the *7mer-A1 site* that comprises the seed match supplemented by an A across from miRNA nucleotide 1; the *7mer-m8* site which comprises the seed match supplemented by a Watson-Crick match to miRNA nucleotide 8; *8mer site* which comprises the seed match supplemented by both m8 and A1 (Figure 16).



Figure 16: 3'UTR of mRNAs contain four main types of canonical seed-matches sites (8mer, 7mer-m8, 7mer-A1 and 6mer) that match the 5' end of a miRNA. Image created in BioRender.com and exported under a paid subscription.

Depending on which type of site is found on the 3'UTR the strength of repression differs with the following hierarchy of efficacy being observed for single canonical sites: 8mer > 7mer-m8 > 7mer-A1 -> 6mer, both at the mRNA and protein level with this differential efficacy of 8mer, 7mer and 6mer sites perhaps attributable to differences in binding affinity (Figure 17) [115,121]. Furthermore, conserved seeds were found to confer more target repression than nonconserved seeds both at the mRNA and protein level [120], perhaps explaining why more

than 60% of protein-coding genes have been found that contain at least one conserved miRNA-binding site [127].

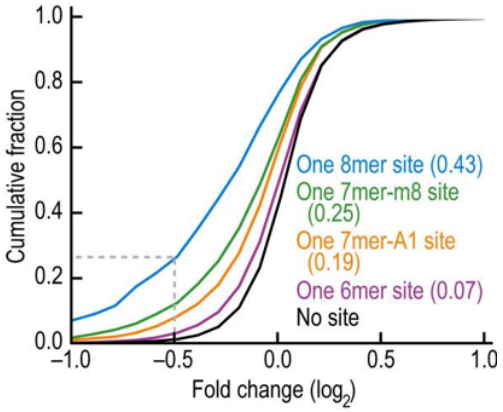


Figure 17: efficacy of repression varies for target genes depending on the type of seed-matched sites they contain, namely 43%, 25%, 19% and 7% repression for 8mer, 7mer-m8, 7mer-A1 and 6mer sites, respectively. Image reproduced from [115] with permission from Elsevier

To ensure effective repression often targets will have multiple (conserved) miRNA-binding sites for the same or different miRNA(s) along their 3'UTR. Having multiple seed sites, as opposed to single ones, is advantageous for two reasons: first, they can allow for stronger repression. For example, experiments in HeLa cells showed that as the seed match count for exogenous miR-1 or miR-124 increased from one to three, the logarithm of the mRNA fold change increased approximately linear for both miRNAs [128], indicating that each seed match contributes multiplicatively to fold change in mRNA level. A similar result was obtained when considering all genes following single transfections of 11 miRNAs into HeLa cells: the repression observed for those genes with two sites, such as two 7-mer sites was almost exactly that expected if the two sites had contributed independently to repression, i.e. a multiplicative effect of repression from the two single sites, a hallmark of independent and non-cooperative behaviour [115] (Figure 18).

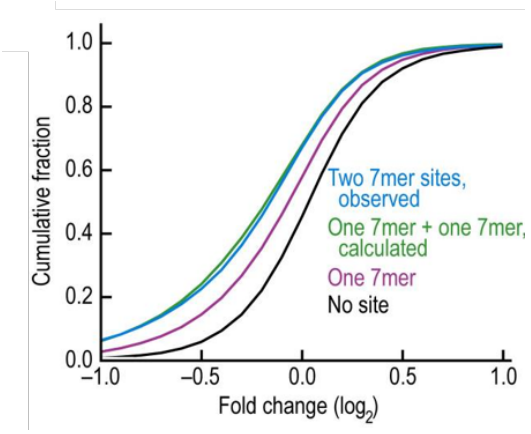


Figure 18: multiple seed matched sites contribute multiplicatively to repression, typical of independent and non-cooperative behaviour. For instance, the observed repression from two 7mer sites is higher than the one observed from a single 7mer site. Image reproduced from [115] with permission from Elsevier

Second, having multiple sites for different miRNAs can furthermore allow redundancy amongst the miRNAs, such that if certain miRNAs become dysregulated other ones are still available to 'take over'. The importance of this phenomenon is perhaps best illustrated by the p21 Cip1/Waf1 protein, a master downstream effector of tumour suppressors, which was found to be directly targeted by 28 different miRNAs in HEK 293 cells, illustrating the necessity of such robust control of this gene's expression levels [129]. In addition to the multiplicative (i.e. non-cooperative) effect of multiple sites in the same target, the level of repression was found to be higher than that expected from independent contributions of the sites when the sites are closer together. This points to a cooperative or synergistic behaviour of miRNAs dependent on the site spacing. Repression was found to be strongest when spacing between two sites that are close together was 8 to ~40nt, pointing to a 'golden range' required for cooperative action [115].

In another study a similar range of seed spacing (13-35nt) was determined to be optimal/necessary for cooperative down-regulation by different miRNAs [130]. Here miR-106b, miR-93, and miR-25 - three miRNAs that are processed from a single intron of the MCM7 gene on chromosome seven (aka mir-106b-25 cluster), were used to determine cooperativity in downregulating the common target BMPR2 (Figure 19). Despite containing seed target sites for all three miRNAs, no detectable knockdown of a luciferase reporter assay containing1.2kb of 3'UTR of the BMPR2 gene was observed following transfection into HEK293 cells. However, when the three sites were moved closer together (BMPR2-Super), a 30% down-

regulation was observed versus the non-specific controls. These results once again confirm how important the spacing between binding sites is for a collaborative effect between multiple miRNAs.

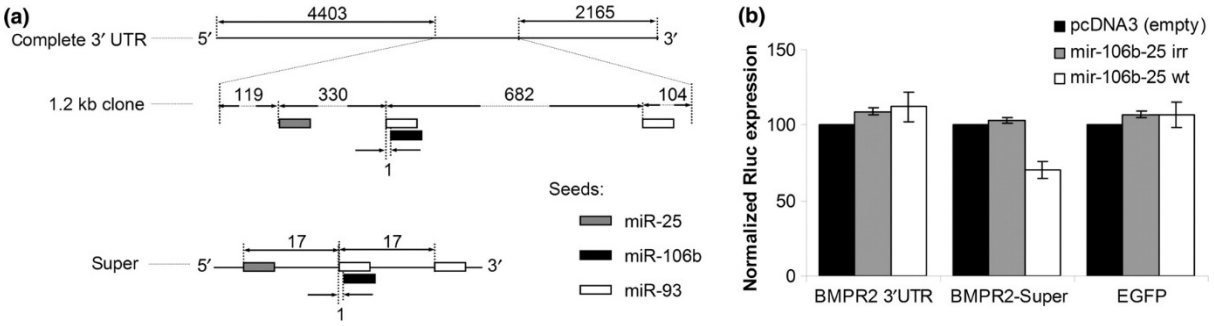


Figure 19: distance contraints between miRNA-binding sites for different miRNAs dictate whether miRNAs exhibit cooperative behaviour or not. MiRs-106b, -93 and -25 suppress the target gene BMPR2 only when the distance between the three seed sites is reduced to ~35nt within each other (BMPR2-Super). Image reproduced from [130] with permission from Oxford University Press

1.13. MicroRNAs cooperate at the pathway level

In addition to cooperation at the gene level miRNAs can also cooperate at the pathway level by targeting many different genes that belong to the same pathway or are involved in regulating the same biological process. For example, in human white adipose tissue a network of miRs-92a, -193b and -126 were shown to regulate production of the pro-inflammatory CCL2 (chemokine ligand 2) in a combinatorial manner [131]. Similarly, another study identified four miRNAs that were up-regulated during monocyte differentiation (miRs-155, -222, -424 and -503) and showed that their simultaneous over-expression triggered specific pro-differentiative changes not stimulated by the over-expression of the individual miRNAs, illustrating how network behaviour can cause different effects to those of an individual miRNA [132]. Furthermore, miRs-126, -21 and -26a were found to jointly regulate the PI3K/AKT and RAF/MAPK signalling pathways [133] (Figure 20), further demonstrating how miRNAs use cooperation to ensure context-dependent cell signalling to drive a specific cellular process.

Cooperation amongst miRNAs, be it at the gene or pathway level or both, is in fact crucial to allow efficient control of dynamic biological systems. A large-scale study looking at synergism

between human miRNAs showed that synergistic miRNAs formed a network that wasn't random, but displayed scale-free, modular and small-world properties, having a similar topology to that of protein-protein networks [134]. Such a network topology is of great advantage as it gives the network robustness causing disturbances to spread slowly through the network, allowing synergistic miRNAs to respond quickly to disturbances. Such a network arrangement also explains why most synergistic miRNA pairs (~80%) also have the same expression tendency in tissues, which not only permits for a rapid response to disturbances but also ensures that miRNAs can promptly implement regulation under specific conditions to quickly adapt to an environmental cue or change. These findings elegantly illustrate how, despite being a myriad of different miRNAs in a cell, they follow well-defined patterns and topologies at a system-wide level to coordinate gene expression at the post-transcriptional level.

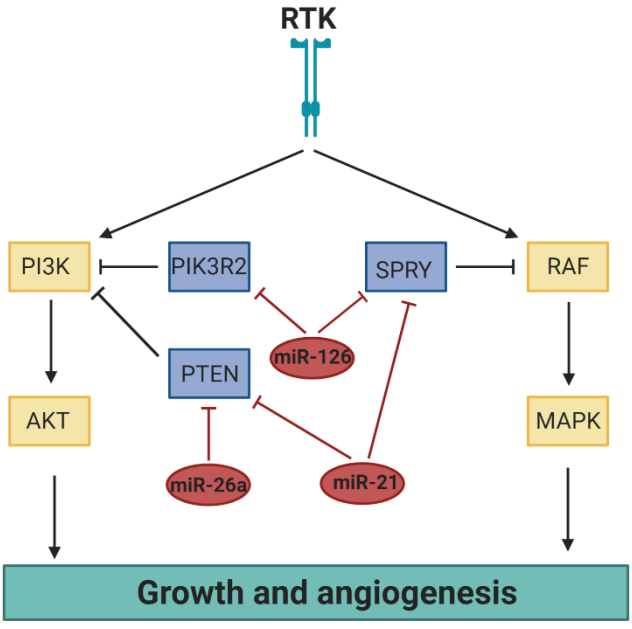


Figure 20: miRs-126, -26a and -21 jointly regulate signalling downstream of the Receptor Tyrosine Kinases (RTK), such as PI3K/AKT and RAF/MAPK signalling pathways. By targeting inhibitors of this pathway the miRNAs act as signal amplifiers, leading to a general upregulation of RTK signalling, in turn driving growth and angiogenesis. Image modified with permission from [133]. Copyright 2010 Springer Nature. Image created in BioRender.com and exported under a paid subscription.

1.14. MicroRNA exhibit target selectivity

Understanding how miRNAs work at the network level, rather than individually is essential because individual miRNA regulation was shown to be selective, with miRNAs effectively 'choosing' which targets to downregulate. For instance, a pull-down assay after miR-34a over-expression in HCT116 or K562 cancer cells lines, showed that not all direct targets (shown in red) were also down-regulated (shown in blue) despite the miRNA binding to them (i.e. pulled down) [135] (Figure 21). In this study, to isolate candidate targets, the authors biotinylated miR-34a at the 3'end of the mature strand (Bi-miR-34a) before transfection into the cells and pulled it down in an Ago-immunoprecipitation assay 24h later. Looking at which mRNA targets were present in the pulled-down Ago proteins, the authors could identify direct targets of miR-34a and further showed these to be enriched in growth factor signalling, cell-cycle progression and DNA repair mechanisms, supporting the role of this miRNA as a tumour suppressor.

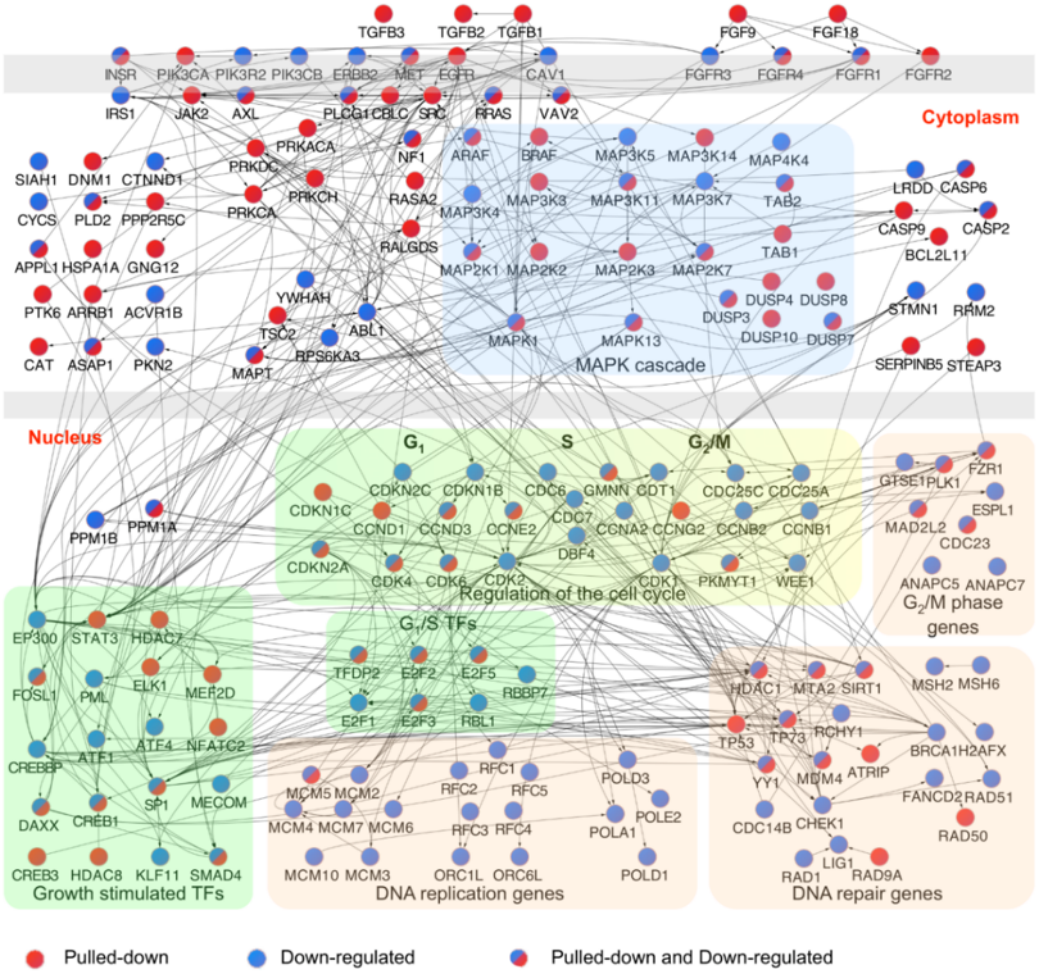


Figure 21: a pull-down assay after miR-34a over-expression shows that not all direct targets (red) are also down-regulated (blue), despite miR-34a binding to the target genes. This points towards target selectivity by miRNAs. Image reproduced from [136] under a Creative Commons License

One of the reasons for this target selectivity could be because miRNAs were shown to introduce thresholds in gene expression acting as switches or fine-tuners depending on the concentration of mRNAs [137] (Figure 22). In this study a two-colour fluorescent reporter system was constructed to monitor protein levels in the presence and absence of regulation by the endogenous miR-20 in HeLa cells. To investigate the miRNA-mediated gene repression the number of miR-20 binding sites or the concentration of miR-20 was varied and the results were correlated with a mathematical model.

In the absence of miRNAs, the mRNA decay rate would be constant causing the mRNA level to increase linearly with the transcription rate. In the presence of miRNAs, however the mRNAs respond in a 'threshold-linear' manner: when the mRNA concentration is low, the few mRNAs that are produced are bound by the existing miRNAs and immediately degraded causing protein production to be highly repressed. As the target mRNAs start to accumulate they gradually titrate away the pool of miRNAs available for repression. At this point protein expression responds sensitively to the mRNA input. Eventually the transcription rate becomes sufficiently high to saturate the miRNA-Ago complexes and reaches a threshold level, where mRNAs can escape the miRNA-induced repression and start accumulating at a rate proportional to their transcription rate.

In this model the threshold can be shifted by changing the affinity of the miRNA-target interaction, k (i.e. via increasing the number of miRNA-binding sites on the 3' UTR) or the relative abundance of miRNAs to their targets (i.e. by increasing the concentration of miRNA via mimics or decreasing it via sponges). As such, these results show that for some miRNA-target interactions miRNA can act both as switches, below the threshold where protein repression is maximal, and fine-tuners, near the threshold where protein expression responds sensitively to the target mRNA input, thus repressing their targets in a non-linear manner.

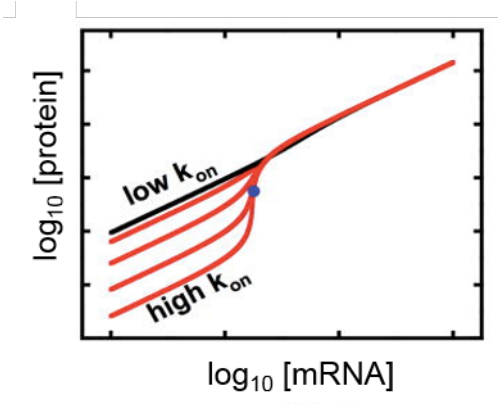


Figure 22: miRNAs repress target genes in a non-linear manner and can act as switches or fine-tuners depending on the mRNA concentration. At low mRNA concentrations miRNAs can immediately degrade the target gene leading to low protein levels. At increasing mRNA concentrations the target mRNAs start to accumulate and gradually titrate away the pool of miRNAs, eventually escaping miRNA repression. Image modified with permission from [138]. Copyright 2011, Springer Nature

1.15. Aims of project

Due to this nonlinear and selective behaviour of miRNAs it can be seen that trying to predict the effects of a single miRNA can be complex. This can become particularly intricate when other (cooperating) miRNAs come into play that display non-linear target repression and target selectivity at their end, because now different combinations of miRNAs can start to shift target thresholds switching on or off different sets of genes, in turn activating different cell signalling pathways. Ultimately, this can lead to a completely different or unexpected behaviour to that of the individual miRNA. Particularly, when miRNAs become dysregulated in diseases, such as DFUs, basing a therapy on an individual miRNA is not enough as the presence of other dysregulated cooperating miRNAs could cause different effects, which means we need to understand the effects of miRNAs at the network level.

As such the aim of this project was to explore miRNA dysregulation in DFU fibroblasts by analysing:

Aim 1: Which miRNAs are dysregulated in DFU fibroblasts vs healthy normal fibroblasts

Aim 2: Explore the biological impact of these dysregulated miRNAs and identify potentially synergistic miRNAs using bioinformatics

Aim 3: Deliver miRNA mimics or inhibitors into healthy fibroblasts *in vitro* to mimic the phenotype observed in the DFU cells and experimentally verify their effect on cellular processes

Aim 4: Deliver the opposite miRNA entities into DFU fibroblasts to restore normal levels of these miRNAs as an attempt to develop a miRNA-based therapy for DFU healing

2. Investigating microRNA dysregulation in diabetic foot ulcer fibroblasts

2.1. Bioinformatics analysis to determine differentially expressed miRNAs in DFU fibroblasts vs nondiabetic healthy fibroblasts

First I needed to understand which miRNAs were differentially expressed (DE) in DFU fibroblasts vs healthy normal fibroblasts. To obtain miRNA expression profiles from DFU fibroblasts and healthy nondiabetic foot fibroblasts I used the publically available GEO dataseries GSE84971 from the paper *'Integrative analysis of miRNA and mRNA paired expression profiling of primary fibroblast derived from diabetic foot ulcers reveals multiple impaired cellular functions'* by Liang L, Stone RC, Stojadinovic O. *Wound Rep Reg.* **24**, 943–953 (2016) [139]. In this paper the authors isolated fibroblasts from tissue samples obtained from the wound edge of diabetic patients with a nonhealing DFU (DFUF, n=4) or healthy, nondiabetic foot skin (NDFF, n=4) and generated miRNA and mRNA gene expression profiles to identify DE miRNAs and mRNAs, respectively (Figure 23). To analyse miRNA expression profiles RNA was extracted from the cultured cell lines and run on the **NanoString nCounter** microRNA expression assay v2 panel[e] containing 800 mature miRNA probes, which yielded 21 differentially expressed miRNAs with $p<0.05$ and with a fold change ≥2. Amongst these, 11 miRNAs were up-regulated and 10 miRNAs were down-regulated in DFUF (Figure 24A). Prior to publishing this paper the same authors showed that diabetic and non-diabetic foot skin displayed only subtle differences at the miRNA and mRNA level [140], which meant that the DE miRNAs identified between DFUF and NDFF in this study were due to ulceration and not caused by the underlying diabetes.

To identify DE mRNAs the authors used Illumina HumanHT-12 v4 Expression BeadChip array containing 47,000 probes and paired the DE mRNA genes with the identified DE

[e] The NanoString nCounter technology uses target-specific colour-coded barcodes that can hybridise directly to target molecules and measures the expression level of a target molecule by counting the number of times the barcode for that molecule is detected. Because of the direct measurement of molecule expression level, this system does not require amplification and is able to simultaneously quantify up to 800 different targets, being sensitive enough to detect low abundance molecules.

miRNAs to create miRNA-mRNA pairs that were disrupted in DFUF. For this, a subset of DE mRNAs were chosen that were predicted as targets of the DE miRNAs and showed an expression in the opposite direction of their targeting miRNAs (miRNA up/mRNA down or miRNA down/mRNA up). Using the criteria p<0.05 and fold change>1.5 for the DE mRNAs, the authors identified 239 DE target genes and 331 reciprocal miRNA-mRNA pairs in DFUF vs NDFF. This allowed to extract functional pathways that were mainly regulated and affected by the disrupted miRNAs in DFUFs. Using bioinformatics analysis the DE pairs were later found to be enriched in several specific cellular functions, including cell proliferation, cell migration, cell differentiation and senescence (Figure 24B), which were later experimentally validated to be indeed disrupted in DFUF.

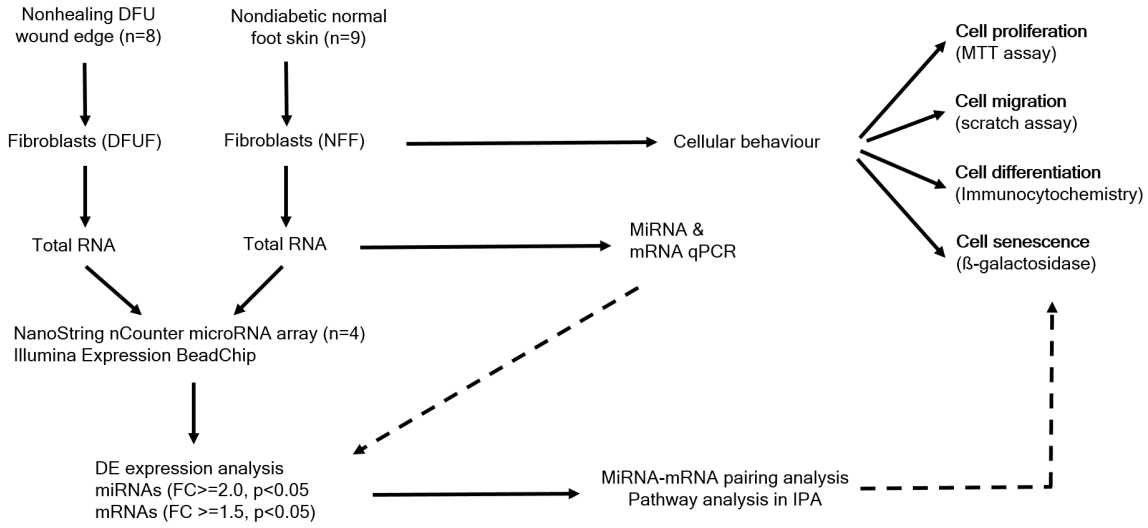


Figure 23: the authors identify DE miRNAs and mRNAs between DFU-derived fibroblasts (DFUF) and nondiabetic foot fibroblasts (NDFF) and link them to cellular functions known to be disrupted in DFUs, such as proliferation, migration and differentiation.

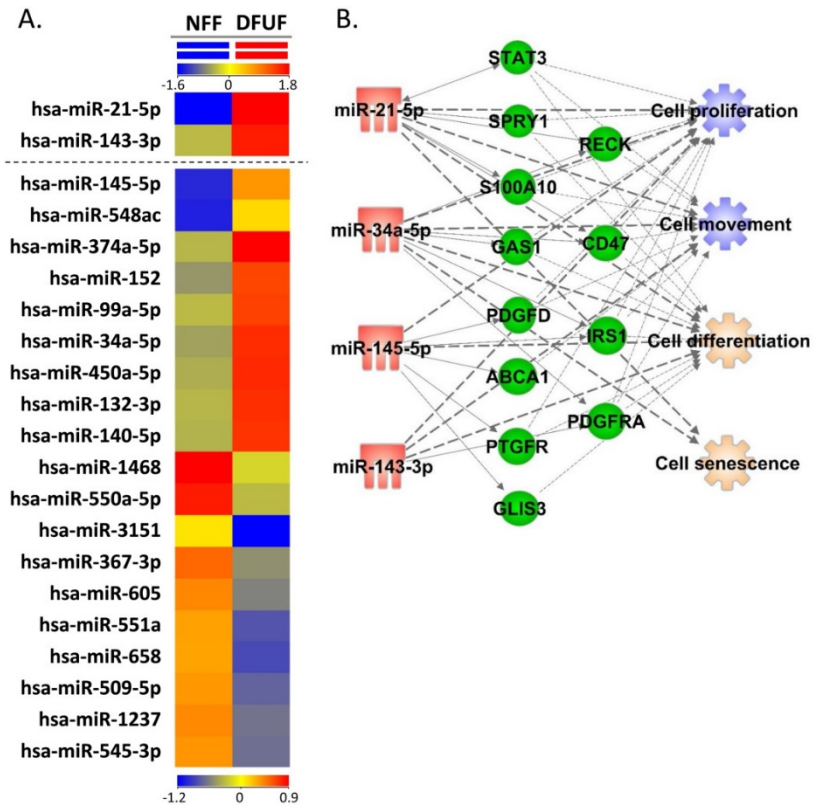


Figure 24: the authors identify 21 DE miRNAs DFUF and NDFF (A) and pair four of these to dysregulated target genes from the same cells to generate miRNA-mRNA networks implicated in disrupting normal cellular processes including cell proliferation, movement or cell differentiation (B). Image taken from [141] and reproduced with permission of the rights holder, John Wiley and Sons

This paper represented the first paper to link DE miRNAs with DE mRNAs in DFU-derived fibroblasts and relate them to impaired processes in wound healing. However, to identify statistically significant DE miRNAs between DFUF and NDFF the authors used student t-test as part of their statistical analysis. Although very common and popular with current methods for DE detection in nCounter data - such as NanoStringNorm and NanoStriDE - t-tests work best when the data being analysed follows a continuous, preferably normal distribution. However, the NanoString nCounter system generates discrete counts that cannot be described by t-tests, but instead should be characterised by a discrete distribution, thus making the method used in this paper not the most appropriate for analysing DE miRNAs. As such I performed my own bioinformatics analysis on the miRNA expression profiles generated in this paper to obtain my own list of DE miRNAs. In turn, this meant I had to find an alternative analysis method that best suited the nature of the data generated by the NanoString nCounter platform in order to identify DE miRNAs.

In the past many different types of tools have been suggested could be applied to analyse nCounter data [142]. One such tool proposed was DESeq, a tool originally developed for analysing count data from RNA-seq because this method uses a negative binomial model for data characterisation. However, nCounter data and RNA-Seq data are different, especially in data normalisation and as such are not compatible to be subjected to the same method of DE analysis. This is because commonly, data normalisation procedures include dividing the raw data by size factors and subtracting the background level. DESeq, however no longer treats the data as discrete making it unsuitable to be analysed as counts. As such, alternative approaches were developed for RNA-Seq data analysis, such as edgeR that treated the size factor as a scaling parameter in the negative binomial model for data normalisation. However, these did not adjust for background noise, nor did they utilise positive controls or housekeeping genes – controls needed by the nCounter platform for the normalisation procedure [f] - thus still being unsuitable to analyse nCounter data.

In 2016 the paper '*NanoStringDiff: a novel statistical method for differential expression analysis based on NanoString nCounter data*' was published by Wang H et. al [142] which described a DE detection method, known as NanoStringDiff specifically designed for nCounter data. This method fully takes into account the discrete nature of the data and utilises all three types of controls that are critical for complete data normalisation. NanoStringDiff utilises a generalised linear model of the negative binomial family to characterise the count data and calculates the size factors needed for normalisation from positive controls, housekeeping genes and negative controls. It uses the likelihood ratio test for DE detection by comparing the maximum of the log of the likelihood under the null hypothesis versus that without any constraint. The chi-square approximation is then used to obtain a P-value, while the Benjamini and Hochberg correction procedure is used to calculate the false discovery rate. Simulations and real data analysis showed that the NanoStringDiff method performed better than any other existing methods in DE detection. For instance, one of the four real nCounter datasets used by the authors to evaluate the performance of NanoStringDiff was the Horbinski data.

[f] The nCounter platform uses three types of controls to normalise the data - positive controls, housekeeping genes and negative controls – which account for lane-to-lane variation, differences in the input sample and non-specific background, respectively.

Horbinski et al. studied human glioma cell lines expressing GFP or GFP with mutated IDH1 - an enzyme involved in regulating cell metabolism, redox states and DNA repair that is frequently mutated in cancers. In this dataset the cells were grown in vitro for 6 days, followed by miRNA profiling. Wang et al. used NanoStringDiff to determine the DE miRNAs in this dataset and compared the results of NanoStringDiff to those obtained by NanoStringNorm, DESeq2, edgeR and NanoStriDE. Choosing 0.01 as the FDR threshold, NanoStringDiff identified 14 DE miRNAs (13 down-regulated and 1 up-regulated). In contrast, DESeq2 identified only 2 DE miRNAs, while both edgeR and NanoStriDE identified only 1 DE miRNA, while NanoStringNorm did not identify any DE miRNAs. The top 5 DE miRNAs from the list - as identified by NanoStringDiff - were further validated via qPCR as down-regulated, while 4 non-DE miRNAs according to NanoStringDiff were validated by qPCR to be indeed non-differentially expressed. Interestingly, these top 5 DE miRNAs were not at all in the top five list for any of the other methods. These findings showed that NanoStringDiff outperforms DE analysis when compared to other existing methods and is most suitable for differential analysis of NanoString nCounter data. As such I decided to use this method to find DE miRNAs between DFUF and NDFF from the miRNA expression profiles generated in the DFU paper.

To analyse the DE miRNAs from this paper the open source R package NanoStringDiff (available at Bioconductor on https://bioconductor.org/packages/devel/bioc/vignettes/NanoStringDiff/inst/doc/NanoStringDiff.pdf) was downloaded and the vignette containing the code for the analysis was followed (supplementary data 2.5.1). Since data normalisation is incorporated in the model framework by including data normalisation parameters estimated from positive controls, negative controls and housekeeping genes, the raw counts of NanoString nCounter data (available from the GEO dataseries GSE84971 under the supplementary file "GSE84971_non-normalized.txt.gz") were put into the package. The count data was then written in the format as specified in the vignette: each row corresponded to one miRNA gene being profiled starting with positive controls, negative controls and housekeeping genes followed by the endogenous genes; each column corresponded to a different sample (patient) being analysed for each category, namely n=3 control samples corresponding to NDFF and n=3 treatment samples corresponding to DFUF (Table 1).

Code Class	Name	Accession	Control 1	Control 2	Control 3	Treatment 1	Treatment 2	Treatment 3
Positive	POS_A(128)	nmiR00813.1	51117	30283	46143	48365	52744	70189
Positive	POS_B(32)	nmiR00809.1	9153	6423	8040	9338	10177	12069
Positive	POS_C(8)	nmiR00811.1	2357	1178	2014	2158	2391	3186
Positive	POS_D(2)	nmiR00822.1	749	444	554	603	786	693
Positive	POS_E(0.5)	nmiR00801.1	133	83	114	135	143	176
Positive	POS_F(0.125)	nmiR00825.1	88	35	82	91	72	110
Negative	NEG_B(0)	nmiR00828.1	52	28	31	61	56	55
Negative	NEG_C(0)	nmiR00803.1	32	25	32	44	42	54
Negative	NEG_A(0)	nmiR00810.1	40	29	29	32	44	36
Negative	NEG_F(0)	nmiR00805.1	14	11	13	5	15	12
Negative	NEG_E(0)	nmiR00827.1	104	74	80	103	135	108
Negative	NEG_D(0)	nmiR00823.1	74	45	60	74	62	61
Housekeeping	Actb|0	NM_001101.2	825	1254	2123	1392	1378	2098
Housekeeping	B2m|0	NM_004048.2	1892	1081	3912	1750	1446	8006
Housekeeping	Gapdh|0	NM_002046.3	1293	1121	1876	1626	1300	2989
Housekeeping	Rpl19|0	NM_000981.3	1496	914	2217	1196	1077	4447
Housekeeping	Rplp0|0	NM_001002.3	2157	1223	3363	1917	1875	4930
Endogenous 1	hsa-let-7a-5p|0	MIMAT0000062	7910	5700	10010	14844	14284	16620
Endogenous 1	hsa-let-7b-5p|0	MIMAT0000063	6231	3903	10943	11372	10414	15491
Endogenous 1	hsa-let-7c|0	MIMAT0000064	201	126	221	249	352	410
Endogenous 1	hsa-let-7d-5p|0	MIMAT0000065	293	155	286	430	550	631
Endogenous 1	hsa-let-7e-5p|0	MIMAT0000066	646	307	633	976	972	1225
Endogenous 1	hsa-let-7f-5p|0	MIMAT0000067	194	161	210	320	354	372
Endogenous 1	hsa-let-7g-5p|0	MIMAT0000414	1660	784	2260	2447	2047	6120
Endogenous 1	hsa-let-7i-5p|0	MIMAT0000415	842	496	972	1450	1915	2190

Table 1: the raw miRNA counts from the dataset from the paper are written in the format specified in the NanoStringDiff vignette and served as input data into the NanoStringDiff R code. Each row corresponds to one miRNA gene being profiled starting with positive controls, negative controls and housekeeping genes followed by the endogenous genes; each column corresponds to a different sample (patient) being analysed for each category; namely n=3 control samples corresponding to NDFF and n=3 treatment samples corresponding to DFUF

This analysis yielded 39 DE miRNAs between DFUF and NDFF with a fold change ≥ 2 and p-value <0.05, amongst which 38 miRNAs were up-regulated and 1 was down-regulated in DFUF compared to NDFF (Table 2).

	logFC	lr	pvalue	qvalue
hsa-let-7i-5p|0	1.025997	4.143597	0.041792	0.512436
hsa-miR-10a-5p|0	1.446321	4.887485	0.027052	0.512436
hsa-miR-1234|0	23.81502	7.79906	0.005227	0.199137
hsa-miR-132-3p|0	1.563076	8.125788	0.004364	0.183747
hsa-miR-136-5p|0	4.340956	15.93964	6.54E-05	0.016284
hsa-miR-140-5p|0	1.481939	6.551819	0.010478	0.335286
hsa-miR-143-3p|0	5.76502	63.83106	1.33E-15	1.07E-12
hsa-miR-145-5p|0	1.523393	8.683076	0.003212	0.15009
hsa-miR-152|0	1.896889	9.370522	0.002205	0.117601
hsa-miR-181a-5p|0	1.440317	7.145477	0.007515	0.250511
hsa-miR-181b-5p+hsa-miR-181d|0	4.151863	4.92473	0.026475	0.512436
hsa-miR-185-5p|0	1.226124	4.154202	0.041531	0.512436
hsa-miR-26b-5p	1.801273	8.591685	0.003377	0.15009
hsa-miR-27a-3p	27.82088	11.48528	0.000701	0.062355
hsa-miR-301a-3p	1.821593	4.304566	0.03801	0.512436
hsa-miR-30a-5p	24.59008	11.51395	0.000691	0.062355
hsa-miR-320e	24.05876	7.36336	0.006657	0.242059
hsa-miR-337-5p	1.220609	4.962779	0.025899	0.512436
hsa-miR-342-3p	2.707672	10.05417	0.00152	0.101336
hsa-miR-34a-5p	1.190555	5.149695	0.02325	0.512436
hsa-miR-34c-5p	25.22607	15.22608	9.54E-05	0.016284
hsa-miR-365a-3p	1.163187	3.858084	0.049507	0.512436
hsa-miR-374a-5p	1.158716	4.888097	0.027042	0.512436
hsa-miR-409-5p	25.50844	9.476536	0.002081	0.117601
hsa-miR-424-5p	30.67986	38.00293	7.06E-10	2.83E-07
hsa-miR-431-5p	2.475173	7.805178	0.00521	0.199137
hsa-miR-432-5p	1.311975	4.007703	0.045293	0.512436
hsa-miR-4454	-1.89124	10.47396	0.001211	0.08805
hsa-miR-450a-5p	1.23255	5.113026	0.023747	0.512436
hsa-miR-455-3p	27.62479	12.30694	0.000451	0.051575
hsa-miR-455-5p	21.39833	8.802321	0.003008	0.15009
hsa-miR-487b	1.422617	5.165403	0.023041	0.512436
hsa-miR-503	1.901533	10.57206	0.001148	0.08805
hsa-miR-532-5p	25.64112	9.763189	0.00178	0.109564
hsa-miR-570-3p	25.01503	7.15166	0.007489	0.250511
hsa-miR-593-3p	28.2444	5.361526	0.020586	0.512436
hsa-miR-601	28.24635	14.84831	0.000117	0.016284
hsa-miR-656	23.15031	4.486338	0.034167	0.512436
hsa-miR-660-5p	29.88738	14.7595	0.000122	0.016284

Table 2: NanoStringDiff identifies 39 DE miRNAs between DFUF and NDFF, amongst which 38 are upregulated and 1 downregulated in DFUF compared to NDFF. LogFC is log2(DFUF/NDFF), lr represents the likelihood ratio test statistic, pvalue represents the p-value and qvalue represents the Benjamini-Hochberg adjusted p-value

These results showed that the majority of DE miRNAs were up-regulated (97%), whereas in the paper the authors identified 21 DE miRNAs amongst which the proportion of upregulated DE miRNAs was very similar to that of downregulated miRNAs (Figure 25).

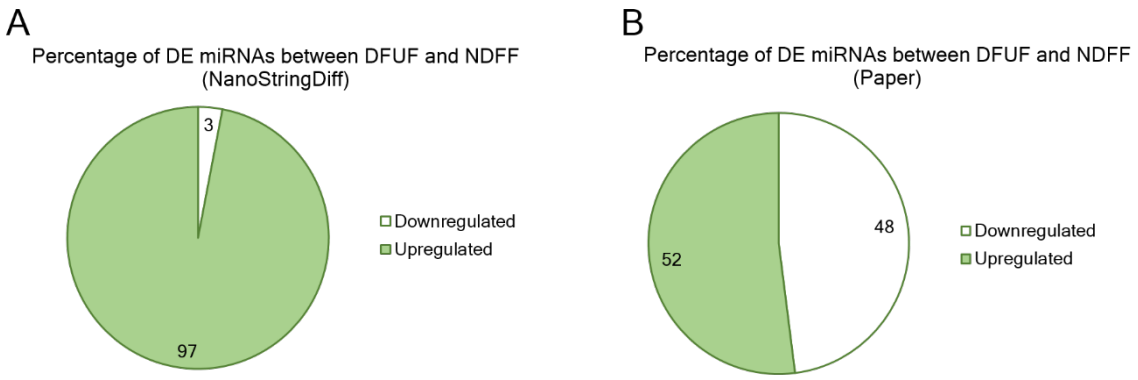


Figure 25: NanoStringDiff identifies 39 DE miRNAs in DFUF vs NDFF amongst which 97% are upregulated, while 3% are downregulated (A), whereas the original paper identifies 21 DE miRNAs amongst which 52% are upregulated and 48% are downregulated (B).

Amongst the two different analyses only 8 coincided for both methods of analysis with NanoStringDiff identifying 31 additional DE miRNAs not identified in the paper, while the paper identified 13 other DE miRNAs not identified by NanoStringDiff (Table 3).

Names	Total	DE miRNAs
NanoStringDiff & Paper	8	hsa-miR-140-5p, hsa-miR-450a-5p, hsa-miR-145-5p, hsa-miR-152, hsa-34a-5p, hsa-miR-143-3p, hsa-374-5p,hsa-132-3p
Paper only	13	hsa-miR-551a, hsa-miR-605, hsa-miR-21-5p, hsa-miR-367-3p, hsa-miR-1237, hsa-miR-545-3p, hsa-miR-3151, hsa-miR-658, hsa-miR-509-5p, hsa-miR-550a-5p, hsa-miR-548ac, hsa-miR-1468, hsa-miR-99a-5p
NanoStringDiff only	31	hsa-miR-181b-5p, hsa-miR-432-5p, hsa-miR-503, hsa-miR-342-3p, hsa-miR-409-5p, hsa-miR-532-3p, hsa-miR-570-3p, hsa-miR-601, hsa-miR-455-5p, hsa-miR-34c-5p, hsa-miR-431-5p, hsa-miR-424-5p, hsa-miR-455-3p, hsa-miR-30a-5p, hsa-miR-185-5p, hsa-miR-1234, hsa-miR-660-5p, hsa-miR-593-3p, hsa-miR-337-5p, hsa-miR-181a-5p, hsa-miR-4454, hsa-miR-320e, hsa-let-7i-5p, hsa-miR-487b, hsa-

		miR-301a-3p, hsa-miR-365a-3p, hsa-miR-10a-5p, hsa-miR-136-5p, hsa-miR-27a-3p, hsa-miR-26b-5p, hsa-miR-656

Table 3: only 8 miRNAs are identified as being DE by both methods of analysis with NanoStringDiff identifying 31 additional DE miRNAs not identified in the paper

Amongst the 8 common miRNAs identified as being DE by both methods, all miRNAs were up-regulated according to both the NanoStringDiff analysis and the paper, thus validating the results of the NanoStringDiff analysis to a certain extent. Furthermore, all the DE miRNAs from the paper that the authors chose to validate via qPCR were also identified as being DE via NanoStringDiff. For instance, the authors chose to validate miR-21-5p, miR-34a-5p and miR-145-5p by qPCR using a larger set of additional cell lines generated from collected samples, DFUF (n=7) and NDFF (n=8). qPCR showed an induction of miR-21-5p in DFUFs by 1.6-fold ($p = 0.029$), miR-34a-5p by 2.5-fold ($p = 0.0001$), and miR-145-5p by 2.2-fold ($p = 0.04$). In the NanoStringDiff analysis miR-21a was not identified as being significantly DE (according to the filtering criteria of FC≥2 and p<0.05), however this can be attributed to the fact that qPCR in the paper confirmed a FC of 1.6 only (less than the threshold of 2 imposed in the NanoStringDiff script), while miR-34a-5p showed a fold change of 2.3 according to NanoStringDiff and miR-145-5p a fold change of 2.8 (similar values to the one observed by the authors via qPCR). These results further confirmed that some of the DE miRNAs identified via NanoStringDiff corresponded to what was being observed and validated via qPCR by the authors in the paper, corroborating that the results are reliable. The remaining 31 DE miRNAs identified by NanoStringDiff alone might reflect what the authors of the NanoStringDiff package mentioned, namely that NanoStringDiff is able to identify additional DE miRNAs not identified by any other method.

2.2. Investigating the biological impact of the DE miRNAs

Next I wanted to find out what signalling pathways and biological functions the 39 DE miRNAs affect in order to gain a deeper understanding of how their dysregulation could bring about delays in the process of wound healing.

The first step involved identifying which genes the DE miRNAs targeted. To achieve this I used a software called Ingenuity Pathway Analysis (IPA) from QIAGEN, a powerful web based software application that allows for analysis and interpretation of data derived from 'omics experiments, such as RNAseq, small RNAseq, microarrays including miRNAs,

metabolomics and proteomics. IPA uses publicly available databases as well as QIAGEN's own manually curated data repository Ingenuity Knowledge Base (updated quarterly) to identify mechanisms, relationships and pathways relevant to a dataset, and is able to predict upstream effectors that may be causing the observed gene expression or downstream biological processes that might be impacted.

To analyse the biological effects of the DE miRNAs I used one of IPA's tools called MicroRNA Target Filter that was specifically created for analysis of miRNA datasets. This tool elegantly explores the biological context of the miRNAs of interest by determining relevant miRNA-mRNA pairings and overlaying the miRNA data onto related networks and pathways. MicroRNA Target Filter draws its miRNA content from multiple miRNA databases, including TargetScan (predicts miRNA targets by searching for the presence of conserved 8mer and 7mer sites that match the seed region of each miRNA), TarBase (contains experimentally demonstrated miRNA-mRNA pairs), miRecords (experimentally validated human, rat and mouse miRNA-mRNA interactions from ~550 published articles) as well as Ingenuity Knowledge Base that contains thousands of manually curated miRNA-related findings from published literature. Furthermore, given the multitude of targets that miRNAs can have, MicroRNA Target Filter additionally allows filtering of the miRNA-mRNA relationships based on database source, confidence level of miRNA-mRNA interaction, tissue, cell type and diseases to quickly prioritise and narrow down the targets in the relevant biological context.

Using IPA the 39 DE miRNAs were input into the MicroRNA Target Filter together with their FC values choosing the following criteria: - confidence (high & experimentally observed), pathway (in Ingenuity Pathway Database), species (human) and tissue (skin, fibroblasts, dermis). These criteria reduced the list to 35 miRNAs targeting 496 mRNAs (the number of miRNAs was reduced from 39 to 35 as MicroRNA Target Filter identifies the miRNAs based on the seed sequence, such that the DE miRNAs that belonged to the same family and thus shared the same sequence were treated as one miRNA). Next these target genes were exported as a list and used as input into the Core Analysis tool of IPA, which determined the enriched canonical pathways, molecular and cellular functions or diseases, as well as predicted upstream regulators and networks in the gene dataset. This analysis showed that the top

enriched pathways involved cancer and growth factor signalling (Table 4), while the top cellular functions included cellular movement and growth (Figure 26).

Ingenuity Canonical Pathways	-log(B-H p-value)
Molecular Mechanisms of Cancer	58.1
Role of Macrophages, Fibroblasts and Endothelial Cells in Rheumatoid Arthritis	53.7
Role of Osteoblasts, Osteoclasts and Chondrocytes in Rheumatoid Arthritis	52.4
Hepatic Fibrosis / Hepatic Stellate Cell Activation	52.1
Colorectal Cancer Metastasis Signaling	46.8
PTEN Signaling	38.6
p53 signalling	24.4
IGF-1 Signaling	21.5
EGF Signaling	18.2
PI3K/AKT Signaling	17.4

Table 4: the top 5 canonical pathways the target genes of the 39 DE miRNAs are enriched in (top of table) include cancer signalling. Interestingly, other enriched canonical pathways include growth factor signalling and signalling involved in cell proliferation and survival. All pathways have a Benjamini-Hochberg (B-H) corrected p-value < 0.05

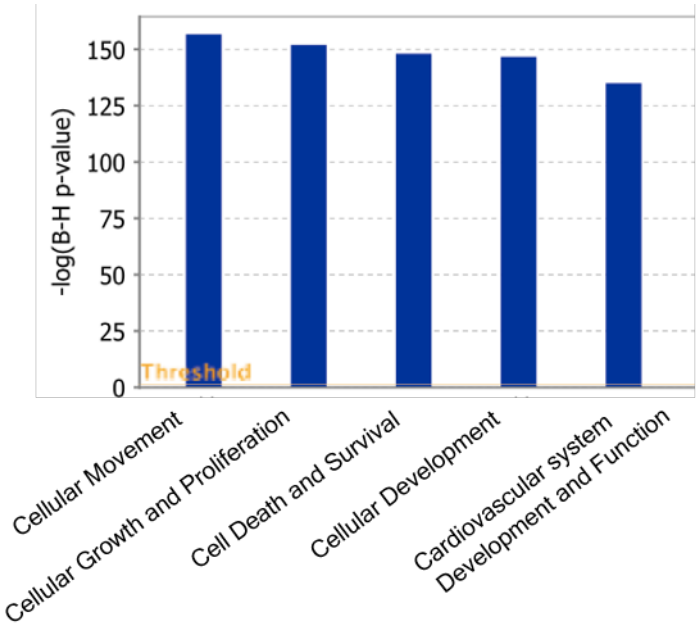


Figure 26: top 5 molecular and cellular functions the target genes of the 39 DE miRNAs are enriched in include cellular movement, proliferation, survival and development. All functions have a Benjamini-Hochberg corrected p-value < 0.05

To corroborate these findings the 496 target genes exported from the MicroRNA Target Filter were further subjected to KEGG pathway analysis, as well as Gene Ontology (GO) enrichment on biological processes analysis in DAVID (https://david.ncifcrf.gov/summary.jsp) and STRING using the whole genome as a statistical background. As expected, the results complemented those obtained from IPA, collectively showing that the highest enrichment in signalling pathways was in cancer signalling and signalling pathways involved in cell proliferation, migration or survival, such as PI3K-AKT signalling, MAPK signalling or RAS signalling pathways that are primarily activated by GFs (Table 5).

#pathway ID	pathway description	observed gene count	false discovery rate
5200	Pathways in cancer	106	1.95E-84
4151	PI3K-Akt signaling pathway	92	1.60E-64
5205	Proteoglycans in cancer	69	1.17E-52
4015	Rap1 signaling pathway	63	2.75E-47
5206	MicroRNAs in cancer	52	4.26E-43
4060	Cytokine-cytokine receptor interaction	65	1.48E-42
4014	Ras signaling pathway	60	8.72E-42

4510	Focal adhesion	57	1.74E-40
5166	HTLV-I infection	62	1.78E-40
4010	MAPK signaling pathway	55	8.68E-33
5215	Prostate cancer	36	8.94E-33
4068	FoxO signaling pathway	40	1.40E-31
5161	Hepatitis B	41	5.51E-30
5218	Melanoma	31	2.82E-29
4668	TNF signaling pathway	36	8.04E-29
5214	Glioma	28	8.12E-27
4390	Hippo signaling pathway	39	8.26E-27
4380	Osteoclast differentiation	34	6.32E-24
5202	Transcriptional misregulation in cancer	38	1.03E-23

Table 5: according to DAVID and String analysis the target genes of the 39 DE miRNAs are enriched in cancer signalling and signal transduction important for cellular pathways controlling cell proliferation and survival, such as PI3K-Akt or Ras signalling

In turn, enriched biological processes were observed in metabolic processes, signal transduction, response to stimuli and cell proliferation (Table 6 top section). Interestingly, the functions that were most enriched at the molecular level were binding of receptor, growth factor or cytokine (Table 6 middle section), while the most enriched cellular components were plasma membrane, cell surface and extracellular region (Table 6 bottom section). Collectively, these findings indicated that the signal transduction involved in the response to stimuli including GFs, was most affected in DFUF, in turn affecting pathways involved in cellular proliferation, migration and survival. Furthermore, given that the majority of the 39 DE miRNAs were over-expressed and that they generally suppress gene expression, these results overall predicted that signal transduction is impaired in DFUF, leading to diminished cellular proliferation, migration and response to stimuli. This supported my hypothesis that miRNA dysregulation might be partially responsible and contributing to delayed wound healing.

	ID	Term	count in gene set	false discovery rate
Biological process	GO:0031325	positive regulation of cellular metabolic process	281	9.35E-107
	GO:0010604	positive regulation of macromolecule metabolic process	271	4.47E-105
	GO:0010033	response to organic substance	259	1.18E-101
	GO:0007166	cell surface receptor signaling pathway	239	3.69E-101
	GO:0071310	cellular response to organic substance	225	5.57E-98
	GO:0070887	cellular response to chemical stimulus	246	1.43E-97
	GO:0009719	response to endogenous stimulus	197	8.35E-95
	GO:0009893	positive regulation of metabolic process	293	1.19E-94
	GO:0007165	signal transduction	331	9.54E-93
	GO:0051239	regulation of multicellular organismal process	239	5.48E-89
	GO:0048522	positive regulation of cellular process	315	1.15E-87
	GO:0042127	regulation of cell proliferation	193	1.54E-87
	GO:0007167	enzyme linked receptor protein signaling pathway	159	3.18E-87
	GO:0042221	response to chemical	289	2.72E-84
	GO:0032270	positive regulation of cellular protein metabolic process	179	9.70E-84
	GO:0051247	positive regulation of protein metabolic process	183	2.15E-82
Molecular function	GO:0005515	protein binding	334	1.18E-90
	GO:0005102	receptor binding	144	3.52E-60
	GO:0005488	binding	402	1.17E-34
	GO:0019899	enzyme binding	118	4.50E-31
	GO:0060089	molecular transducer activity	132	1.58E-29
	GO:0019838	growth factor binding	34	4.47E-28
	GO:0004871	signal transducer activity	118	7.22E-26
	GO:0004872	receptor activity	111	3.14E-25
	GO:0038023	signaling receptor activity	97	1.13E-21
	GO:0005126	cytokine receptor binding	41	1.63E-21
	GO:0019199	transmembrane receptor protein kinase activity	26	9.10E-20
	GO:0004672	protein kinase activity	62	1.42E-19
	GO:0097367	carbohydrate derivative binding	133	4.53E-19
	GO:0003674	molecular function	414	1.06E-18
	GO:0016773	phosphotransferase activity, alcohol group as acceptor	66	1.15E-18
	GO:0044212	transcription regulatory region DNA binding	63	7.17E-18
	GO:0008083	growth factor activity	24	8.86E-18
Cellular component	GO:0005886	plasma membrane	259	3.10E-42
	GO:0071944	cell periphery	258	9.43E-41
	GO:0044459	plasma membrane part	171	1.04E-38
	GO:0005615	extracellular space	122	2.49E-36
	GO:0031226	intrinsic component of plasma membrane	132	9.97E-34
	GO:0009986	cell surface	86	2.71E-32
	GO:0005887	integral component of plasma membrane	126	1.19E-31
	GO:0005576	extracellular region	230	7.94E-30
	GO:0044421	extracellular region part	206	2.29E-29

Table 6: according to DAVID and String analysis the 39 DE miRNAs are enriched in biological processes involving response to stimuli, signal transduction and cell proliferation (top section); molecular functions involving binding of

receptors, cytokines or GFs (middle section) and cellular components involving plasma membrane and cell surface (bottom section)

Additional search in the literature showed that some of the DE miRNAs identified via NanoStringDiff analysis were previously found to be implicated in aged skin, senescence and ECM remodelling.

For instance, miR-181a, miR-181b, miR-30 and miR-152 were shown to be up-regulated in senescent human keratinocytes or dermal fibroblasts in ageing skin [143]. MiR-181a and miR-181b, for example were found to be upregulated during replicative senescence in keratinocytes targeting SIRT1, a NAD^+ dependent deacetylase involved in regulating cellular stress responses, immune responses and replicative senescence [144]. Similarly, the expression of miR-30 was shown to increase during fibroblast senescence directly repressing B-Myb, a transcription factor that controls a variety of genes involved in cellular proliferation [145]. Also, miR-181a and miR-152 were shown to induce senescence in proliferating human dermal fibroblasts and to play a role in ECM remodelling by downregulating their direct targets collagen XVI (COL16A1) and integrin α5 (ITGA5), respectively [146]. Collagen XVI is an important component of the skin ECM, ensuring mechanical anchoring in the dermal-epidermal junction zone, while integrin α5 promotes cell adhesion and migration on fibronectin.

Similarly, miR-424, miR-487b and miR-181a (identified via NanoStringDiff alone) and miR-34a (identified by both NanoStringDiff and the paper) were found to be DE between young (<10 yrs) and aged (>60 yrs) human dermis [147]. Amongst these, miR-34a and miR-424 were further found to be up-regulated in senescent human dermal fibroblasts (HDFs) when cultured at high passages, with transfection of miR-34b-5p mimics into HDFs significantly inducing cell cycle arrest and decreasing the expression of COL1A1 and elastin.

Another study identified some of the miRNAs from the NanoStringDiff analysis as being upregulated in serum of type 1 diabetic children compared to healthy controls, including miR-152, miR-30a-5p, miR-181a and miR-27a [148].

Given that all these miRNAs were over-expressed in DFUF according to NanoStringDiff, this could explain how they may contribute to altered ECM deposition and increased senescence, common phenotypes observed in DFUs. Overall these findings corroborate that the list of DE

miRNAs identified via NanoStringDiff is most likely physiologically relevant to the DFU phenotype observed in ulcerated cells or systemic disease, such as diabetes.

2.3. Investigating miRNA clusters amongst the DE miRNAs

To gain more biological insight into the DE miRNAs from the NanoStringDiff dataset I furthermore mapped the miRNA coding genes to their genomic location to check if any of the miRNAs clustered together.

MiRNA clusters - according to the miRBase database definition – are miRNA genes that are located within a short distance on the same segment of the chromosome, usually within 10kb. Many of the miRNA clusters are evolutionary conserved (with miRBase identifying over 40% of human miRNAs and over 30% of worm and fly miRNAs to be within 10kb of another miRNA [149]) and may have one core promoter region and transcriptional start site causing all the miRNA genes within that cluster to be expressed within one single RNA transcript [150]. Because of this common promoter or a common regulatory machinery, many cluster members tend to display similar expression, either being increased or decreased together as part of normal processes, such as adult aging [151] or in pathological states, such as cancer where for instance, all three miRNAs of the miR-23a~27a~24-2 cluster were found to be simultaneously up-regulated or down-regulated in various carcinomas [152]. Likewise, miRNAs part of a cluster are often found to cooperate with each other by regulating different genes of the same pathway to jointly drive a phenotype, such as the members of the miR-106b~93~25 cluster that were found to be abnormally upregulated in gastric cancer and to cooperatively target the cell cycle Cip/Kip family proteins [153].

To map the miRNAs to their genomic locations the BioMart tool in Ensembl (https://www.ensembl.org/info/data/biomart/index.html) and the Pubmed Gene resource (https://www.ncbi.nlm.nih.gov/gene/) were used, which yielded the chromosome and the band name of each miRNA gene's location (Table 7).

Description	Band	Chromosome Name
microRNA 1234	q24.3	8
microRNA 342	q32.2	14
microRNA 26b	q35	2
microRNA 365a	p13.12	16
microRNA 450a-1	q26.3	X
microRNA 337	q32.2	14
microRNA 34c	q23.1	11
microRNA 455	q32	9
microRNA 487b	q32.31	14
microRNA 181a-1	q32.1	1
microRNA 27a	p13.12	19
microRNA 30a	q13	6
microRNA 136	q32.2	14
microRNA 152	q21.32	17
microRNA 656	q32.31	14
microRNA 660	p11.23	X
microRNA 181b-1	q32.1	1
microRNA 601	q33.3	9
microRNA 301a	q22	17
microRNA 503	q26.3	X
microRNA 140	q22.1	16
microRNA 185	q11.21	22
microRNA 34a	p36.22	1
microRNA 143	q32	5
microRNA 10a	q21.32	17
microRNA 132	p13.3	17
microRNA 145	q32	5
microRNA 4454	q32.2	4
microRNA 432	q32.2	14
microRNA 431	q32.2	14
microRNA 409	q32.31	14
microRNA 320e	q13.32	19
microRNA 374a	q13.2	X
microRNA 424	q26.3	X
microRNA let 7i	q14.1	X
microRNA 455	q32	9
microRNA 532	p11.23	X
microRNA 570	q29	3

microRNA 593	q32.1	7

Table 7: genomic mapping shows the exact location the miRNA genes of the DE miRNAs from the NanoStringDiff analysis are mapped to on the chromosomes. This includes the band and the chromosome name

The genomic mapping results showed that the DE miRNAs were enriched in two chromosomes, namely chromosome 14 and chromosome X, with 7 miRNA genes located on either chromosome (Figure 27).

Interestingly, the 7 miRNAs that mapped to chromosome 14 (miRs- 136, -337, -409, -431, -432, -487b, -656) mapped to the region 14q32, a chromosomal region that holds the largest cluster of miRNAs in the human genome comprising 54 miRNAs (Figure 28). This chromosomal region holds the imprinted gene cluster Dlk1-Dio3 that apart from hosting the miRNA genes, also contains a variety of other genes, including the paternally expressed protein-coding genes DLK1, RTL1 and DIO3 and the maternally expressed noncoding RNA genes Gtl2 (MEG3), RIAN (MEG8) and Mirg (MEG9), as well small nucleolar RNAs (snoRNAs) that primarily guide methylation of other RNAs [154].

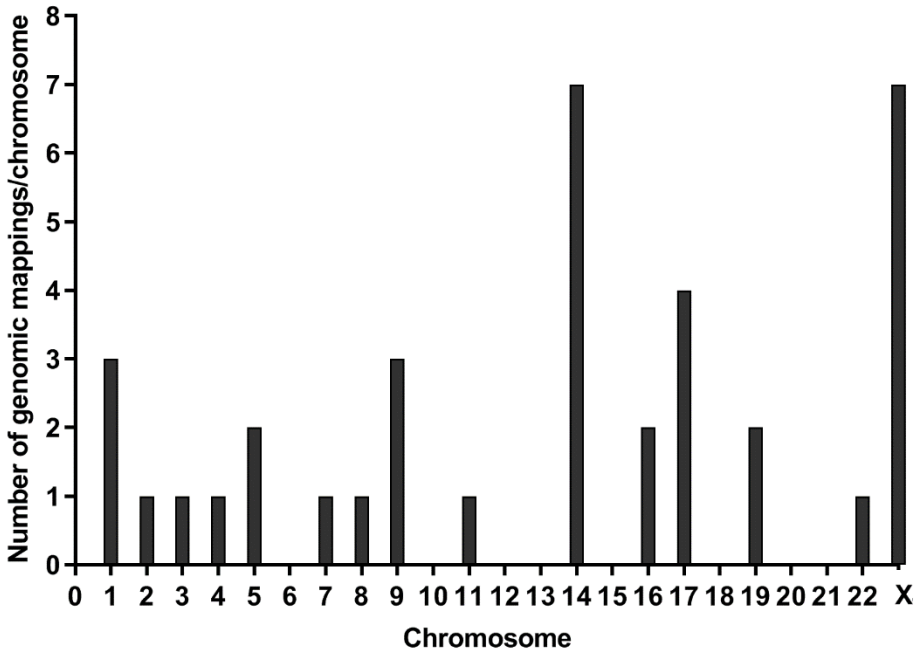


Figure 27: genomic mapping of the miRNA-coding genes of the DE miRNAs from the NanoStringDiff dataset shows the miRNA-coding genes are scattered across many chromosomes and display enrichment in chromosome 14 and chromosome X

The Dlk1-Dio3 region has been shown to play important functions in oncogenesis, malignant growth, proliferation and cell survival, and cellular interactions with the ECM - processes that

were also enriched in the GO terms of the DE miRNA targets- while disruptions of the Dlk1-Dio3 region have been linked to disease pathogenesis and increased tumorigenicity [155]. For instance, four of the miRNAs of the 14q32 cluster (miR-329, -487b, -494 and -495) were shown to be highly involved in neovascularisation showing antiangiogenic properties in an hindlimb ischemia mouse model via targeting proangiogenic genes including FGFR2, VEGFA and IRS1 [156]. Amongst these, however only miR-487b was upregulated in the dataset from NanoStringDiff. Other miRNAs from the Dlk1-Dio3 cluster including miRs-300, -382, -494, -495, -539, -543 and -544 were shown to function cooperatively to repress the EMT transition by targeting the transcription factor TWIST1, a potent EMT inducer [157], while MEG3 was shown to act as a growth suppressor in tumour cells by activating p53. Collectively these findings suggest that the Dlk1-Dio3 region overall exerts a tumour suppressive role.

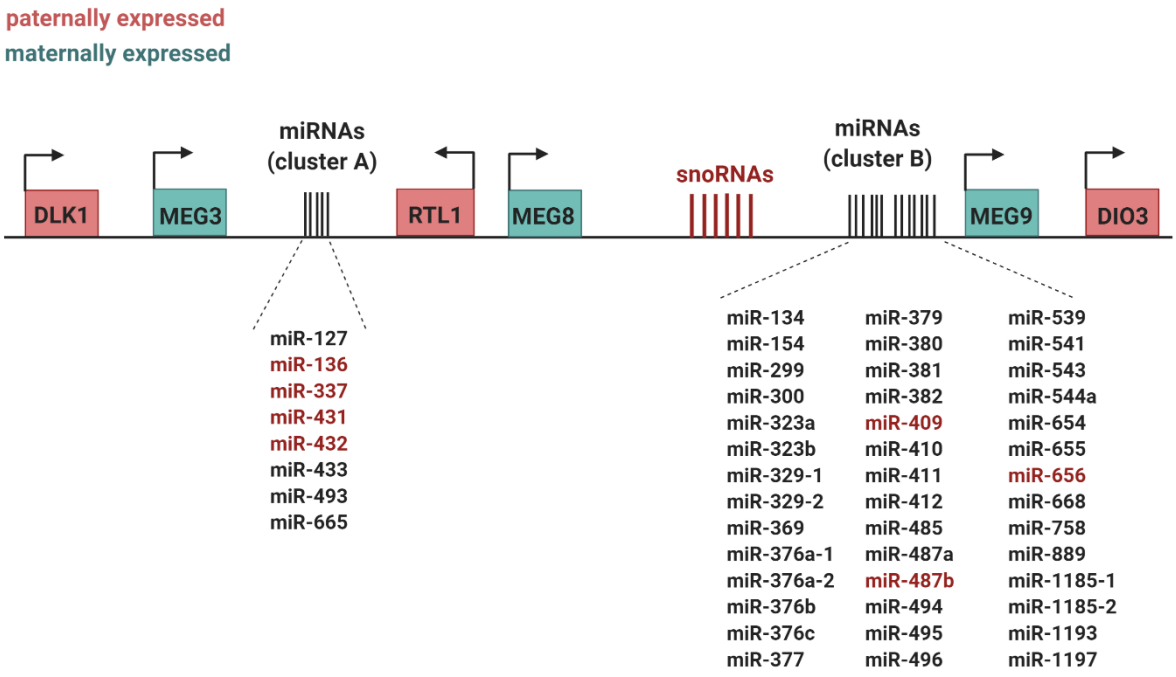


Figure 28: the Dlk1-Dio3 chromosomal region (14q32) contains maternally and paternally expressed genes and holds the largest cluster of miRNAs comprising 54 human miRNAs. Seven of the DE miRNAs from the NanoStringDiff analysis (shown in red) were mapped to this chromosomal region, suggesting it might be implicated in the pathogenesis of DFUF. Image created in BioRender.com and exported under a paid subscription

Given that all 7 DE miRNAs from the NanoStringDiff dataset were up-regulated in the DFUF, it may suggest that this chromosomal region is activated and thus may be implicated in the DFU pathogenesis in fibroblasts. Indeed, upregulation of these genomic imprinted Dlk1-Dio3 miRNAs might be driven by low global DNA methylation levels [158], a phenomenon previously

observed in DFU-derived fibroblasts [159]. Furthermore, given the tumour suppressive role this chromosomal region exerts, it further suggests its activation might contribute to impairing cellular processes important for wound healing, such as proliferation or migration and thus might be interesting to investigate in the future regarding DFU pathogenesis.

2.4. Finding miRNAs that work together by targeting common pathways

Having identified DE miRNAs in DFUF vs NDFF I then investigated which of these DE miRNAs are likely to cooperate at the pathway level as synergistic networks to disrupt signal transduction - according to the original hypothesis of this project.

To infer miRNA networks I started looking for miRNAs that target genes belonging to the same signalling pathway or found across multiple interacting signalling pathways that are important for wound healing. To achieve this the DE miRNAs from the NanoStringDiff were overlayed onto several of the enriched pathways according to the Core Analysis in IPA, such as PI3K-Akt signalling (Figure 29), EGF signalling (Figure 30), IGF-1 signalling (Figure 31) or ERK/MAPK signalling (Figure 32) to check what genes they targeted.

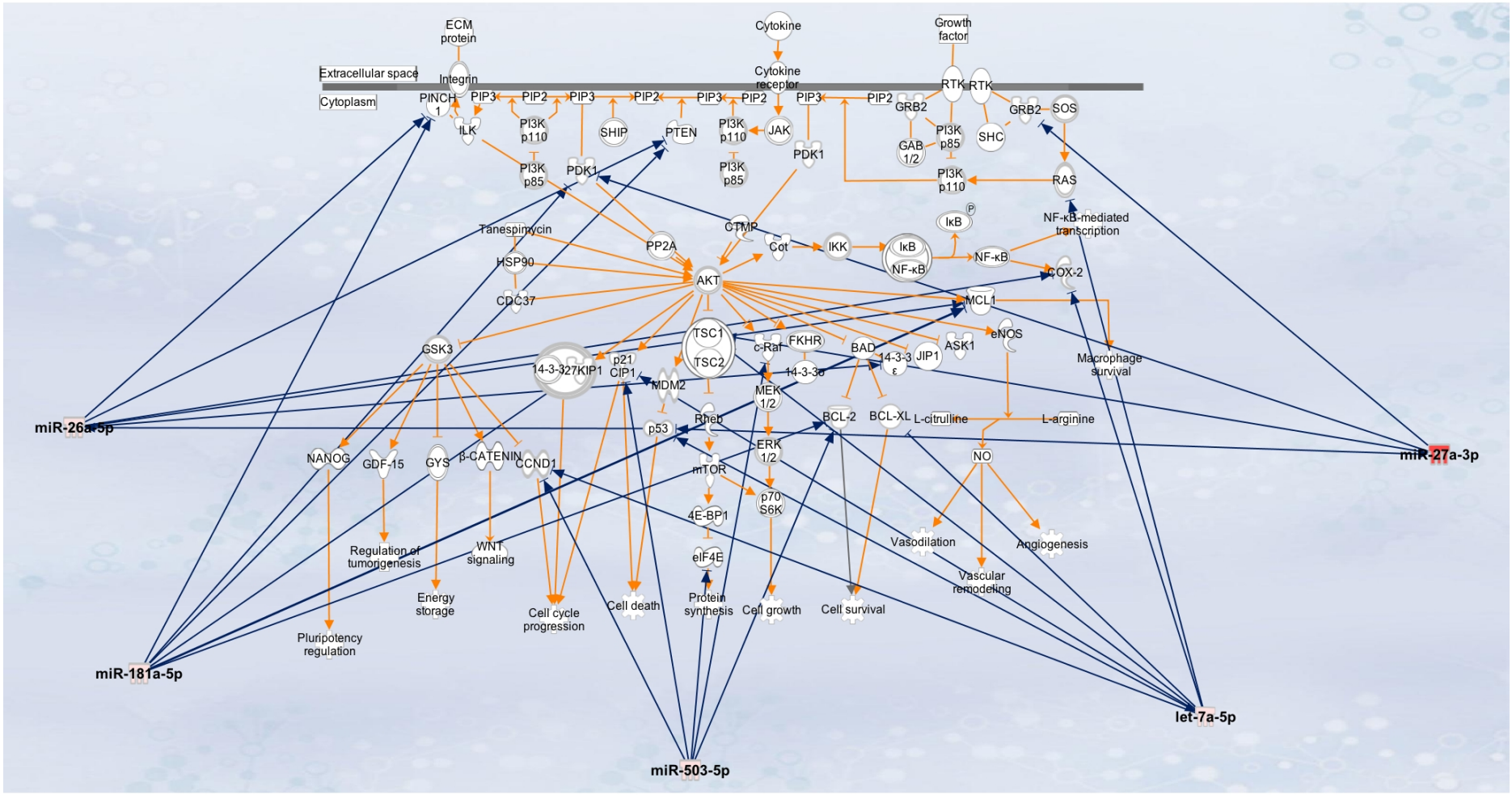


Figure 29: DE miRNAs from the NanoStringDiff dataset are predicted to target many signalling components of the enriched PI3K/AKT signalling pathway, showing how miRNAs can potentially work together at the pathway level to control signal transduction. Image created in Path Designer in IPA.

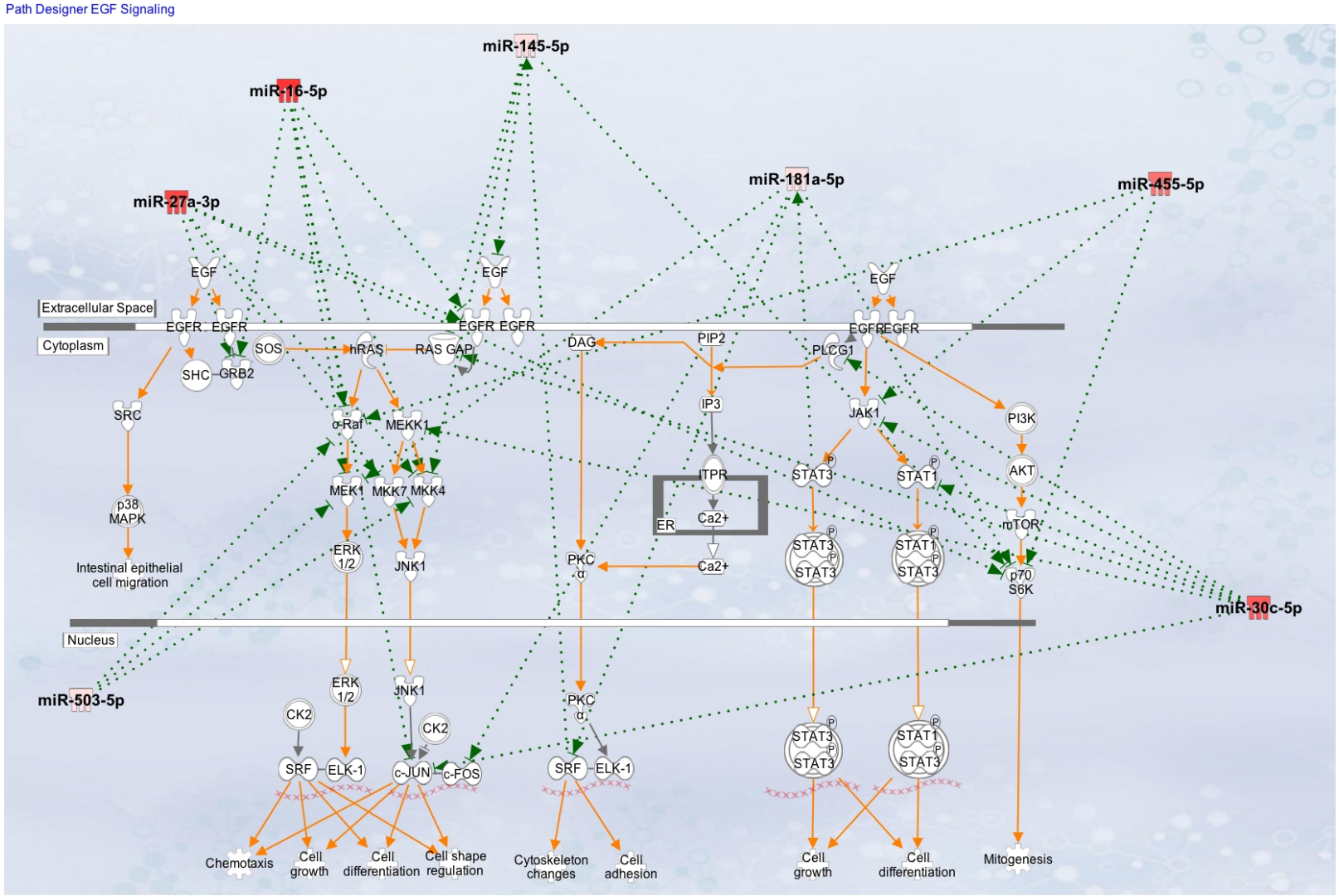


Figure 30: DE miRNAs from the NanoStringDiff dataset are predicted to target many signalling components of the enriched EGF signalling pathway, showing how miRNAs can potentially work together at the pathway level to control signal transduction. Image created in Path Designer in IPA.

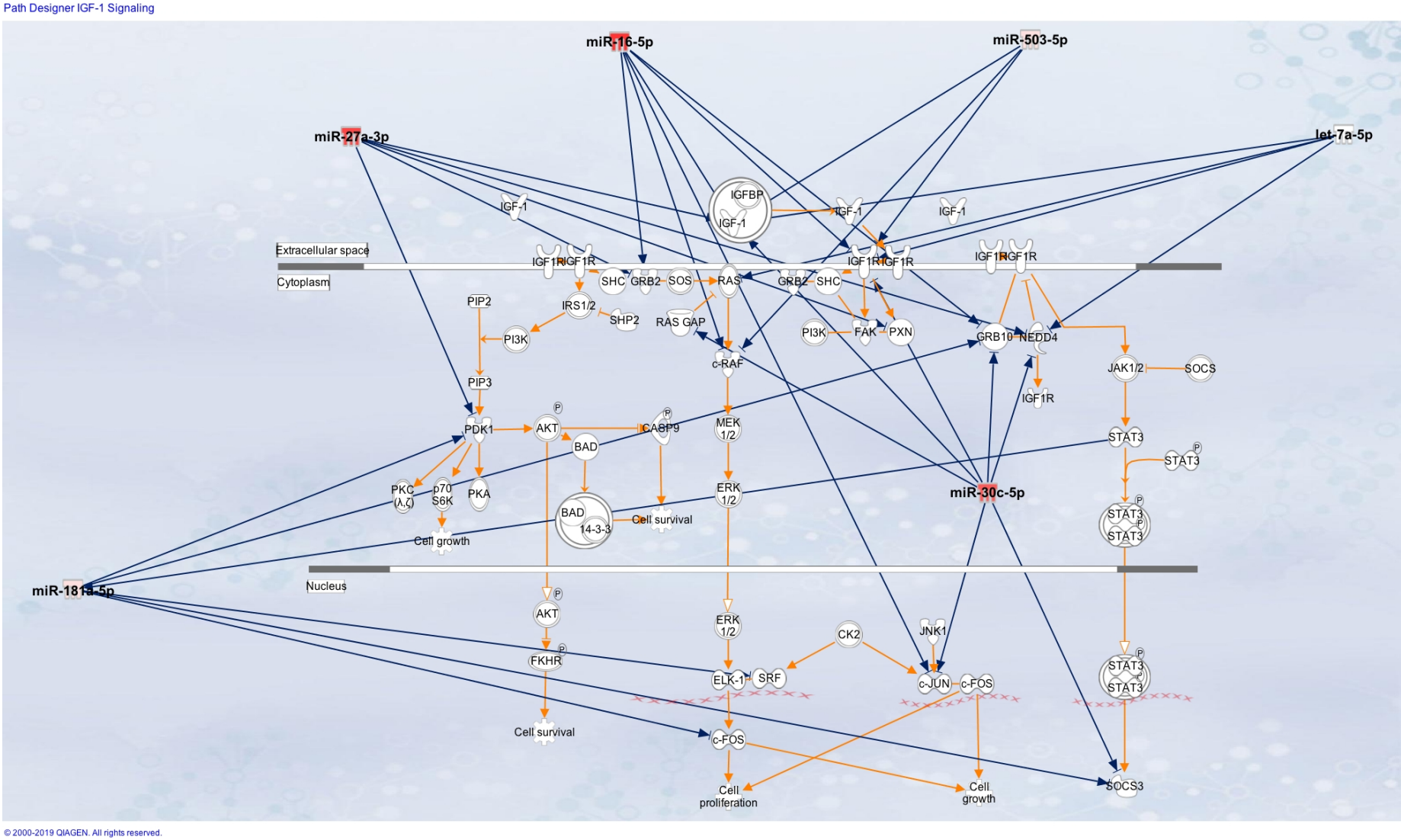


Figure 31: DE miRNAs from the NanoStringDiff dataset are predicted to target many signalling components of the enriched IGF-1 signalling pathway, showing how miRNAs can potentially work together at the pathway level to control signal transduction. Image created in Path Designer in IPA.

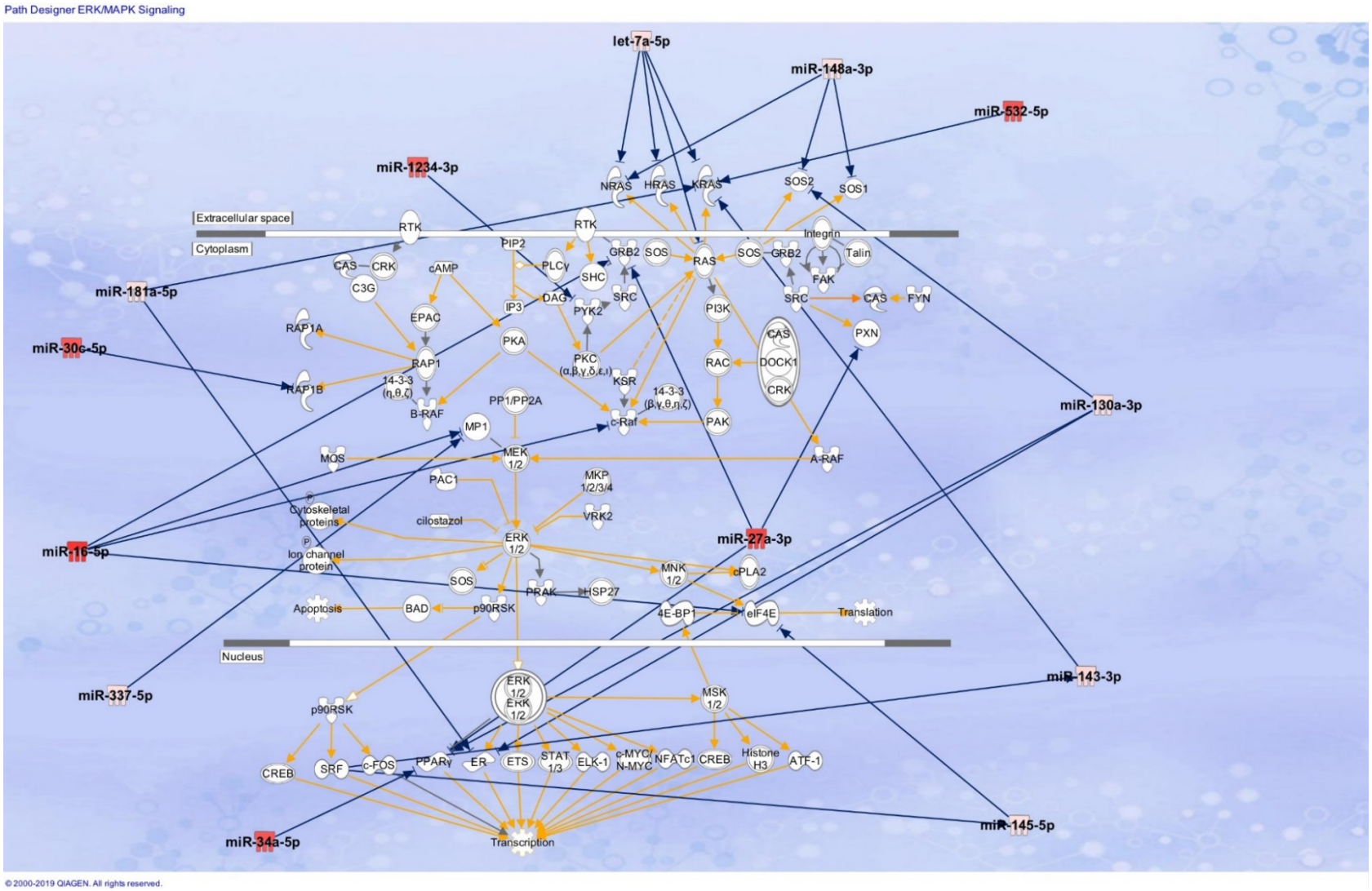


Figure 32: DE miRNAs from the NanoStringDiff dataset are predicted to target many signalling components of the enriched ERK/MAPK signalling pathway, showing how miRNAs can potentially work together at the pathway level to control signal transduction. Image created in Path Designer in IPA.

Amongst these 39 DE miRNAs those that targeted only one or two genes in a pathway were removed from the miRNA-pathway network and when overlaying these across multiple IPA pathways (~10) it was noticed there was a set of miRNAs that kept re-occurring, namely miR-145, -148, -16, -27a, -503, -30c, and -181a, while the DE miRNAs from cluster A on the Dlk1-Dio3 chromosomal region were either not present or targeted only one gene. Furthermore, miRNA-mRNA networks displaying the connections between these miRNAs and their target genes (from the original list of 496 genes of all DE miRNAs) showed that many of these genes were commonly targeted by pairs of miRNAs or all of them, suggesting these miRNAs might work together both at the pathway and gene level (Figure 33). Many of these genes were key targets important for growth factor signalling, such as IGF1R, INSR, KRAS, JUN, c-RAF, GRB2 and SOS1, which corroborated the previous results showing enrichment in GF signalling in the NanoStringDiff dataset (Table 4 and Table 5).

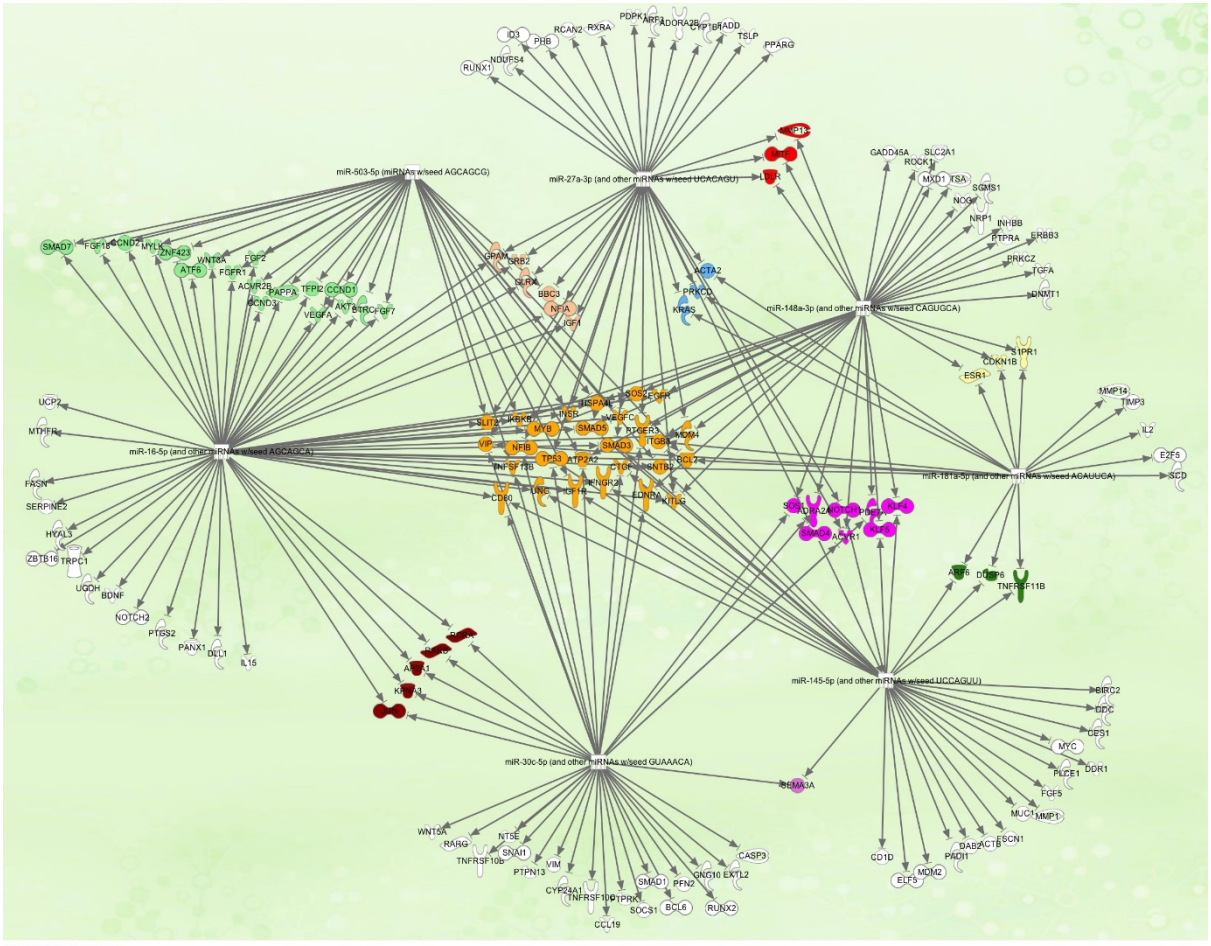


Figure 33: miRNA-mRNA networks between 7 of the DE miRNAs from the NanoStringDiff analysis (miRs-145, -143, -16, -27a, -503, -30c and -181a) show strong target sharing, with many genes being targeted by multiple miRNAs. Image created in Path Designer in IPA.

Furthermore, PPI networks [g] between the target genes of these 7 DE miRNAs showed strong interactions between the proteins (PPI enrichment p-value < $1.0*10^{-16}$), with each protein connecting on average to 18 other proteins (Figure 34). Given that the set of genes showed such strong protein-protein connectivity, it suggests that the proteins are physically interacting to achieve specific functions and perhaps the miRNAs that are targeting them also cooperate.

[g] PPI networks reveal physical interactions between proteins in the cell that are specific and occur within defined binding regions in the proteins. Protein interactions can be both stable and transient and serve a specific function, such as membrane transport, cell metabolism or signal transduction when phosphorylation of a protein causes conformational changes in its shape allowing other proteins to bind to it and become activated, in turn activating a signalling cascade downstream.

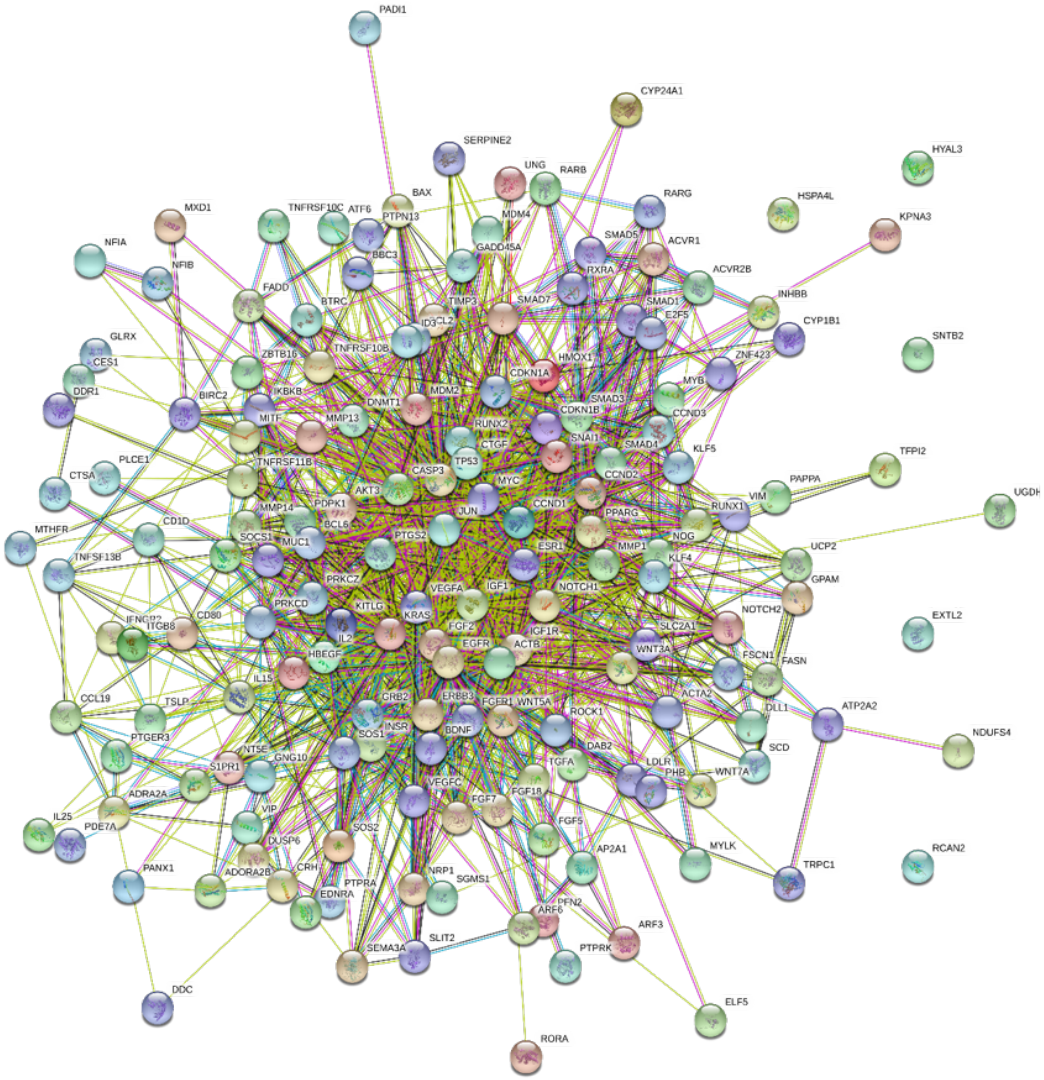


Figure 34: PPI network between the proteins targeted by 7 of the DE miRNAs from the NanoStringDiff dataset (miRs-145, -143, -16, -27a, -503, -30c and -181a) shows very strong interactions, implying the proteins are involved in regulating a common function

In addition, GO analysis of biological functions and pathway enrichment (both from KEGG and Core Analysis in IPA) further showed that the genes targeted by these 7 miRNAs were involved in cancer and GF signalling (Table 8), as well as regulation of signal transduction and cellular response to stimuli (Table 9).

Pathway	p-value
Molecular mechanisms of cancer	2.53E-25
MicroRNAs in cancer (KEGG)	5.26E-30
Colorectal cancer metastasis signalling	5.15E-22
PI3K-Akt signalling pathway (KEGG)	1.13E-25
PTEN signalling	2.13E-18
MAPK signalling pathway (KEGG)	3.36E-18

Table 8: Seven of the DE miRNAs from the NanoStringDiff dataset (miRs-145, -143, -16, -27a, -503, -30c and -181a) are enriched in pathways cancer signalling and signalling pathways important for cell growth and proliferation, such as PI3-Akt or MAPK signalling pathway.

Molecular and biological function/process	p-value
Cellular movement	1.15E-66
Cell death and survival	3.07E-63
Cellular growth and proliferation	5.08E-60
Regulation of signal transduction (GO)	5.94E-35
Cellular response to stimulus (GO)	3.56E-36

Table 9: Seven of the DE miRNAs from the NanoStringDiff dataset (miRs-145, -143, -16, -27a, -503, -30c and -181a) are enriched in processes involving cellular movement, growth and proliferation as well as response to stimuli.

Together with this data it was concluded that the set of target genes by these 7 DE miRNAs was involved in signal transduction regulating cellular proliferation and movement, which might explain the closely interacting proteins as well.

From the set of 7 DE miRNAs three miRNAs were ultimately chosen for experimental validation, namely miRs-181a, -27a and -30a that were believed to cooperate based on the pathways they targeted and the genes they were predicted to have in common. These three miRNAs were predicted to affect the MAPK-Erk signalling pathway and the PI3K-Akt signalling pathways (Figure 35). Given that all these miRNAs were upregulated in DFUF vs NDFF, I hypothesised they could work together to suppress gene expression along these two major signalling pathways, impairing cellular growth, proliferation and migration, in turn, leading to delayed wound healing.

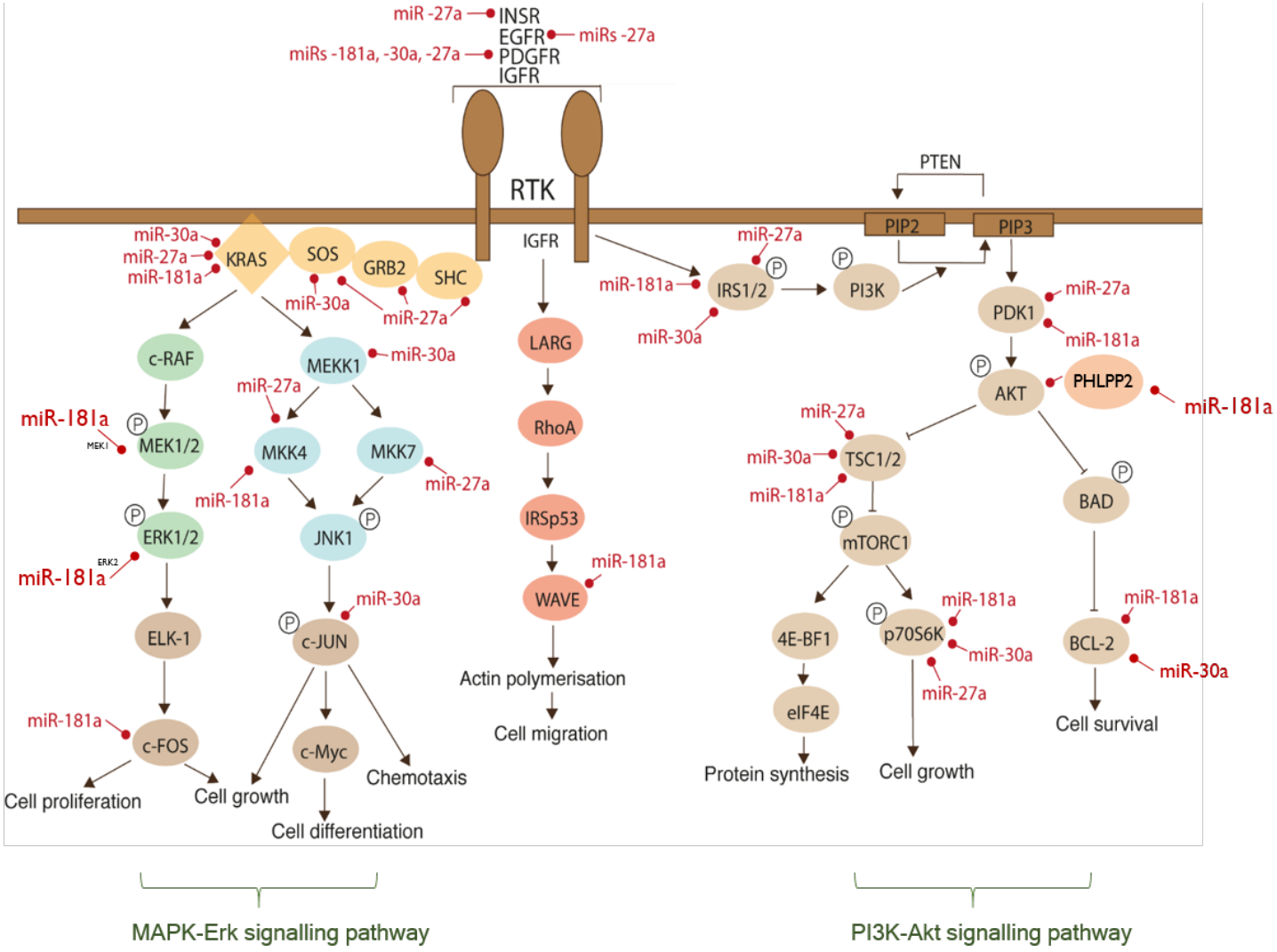


Figure 35: miRs-181a, -27a and -30a from the NanoStringDiff dataset are predicted to commonly target the MAPK-ERK signalling pathway and the PI3K-AKT signalling pathway, implying they might cooperate at the pathway level to jointly control signal transduction along these pathways

The PI3K/AKT and MAPK/ERK signalling pathways have been shown to play essential roles in wound healing [160].

ERK1/2 activation, for instance is one of the earliest events that occurs after wounding to signal injury [161,162]. Both epithelial and fibroblast cells at the wound edge display a rapid and transient activation of ERK in the first 10 minutes following injury ("first wave"), followed by a slow and sustained ERK activation 3-5 hours post wounding ("second wave") in the migratory cells displaying an elongated shape. This remarkable "two-wave" activation of ERK1/2 is necessary for epithelial cell sheet movement [161] and plays crucial roles in driving and regulating directional migration in cultured fibroblasts [162], as demonstrated by pharmacological inhibition of MEK1/2 upstream of ERK. The MAPK/Erk pathway, however is attenuated during diabetic wound healing. In a rat wound healing model protein levels of key components of this pathway SHC and ERK1/2 were found to be lower in the wounded skin of diabetic rats compared to wounded nondiabetic rats, contributing to impaired wound healing [160].

Similarly, the PI3k-Akt pathway plays important roles in cell growth and proliferation, cell migration and epithelial mesenchymal transition (EMT) [163], as well as re-epithelialisation [164], collagen I expression and ECM deposition [165] and neovascularisation [166] – all key processes for effective wound resolution. During normal wound healing, the Akt-mTOR pathway is upregulated in response to injury to drive wound repair [167]. For instance, induction of p-Akt (Ser473) and pS6 were observed in the basal epidermal layer of the migrating epithelial tongue compared to intact adjacent skin in mice, driving re-epithelialisation [164].

However, in diabetes and diabetic wound healing the PI3K/Akt signalling pathway was found to be significantly attenuated, contributing to impaired wound healing [168]. For instance, expression of key proteins (including Akt, mTOR, p70S6K and eIF4E) in this pathway, especially phosphorylated levels of these proteins, were found to be much lower in wounded skin tissue from diabetic rats compared to nondiabetic wounds [169]. Reduced activity of this pathway leads to reduced gene transcription and protein translation, resulting in reduced cell growth and survival, decreased cellular migration and proliferation – all processes crucial for wound healing.

Furthermore, these 3 miRNAs were predicted to target (and suppress) KRAS and IRS1/2, key genes in the signal transduction pathways coordinating the cellular events. KRAS belongs to the RAS family of small GTPases that act as on/off switches in cell signalling. Cycling between the "on" state - when bound to GTP- and "off" state - when bound to GDP – KRAS plays a key role in activating downstream proteins that are involved in cell growth, proliferation and cell survival, acting as an oncogene. In fact, KRAS is one of the most frequent mutation in many cancers, including pancreatic, colorectal and lung cancer, being deemed 'undruggable' by small molecule drugs due to lack of deep hydrophobic pockets [170]. Finding a miRNA combination that suppress KRAS expression could potentially also be translatable into a miRNA-based therapy for cancer treatment.

IRS1 and IRS2 play key roles in transmitting signals from the insulin receptor (IR) and insulin-like growth factor 1 receptor (IGF-1R) to intracellular pathways PI3K/Akt and MAPK/Erk by activating PI3K and GRB2, respectively. Deregulation in IRS1/2 expression or activity has been associated with impaired insulin signalling in diabetes. For instance, both IRS1 and IRS2 protein levels were found to be decreased in wounded skin of diabetic rats compared to wounded skin of nondiabetic rats contributing to impaired wound healing [160]. This made me further believe that upregulation of the DE miRNAs in DFUF could contribute to IRS1/2 suppression.

Altogether this analysis showed that these three miRNAs are involved in regulating pathways important for wound healing and that they are predicted to target common pathways and thus potentially display cooperation. As such the next step was to experimentally validate this miRNA combination *in vitro* with the following aims:

Aim 1: Deliver miRNA mimics of miRs-181a, -27a and -30a into nondiabetic healthy fibroblasts to over-express their levels, thus mimicking the upregulation observed in DFUF according to the NanoStringDiff bioinformatics analysis.

Aim 2: Investigate their individual and collective impact on cellular processes, such as proliferation and check if these three miRNAs work together as a network. *Hypothesis: miRs-181a, -27a and -30a work together as a network to suppress cell proliferation by cooperating at the pathway level,* thus showing how DE miRNAs can synergise in DFUF to impair wound healing.

Aim 3: If over-expression of these 3 miRNAs suppresses proliferation, deliver inhibitors of these miRNAs into DFU – derived fibroblasts to inhibit their levels and de-repress the attenuated proliferation as a miRNA-based therapy for wound healing.

2.5. Supplementary data

2.5.1. R script to analyse DE miRNAs using the NanoStringDiff vignette

Once the csv file was defined it was imported into R Bioconductor and subjected to the following script for analysis of DE miRNAs of NanoString nCounter Data:

```
source("https://bioconductor.org/biocLite.R")

biocLite()

biocLite("NanoStringDiff")

biocLite("Biobase")

library("BioBase")

library("NanoStringDiff")


designs=data.frame(group=c("Control","Control","Control", "Treatment", "Treatment", "Treatment"))

designs

directory <- "/Users/mara_pop/Desktop"

path <- paste(directory, "nanostring2.csv", sep ="/", collapse = NULL)

NanoStringData=createNanoStringSetFromCsv(path,header=TRUE,designs)

head(exprs(NanoStringData))

pData(NanoStringData)

pheno=pData(NanoStringData)

group=pheno$group

design.full=model.matrix(~0+group) #create a design (or model) matrix

design.full
```

```
contrast=c(-1,1) #compare treatment to control (i.e. DFUF miRNA expression vs NFF)

NanoStringData=estNormalizationFactors(NanoStringData) #estimate normalisation factors

pf <- positiveFactor(NanoStringData)

pf

nf <- negativeFactor(NanoStringData)

nf


hf <- housekeepingFactor(NanoStringData)

hf

result=glm.LRT(NanoStringData,design.full, Beta= ncol(design.full), contrast=contrast) #generalise linear model likelihood ratio test

result$table #display the FC, lr, pvalue and qvalue for all the miRNA genes

write.csv(result$table, file="results nanostring.csv")

str(result)

result$mean.reduce

result$mean.full #estimates mean value for every gene in the group (treatment or control across all replicates) which is used to compute the fold change values

#traceback() # allows debugging after an error occurs (call immediately after error appears)

significant_res <- result$table[abs(result$table[1]) >=1.0 & result$table[3] < 0.05 & !is.na(result$table[3]),] #show miRNAs with an absolute FC>2 and p-value<0.05

significant_res

write.csv(significant_res, file="significant miRNAs nanostring2.csv") #write file with the significant miRNAs and all their values
```

3. Isolation and characterisation of primary skin cells

3.1. Isolation of primary skin cells from amputated human lower limb tissues

To investigate the impact of miRNA dysregulation on wound healing *in vitro* I isolated primary fibroblasts and keratinocytes from the skin of amputated human lower limb tissues, such as feet or toes that were diabetic and ulcerated, diabetic non-ulcerated or nondiabetic non-ulcerated to allow a comprehensive study (Figure 37).

Following the guidelines established by the Imperial College Healthcare NHS Trust Tissue Bank prior to the amputation patients were given an information leaflet (v4 4/7/14) describing the use of their leftover tissue for research and teaching purposes and asked for their consent in written. Post-surgery the discarded tissues were transported back to the cell culture lab on the same or following day, where the donors' personal information was removed and each sample given a unique code that anonymised the donors. All tissues were processed over 2 days to isolate primary keratinocytes from the epidermis - top layer of the skin - and fibroblasts from the dermis - middle layer of the skin (Figure 36).

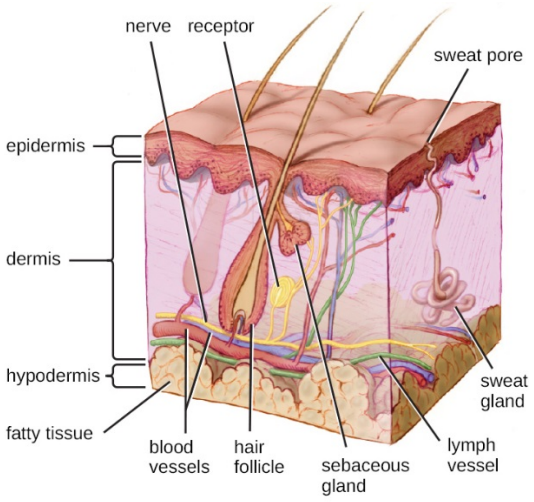


Figure 36: skin consists of three layers (epidermis, dermis and fat) with many structures embedded throughout, such as sweat glands, hair follicles, sebaceous glands, blood vessels and nerves.

Day 1:

Upon arrival each amputated tissue was cleaned on the surface 3-4 times with sterile iodine and chlorhexidine wipes, followed by ethanol wipes to ensure the epidermis was clean of dirt. Next, small pieces of skin from the top/bottom and wound edge/away from the wound edge (i.e. non-ulcerated area) of the amputated tissues were cut out and kept in a strong antibiotic-antimycotic solution (3xABAM in PBS or DMEM) for 30-60 min to remove any bacterial and fungal contaminants present. Following decontamination a few small strips (~1x0.5 cm^2) were placed sideways in cryomoulds and embedded in OCT on dry ice for crysectioning and histological H&E staining to study the skin morphology. For the remaining pieces the adipose layer was removed with scissors, leaving behind a thin layer of skin (~6-7mm thick) containing the epidermis and dermis only. These were placed in a dispase solution (5U/mL) at 4°C overnight to enzymatically digest the basement membrane allowing separation of the epidermis from the dermis (Figure 38).

Day 2:

Following the dispase treatment the epidermis was peeled of the dermis using forceps and both the epidermis and dermis were minced separately into very small pieces using a scalpel or scissors, respectively. The minced epidermis was placed into warm trypsin-EDTA solution (0.25%) at 37°C for 30 min to extract the keratinocytes, while shaken every 5 min to aid dissociation. The effect of trypsin was subsequently inhibited with Defined Trypsin Inhibitor in a 1:1 ratio and the resulting solution was passed through a 70 μm cell strainer to retain the skin pieces and allow only the dissociated cells to pass through. The cell solution was centrifuged at 1400rpm for 8min, followed by re-suspension of the pellet in Epilife medium (supplemented with EDGS) and seeding into T75 flasks (pre-coated with coating matrix 1:100 for 30min at room temperature). The resulting keratinocytes displayed the characteristic eye-shaped or fried-eye morphology (Figure 39 – step 6).

The minced dermis was placed into high glucose DMEM (supplemented with 20% FBS, 2.5 mM L-glutamine, 1xABAM) containing collagenase type I at 5-10 mg/mL and placed on an orbital shaker for 3-6h to isolate the fibroblasts. Following enzymatic digestion of the dermis the resulting collagenase solution was passed through 70μm and 40μm cell strainers, respectively followed by centrifugation at 1400 rpm for 8 min, re-suspension of the cell pellet

and seeding into T75 flasks. The resulting fibroblasts displayed the characteristic spindle-shaped morphology (Figure 39 – step 5). Once the fibroblasts reached confluency, they were passaged and the composition of the medium was changed to high glucose DMEM supplemented with 10% FBS, 2.5 mM L-glutamine and 1x Penicillin-Streptomycin (i.e. full DMEM) [h] as the cells no longer required such a high amount of FBS or such a strong antibiotic-antimycotic solution.

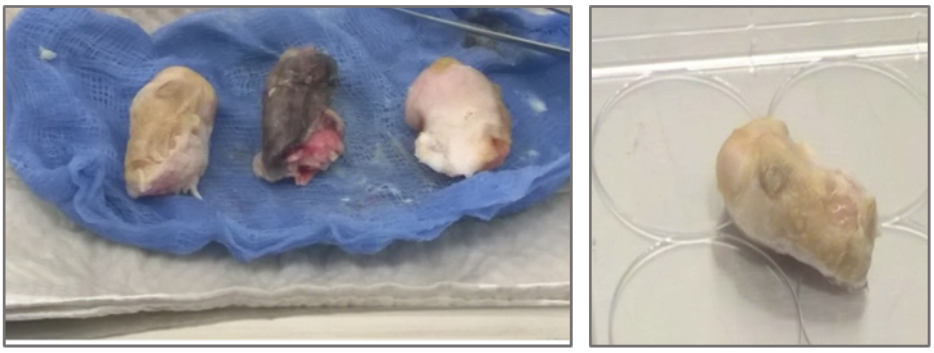
To isolate the fibroblasts enzymatic digestion of the dermis was chosen as the preferred method - as opposed to outgrowth of fibroblasts from explanted tissue pieces - because this method is much faster and yields higher recovery of cells from the skin sample. Also, as many tissue samples came from elderly people who were diabetic or had a non-healing ulcer (see donor demography in supplementary data 3.4.1), there was a risk that fibroblast motility might be impaired and as such have reduced ability to migrate out of the skin and adhere to the surface of the culture vessel (a process that needs to happen during the outgrowth procedure). Once the primary cell populations were isolated from the biological samples all cells were grown in incubators maintained at 37°C in normoxic atmosphere with 5% CO_2 and 95% humidity. The standard protocols for subculturing were followed (supplementary data 3.4.4 and 3.4.5) and the cells were regularly tested for mycoplasma contamination (supplementary data 3.4.2) – either by myself or by the departmental TC lab technician Kosta Rolev.

[h] The Penicillin-Streptomycin stock solution (100x) contained 10,000 units penicillin and 10 mg streptomycin/mL.

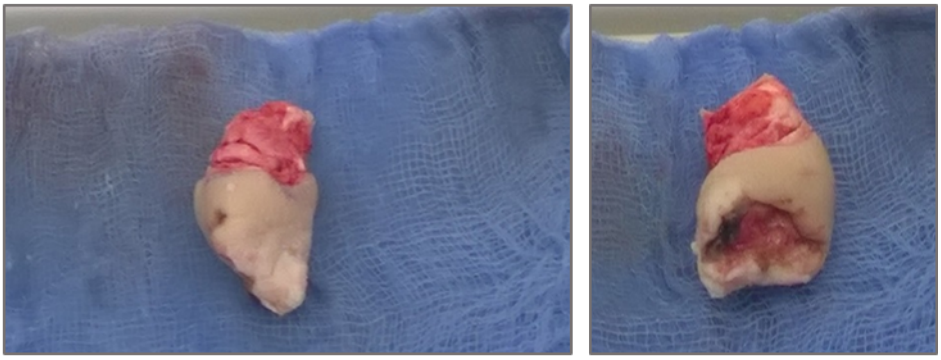
NDT20170207 – nondiabetic forefoot



NDT20161129 – nondiabetic toes



DT20170126 – diabetic toe with non-healing ulcer



DT20170328 – ulcerated diabetic toes



Figure 37: representative images of amputated human biological tissues used for isolation of primary skin cells. The tissues are nondiabetic non-ulcerated, diabetic ulcerated or diabetic non-ulcerated

Processing of amputated tissues

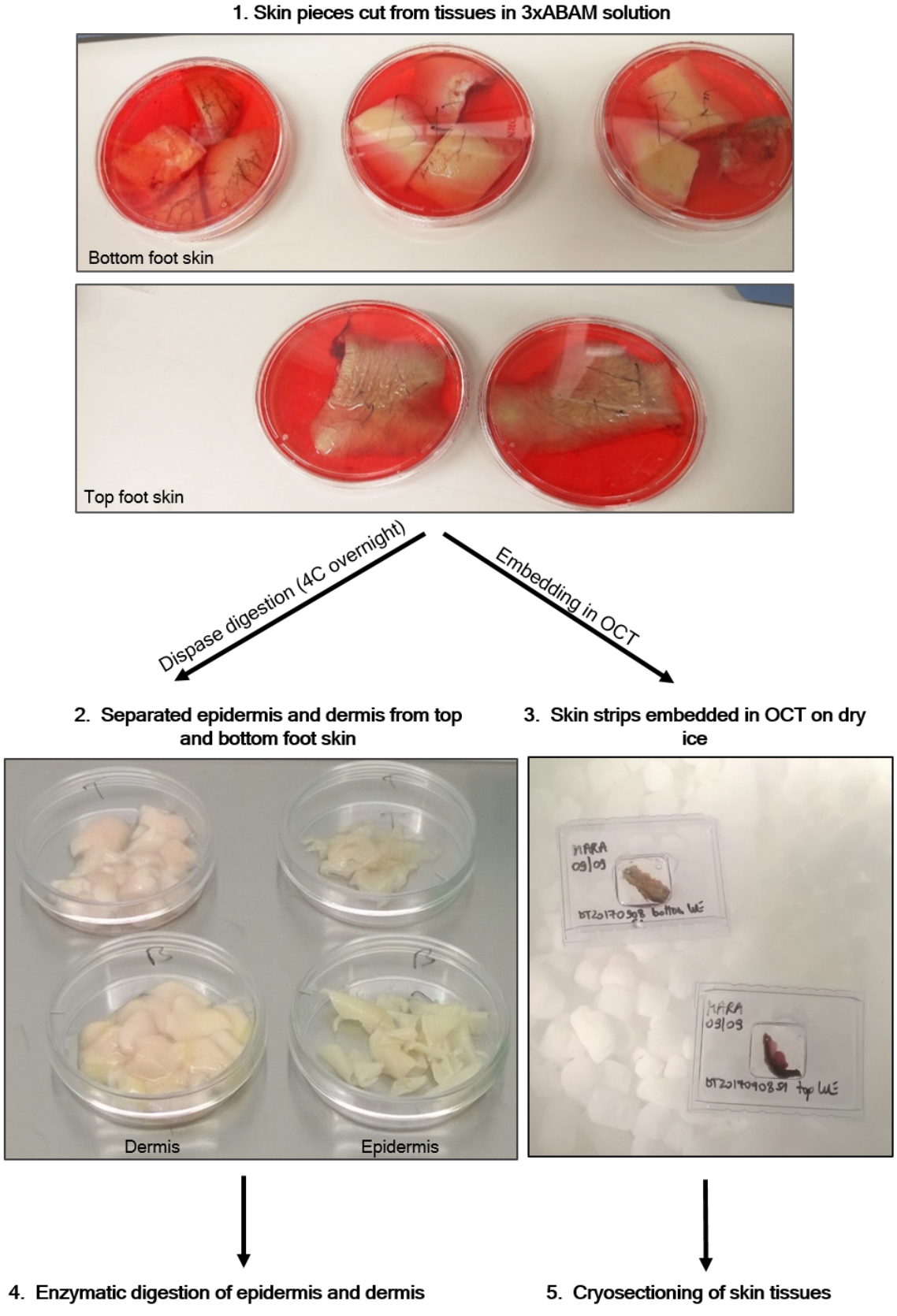


Figure 38: skin pieces cut from amputated limbs are kept in strong antibiotic solutions prior to being subjected to dispase digestion to isolate the epidermis from the dermis or being embedded in OCT for cryosectioning

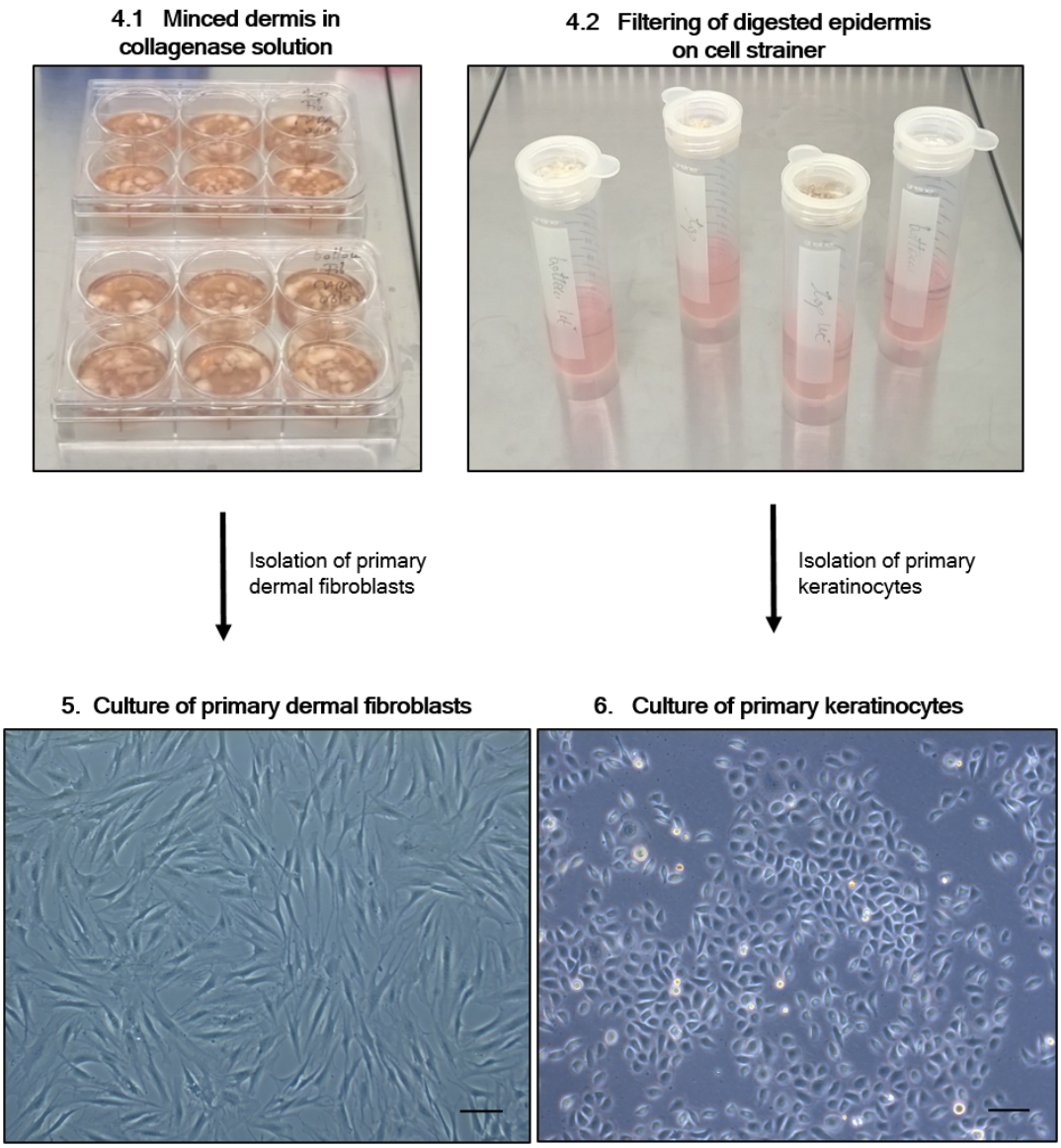


Figure 39: after dispase separates the dermis from the epidermis primary fibroblasts and keratinocytes are isolated via enzymatic digestion involving collagenase I and trypsin-EDTA, respectively. Scale bars are 200 µm.

At all points during the processing of the tissues the top and bottom skin were kept separate (Figure 38 – step 1) to allow distinguishing between the plantar skin (from the bottom of foot) and non-plantar skin (top foot) as fibroblasts were shown to display 'positional identity', displaying distinct characteristic phenotypes – a phenomenon known as topographic differentiation - depending on the anatomical location on the body they were isolated from [171,172]. These gene expression profiling studies found marked differences in gene expression related to positional identity, cell fate determination, cell migration and ECM synthesis and remodelling, showing that distinguishing between the anatomical sites of isolation is very important when studying fibroblast behaviour.

Fibroblasts, however have been further shown to display heterogeneity within the dermis from the same isolation site. This is because the dermis hosts several fibroblast populations, namely the papillary fibroblasts residing in the papillary dermis, the reticular fibroblasts found in the reticular dermis and those associated with hair follicles – the dermal papilla and dermal sheath fibroblasts [173] (Figure 40). These fibroblast subpopulations can be morphologically and physiologically distinct, exhibiting different rates of growth and cellular markers, as well as distinct patterns of growth factor and cytokine secretion and ECM components, reflecting the different roles they play in skin homeostasis and during cutaneous injury [174,175]. In fact the local environment these different fibroblast subtypes reside in is also different, with the papillary and reticular dermis displaying different structural composition as shown by an H&E stained skin section of one of our amputated nondiabetic tissue samples (Figure 41). For instance, the papillary dermis is superficial, contains more cells (blue dots) than the reticular dermis and consists of thin collagen fibres that are loosely connected, whereas the reticular dermis is thick, is mainly acellular and contains a dense meshwork of thick collagen fibres.

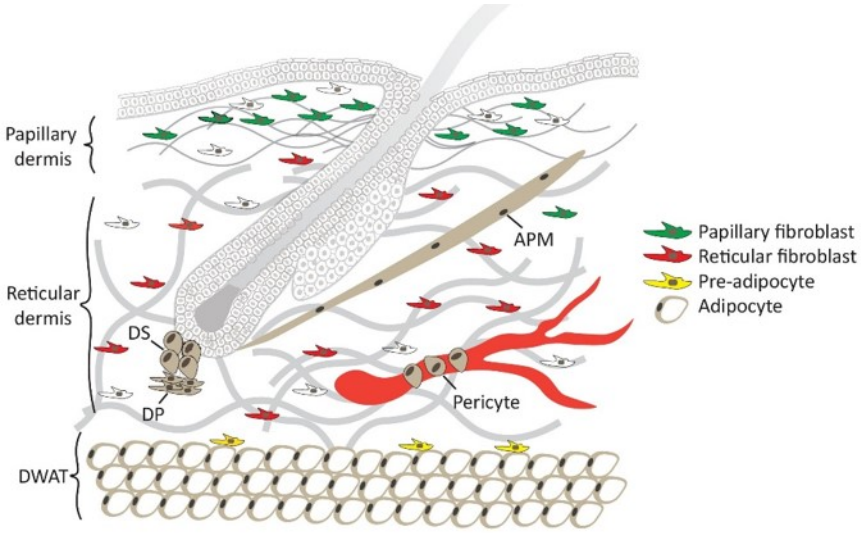


Figure 40: the dermis consists of papillary dermis, reticular dermis and Dermal White Adipose Tissue (DWAT) and contains distinct fibroblast subpopulations including papillary, reticular, dermal papilla and dermal sheath fibroblasts. These fibroblast populations can be morphologically and physiologically distinct, exhibiting different rates of growth, cellular markers and cytokine secretion, and play distinct roles during homeostasis and wound healing. Abbreviations: DS (dermal sheath), DP (dermal papilla), APM (arrector piri muscle). Image reprinted from [176] and reproduced under a Creative Commons CC-BY Licence

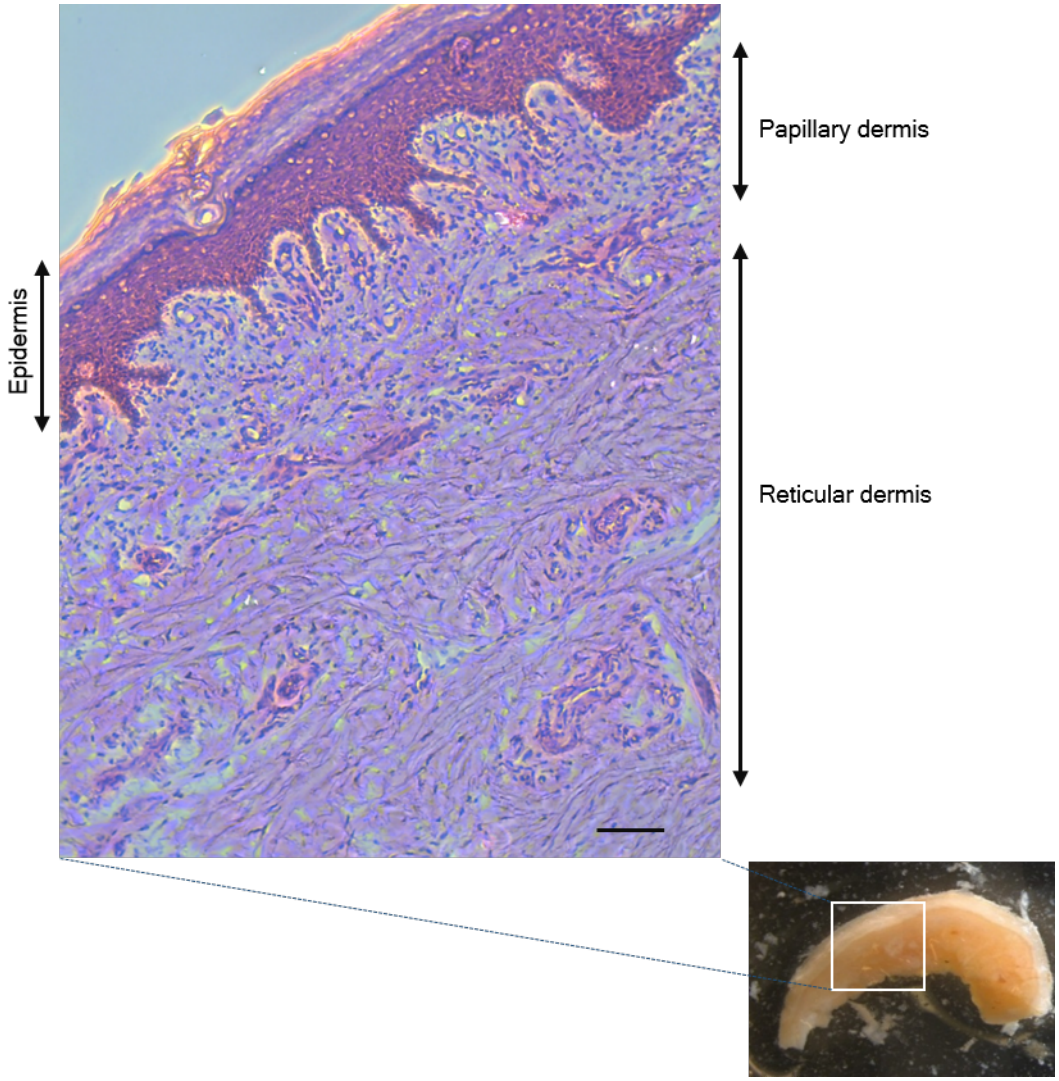


Figure 41: H&E stained skin from a nondiabetic bottom foot amputated tissue clearly shows the epidermis, papillary dermis and reticular dermis and identifies the structural differences between these. The papillary dermis contains more cells (blue dots) and thinner collagen fibres than the reticular dermis which is mainly acellular and contains dense collagen fibres. For H&E staining 16 µm thick sections were cut with the cryostat from the frozen skin tissue embedded in OCT and adsorbed onto SuperFrost glass slides. Skin sections were visualised with the light microscope. Scale bar: 100 µm

As collagenase type I was used during the processing of the biological samples for enzymatic digestion of the dermis, the isolated dermal fibroblasts were most likely a heterogenous mixture of papillary and reticular fibroblasts, but no hair follicle associated fibroblasts (as follicular fibroblasts cannot be enzymatically digested using standard protocols). Although the exact ratio of papillary: reticular fibroblasts was never determined in the isolated fibroblast populations, it was shown by Dr Helena Topouzi (post-doctoral researcher in Dr Claire Higgins' lab at Imperial College London) that during routine subculturing the papillary fibroblasts tend to take over the cell population due to their increased proliferation rate, with

>70% of the population being papillary fibroblasts. As such, for all intent and purposes, it can be assumed that the fibroblasts used in all experiments were most likely papillary fibroblasts.

Furthermore, as the enzymatic digestion of the dermis might allow for other cell types that reside within the dermis to attach to the culture flasks, i.e. macrophages or endothelial cells from microvasculature I verified that the fibroblast culture was 'clean' and devoid of other cell types. For this purpose primary fibroblast cultures were immunostained for vimentin – an intermediate filament that is expressed in mesenchymal cells – and collagen I – an ECM component that is expressed and synthesised primarily by fibroblasts [i]. The staining showed the nuclear signal overlaid with the Collagen I/Vimentin staining in all imaged cells (Figure 42), while the negative control showed no expression of Collagen I or Vimentin (supplementary data 3.4.3). This confirmed the fibroblast cell culture was clean and that the isolated fibroblasts expressed their identity.

[i] Although other cell types, such as podocytes (found in kidneys) and Leydig cells (found in testis) were shown to be capable of producing collagen I in a reporter mouse [226] these cells do not reside in the skin, which means that the cells stained for collagen I in the skin samples must be fibroblasts.

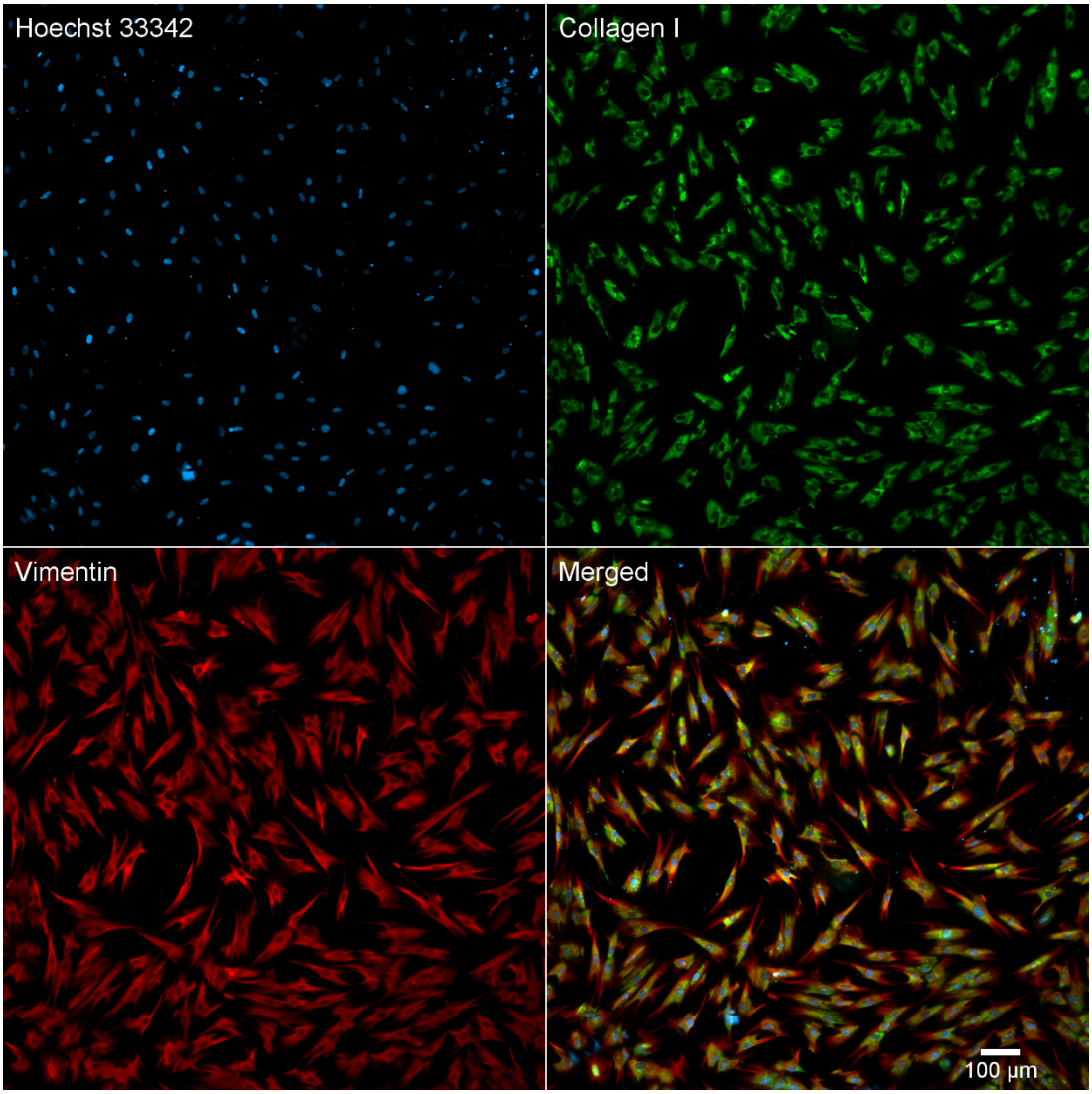


Figure 42: immunostaining of the isolated fibroblast populations shows the cells express both vimentin (red) and collagen I (green), markers of fibroblasts. The nuclear staining (blue) overlays with the collagen I/vimentin staining in all cells, confirming the cell culture is 'clean'. Incubation with primary antibodies against vimentin (raised in chicken, 1:200) and against collagen I (raised in rabbit, 1:400) occurred in 5% goat serum in PBS overnight at 4°C. Incubation with secondary antibodies included goat anti-chicken 633 (1:200) and goat anti-rabbit 488 (1:200) in PBS for 1h at room temperature in the dark. Cells incubated with the secondary antibodies only served as the negative control.

3.2. Characterisation of the isolated primary fibroblasts

3.2.1. Growth rate and doubling times

Once the fibroblasts were isolated from the amputated skin samples and expanded in culture, I proceeded to characterise their behaviour *in vitro*.

First, I determined the growth rate and the doubling time of the isolated primary fibroblasts to get an idea of how fast they grow and how many passages they can be used for throughout experiments. Primary cells are taken directly from living tissue and are representative of the in vivo state, but unlike (immortalised) cell lines they have a limited lifespan being able to undergo a certain number of passaging before becoming senescent.

Primary fibroblasts from two nondiabetic donors were seeded in 96-well plates and the cell number was counted every day over a period of 9 days. This testing revealed that the cell growth followed the characteristic sigmoidal shape, starting with a slow lag phase, followed by the log phase denoting exponential growth rate and the plateau denoting the stationary phase (Figure 43). In this case the fibroblasts started the log phase at ~3,000 cells/well or ~9,000/cm^2, which showed that this is the minimal density at which they should be seeded for experiments to ensure the cells are in the active growth phase. It is important that the cells are actively growing during experiments as in this way any stimulatory effect should have an effect and allow comparisons amongst different conditions and donors.

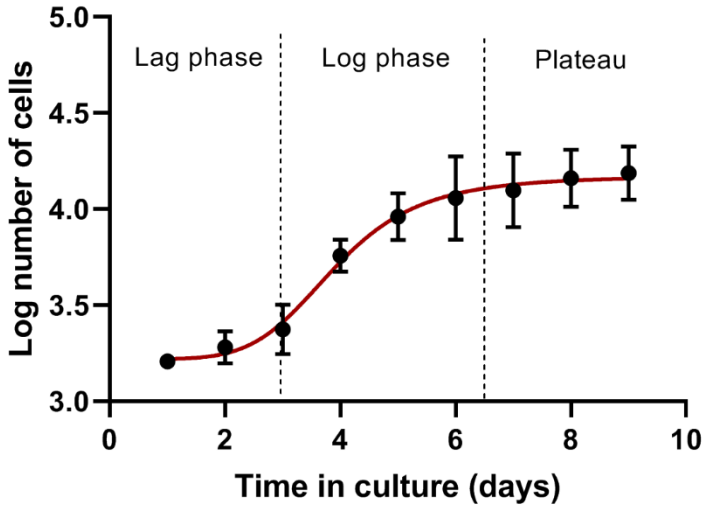


Figure 43: the isolated fibroblasts (nondiabetic) display the characteristic sigmoidal growth curve in culture consisting of the lag phase, log phase and plateau. To obtain the growth curve nondiabetic fibroblasts were seeded at 1,600 cells/well in a 96-well plate in full DMEM medium. Each day the cells were trypsinised from one column on

the well plate at a time (representing each day of growth) and their cell number was counted with the haemocytometer. Nonlinear regression was used to fit the sigmoidal curve to the data points. Data points are plotted as mean ± SD. N=2, n=6/donor.

Second, I monitored the doubling time of the fibroblasts over several passages. For this cells from three nondiabetic donors were seeded at 8,000 cells/cm^2 in culture flasks and their number counted when they reached 90-95% confluency. As the cells were in the log phase at this seeding density according to the growth curve (Figure 43), the following formula could be used to determine their doubling time:

$$t_{doubling} = \frac{ln2 * \Delta t}{\ln(\frac{N_t}{N_0})}$$

, where N_t = number of cells at time t, N_0 = number of cells at t0 and Δt= time in days.

This testing showed the average doubling time of the cells is ~2.5 days throughout to P7, whereas it increases slightly to ~3 days at P8 (Figure 44). As such, all the experiments from now on were done with fibroblasts at P3-7, being confident that they are still actively proliferating and haven't reached senescence.

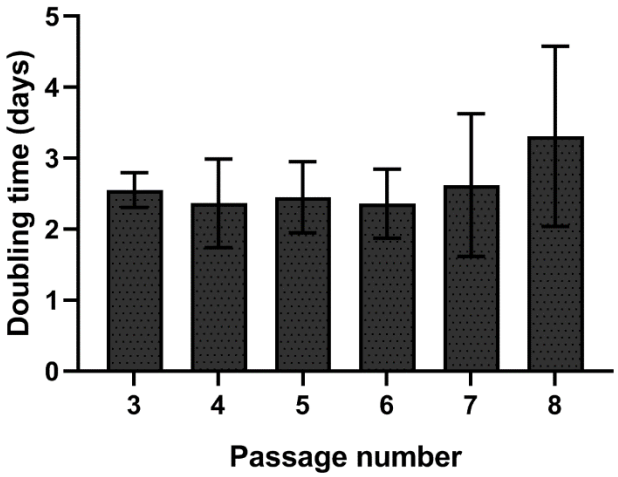


Figure 44: the isolated fibroblasts (nondiabetic) have a doubling time ~2.5 days that gets maintained across many passages. To obtain the doubling time the cells were seeded at 8,000 cells/cm^2 in culture flasks and their number was counted when the cells reached 90-95% confluency. Data is plotted as mean ± SD. N=3

3.2.2. Response to growth factor stimulation

Lastly, I checked that the isolated fibroblasts displayed functional behaviour *in vitro* by measuring their proliferative response to GF stimulation. For this, nondiabetic fibroblasts were stimulated in 0.1% FBS with PDGF-BB, a potent mitogenic GF for cells of mesenchymal origin such as fibroblasts and proliferation was measured 2 days later via Presto Blue.

Presto Blue is a dye that relies on the metabolic activity of cells to measure cell viability. Upon entering a living cell, Presto Blue reagent is reduced from resazurin, a blue compound with no intrinsic fluorescence to resorufin which is red in colour and highly fluorescent. This conversion is proportional to the number of metabolically active cells, allowing cell proliferation to be determined in a linear fashion (Figure 45 top). The results showed the primary fibroblasts responded to PDGF-BB in a dosage-dependent manner, reaching ~60% increase in proliferation at 100 ng/mL PDGF-BB compared to unstimulated fibroblasts (Figure 45 bottom), and thus behaved as expected.

Overall these characterisation studies showed the isolated primary fibroblasts were *bona fide* fibroblasts that displayed characteristic morphology and functional behaviour and hence could be reliably used for the experimental testing of the miRNA combination.

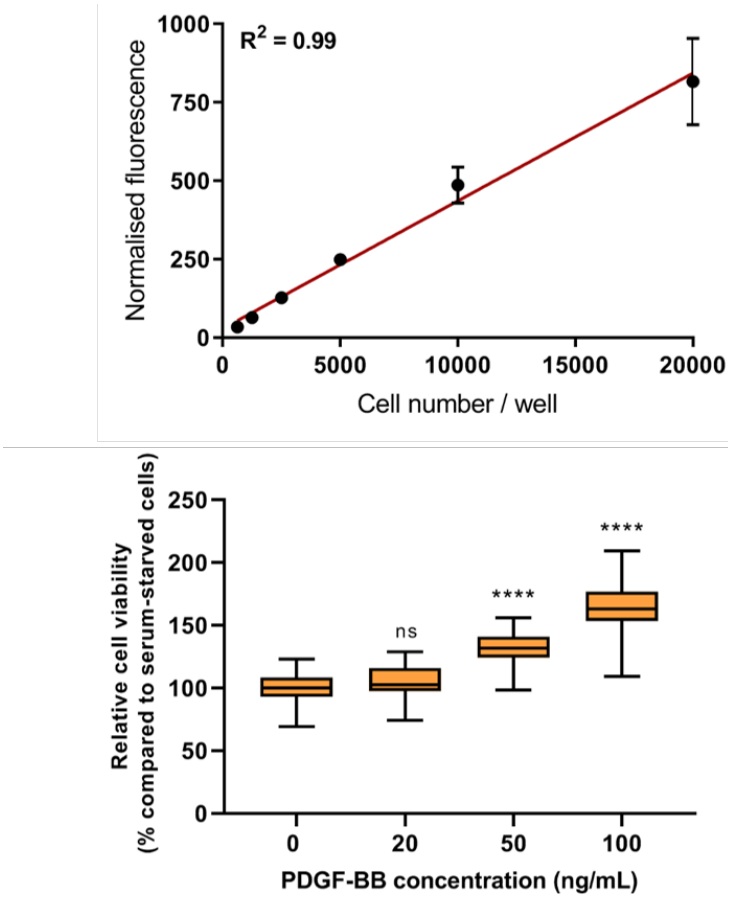


Figure 45: (Top) Presto Blue measures proliferation in a linear manner. To obtain the standard curve 1:2 serial dilutions of fibroblasts were generated in a range of 625-10,000 cells/well in a 96-well plate, followed by incubation with Presto Blue (1:10 dilution) for 1h at 37°C. Data points are plotted as mean ± SD; (Bottom) PDGF-BB stimulation in a concentration range of 20-100 ng/mL has a dosage-dependent proliferative effect on nondiabetic fibroblast populations cells as measured via Presto Blue 48h post-stimulation. Prior to stimulation with PDGF-BB cells were serum-starved in 0.1% FBS for 24h. Box & whiskers plot span min to max. Analysis of statistical significance was performed via one-way ANOVA, followed by posthoc Dunnett's multiple comparisons test. **** $p<0.0001$. N=4, n=8/donor

3.3. Methods

3.3.1. H&E staining of skin samples

Frozen skin sections embedded in OCT were cut with the cryostat 16 μm thick and adsorbed onto SuperFrost glass slides. H&E staining was used to show the structure of the resulting skin tissue. Briefly, the skin tissues were re-hydrated in ethanol of decreasing strengths (100%, 95% and 70%), stained with Hematoxylin Harris, differentiated in 1% acid alcohol once, stained with diluted Eosin Y, followed by de-hydration in ethanol of increasing strengths (70%, 95% and 100%) and mounting with DPX mounting medium (for detailed protocol for H&E staining see supplementary data 3.4.6).

3.3.2. Obtaining the growth curve of fibroblasts

Nondiabetic fibroblasts were seeded at 1,600 cells/well in a 96-well plate in full DMEM medium. Each day the cells were trypsinised and their cell number counted for 9 days in a row. Nonlinear regression was used to fit the sigmoidal curve to the data points.

3.3.3. Generating the Presto Blue calibration curve with fibroblasts

To obtain the calibration curve of Presto Blue 1:2 serial dilutions of fibroblast cells were generated in a range of 625-10,000 cells/well in a 96-well plate, followed by incubation with Presto Blue in a 1:9 ratio (10 μL Presto Blue + 90 μL full DMEM/well) for 1h at 37°C. Fluorescence was measured with the Varioskan Flash plate reader at 560 nm excitation and 590 nm emission. Wells containing DMEM only were used to obtain the background values, which were subtracted from all experimental values to obtain the normalised fluorescence values. Linear regression analysis was done to obtain the R^2 value.

3.3.4. Growth factor stimulation of fibroblast populations

Fibroblasts were seeded at 7,000 cells/well in antibiotic-free DMEM (supplemented with 10% FBS and 2.5 mM L-glutamine) and left to adhere overnight. The following day the cells were washed three times with PBS (200 μL/well) and serum-starved in 0.1% FBS for 24h. The cells were then stimulated with PDGF-BB in a range of 20-100 ng/mL, respectively for 48h. Proliferation was measured via Presto Blue (1h incubation at 37°C) and the fold change in proliferation was calculated relative to serum-starved cells.

3.3.5. Immunostaining of fibroblast populations with collagen I and vimentin

Primary nondiabetic fibroblasts isolated from amputated tissues were seeded at 50,000 or 100,000 cells/cover slip in 6-well plate in full DMEM and left to adhere overnight. The following day the cells were stained with Hoechst 33342 (7 min at room temperature) and fixed in 4% PFA (10 min at room temperature). Following 3 washes in PBS the cells were permeabilised in 5% goat serum in 0.3% Triton-X in PBS (30 min at room temperature) to block any non-specific binding. The cover slips were then incubated with primary antibodies against vimentin (raised in chicken, 1:200) and against collagen I (raised in rabbit, 1:400) in 5% goat serum in PBS (overnight at 4°C). The following day the cover slips were washed in 0.1% Triton-X in PBS three times and incubated with the secondary antibodies goat anti-chicken 633 (1:200) and goat anti-rabbit 488 (1:200) in PBS (1h at room temperature in the dark). Following three final washes in PBS the cover slips were mounted onto microscope slides using Vectashield mounting medium. The cells were imaged with the Inverted Widefield Zeiss Axio Observer microscope in the three channels: DAPI, Alexa 488 and Alexa 633. Cells incubated with the secondary antibodies only served as the negative control. The images were subsequently processed in FIJI.

3.3.6. Statistical analysis and graph generation

All statistical analysis was done in GraphPad Prism (Version 7 and 8). All graphs showing experimental data were plotted in GraphPad Prism (Version 7 and 8).

3.4. Supplementary data

3.4.1. Donor demography

Type of tissue	Code	Age	Sex	Reason for amputation
Nondiabetic non-ulcerated	NDT20161129	66 yrs	M	Toes from below knee amputation due to occlusive arterial disease
	NDT20170207	49 yrs	F	Forefoot from above knee amputation due to chronic pain caused by damaged lymph nodes
	NDT20171026S1		M	Forefoot from below knee amputation due to traumatic injury
	NDT20180710	47 yrs		Forefoot amputated due to traumatic injury
Diabetic ulcerated	DT20170126	72 yrs	M	Toes with diabetic nonhealing ulcer, suspected osteomyelitis
	DT20170209	70 yrs	M	Toes with infected DFU
	DT20170328	56 yrs	M	Ulcerated diabetic toes
	DT20171110			Nonhealing chronic leg ulcer
Diabetic non-ulcerated	DT20170316	74 yrs	M	Nonulcerated necrotic diabetic toes
	DT20170126	72 yrs	M	Toes with diabetic nonhealing ulcer, suspected osteomyelitis - tissue isolated away from wound edge
	DT20170328	56 yrs	M	Ulcerated diabetic toes - tissue isolated away from wound edge

Table 10: demography of the amputated tissue samples shows that most of the donors are male and elderly. Mean age: 62±10 years. Some of the information is missing.

3.4.2. Mycoplasma testing

Mycoplasmas are tiny bacteria that can alter DNA, RNA and protein synthesis, introduce chromosomal alterations and change the expression of hundreds of genes, potentially biasing experimental results. As they lack a cell wall they are resistant to antibiotics, such as Penicillin-Streptomycin that is commonly added to the cell culture media. Contamination by mycoplasmas can go undetected for long periods of time as it cannot be visualised neither by the naked eye - due to the lack of medium turbidity typically produced by bacterial and fungal contamination nor by optical microscopy - due to their tiny size (~100nm).

The presence of mycoplasmas was tested via PCR using the PCR mycoplasma test kit II which detects the presence of mycoplasma 16s ribosomal RNA with high sensitivity and specificity. For PCR 3-4 day old supernatant from 90% confluent T75 flasks from various donors was collected and the test was run according to the manufacturer's protocol. Briefly, the supernatant was centrifuged at 15,000xg for 10 min to sediment any mycoplasma present, followed by re-suspension of the pellet in buffer and heat inactivation at 95°C. Next, PCR was performed on the samples, including positive and negative controls and the amplified fragments were detected by agarose gel electrophoresis.

All tested samples came out negative as the DNA bands aligned with the negative controls and not the positive controls (Figure 46), thus confirming the isolated fibroblast populations were not contaminated by mycoplasma.

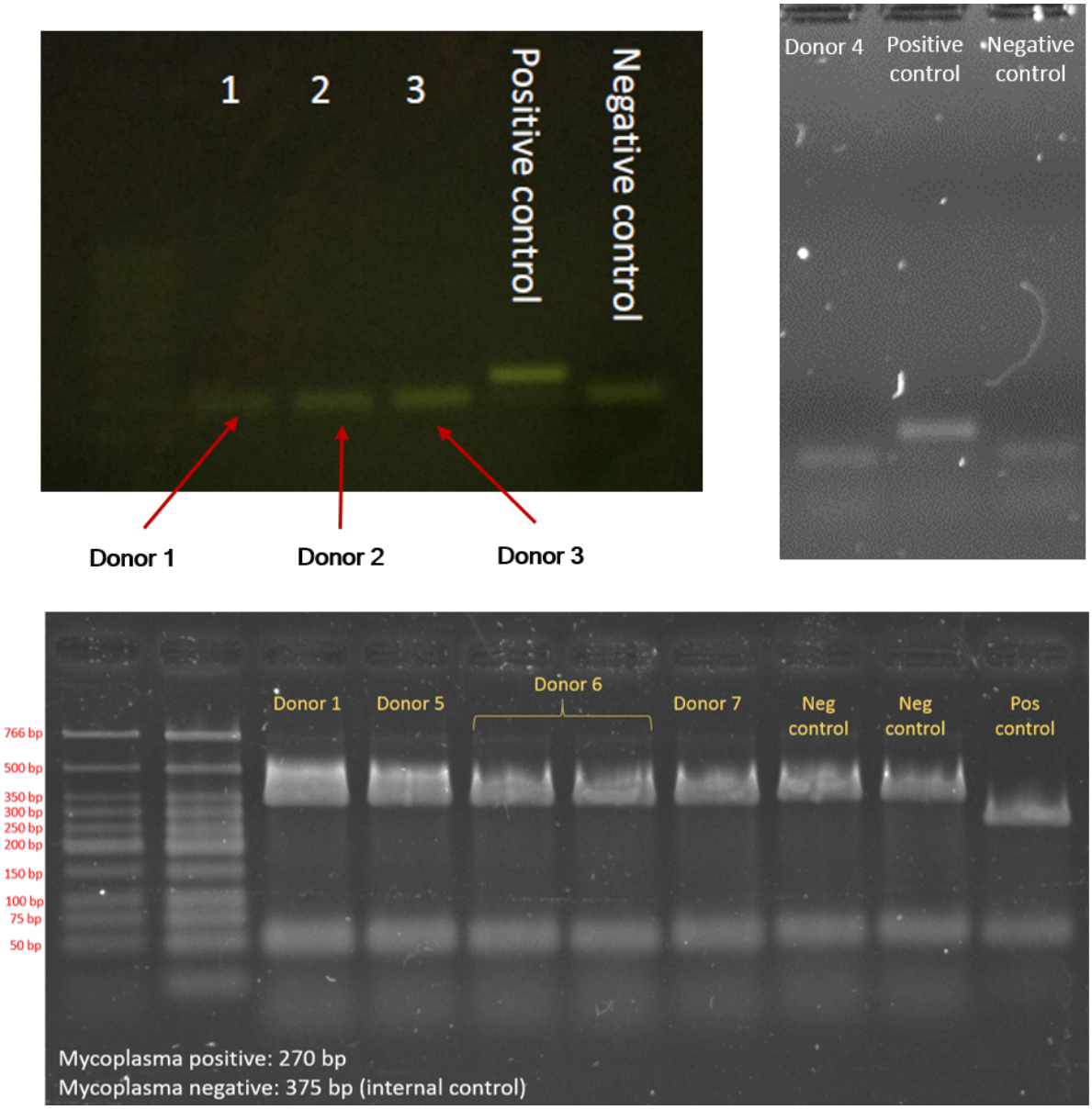


Figure 46: all fibroblast populations tested for mycoplasma contamination by PCR are negative as all DNA bands align with the negative controls and not the positive control. Bands were detected by agarose gel electrophoresis. For PCR 3-4 day old supernatant from 90% confluent T75 flasks was collected from various donors.

3.4.3. Immunostaining of fibroblasts cell populations with collagen I and vimentin for the negative control

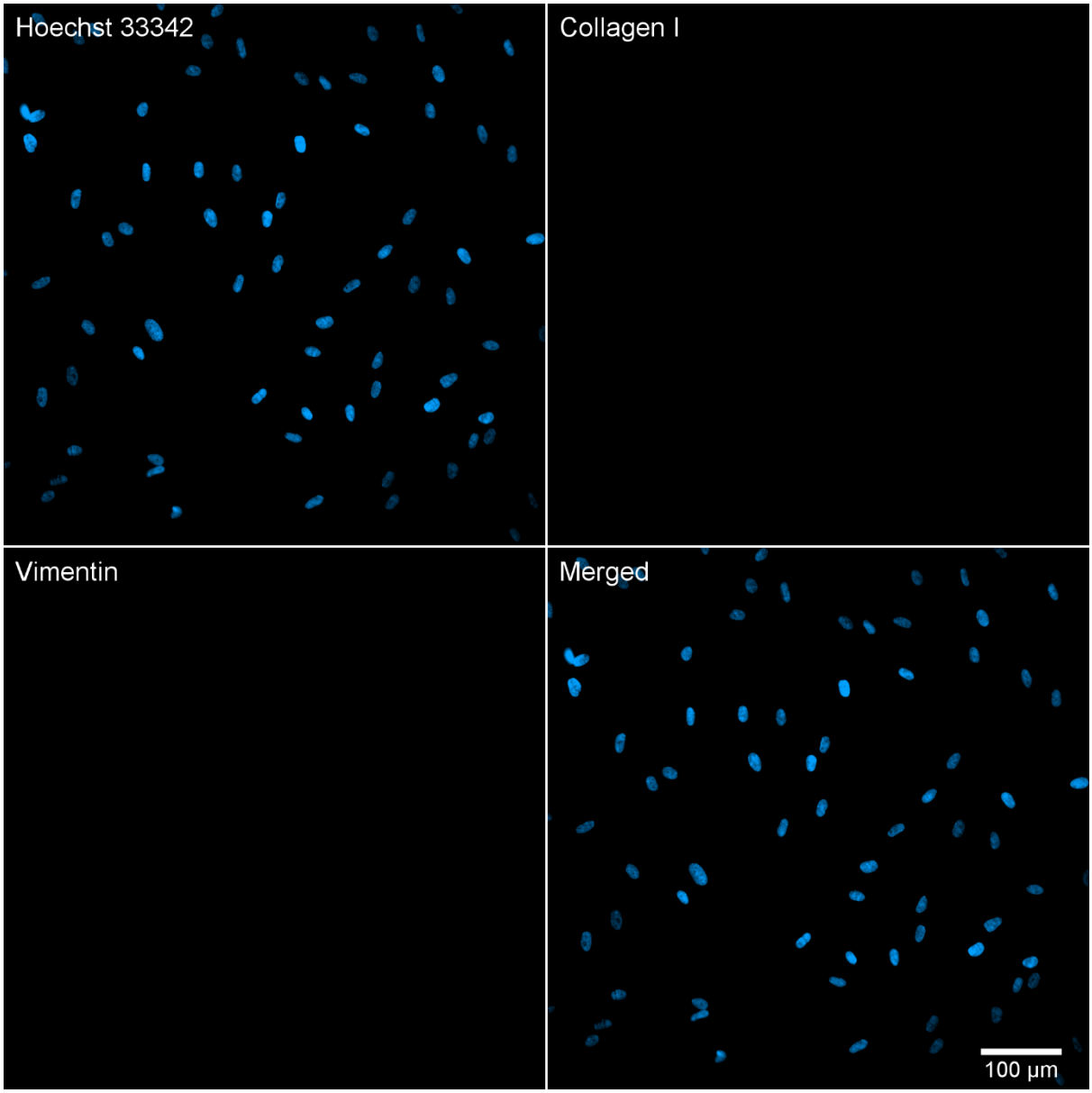


Figure 47: the negative control used during the immunostaining of the fibroblasts shows no sign of vimentin or collagen I expression, hence confirming the positive signal observed in the immunostained fibroblasts containing the primary and secondary antibodies is true

3.4.4. Protocol for culturing primary fibroblasts

Subculturing:

- Check cells under the microscope for contamination, colour change of medium etc.
- Aspirate the medium and wash the cells twice with 5 mL PBS (T25) or 10 mL PBS (T75).
- Add 1 mL trypsin-EDTA (T25) or 2 mL (T75) to the flask for 5 min at 37°C until the cells have detached.
- Inhibit the trypsin with 4 mL DMEM medium (T25) or 8 mL (T75) and re-suspend up and down 5 times. Transfer the cell suspension into a Falcon tube.
- Place the tube into the centrifuge and spin at 1400 rpm for 5 min around 20°C – make sure to balance the centrifuge with another tube of the same volume.
- Aspirate the supernatant carefully making sure not to dislodge the cell pellet.
- Re-suspend the cell pellet in 2-4 mL medium until the cell pellet is disrupted (go up and down ca. 20 times with the pipette tip).
- Count the cells twice by removing 10 µL of cell suspension for the haemocytometer.
- Split the cells in the appropriate ratio (1:2 to 1:4) for subculturing or use immediately for assays. When seeding the cells for expansion seed them at 4,000-5,000 cells/cm^2.
- Feed the cells every 3-4 days by removing the medium and replacing with fresh medium: 5 mL for T25 or 10 mL for T75.

Freezing:

- Obtain the cell pellet as described above.
- Resuspend the cell pellet in freezing medium (90% FBS + 10% DMSO) and add 1 mL of cell suspension into each cryovial.
- Place the cryovials into 'Mr Frosty' that has warmed up to room temperature and place it into -80°C freezer.
- Transfer the cryovials into the -140°C freezer the next day for long-term storage.

Thawing:

- When thawing the cells, hold the cryovial into a beaker with warm water, gently shaking it until the cells defrost to allow rapid thawing.
- Pipet the cell suspension dropwise into 9 mL of pre-warmed DMEM medium while gently shaking the Falcon tube.
- Centrifuge the cells at 1400 rpm for 5 min and aspirate the supernatant to remove the DMSO. Resuspend the cells in fresh DMEM and seed the cells at 5,000/cm^2.

3.4.5. Protocol for culturing primary keratinocytes

Subculturing:

- Coat the flask with diluted coating matrix:
    - T25: 1.7 mL dilution medium + 17 µL coating matrix (100:1)
    - T75: 5 mL dilution medium + 50 µL coating matrix (100:1)
- Ensure the entire bottom surface of the flask is covered and leave to settle for 30 min at room temperature. When the time is up, aspirate the medium. The coated flasks can be used immediately or stored in the fridge for up to 1 week.
- Aspirate the Epilife medium from the flask.
- Add 1 mL TryplE (T25 flask) or 2 mL TryplE (T75 flask) and incubate at 37°C for 5-10 min until the keratinocytes have detached.
- Dilute the TryplE in 4 mL Epilife (T25 flask) or 8 mL Epilife (T75) by mixing up and down 5-6 times *.
- Transfer the cell suspension into a Falcon tube.
- Centrifuge at 300xg for 4 min at ca. 20°C.
- Remove the supernatant and resuspend the cell pellet 50 times with a 1000 µL pipette tip.
- Count the cells with the haemocytometer using 10 µL of cell suspension.
- Split the cells at 7,000-8,000 cells/cm^2. Feed the keratinocytes every 2-3 days.
- Split the cells again when they start touching to avoid differentiation.

*To detach the keratinocytes Trypsin-EDTA can also be used, but in this case DTI must be used to inhibit the effects of trypsin in a 1:1 ratio following cell detachment.

Freezing:

- Obtain the cell pellet as described above.
- Resuspend the cell pellet in freezing medium (Synth-a-Freeze) and add 1 mL of cell suspension into each cryovial.
- Place the cryovials into 'Mr Frosty' that has warmed up to room temperature and place it into -80°C freezer.
- Transfer the cryovials into the -140°C freezer the next day for long-term storage.

3.4.6. Protocol for H&E staining of skin samples

Step 1: Re-hydrate in alcohol to help with adhesion of the aqueous stains

- 100% ethanol, 2 changes (2 min each)
- 95% ethanol, 1 change (2 min)
- 70% ethanol, 1 change (2 min)

Step 2: Stain with Harris Hematoxylin solution (8 min)

- Wash off excess solution with distilled water

Step 3: Differentiate in 1% acid alcohol once (1 min)

- Wash off with distilled water

Step 4: Stain with 2:3 diluted Eosin Y solution (1 min)

- Wash off excess with distilled water

Step 5: De-hydrate in alcohol as mounting medium as hydrophobic

- 70% ethanol, 1 change (2 min)
- 95% ethanol, 1 change (2 min)
- 100% ethanol, 1 change (2 min)

Step 6: Mount with DPX mounting medium (1 drop/cover slip)

- Allow the slide to dry in the fume hood

Step 7: Image the H&E stained skin tissue with the light microscope

4. Testing the differentially expressed miRNAs for cooperative effects *in vitro*

Following the bioinformatics analysis on DE miRNAs in DFU fibroblasts vs healthy normal fibroblasts and the isolation of *bona fide* primary fibroblasts the next step was to experimentally validate the hypothesis that miR-181a, miR-27a and miR-30a work together as a network at the pathway level to disrupt cell signalling important for wound healing (Chapter 2). This involved a) transfecting mimics of miRs-181a, -27a and -30a into nondiabetic fibroblasts to over-express their levels, thus mimicking the phenotype of DFU fibroblasts according to the NanoStringDiff analysis, b) looking for synergy at the pathway level via proliferation assays and c) investigating the biological impact of the individual and combinatorial dysregulation of these miRNAs in the context of diabetic wound healing.

4.1. Purchase and characterisation of the miRNA mimics

Human miRIDIAN microRNA mimics of the three miRNAs to be transfected, miR-181a-5p, miR-30a-5p and miR-27a-3p were purchased from Dharmacon (Table 11). These synthetic mimics are double-stranded oligonucleotides designed to mimic the function of endogenous mature miRNAs to facilitate gain-of-function studies (Figure 48). MiRIDIAN miRNA mimics are chemically enhanced to preferentially program RISC with the active miRNA strand, thereby maximising the chance of RISC loading. Once loaded RISC binds to the 3'UTR of the target mRNAs to maintain low endogenous protein level, thus augmenting the function of endogenous miRNAs to further decrease protein levels. This not only facilitates easier detection of the miRNA effects on a target gene, but further allows miRNA mimics to induce a specific phenotype. As miRNA mimics cause the miRNA of interest to become over-expressed, their gain-of-function effect is best observed in cells with low endogenous miRNA levels.

To ensure the effects observed with the miRNA mimics are specific and aren't simply caused by the presence of exogenous miRNA in the cells, a miRNA mimic negative control based on C. elegans miRNA sequence was used for normalisation (e.g. scramble miRNA). This miRNA, cel-miR-67 has been chemically modified in the same way as the miRIDIAN microRNA mimics and confirmed by the manufacturers to have minimal sequence identity with miRNAs

in human, rat or mouse thus minimising off-target effects. To further confirm transfection of miRNA mimics is successful and they become functional following delivery two miRNA mimic positive controls were purchased: 1) miRIDIAN miR mimic transfection control with Dy547, a non-targeting miRNA mimic based on the C. elegans cel-miR67 labelled with Dy547 (absorbance/emission max: 557/570 nm) was used to check the distribution of the miRNA throughout the cell and 2) miR mimic positive control against the housekeeping gene GAPDH was used to validate this gene was indeed getting knocked down and hence the transfection method was working.

All miRNA mimics were received from the supplier in lyophilised form. These were subsequently resuspended in 1x siRNA buffer at 100 µM final concentration, aliquoted and stored at -20°C for long-term storage.

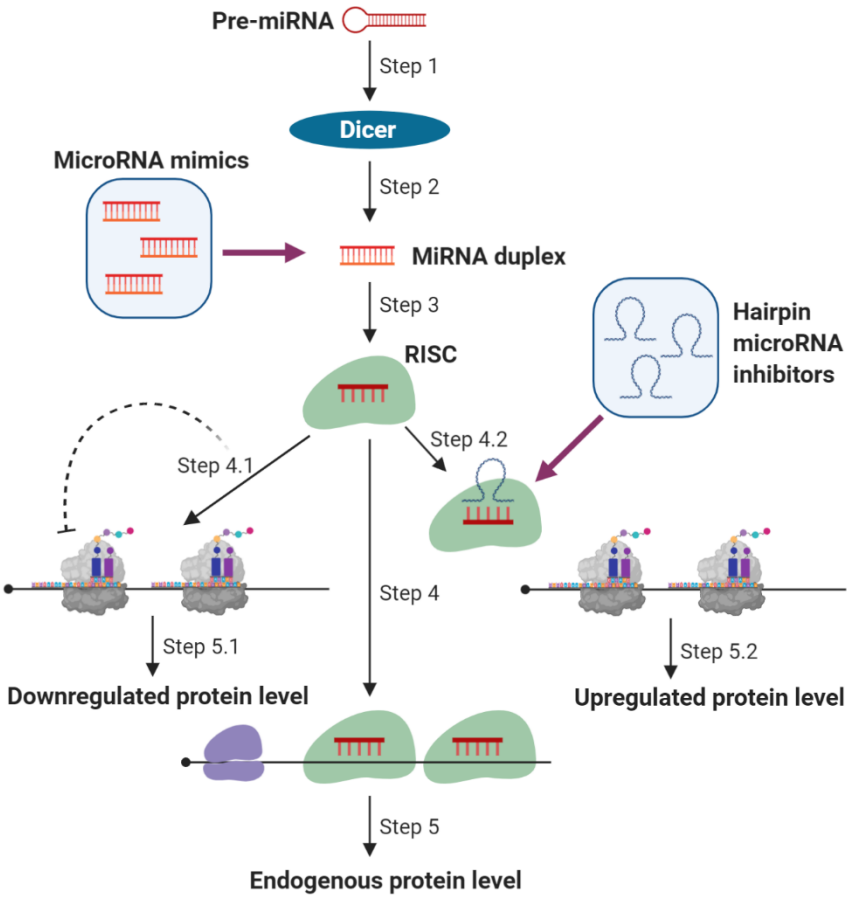


Figure 48: miRNA mimics and inhibitors augment or attenuate the effect of endogenous miRNAs. Steps 1&2 describe the formation of mature miRNA duplexes after the pre-miRNA is exported into the cytoplasm. Once miRNA duplexes are loaded into RISC, the inactive strand becomes cleaved resulting in the formation of programmed RISC (step 3). This binds to the 3'UTR of a target mRNA (step 4) to suppress gene expression (step 5). MiRNA

mimics of mature miRNAs increase the expression level of miRNAs to further downregulate protein levels (Step 4.1). MiRNA inhibitors bind to the endogenous miRNAs and prevent them from binding to the target mRNAs, thus upregulating protein levels (Step 5.2). Figure created with BioRender.com and exported under a paid subscription.

miRIDIAN microRNA mimic ID	**miRBase Accession No.**	**Sequence**
hsa-miR-181a-5p mimic	MIMAT0000256	AACAUUCAACGCUGUCGGUGAGU
hsa-miR-30a-5p mimic	MIMAT0000087	UGUAAACAUCCUCGACUGGAAG
hsa-miR-27a-3p mimic	MIMAT0000084	UUCACAGUGGCUAAGUUCCGC
cel-miR-67 mimic negative control	MIMAT0000039	UCACAACCUCCUAGAAAGAGUAGA
miR mimic transfection control with Dy547	MIMAT0000039	UCACAACCUCCUAGAAAGAGUAGA
miR mimic housekeeping positive control (GAPD)	Not provided	Not provided

Table 11: miRNA mimics of miR-181a, -27a, -30a were bought from Dharmacon together with negative and positive miR mimic controls. MiRNA mimics are double-stranded oligonucleotides designed to mimic the function of endogenous mature miRNAs to facilitate gain-of-function studies.

Mature miRNA mimics were chosen for transfection - instead of pre-miRNAs - as they can be directly incorporated into RISC (Figure 48), given that in diabetes the miRNA processing machinery, such as Dicer expression, was shown to be impaired in unwounded diabetic skin compared to non-diabetic unwounded skin [108]. Also, they allow transient over-expression of miRNAs as opposed to the stable expression of short hairpin RNAs (shRNA) - transfected via viral vectors - that has been associated with cytotoxic effects [177].

Prior to transfecting the miRNA mimics into cells I confirmed the size and integrity of the purchased miRNA mimics by running them on a denaturing urea 15% polyacrylamide gel. This allows separation and visualisation of single stranded DNA and RNA oligos of 20-800 bases in length. Briefly, 50ng of each of the miRNA mimics were loaded into the pre-heated gel, together with 10/60 DNA ladder marker oligos and run at 180mV/10mA for 80 min. To aid with the visualisation of the bands the gel was stained with Sybr Gold (1x) and visualised with the Gel Documentation System.

Results from this testing showed that the miRNA mimics created two distinct bands of sizes ~25 nt and ~40 nt, respectively (Figure 49). The first band corresponded to the denatured single-stranded microRNA mimic, whereas the higher weight band likely corresponded to the double stranded miRNA mimic. This showed the mimics were not denatured (lack of smears) and had the correct sizes. Similarly, the purity of the miRNA mimics was shown to be high (A260/A280 >2.0 and A260/A230 > 2.0) via Nanodrop 2000, further confirming that the miRNA mimics should perform as expected.

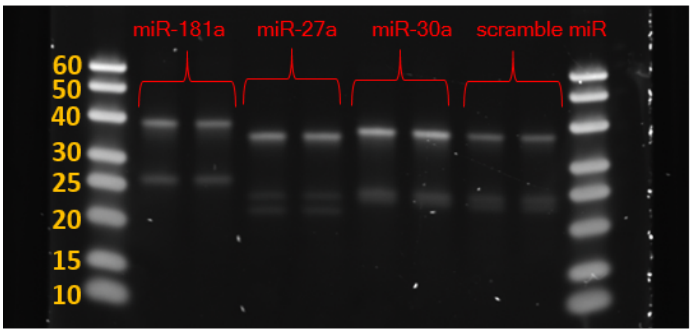


Figure 49: denaturing 15% polyacrylamide gel shows mature miRNA mimics of miR-181a, -27a, -30a and scramble miRNA create two distinct bands of ~25nt and ~40nt and confirms they are not denatured as seen by the lack of smeared appearance. To detect the RNA bands the gel was stained with Sybr Gold.

4.2. Liposomal-based transfection of miRNA mimics into primary dermal fibroblasts

To deliver the miRNA mimics into the primary fibroblasts I chose a lipid-based transfection method involving lipofectamine. Lipofectamine contains lipid subunits that can form cationic liposomes (i.e. positively charged lipids) in an aqueous environment and complex with negatively charged nucleic acids, such as DNA or RNA. This entrapment of the cargo helps mask their negative charge and overcome the electrostatic repulsion of the negatively charged cell membrane. The resulting liposome-RNA complexes go on to bind the negatively charged cell membrane and become internalised via fluid endocytosis [178] (Figure 50). Once inside the cell the cargo starts its journey in early endosomal vesicles which subsequently fuse with sorting endosomes, in turn transferring their contents to the late endosomes [179]. These acidified vesicles (pH 5-6) subsequently relocate their endosomal content to lysosomes, which are further acidified (pH ~4.5) and contain nucleases to degrade the RNA. To avoid degradation in the lysosomes the RNA must escape from the endosomes into the cytosol, where they can associate with RISC to be processed accordingly. Endosomal escape is a major barrier for

efficient RNA delivery and it is unknown how RNA escapes to become functional. Nevertheless, uptake of cargo via liposomal-based delivery is fairly quick with internalisation occurring within 6h, making this transfection method one of the most commonly used amongst researchers. Liposomal-based delivery, however is highly dependent on cell type and origin, i.e. primary vs cell lines which meant that I first needed to test if this method successfully transfected small RNAs into primary dermal fibroblasts.

To verify uptake of the miRNA mimics and their cellular distribution in the fibroblasts I transfected dy547-labelled miR mimic into primary dermal fibroblasts via lipofectamine RNAiMAX – a type of lipofectamine that works best for small RNAs - according to the manufacturer's protocol (methods 4.8.2). As transfection efficiency via lipofectamine is further known to depend on cell confluency, nondiabetic fibroblasts were seeded into cell culture plates at different cell densities (9,000-25,000 cells/cm^2) in antibiotic-free DMEM and left to adhere overnight, followed by transfection at 10-30 nM final concentration. 24h later the cells were stained with nuclear dye Hoechst 33342 and fixed in 4% PFA for microscopy imaging. Fibroblasts without dy547 miR mimic served as negative control.

The results showed that dy547-labelled miR mimic was uptaken very efficiently into the primary fibroblasts (at all cell densities tested – supplementary data 4.9.1) with no fluorescence observed in the negative control (Figure 51). Close-up images of the transfected fibroblasts further showed punctate uptake of the fluorescently-tagged miRNA (Figure 51), consistent with liposomal-based transfection of small RNAs [180].

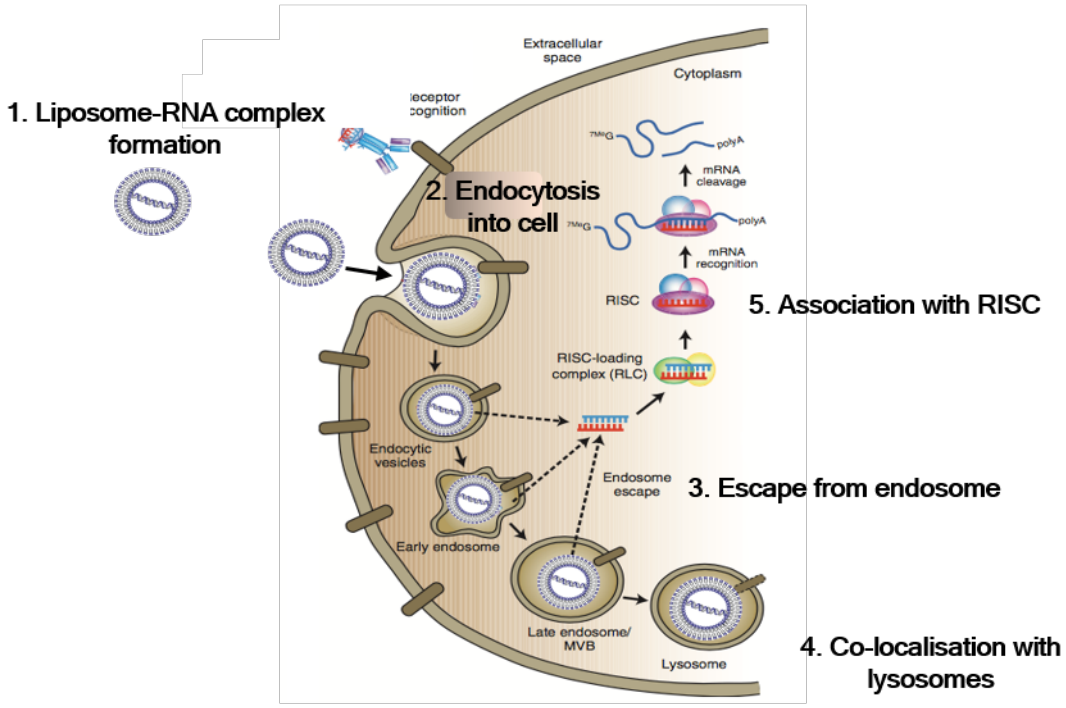


Figure 50: liposomal-based transfection of cargo relies on the endosomal pathway, starting with uptake of liposome-RNA complexes (1) into the cytoplasm via endocytosis (2), followed by escape of cargo from the endosomes (3) to associate with RISC (5) or co-localisation with lysosomes (4). Image modified from [179] with permission of the rights holder, The Company of Biologists

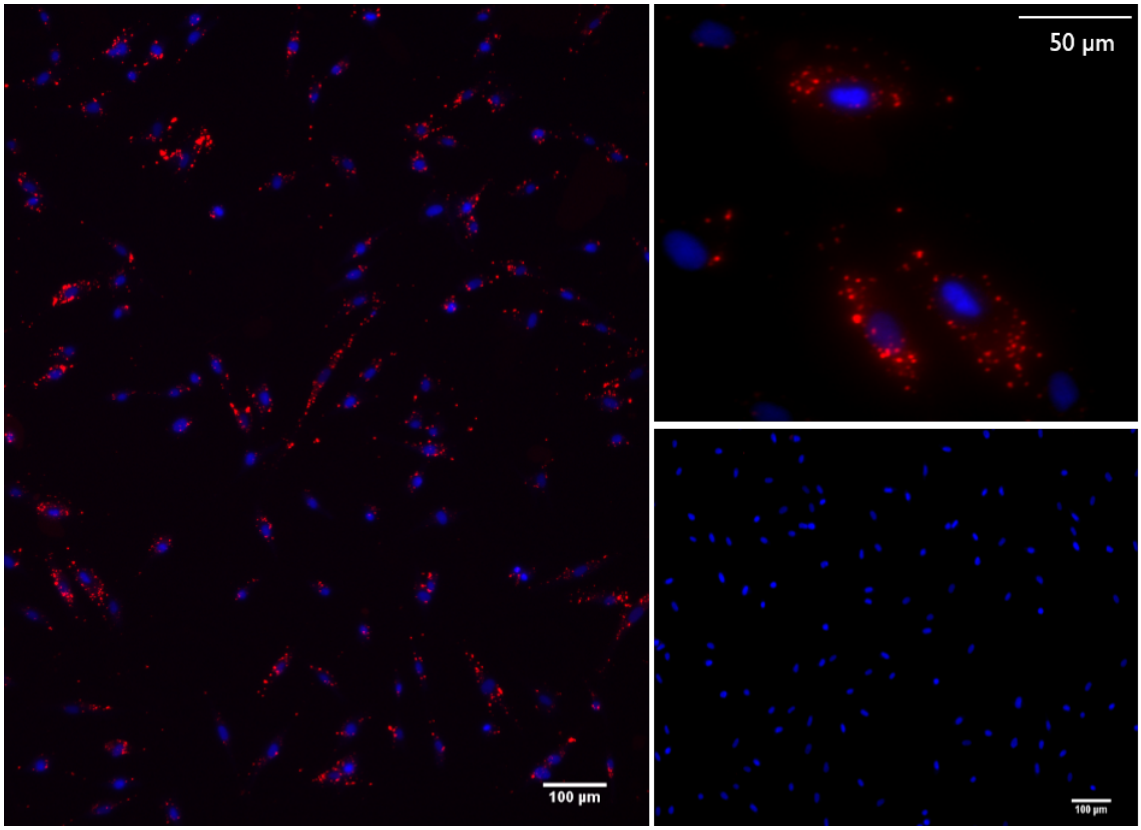


Figure 51: dy547-labelled miRNA (red) transfected into primary dermal fibroblasts via lipofectamine RNAiMAX at 10-30 nM shows successful uptake 24h post-transfection (left). Close-up images display punctate uptake of the cargo consistent with liposomal-based delivery methods (top right); negative control involving fibroblasts without dy547-labelled miRNA shows no sign of autofluorescence (bottom right). Blue dye denotes the nuclear staining Hoechst 33342.

To confirm, however that the dy547-labelled miRNA didn't get stuck to or in the surface of the cell, but entered to become functional, I further transfected a miRNA mimic positive control against the housekeeping gene GAPDH into the dermal fibroblasts at 100nM via lipofectamine RNAiMAX. GAPDH expression was measured 48h post-transfection via Taqman-qPCR and its fold change compared to that following transfection of scramble miRNA mimic at 100nM or untreated cells. Prior to qPCR the integrity and purity of the extracted RNA was checked and confirmed to be high (supplementary data 4.9.2). To determine the fold change in gene expression the $2^{-\Delta\Delta CT}$ method was used - with Beta Actin (ACTB) gene serving as the normalisation gene - after confirming that the amplification efficiency of the RT products is high (supplementary data 4.9.4).

Transfection with the miR mimic positive control showed that GAPDH exhibited a negative fold change of ~40 corresponding to 98% gene knockdown (Figure 52). Such large knockdown meant that the miR positive control displayed a similar behaviour and effect to siRNAs - as opposed to the known fine-tuning effect of miRNAs – as transfection of primary dermal nondiabetic fibroblasts with CAV1 siRNA showed a comparable fold change in CAV1 gene expression (supplementary data 4.9.6).

Overall, these results confirmed that lipofectamine RNAiMAX successfully transfected primary dermal fibroblasts with small RNAs and that the protocol devised for transfection was adequate.

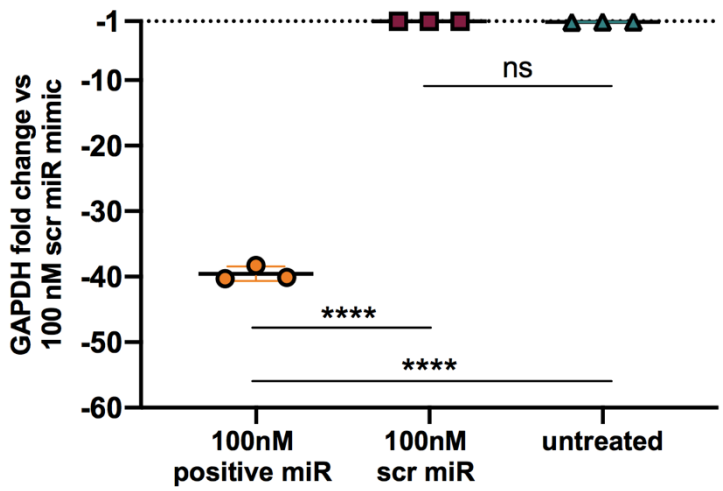


Figure 52: Transfection of positive miR mimic against GAPDH via lipofectamine RNAiMAX at 100 nM into primary dermal fibroblasts causes large suppression of GAPDH gene expression 48h post-transfection, confirming liposomal-based delivery of miRNAs works efficiently. The fold change in GAPDH gene expression was determined using the $2^{-\Delta\Delta CT}$ method. Data points show mean ± SD. Analysis of statistical significance was performed via one-way ANOVA, followed by Tukey's multiple comparisons test. **** $p<0.0001$. N=1, n=3

4.3. Transfection of miRNA mimics into fibroblasts to check for synergy

To test for synergy miRNA mimics of miR-181a-5p, miR-27a-3p and miR-30a-5p were transfected individually and in combination into nondiabetic dermal fibroblasts at 300 nM final concentration/well according to the 'synergy' protocol (methods 4.8.2 - Table 15). This protocol involved spiking each miRNA mimic with scramble miR mimic to ensure the same total amount of miRNA mimic was transfected in each condition.

First, I checked that the three miRNAs became indeed over-expressed following transfection and to what degree. To verify this nondiabetic fibroblasts were seeded in antibiotic-free DMEM (supplemented with 10% FBS, 2.5 mM L-glutamine) and left to adhere overnight, followed by transfection of miRNA mimics individually and in combination of all three. Taqman-qPCR was performed 48h post-transfection to determine the fold change in miRNA compared to the basal levels in the fibroblasts transfected with 300 nM scramble miR mimic. RNU44, a small nucleolar RNA served as the normalisation gene. Prior to running qPCR the integrity and purity of the extracted small RNA was checked together with the amplification efficiency of the miRNA genes during qPCR and confirmed to be high (supplementary data 4.9.3 and 4.9.5). Furthermore, the expression of RNU44 was confirmed to be unaffected following transfection of the functional miRNA mimics and hence suitable as a normalisation gene (supplementary data 4.9.7).

These results confirmed that all three miRNAs became over-expressed very well following transfection, both when delivered individually - at 100 nM/well spiked with scramble miR mimic - and in combinations of three - each at 100 nM/well (Figure 53). The fold change of miRNA over-expression between individual and combined transfections displayed no statistically significant difference, which meant that I could reliably test for synergy as the miRNAs showed similar level of expression in each condition.

Furthermore, the high amount of over-expression observed in the data (fold change of several thousands) was consistent with other published reports on transfection of miRNA mimics via liposomal-based delivery methods [181]. Many times, these fold changes detected have such high values because Taqman-qPCR detects miRNA mimics that may be trapped in endosomes or lysosomes, as well as those corresponding to functional levels [181].

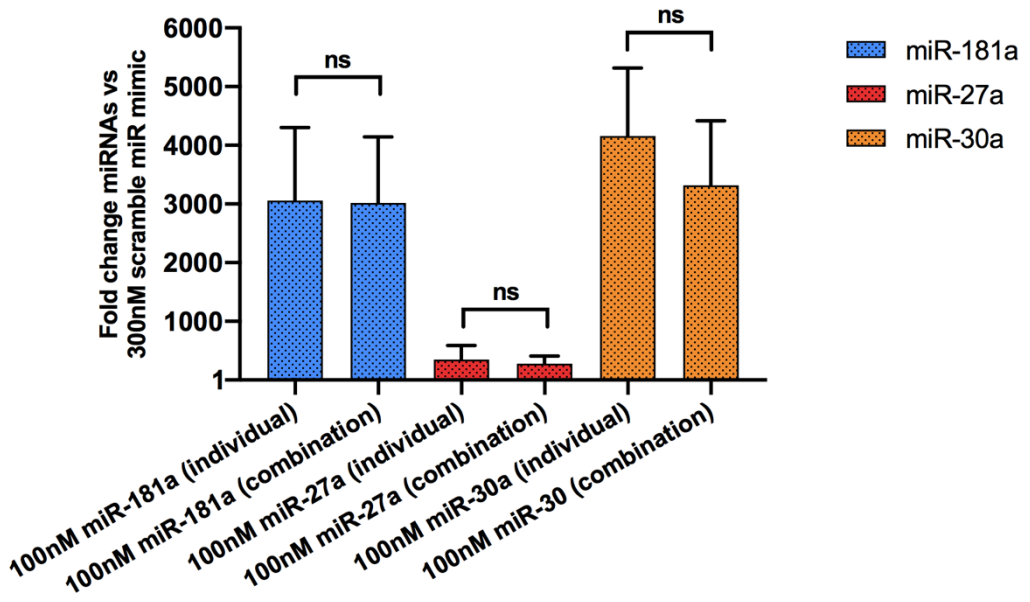


Figure 53: individual and combined transfection of miR-181a, -27a, -30a mimics into primary dermal nondiabetic fibroblasts via lipofectamine RNAiMAX at 300nM final concentration shows large over-expression 48h later. No statistical difference is observed between the individual and the combined transfection, confirming that miRNAs become expressed to a similar amount even when delivered in combination. For the individual transfections the functional miRNAs (100 nM) were spiked with scramble miRNA mimic (200 nM) to ensure the same total amount of miRNA mimic was transfected in each condition. Bars denote mean ± SD. Statistical analysis to determine significance over cells transfected with scramble miRNA was done via one-way ANOVA, followed by posthoc Tukey's multiple comparisons test. N=2, n=3/donor.

To understand why the three miRNAs of interest became over-expressed to different extents, I measured the expression levels of miRs-181a, -27a and -30a in untreated primary dermal fibroblasts or following transfection of 300 nM scramble miR mimic. Plotting the results as relative expression to RNU44 revealed that miR-27a, for instance was highly expressed in the cells (average CT value ~25), which could explain why this miRNA expression displayed the lowest fold change following transfection of miR-27a mimic (~300-fold change increase). On the other hand, miR-181a displayed low endogenous expression (average CT value ~29), which may reflect the very high fold changes observed after transfection of miRNA mimic (Figure 54).

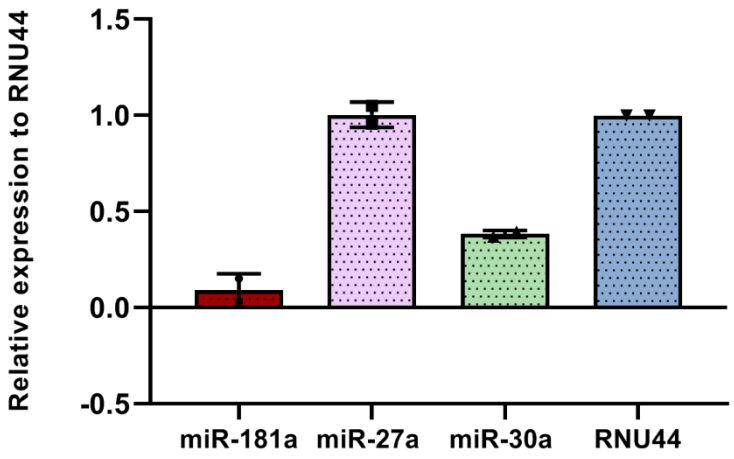


Figure 54: Taqman-qPCR measurements of the endogenous levels of miR-181a, -27a and -30a show that miR-181a is very lowly expressed, followed by miR-30a and miR-27a which shows the highest endogenous expression in primary dermal nondiabetic fibroblasts. Expression values were calculated relative to expression of RNU44. Bars denote mean ± SD. N=2

4.4. Testing for synergy at the pathway level

After confirming that the miRNAs of interest were indeed becoming over-expressed, I tested for synergy at the pathway level. To accomplish this mimics of miRs -181a, -27a and -30a were delivered at 300 nM final concentration into nondiabetic dermal fibroblasts individually, pairwise and in combination of three according to the 'synergy' protocol (methods 4.8.2). This protocol involved delivering each functional miRNA mimic at 100 nM, while spiking it with scramble miRNA mimic to ensure the final concentration of miRNA mimic was the same in each condition. Proliferation was measured 5 days post transfection via Presto Blue and the fold change in cell viability was compared to fibroblasts transfected with 300nM scramble miR mimic. Scramble miRNA was previously confirmed to have no notable effects on cell proliferation at 10-300 nM compared to untreated cells (supplementary data 4.9.9).

The proliferation assays showed that miR-181a over-expression caused an increase in cell proliferation, miR-27a over-expression led to a decrease in cell proliferation, and miR-30a over-expression caused an increase in proliferation albeit to a more modest degree. However, there was no sign of synergy (at the pathway level) neither amongst any two miRNA pairs nor amongst all three of them (Figure 55).

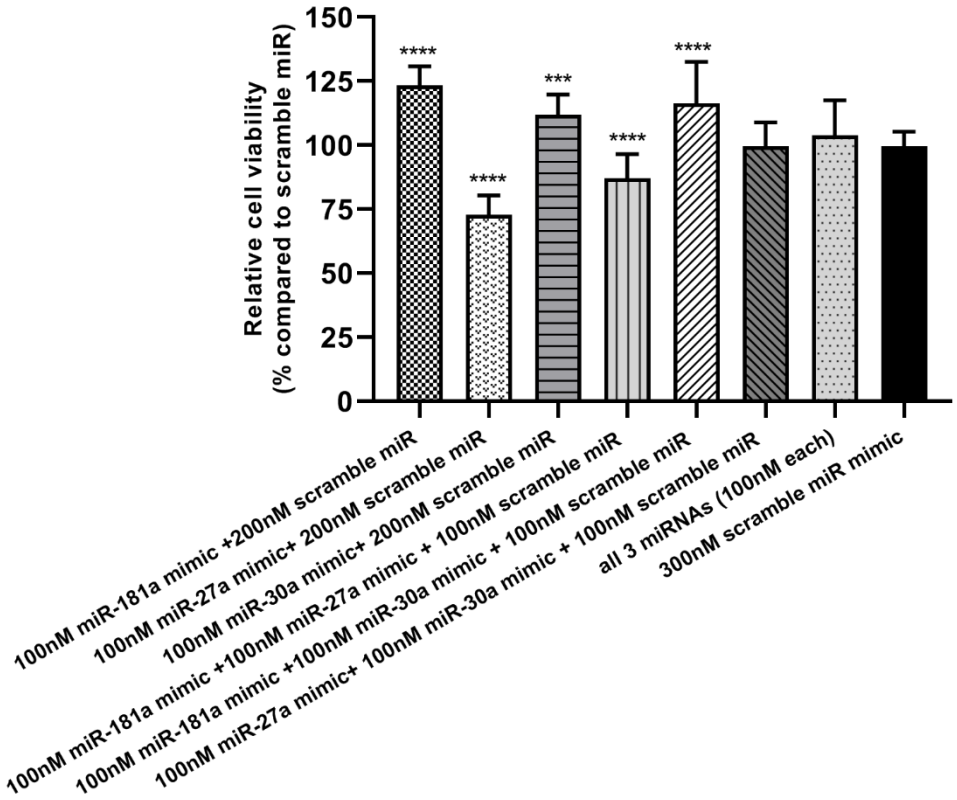


Figure 55: to test for synergy miRNA mimics of miR-181a, -27a and -30a were transfected into primary dermal nondiabetic fibroblasts via lipofectamine RNAiMAX at 300nM final concentration individually, pairwise and in triple combination. Over-expression of each of the miRNAs has a biological effect on cell proliferation, however they show no sign of synergy. Proliferation was measured 5 days post-transfection via Presto Blue. Bars denote mean ± SD. For analysis of statistical significance one-way ANOVA was used, followed by posthoc Dunnett's multiple comparisons test. *** $p<0.001$, **** $p<0.0001$. N=3, n=9/donor

These results were somehow unexpected as my initial hypothesis suggested that all these three miRNAs should work as tumour suppressors affecting signalling pathways important for cell growth and proliferation. Based on the bioinformatics analysis I predicted that the key genes these miRNAs targeted were involved in regulating cell growth, proliferation and apoptosis such that over-expressing their levels should overall have a suppressive effect on cell proliferation (which would explain their upregulation in DFU fibroblasts according to the NanoStringDiff analysis). However, it may be that this expectation was somewhat too easy as miRNAs are known to have dual behaviour depending on cell type and disease state. MiR-181a and miR-27a, for instance were shown to act both as tumour suppressors or oncogenes in various cell types depending on the genes they were targeting (Table 12), such that it becomes difficult to predict the effect a miRNA will have, yet alone in combinations.

miR-181a	'MicroRNA-181a **enhances** cell proliferation in acute lymphoblastic leukemia by targeting EGR1' [182]
	'MicroRNA-181a **promotes** proliferation and inhibits apoptosis by suppressing CFIm25 in osteosarcoma' [183]
	'MicroRNA-181a **inhibits** activated B-Cell-Like Diffuse Large B-Cell Lymphoma progression by repressing CARD11' [184]
	'MiR-181a-5p **inhibits** cell proliferation and migration by targeting KRAS in non-small cell lung cancer A549 cells' [185]
miR-27a	'MicroRNA-27a **promotes** proliferation and suppresses apoptosis by targeting PLK2 in laryngeal carcinoma' [186]
	'MicroRNA-27a **promotes** proliferation, migration and invasion by targeting MAP2K4 in human osteosarcoma cells' [187]
	'MicroRNA-27a functions as a **tumor suppressor** in renal cell carcinoma by targeting epidermal growth factor receptor' [188]
	'MicroRNA-27a functions as a **tumour suppressor** in esophageal squamous cell carcinoma by targeting KRAS' [189]

Table 12: miR-181a and miR-27a work as tumour suppressors or oncogenes depending on the genes they target, cell type and disease state such that it becomes difficult to predict the effects of a miRNA *in vitro*

Following testing the effect of the miRNA mimics on fibroblast proliferation I proceeded to check whether the three miRNAs affected the expression of the target genes KRAS and IRS1 as the bioinformatics analysis in IPA predicted (Figure 35). For this miRs-181a, -27a and -30a were transfected into nondiabetic dermal fibroblasts at 300nM final concentration according to the 'synergy' protocol (100nM each miRNA) individually and in combination of three. The expression of these two genes was measured via Taqman-qPCR 48h later and the fold change calculated relative to fibroblasts transfected with 300nM scramble miR mimic. Beta actin (ACTB) served as the internal normalisation gene after it was confirmed to remain unaffected by the over-expression of the functional miRNAs (supplementary data 4.9.8).

The results showed that all three miRNAs cause a suppression of KRAS expression with miR-181a having the most significant impact (~2-fold change). No sign of cooperativity/synergy was observed amongst the three miRNAs (Figure 56), somewhat expected as the seed sites for the miRNAs were spread >35 nt apart - the 'golden' distance needed for miRNA cooperativity at gene level. Although knockdown of KRAS could be attributed both to direct or indirect effects of the miRNAs, luciferase assays were not performed to validate the direct repression by the miRNAs as previous literature findings confirmed KRAS to be a functional target of miR-181a [185], miR-27a [190] and miR-30a [191] in various different cancers.

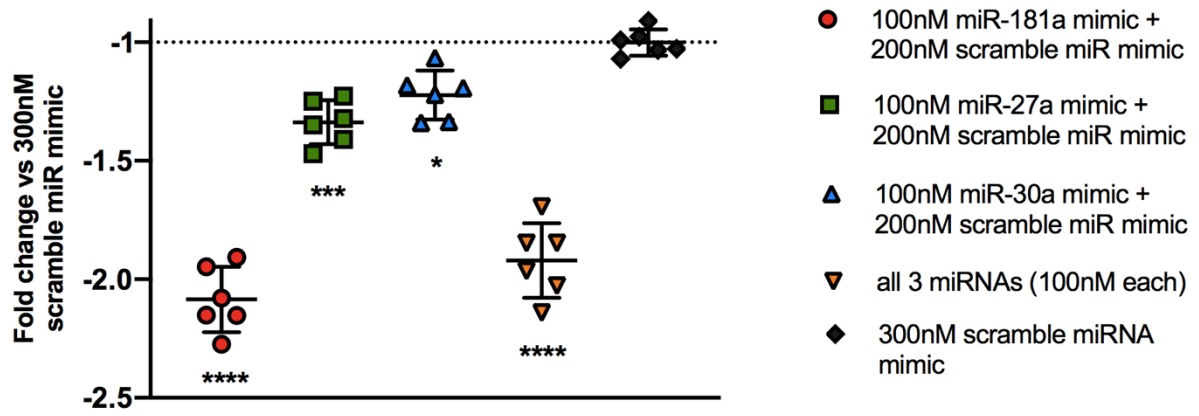


Figure 56: KRAS becomes repressed by varying amounts following individual transfection of miRs-181a (52 ±3%), -27a (25±5%), -30a (18±7%) or in triple combination (48±4%), however no sign of synergy is observed. Fold change values are normalised to scramble miR mimic showing a fold change of -1. MiRNA mimics were transfected via lipofectamine RNAiMAX at 300 nM final concentration and KRAS expression was measured via Taqman-qPCR 48h post-transfection. Data points denote mean ± SD. Analysis of statistical significance was performed via one-way ANOVA, followed by posthoc Tukey's multiple comparisons test. * $p<0.05$, *** $p<0.001$, **** $p<0.0001$. N=2, n=3/donor

The difference in knockdown efficiency between the three miRNAs could be attributed to the type and number of canonical sites present on KRAS: one *8mer* site and one *7mer-A1* site for miR-181a, two *7mer-A1* sites for miR-27a and one 7mer-m8 site for miR-30a (Table 13). Following the known hierarchy of repressive efficiency for canonical sites (8mer > 7mer-m8 > 7mer-A1 > 6mer), miR-181a caused stronger KRAS suppression than miR-27a or miR-30a. MiR-27a, however caused stronger suppression than miR-30a as it had two binding sites on KRAS as opposed to only one for miR-30a - despite the latter being a more efficient 7mer-m8 site -, further reinforcing how multiple miRNA binding sites offer stronger suppression over single ones. Interestingly, despite over-expression of all three miRNAs leading to knockdown of KRAS, albeit to different degrees, miRs-181a and miR-30a caused an increase in fibroblast proliferation, while miR-27a caused a decrease in proliferation. This phenomenon further highlighted the complexity of miRNA regulation of cell signalling, where despite targeting a certain gene with a specific function, they can lead to a different functional effect due to their ability to target many other genes as well.

MiRNA	Position of KRAS 3'UTR	Type of seed-matched site
hsa-miR-181a-5p	633-640	8 mer
	4377-4383	7mer-A1
hsa-miR-27a-3p	343-349	7mer-A1
	4583-4589	7mer-A1
hsa-miR-30a-5p	4367-4373	7mer-m8

Table 13: miRs-181a, -27a and -30a have different types of canonical sites on the 3'UTR of KRAS, which could be responsible for the difference in KRAS repression efficiency observed after over-expression of the miRNAs according to the Targetscan Human database Version 7.2 on human KRAS ENST00000256078.4

IRS1, on the other hand, was shown to be knocked down in a relatively modest manner following miRNA transfection (except miR-27a whose over-expression didn't affect IRS1 gene expression), with the largest suppression observed when the miRNAs were delivered in combination (Figure 57). No sign of synergy was observed however, once again perhaps as expected, given the distance between the seed sites amongst these three miRNAs was not 'right' for cooperation.

Nevertheless, overall these results showed that miRs-181a, -27a and -30a target major nodes along key cell signalling pathways important for wound healing. This reinforced the involvement of these three miRNAs in regulating signal transduction important for cell growth and proliferation in dermal fibroblasts according to the original hypothesis of the PhD project.

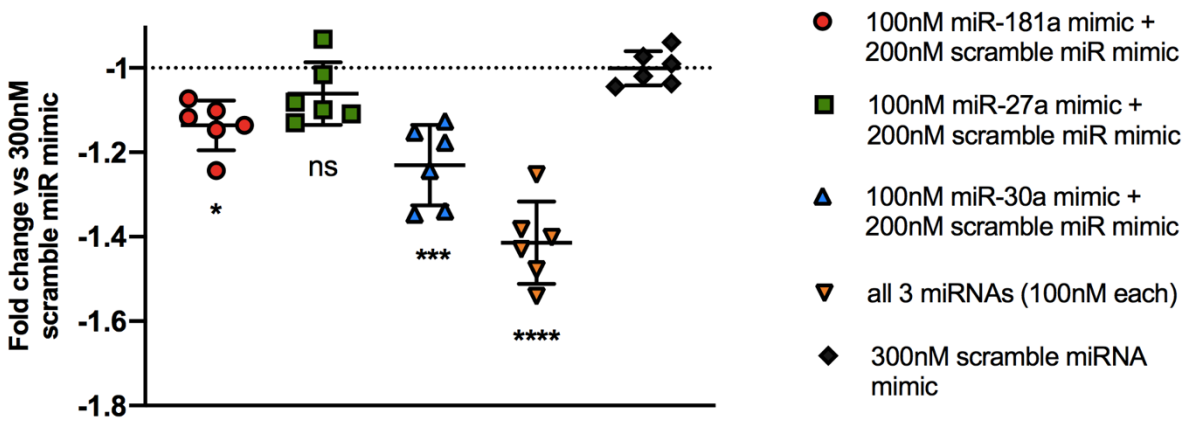


Figure 57: IRS1 becomes repressed moderately after individual transfection of miRs-181a (12±4%), -27a (5±7%), -30a (18±6%) or in triple combination (29±5%), however no sign of synergy is observed. Fold change values are normalised to scramble miR mimic showing a fold change of -1. MiRNA mimics were transfected via lipofectamine RNAiMAX at 300 nM final concentration and IRS1 expression was measured via Taqman-qPCR 48h post-transfection. Data points denote mean ± SD. Analysis of statistical significance was performed via one-way ANOVA, followed by posthoc Tukey's multiple comparisons test. * $p<0.05$, *** $p<0.001$, **** $p<0.0001$, ns means $p>0.05$. N=2, n=3/donor

4.5. Exploring the individual role of miRNAs

Despite the three miRNAs showing no sign of synergy, they were identified as being interesting in the context of DFUs according to the bioinformatics analysis (chapter 2) and therefore also worth testing individually. As such, I proceeded to investigate the separate roles of some of these miRNAs, such as miR-181a or miR-27a by transfecting them at 100nM into non-diabetic, diabetic non-ulcerated and diabetic ulcerated dermal fibroblasts. Proliferation was then measured 5 days later via Presto Blue and the fold change in proliferation compared to cells transfected with scramble miRNA mimic.

Interestingly, I noticed that miR-181a had a divergent behaviour between diabetic and non-diabetic dermal fibroblasts, leading to an increase in cell proliferation in nondiabetic fibroblasts, but a decrease in proliferation in diabetic ulcerated and diabetic non-ulcerated fibroblasts (Figure 58). MiR-27a over-expression, however consistently caused a decrease in cell proliferation of the fibroblasts - regardless of the disease state (ulcerated or non-ulcerated) – further supporting the hypothesis that miR-181a mimic drives a divergent behaviour in diabetic fibroblasts. Moreover, the fact that diabetic non-ulcerated and diabetic ulcerated fibroblasts were displaying similar response in cell proliferation following miR-181a over-

expression was consistent with literature findings that diabetic fibroblasts (ulcerated or non-ulcerated) commonly diverge in behaviour from nondiabetic fibroblasts [159].

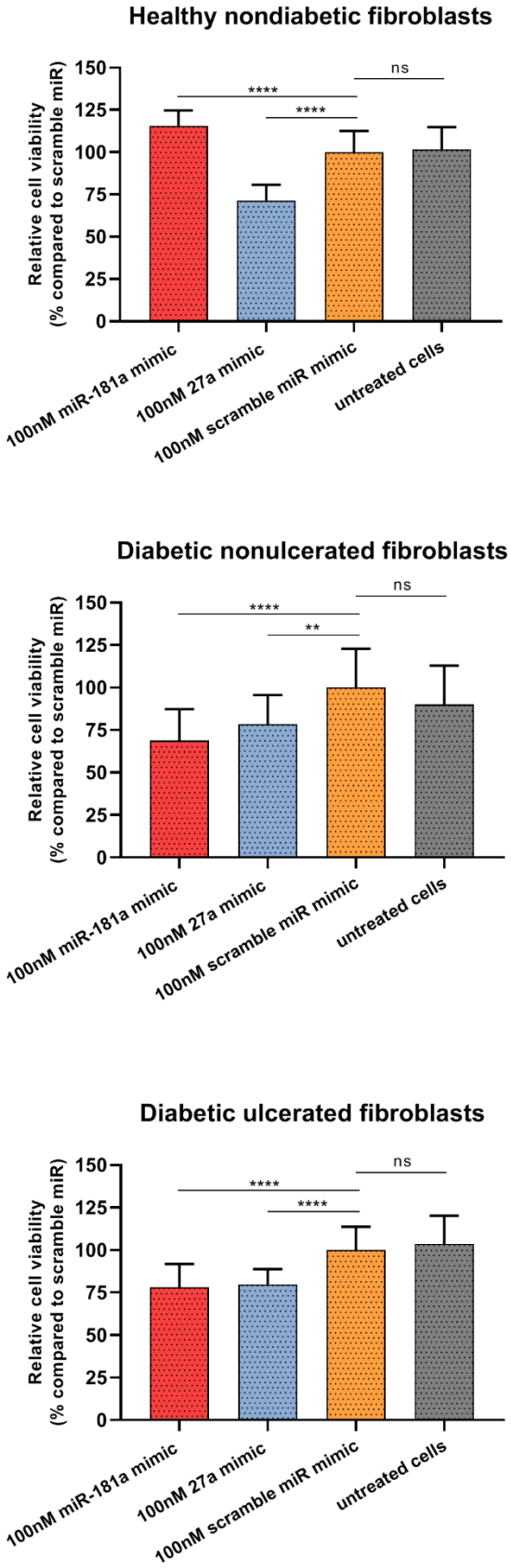


Figure 58: miR-181a exhibits dual behaviour between nondiabetic and diabetic fibroblasts, increasing proliferation in nondiabetic fibroblasts, but decreasing proliferation in diabetic ulcerated and diabetic non-ulcerated fibroblasts. MiR-27a has a suppressive effect on proliferation in all three sets of fibroblast populations. MiRNA mimics were

transfected into the fibroblasts via lipofectamine RNAiMAX at 100 nM and proliferation was measured 5 days post-transfection via Presto Blue. Bars denote mean ± SD. Analysis of statistical significance was performed via one-way ANOVA, followed by posthoc Tukey's multiple comparisons test. **p<0.01,**** p<0.0001. N=3, n=9/donor for each set of fibroblast populations

Interestingly, when checking the endogenous (basal) expression of these two miRNAs in the untreated fibroblast populations miR-181a exhibited upregulation in the diabetic fibroblasts, whereas miR-27a did not (Figure 59). Whether over-expression of miR-181a might contribute to the divergent behaviour in the diabetic vs non-diabetic fibroblasts, still remains to be elucidated.

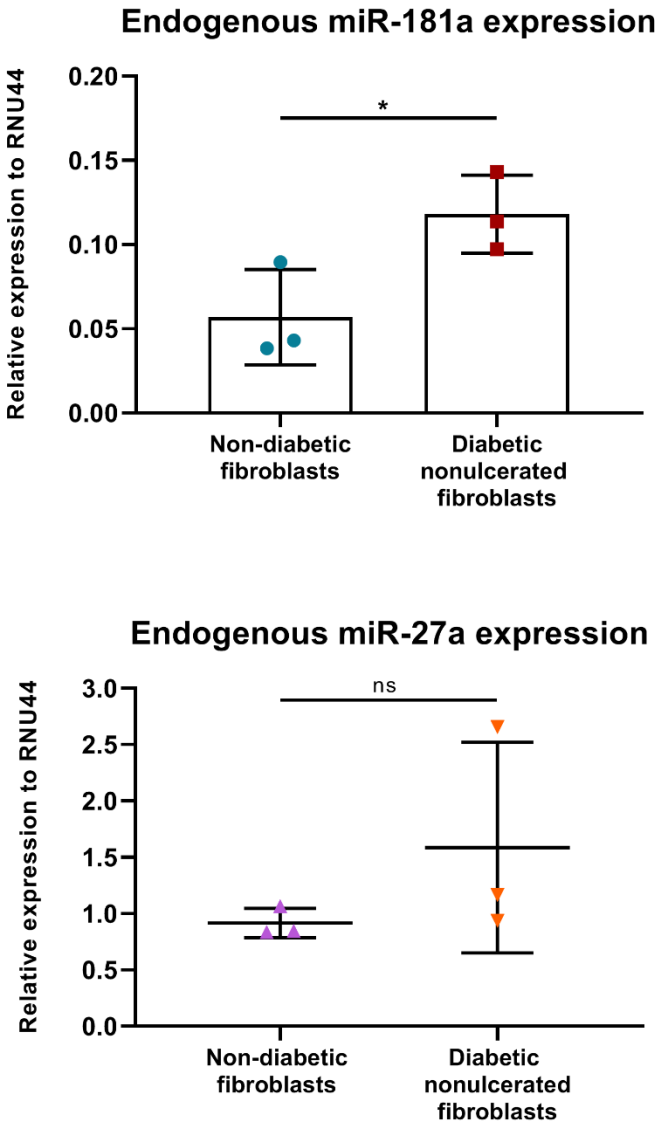


Figure 59: miR-181a is upregulated in diabetic fibroblasts compared to nondiabetic fibroblasts, whereas miR-27a shows no statistical difference. However, due to the high variability of expression amongst the populations, further donors are required to validate these observations and be able to draw a definitive conclusion on the difference in

endogenous expression of these two miRNAs in diabetic vs nondiabetic fibroblasts. Bars denote mean ± SD and data points represent relative expression to RNU44. Statistical analysis to determine significance was performed via two-tailed unpaired t-test. *p<0.05, N=3

Nevertheless, collectively these findings reinforced the original hypothesis that miR-181a and miR-27a over-expression may suppress cell proliferation in DFU cells and that downregulation via miRNA inhibitors could be a potential miRNA-based therapy for accelerating DFU healing.

To further confirm that the effects of the miR-181a and miR-27a mimics were indeed caused by over-expression of these miRNAs, I performed loss-of-function studies using miRIDIAN miR-181a or miR-27a hairpin inhibitors (Dharmacon) to check if the opposite effect to miRNA mimics would be observed on cell proliferation (Table 14). miRIDIAN microRNA hairpin inhibitors are single-stranded chemically-enhanced RNA oligonucleotides designed to bind to and sequester the complimentary, mature miRNA strand. This, in turn, prevents interaction of the mature miRNAs (loaded into RISC) with the complementary mRNA targets in the cells, leading to increased protein levels (Figure 48).

miRIDIAN microRNA mimic ID	**miRBase Accession No.**	**Sequence**
miRIDIAN microRNA human hsa-miR-181a-5p - Hairpin inhibitor	MIMAT0000256	AACAUUCAACGCUGUCGGUGAGU
miRIDIAN microRNA human hsa-miR-27a-3p – Hairpin inhibitor	MIMAT0000084	UUCACAGUGGCUAAGUUCCGC
miRIDIAN microRNA hairpin inhibitor negative control #1	MIMAT0000039	UCACAACCUCCUAGAAAGAGUAGA

Table 14: miRNA inhibitors against miR-181a and miR-27a were purchased from Dharmacon for loss-of-function studies. The hairpin inhibitor negative control allows to normalise for any effects caused by scramble miRNA inhibitor alone

MiR-181a or miR-27a hairpin inhibitor were transfected into nondiabetic or diabetic non-ulcerated primary fibroblasts at 100 nM via lipofectamine RNAiMAX and proliferation was measured 5 days later via Presto Blue and compared relative to cells transfected with 100nM scramble miRNA hairpin inhibitor – serving as a negative control. The scramble miRNA hairpin inhibitor was based on the C. elegans cel-miR-67 sequence and had an identical design and modification as miRIDIAN miRNA hairpin inhibitors, allowing to rule out any non-specific effects caused by the presence of scramble miRNA inhibitor alone.

The results showed that down-regulating miR-181a expression levels in nondiabetic fibroblasts caused a suppression of cell proliferation (Figure 60), while in diabetic non-ulcerated fibroblasts there was a trend of fibroblast proliferation to go up (Figure 61). Although none of the results were statistically significant, due to the low endogenous expression of miR-181a I expected delivery of miRNA inhibitor to have no significant impact. Down-regulation of miR-27a expression levels, on the other hand caused a robust increase in cell proliferation in both nondiabetic (Figure 60) and diabetic non-ulcerated fibroblast populations (Figure 61) due to its high endogenous expression. Nonetheless, all trends observed were the opposite of those caused by miRNA mimics delivery.

Furthermore, to confirm that the levels of miR-181a or miR-27a were indeed getting suppressed following transfection of the hairpin inhibitors, Taqman-qPCR was done 48h post transfection of antimiRs into nondiabetic fibroblasts. The fold change in miR-181a or miR-27a expression was calculated relative to cells transfected with 100nM scramble miRNA inhibitor. This showed that miR-181a was getting knocked down by ~6-fold change, whereas miR-27a was suppressed by ~12-fold change (Figure 62), thus confirming that both miRNAs were indeed getting suppressed following transfection.

Collectively these findings supported the conclusion that the cellular effects caused by the miR-181a and miR-27a mimics were genuine.

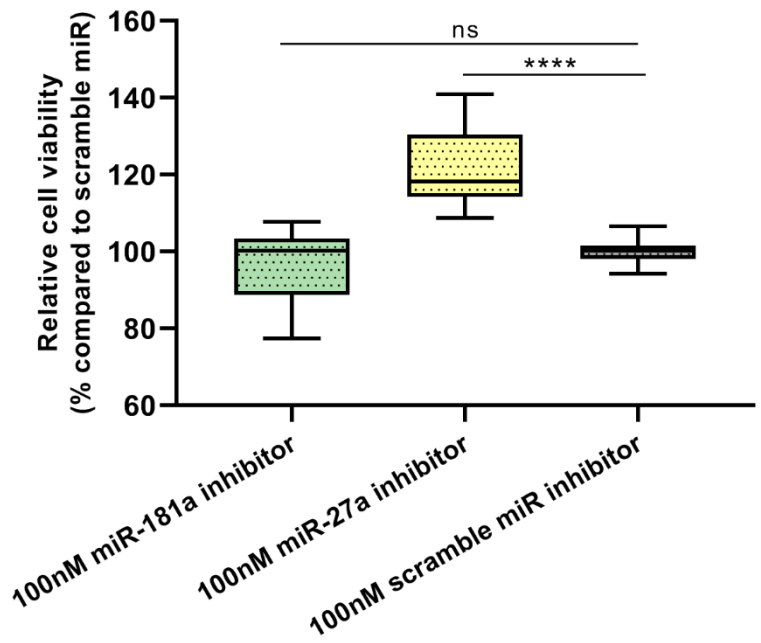


Figure 60: transfection of miR-181a inhibitor at 100 nM via lipofectamine RNAiMAX shows a trend of suppression on primary dermal nondiabetic fibroblasts, while inhibition of miR-27a exerts a proliferative effect. Proliferation was measured 5 days post-transfection via Presto Blue. Box and whisker plots span min to max. Statistical analysis was performed via one-way ANOVA, followed by posthoc Tukey's multiple comparisons test. ****p<0.0001. N=3, n=3/donor

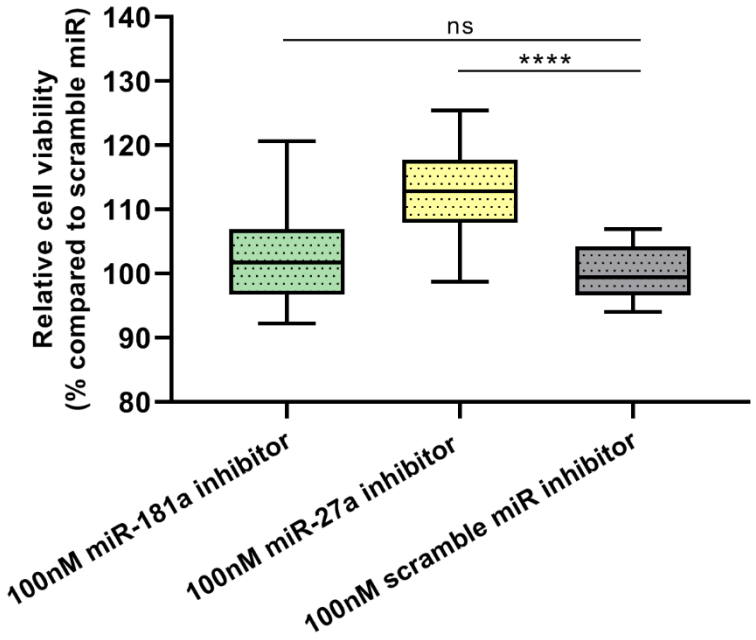


Figure 61: transfection of miR-181a inhibitor at 100 nM via lipofectamine RNAiMAX seems to exhibit a trend of stimulatory effect on diabetic non-ulcerated fibroblasts, while inhibition of miR-27a exerts a proliferative effect. Proliferation was measured 5 days post-transfection via Presto Blue. Box and whisker plots span min to max.

Statistical analysis was performed via one-way ANOVA, followed by posthoc Tukey's multiple comparisons test. ****p<0.0001. N=3, n=3/donor

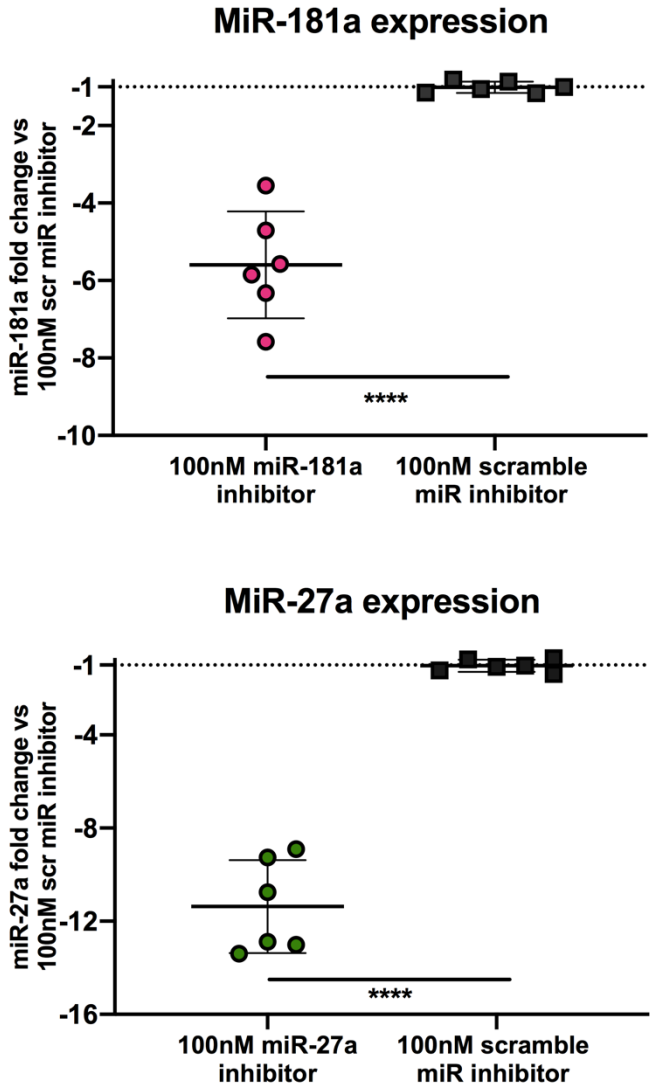


Figure 62: Taqman-qPCR confirms that transfection of miRNA inhibitors into nondiabetic fibroblasts at 100 nM via lipofectamine RNAiMAX represses expression of miR-181a or miR-27a 48h later. Data points denote mean ± SD. Statistical analysis was performed via two-tailed unpaired t-test. ****p<0.0001. N=2, n=3/donor

4.6. Exploring the role of miR-181a

Given the divergent behaviour caused by miR-181a mimic in diabetic vs non-diabetic fibroblasts I decided to explore in more detail the signalling pathways this miRNA was acting through. Since miR-181a over-expression led to an increase in cellular proliferation, I hypothesised that either MAPK/ERK signalling pathway or the PI3K/AKT signalling pathway became activated. However, transfection of miR-181a mimic led to KRAS suppression (Figure 56) and as RAS activation is the primary driver of downstream activation of the MAPK/ERK pathway components, I hypothesised that the effects of miR-181a were acting through the PI3K/AKT signalling pathway instead – something that was observed with miR-181b in the case of hepatic stellate cells [192].

The PI3K/AKT signalling pathway is a crucial regulator of normal cellular processes involved in cell growth, proliferation, glucose metabolism, survival and apoptosis (Figure 63). It contains three significant nodes including Phosphatidylinositol 3-kinase (PI3K), AKT – a serine/threonine protein kinase also known as protein kinase B (PKB) and mammalian target of rapamycin (mTOR) along the pathway that are typically activated by upstream signalling of tyrosine kinases. The primary role of PI3K is to convert phosphatidylinositol 4,5-bisphosphate (PIP_2) to PIP_3 (phosphatidyl inositol 3,4,5 tri-phosphate), which binds AKT resulting in its translocation to the plasma membrane. Here, AKT becomes activated through phosphorylation by 3-phosphoinositide-dependent kinase 1 (PDK1) at Thr308 and the second mTOR complex, mTORC2 at Ser473. Activated Akt then goes on to phosphorylate a large number of downstream substrates, including mTORC1, GSK3α/β, TSC2 that overall promotes cell growth and protein synthesis, G1 cell cycle progression and cell survival (through signalling via p70 S6 kinase and inhibition of 4E-BP1).

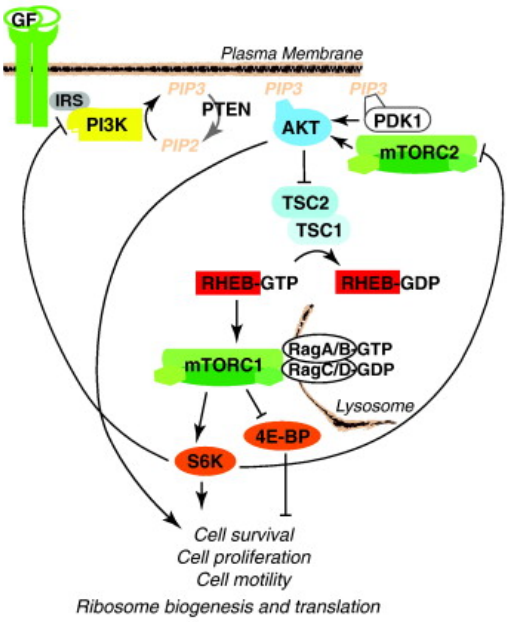


Figure 63: the PI3K/AKT signalling pathway plays key roles in regulating survival, proliferation, cell motility and protein production. Image reproduced from [193] with permission of the rights holder, Elsevier

To verify that PI3K/AKT was the pathway miR-181a was exerting its effects through the chemical modulator Ly294002 - a known potent inhibitor of PI3K family members [194] – was used to inactivate this signalling pathway. Ly294002 is known to block PI3K-dependent AKT phosphorylation and kinase activity causing cell cycle arrest predominantly at the G1 phase of the cell cycle [195]. As such, if the PI3K/AKT signalling pathway was involved, transfection with miR-181a mimic would no longer cause an increase in fibroblast proliferation as its signalling effects could no longer pass through the blocked pathway.

First, however, I confirmed Ly294002 had an inhibitory effect on primary dermal nondiabetic fibroblasts by treating the cells with the chemical compound (50 μM in 10% FBS) for different lengths of time (24h or 72h) and measuring proliferation 3 days later. Untreated fibroblasts or fibroblasts kept in DMEM supplemented with DMSO in the same ratio as for Ly294002 dilution (1:1000) served as the control to rule out any toxic effect DMSO alone might have on cell proliferation. This latter control was used because Ly294002 (Cell Signalling Technologies) came from the supplier in lyophilised form and had to be dissolved in DMSO.

This testing revealed Ly294002 treatment strongly suppressed fibroblasts proliferation, even in the presence of 10% FBS, with the 24h long treatment suppressing cell proliferation by ~40% and 72h long treatment by ~60% (Figure 64). Furthermore, the effects caused were long-term

as fibroblasts didn't seem to recommence cell proliferation even after the medium was switched back to the normal medium (in the case of 24h Ly294002 treatment). Although the phosphorylation level of AKT in fibroblasts was not checked following exposure to Ly294002, given the strong suppressive effect this caused on cell proliferation I was confident that Ly294002 was inhibiting the PI3K/AKT signalling pathway as expected.

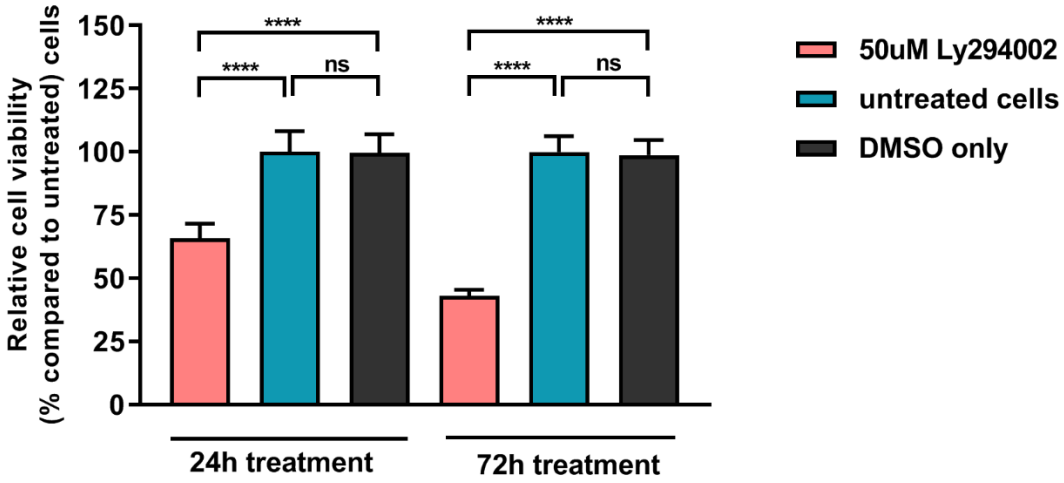


Figure 64: treatment with Ly294002, a potent PI3K inhibitor, at 50 μM in 10% FBS for different lengths of time (24h or 72h) causes a large suppressive effect on nondiabetic fibroblast proliferation 3 days later, illustrating the important role PI3K/AKT signalling plays in controlling cell proliferation. Untreated fibroblasts or fibroblasts kept in DMEM supplemented with DMSO in the same ratio as for Ly294002 dilution (1:1000) served as the control to rule out any toxic effect DMSO alone might have on cell proliferation. Bars denote mean ± SD. Statistical analysis was done via one-way ANOVA, followed by posthoc Tukey's multiple comparisons test. ****p<0.0001, n=15

After confirming the inhibitory effect of Ly294002 on fibroblast proliferation, nondiabetic fibroblasts were transfected with 100nM miR-181a mimic or scramble miR mimic in the presence or absence of Ly294002 for 5 days, followed by measuring proliferation via Presto Blue. The fold change in proliferation was calculated relative to cells transfected with 100 nM scramble miR mimic in the absence of Ly294002.

Treatment with Ly294002 caused a strong inhibitory effect on fibroblast proliferation, leading to a ~60% suppression between cells transfected with 100nM scramble miR mimic in the presence or absence of Ly294002 (Figure 65). In the absence of Ly294002 miR-181a caused an increase in cell proliferation - as usual - whereas in the presence of Ly294002 miR-181a over-expression not only did not increase cell proliferation – suggesting that PI3K/AKT signalling was the pathway this miRNA was mediating its effects through – but instead it suppressed

proliferation even further, similar to the effects caused by miR-181a mimic in diabetic non-ulcerated and DFU fibroblasts (Figure 58).

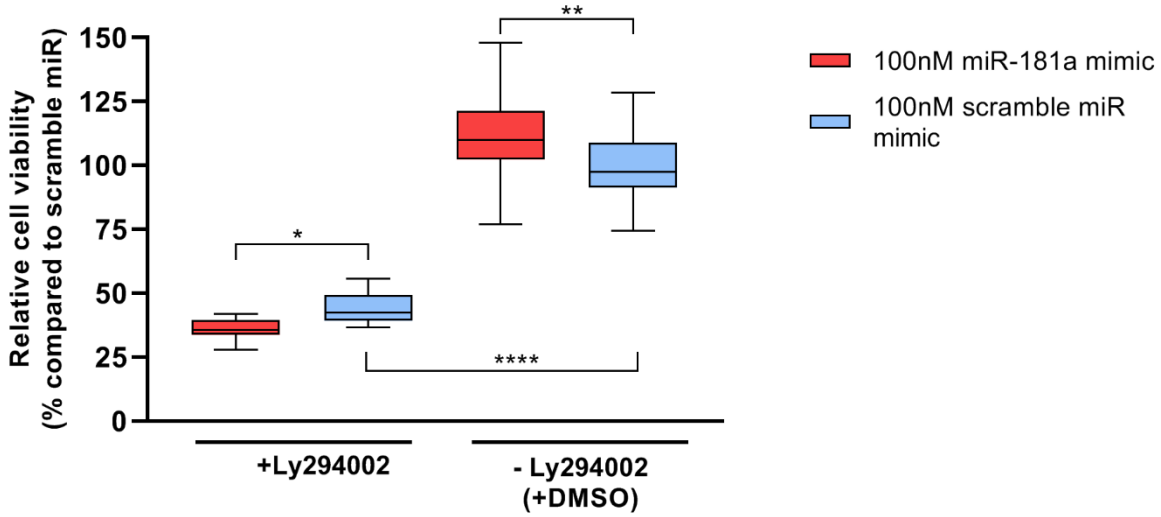


Figure 65: over-expression of miR-181a exerts its proliferative effects on nondiabetic fibroblasts through the PI3K/AKT signalling pathway as blocking this pathway via Ly294002 treatment abolishes the stimulatory effect miR-181a has on fibroblasts. Cells were transfected with 100 nM miR-181a mimic or scramble miR mimic in the presence or absence of Ly294002 for 5 days, followed by measuring proliferation via Presto Blue. Box and whisker plots show min to max. Statistical analysis was done via one-way ANOVA, followed by posthoc Tukey's multiple comparisons test. *p<0.05, **p<0.01, ****p<0.0001. N=3, n=9/donor

In diabetes, it is known that the PI3K/AKT signalling pathway is impaired, emphasising perhaps the idea that miR-181a may have a divergent behaviour on cell proliferation depending on whether the PI3K/AKT signalling is inhibited or not. Overall, these findings suggested that miR-181a over-expression was increasing cell proliferation by potentially activating the PI3K/AKT signalling pathway.

To check which targets along the PI3K/AKT signalling pathway miR-181a might cause an increase in cellular proliferation, I checked the expression of tumour suppressor PTEN - a lipid phosphatase that catalyses the dephosphorylation of PIP_3, thus negatively regulating AKT signalling- and P70 S6K – a kinase that acts downstream of mTORC1 to promote cell proliferation and cell growth (Figure 63).

Nondiabetic fibroblasts were transfected with 100nM miR-181a mimic or 100nM scramble miR mimic and the fold change in PTEN or RPS6KB1 (gene coding for p70 S6K) was measured 48h later by Taqman-qPCR. The fold change in gene expression was determined relative to

cells transfected with 100nM scramble miR mimic using Beta Actin as the internal normalisation gene.

Interestingly, PTEN expression was upregulated by ~2-fold change while RPS6KB1 was modestly down-regulated by ~1.3-fold change (Figure 66). These results were somewhat surprising as I expected that PTEN expression would be suppressed, thus increasing the activity of PI3K/AKT signalling. Similarly, the expression of RPS6KB1 was only moderately suppressed, possibly because of upstream activation from AKT/mTORC1 signalling. It might be, however, that PI3K/AKT signalling pathway is becoming activated through inhibition of PHLPP2 – a phosphatase that dephosphorylates AKT1 and AKT3, thus negatively regulating AKT activity – previously confirmed to be a direct target of miR-181a in human keloid fibroblasts [196].

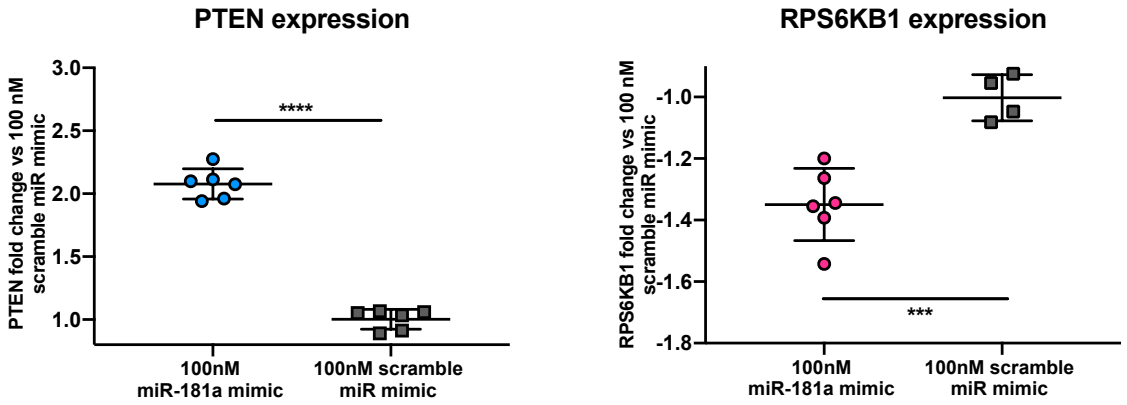


Figure 66: miR-181a over-expression causes upregulation of PTEN and downregulation of RPS6KB1 48h post-transfection of miR-181a mimic into primary nondiabetic fibroblasts, suggesting that the PI3K/AKT signalling pathway is becoming activated through other nodes. MiR-181a mimic was transfected at 100nM via lipofectamine RNAiMAX. Fold changes were calculated relative to scramble miR mimic displaying a fold change of 1 or -1, respectively. Data points denote mean ± SD. Statistical analysis was performed via two-tailed unpaired t-test. ***p<0.001, ****p<0.0001. N=2, n=3/donor

To further confirm the observed changes to gene expression following transfection of miR-181a mimic, I transfected antimiR-181a into nondiabetic fibroblasts and measured the expression of KRAS and PTEN. These two genes were chosen because they showed large fold changes when miR-181a was over-expressed, namely 2-fold downregulation or upregulation, respectively. Taqman-qPCR was performed 48h post-transfection of miR-181a inhibitor and the fold change was calculated relative to cells transfected with 100nM scramble miR inhibitor. Although the effects of antimiR-181a on KRAS and PTEN expression were not exactly the

opposite to those of miR-181a mimic, the results showed that KRAS was no longer suppressed and PTEN was no longer upregulated with the p-value > 0.05 in both cases (Figure 67). This milder effect could be attributed once again to the low endogenous expression of miR-181a, such that delivery of the antimiR should cause no substantial impact.

Nonetheless, these findings confirmed that the effects miR-181a mimic was exerting on fibroblast signalling were reliable.

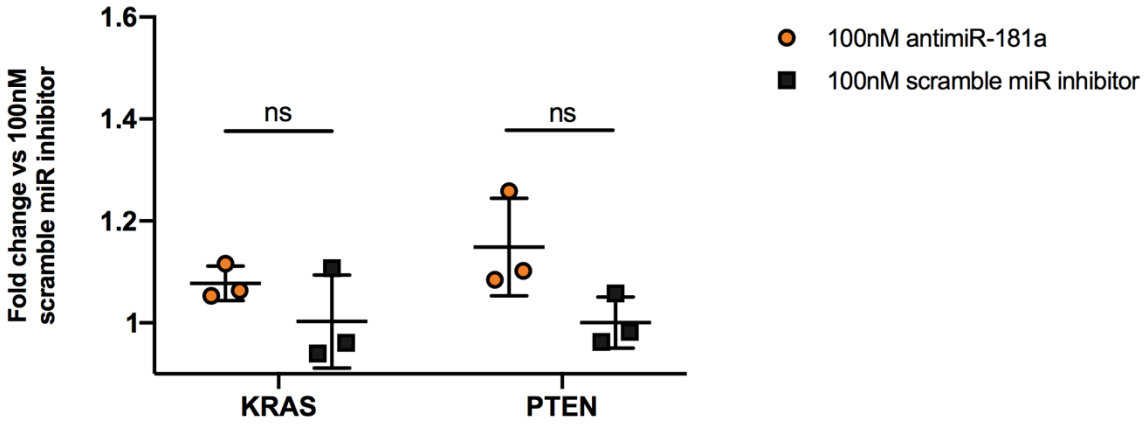


Figure 67: inhibiting miR-181a expression via transfection of 100nM antimiR-181a using lipofectamine RNAiMAX causes KRAS to no longer to be downregulated and PTEN no longer to be upregulated 48h post-transfection, displaying opposite effects to those of miR-181a mimic. Data points denote mean ± SD. Statistical analysis was performed via unpaired two-tailed t-test, ns means p>0.05. n=3

However, it was clear that understanding the effects of miR-181a mimic on cell signalling and the reason behind the dual behaviour of miR-181a in the nondiabetic vs diabetic cells was more complicated than possible to describe using single high probability targets on the relevant pathways. As such, I decided to use Reverse Phase Protein Arrays (RPPA) analysis on three nondiabetic and three diabetic non-ulcerated fibroblast populations to investigate which cell signalling proteins change following transfection of miR-181a mimic. RPPA detects expression levels and activation status of hundreds of signalling proteins in a high throughput manner with great sensitivity and accuracy [197]. Minimal amounts of samples, i.e. ng of protein lysates are spotted onto nitrocellulose-coated arrays that get probed with a specific antibody - one antibody/slide (Figure 68). Over 1,000 samples can be assayed on a single array, allowing for comparison of many different samples and conditions in a single study, which reduces the complexity of normalisation and analysis across assays. Traditionally, RPPA has been an invaluable tool for researchers investigating protein signalling changes occurring in cancer.

Recently, however, it has been increasingly finding uses in other fields as well, such as wound healing for studying keratinocyte protein signalling in DFUs [198].

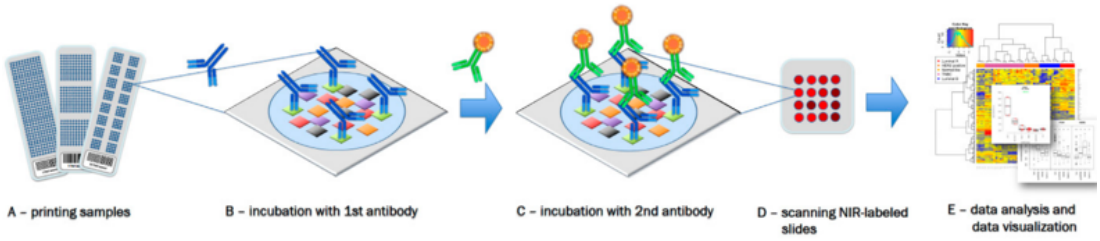


Figure 68: RPPA allows high throughput detection of expression levels and activation status of signalling proteins. It consists of spotting cell lysates from multiple samples on arrays that get probed with one antibody at a time, followed by scanning the spotted slides to generate data reports. Image reproduced from [199] under the terms and conditions of the Creative Commons Attribution License

Cell lysates from six samples were submitted to the RPPA Core Facility at the MD Anderson Cancer Centre (Texas, US) for RPPA analysis (https://www.mdanderson.org/research/research-resources/core-facilities/functional-proteomics-rppa-core.html). Briefly, fibroblasts were seeded in 6-well plates in antibiotic-free DMEM (supplemented with 10% FBS and 2.5 mM L-glutamine) and left to adhere overnight. The following day cells were transfected with miR-181a mimic or scramble miR mimic at 100 nM via lipofectamine RNAiMAX or left untreated – these served as the baseline control in each fibroblast population. 72h post-transfection the cells were washed with PBS, lysed in the lysis buffer provided by the facility and spun down to pellet the cellular debri. The supernatant was subsequently removed, mixed with 4xSDS (containing Be-Mercaptoethanol 1:10) to be denatured at 95°C for 5 min, followed by long-term storage at -80°C until sample submission. All samples had a protein concentration of 0.5-1.5 µg/µL - according to the facility's requirements - as measured by the Pierce BCA Protein Assay and were submitted for RPPA analysis in January 2020. Given the turnaround time of 8-10 weeks after sample submission means that the results could not be included in this version of the thesis.

4.7. Investigating dosage-dependent effects of miRNAs via lipofectamine RNAiMAX

After having explored the biological effects of miR-181a and miR-27a in more detail, I redirected my attention to the original quest of investigating combinatorial effects of the three chosen miRNAs. A lingering belief persisted that - despite no synergy being observed at the concentrations tested (100 nM) - synergy might exist at other concentrations of miRNAs. MiRNAs are believed to exert dosage-dependent effects on cells, which led me to hypothesise that different relative concentrations of miRs-181a, -27a and -30a might potentially have cooperating effects. This, in turn, led me to investigate whether, first of all, delivery mediated via lipofectamine RNAiMAX could control the dosage of miRNA transfected into cells.

To verify this miR-181a mimic was transfected at 10-100 nM into nondiabetic dermal fibroblasts [j] and miR-181a expression was measured 48h post transfection via Taqman-qPCR. The fold change in miR-181a expression was calculated relative to fibroblasts transfected with 100nM scramble miR mimic. Results showed that the fold change in miR-181a expression was very similar across all concentrations, suggesting that lipofectamine RNAiMAX cannot control the miRNA dosage delivered (Figure 69).

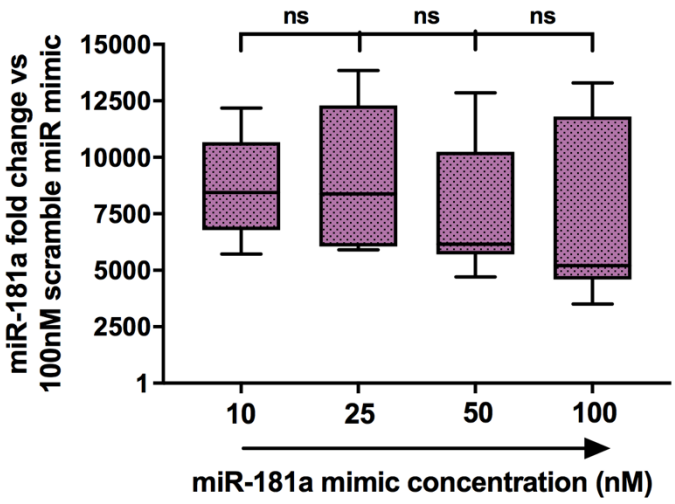


Figure 69: lipofectamine RNAiMAX cannot control the amount of miR-181a delivered into primary dermal fibroblasts as transfection of miR-181a mimic at 10-100nM causes similar levels of miR-181a overexpression at all concentrations of mimic 48h post-transfection (p=0.5186). The fold change in miR-181a expression was calculated

[j] This concentration range of miR-181a mimic was chosen according to the manufacturer's suggestions of concentrations to be tested with miRNAs, as well as literature search which showed that this is one of the most common ranges of miRNA mimics to use for gain-of-function studies

relative to fibroblasts transfected with 100 nM scramble miR mimic. Box and whisker plots span min to max. Statistical analysis was performed via one-way ANOVA. N=3, n=3/donor

However, given that it was unknown how much of the miR-181a becomes functional at the various concentrations transfected – due to the limitation of liposomal-based delivery method - I measured the expression of KRAS and PTEN in the same RNA samples via Taqman-qPCR to check if a difference could be observed at the gene level instead. The fold change in these two genes was determined relative to fibroblasts transfected with scramble miR mimic, with ACTB serving as the internal normalisation gene. Similar to miR-181a over-expression levels, the fold changes of KRAS or PTEN turned out to be similar across all concentrations tested (Figure 70). The finding that transfection of miR-181a mimic at increasing concentration via lipofectamine RNAiMAX causes no differential effect at the mRNA level on target genes, reinforced that lipofectamine RNAiMAX cannot control the dosage of miRNA delivered.

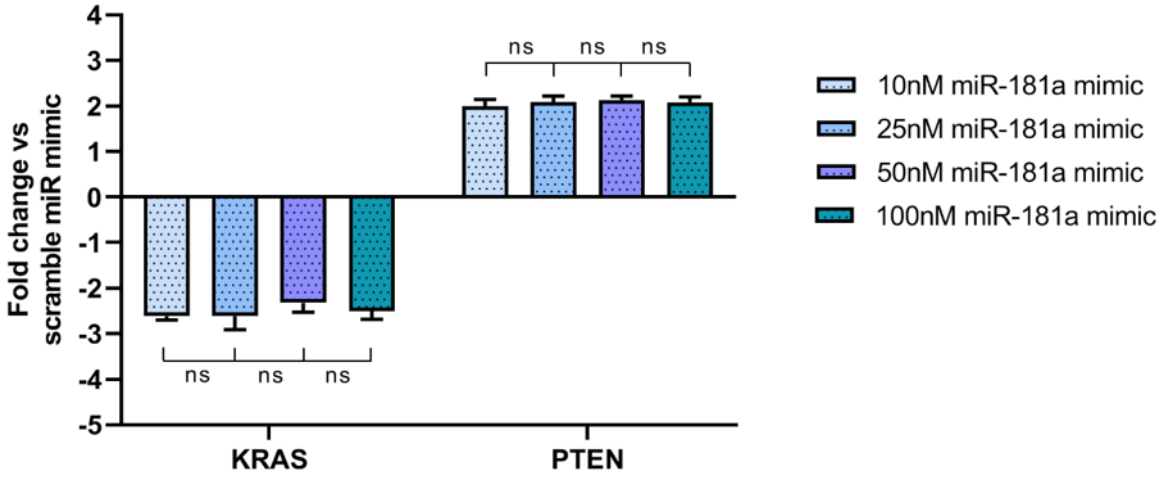


Figure 70: 48h post-transfection of miR-181a mimic into primary dermal fibroblasts via lipofectamine RNAiMAX KRAS and PTEN become suppressed and upregulated, respectively by the same amount at all concentrations of miR-181a mimic transfected (p=0.0743 for KRAS and p=0.3199 for PTEN). This reinforced that lipofectamine RNAiMAX cannot control the dosage of miRNA delivered. Bars show mean ± SD. Statistical analysis was performed via one-way ANOVA. N=3, n=3/donor

To further support the findings that lipofectamine RNAiMAX cannot control the miRNA dosage transfected I tested the effects of miR-181a or miR-27a mimics at 10-100 nM on proliferation in nondiabetic fibroblasts to check if changes may occur in cell behaviour at the various concentrations. 5 days post transfection of the miRNA mimics proliferation was measured via Presto Blue and the fold change was determined relative to fibroblasts transfected with scramble miR mimic at 10-100 nM, respectively. This testing showed that

miR-181a over-expression caused an increase in cell proliferation at all mimic concentrations (Figure 71), while miR-27a over-expression caused a ~25% suppression in cell proliferation at all concentrations of mimic tested (Figure 72).

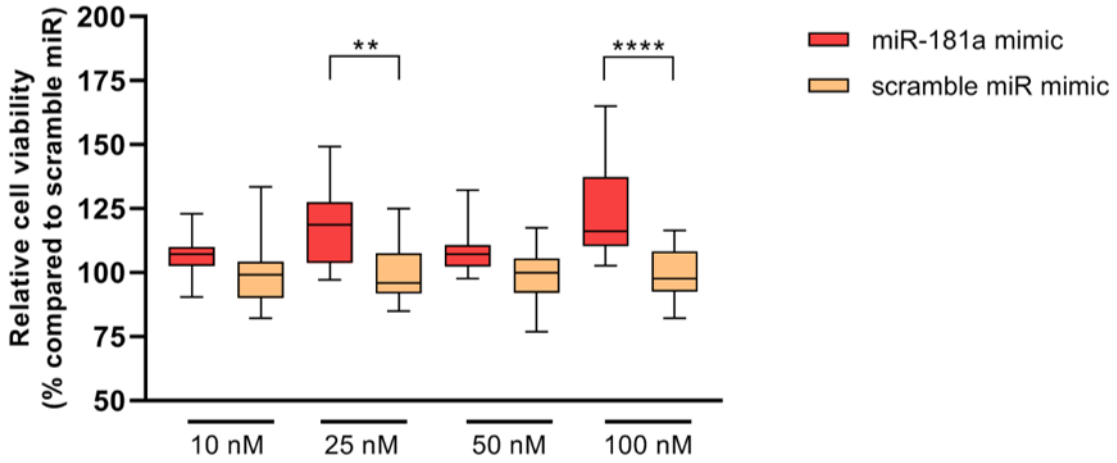


Figure 71: transfection of miR-181a mimic at 10-100 nM via lipofectamine RNAiMAX into nondiabetic dermal fibroblasts increases cell proliferation at all concentrations of miR-181a mimic tested, showing no differential behaviour. Proliferation was measured 5 days post transfection via Presto Blue and the fold change was determined relative to fibroblasts transfected with scramble miR mimic at 10-100 nM, respectively. Box and whisker plots span min and max. Statistical analysis was performed via one-way ANOVA, followed by posthoc Tukey's multiple comparisons test. **p<0.01, ****p<0.0001. N=2, n=9/donor

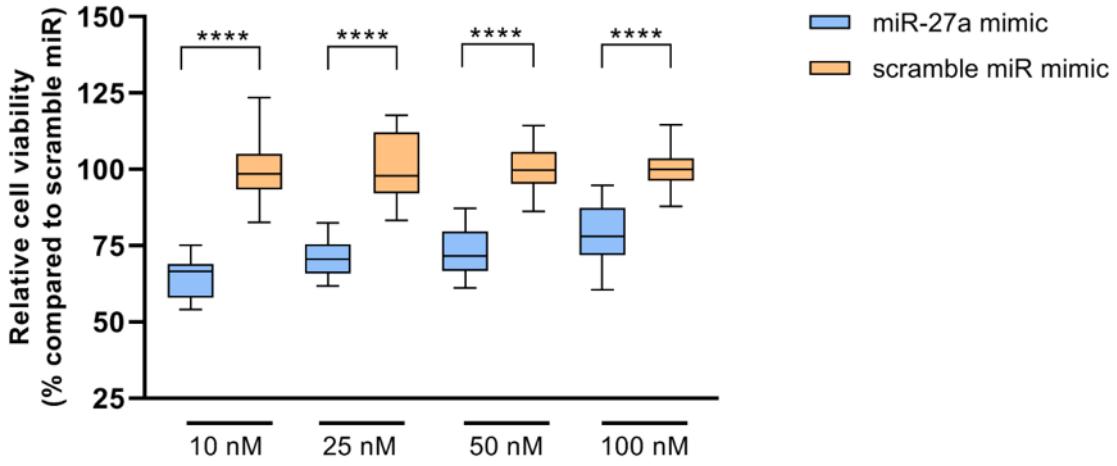


Figure 72: transfection of miR-27a mimic at 10-100 nM via lipofectamine RNAiMAX into nondiabetic dermal fibroblasts causes suppression of cell proliferation at all concentrations of miR-27a mimic tested, exhibiting no differential behaviour in between these concentrations. Proliferation was measured 5 days post transfection via Presto Blue and the fold change was determined relative to fibroblasts transfected with scramble miR mimic at 10-100 nM, respectively. Box and whisker plots span min and max. Statistical analysis was performed via one-way ANOVA, followed by posthoc Tukey's multiple comparisons test. **p<0.01, ****p<0.0001. N=2, n=9/donor

Finally, to rule out any cell specific effects of liposomal-based transfection miR-181a mimic was also transfected into HUVEC (endothelial cells) at 10-100 nM and proliferation was measured 3 days later relative to HUVEC transfected with scramble miR mimic. The same effect on cell proliferation was observed with HUVEC as with fibroblasts, namely miR-181a over-expression increased cell proliferation at all concentrations of mimic tested (Figure 73). These results overall suggested that although lipofectamine RNAiMAX works very well at transfecting miR mimics into primary dermal fibroblasts (or HUVEC), it cannot control the dosage of miRNA delivered. In turn, this precludes the ability to study dosage-dependent effects of miRNAs.

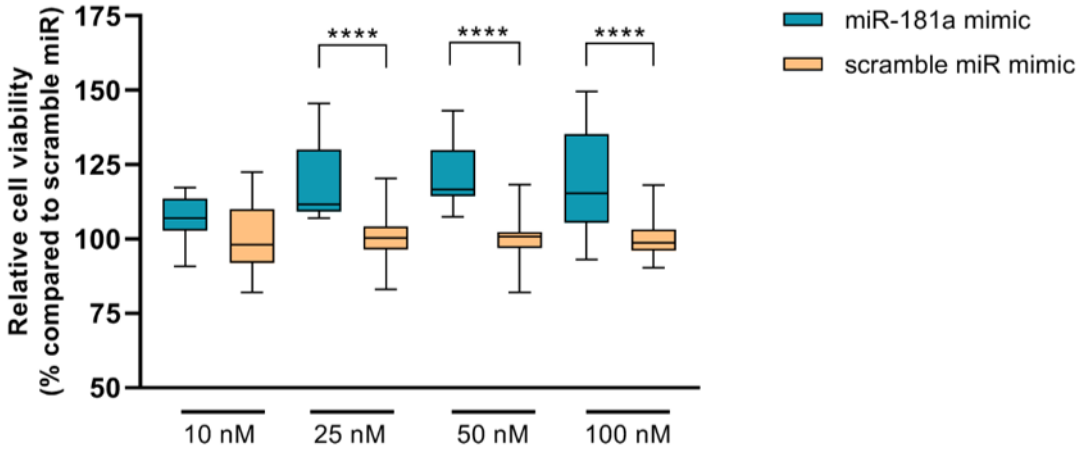


Figure 73: transfection of miR-181a mimic at 10-100 nM via lipofectamine RNAiMAX into HUVEC increases cell proliferation at all concentrations of miR-181a mimic tested, showing no differential effects. Proliferation was measured 5 days post transfection via Presto Blue and the fold change was determined relative to HUVEC transfected with scramble miR mimic at 10-100 nM, respectively. Box and whisker plots span min and max. Statistical analysis was performed via one-way ANOVA, followed by posthoc Tukey's multiple comparisons test. **p<0.01, ****p<0.0001. N=2, n=9/donor

Being able to control how much miRNA gets delivered into a cell is crucial as dose-dependent effects of miRNAs may lead to dual behaviour in certain cell types. One such example includes miR-17-92 that was shown to decrease HCT116 cell viability at low doses (0.00003 μg plasmid), but increase cell viability at high doses (0.3 μg plasmid) [200]. However, despite their wide implication and importance, dosage-dependent effects of miRNAs remain vastly unexplored with most studies performed at one concentration of miRNA only. These approaches, however might only provide a snapshot of a miRNA's effects as miRNAs were shown to target genes based on a narrow range of functional dose, i.e. an optimal range that

causes maximal target suppression beyond which the particular mRNA is no longer a viable target (Figure 74). This functional dose may be different for each target gene with factors such as expression levels of the targets, number of miRNA-binding sites on the target mRNA and feedback loops being able to shift this narrow window for effective gene suppression. In turn, this means that for any given concentration of miRNA different targets will be suppressed by different amounts, which can result in selective downregulation of target genes at different doses.

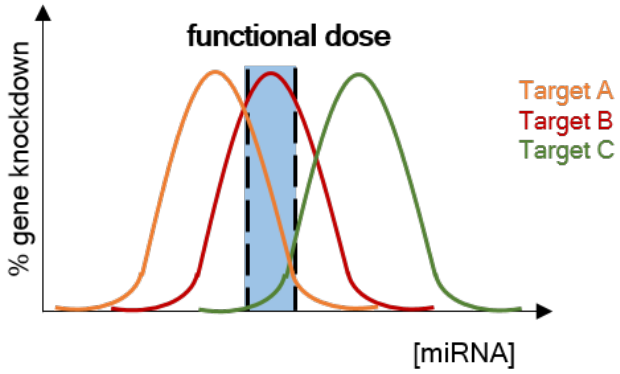


Figure 74: MiRNAs have different functional doses for different target genes causing dose-dependent mRNA target selection. I believe that the trend of gene knockdown at increasing miRNA concentrations most likely follows a Gaussian trend. Functional dose is defined as a narrow range of miRNA concentration that causes maximal target suppression beyond which the particular mRNA is no longer a viable target

For instance, a study showed that transfection of let-7a-7f plasmid into Huh-7 cells via lipofectamine 2000 caused suppression of its target gene cMYC at 0.03 μg, but caused its over-expression at 0.3 μg, while for target gene CCND1 suppression occurred at 0.00003 μg and 0.003 μg but not in between [200] (Figure 75). Notably, the functional dose for cMYC required a 1000-fold stronger dose for its suppression compared to CCND1, illustrating how functional doses can span several orders of magnitude for different target genes.

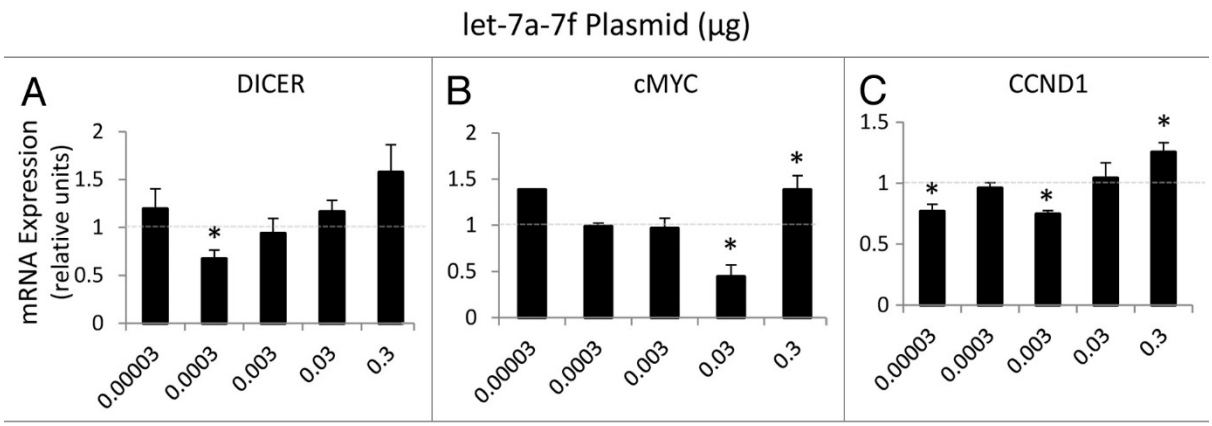


Figure 75: transfection of let-7a-7f plasmid into Huh7 cells via lipofectamine 2000 causes different amounts of repression of its target genes cMYC and CCND1 at the different concentrations tested. Image reproduced from [200] with permission of the rights holder, Taylor & Francis

Furthermore, as miRNAs do not work individually this dose-dependent mRNA target selection becomes even more complex when combinations of miRNAs, with potentially overlapping targets, are taken into account. This is because different relative concentrations of miRNAs can start suppressing different sets of genes, leading to activation of different signalling pathways, in turn triggering different cellular responses (Figure 76).

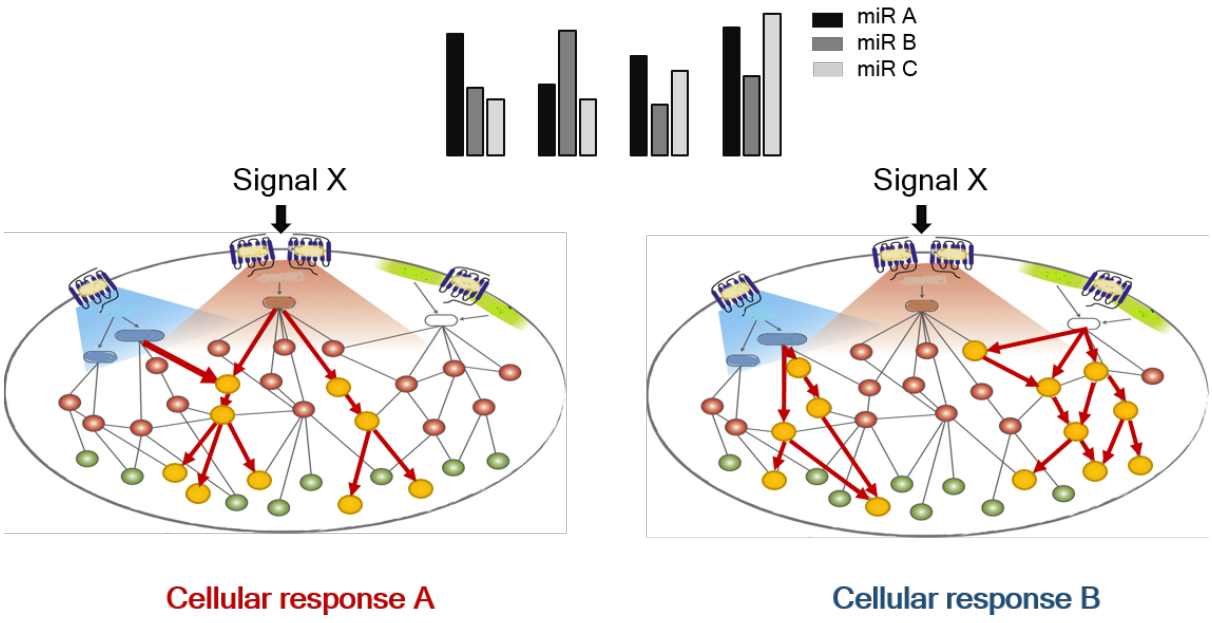


Figure 76: miRNA combinations can trigger different effects at varying relative concentrations of miRNA by changing the sets of genes targeted, in turn activating different cellular pathways leading to different cellular behaviour. Image modified from [201] with permission of the rights holder, Elsevier

As such, we need to study the incremental effects of miRNA dosage to gain a more complete understanding of how miRNAs regulate cellular behaviour - either individually or in combinations - which means a method is required that can precisely control how much miRNAs is delivered into the cell. Although the one study presented here indicated that dose-dependent transfection of miRNA could be achieved, the authors transfected miRNA-coding plasmids into cells (as opposed to mature miRNA mimics). This might not be so useful in certain diseases like diabetes where the miRNA-processing machinery is impaired and may not be able to process the miRNA gene-encoding plasmids efficiently or for cell types, where liposomal-based transfection does not work. However, even in the case of transfection of mature miRNA mimics I showed that liposomal-based delivery offered no control over how much miRNA was entering the fibroblasts. This is mainly because this method of delivery relies on the endosomal pathway to transfect miRNAs, which is a primarily stochastic mechanism.

Overall, these results collectively showed it is likely necessary to use a different approach to achieve controlled delivery of miRNAs.

4.8. Methods

4.8.1. Testing the integrity and size of the miRNA mimics or small RNAs extracted via the miRVana microRNA kit

~50ng of RNA (microRNA mimics or total RNA extracted) was run on a pre-cast 15% denaturing urea polyacrylamide gel in XCell sure-lock mini cells according to the manufacturer's instruction: 5 μL RNA mixed with 5 μL of TBE-Urea sample buffer (2x) was loaded into the wells. The RNA samples were then heated at 95°C for 4min in a hotplate and then immediately chilled in ice. Prior to loading the samples the gel was pre-run at 180V and ca. 10mA in constant voltage mode for 45 min to ensure homogenous distribution of the heat throughout the gel and avoid the 'smile' effect. To quantify the size of the microRNA mimics a 10/60 DNA ladder was further used following the same procedure: 1 μL of ladder was added to 4 μL RNAse-free deionised water and 5 μL of TBE Urea sample buffer (2x) to yield 10 μL total volume. The gel was run for ~80 min at 180V and ca. 10mA in constant voltage mode at which point the tracking dyes bromophenol blue and xylene cyanol contained in the TBE-urea sample buffer migrated three-quarters down the gel (Figure 77). Once this finished the gel was removed from the cast and stained with freshly-made 1xSybr Gold in 1xTBE for 20 min at room temperature in the dark on the orbital shaker. The bands were then visualised with a Gel Documentation System using the Sybr gold filter, UV epi-illumination and 3000-5000 ms exposure time.

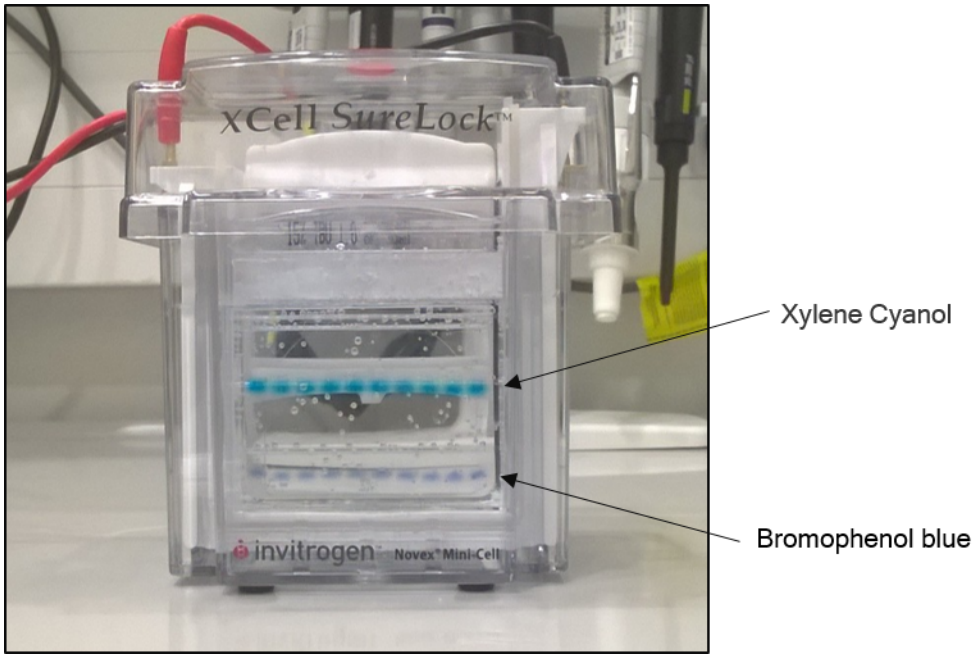


Figure 77: xylene cyanol and bromopheol blue are tracking dyes used in loading gels that aid to keep a visual track over how far down the gel DNA or RNA has migrated. Image shows a loaded pre-cast 15% denaturing urea polyacrylamide gel in XCell SureLock mini cells after having run for 80 min at 180V and 10mA in constant voltage mode

4.8.2. Protocol for miRNA mimics or inhibitors transfection via lipofectamine RNAiMAX

	96-well plate	**24-well plate**	**12-well plate**
Surface area of well	0.32 cm^2	2 cm^2	4 cm^2
Final volume/well	100 µL	500 µL	1000 µL
Number of adherent cells	5-8x10^3	18-25x10^3	40-50x10^3
Opti-MEM	50 µL	100 µL	200 µL
Lipofectamine RNAiMAX	3 µL	6 µL	12 µL
Opti-MEM	50 µL	100 µL	200 µL
miRNA stock (10-100 µM)* **(for synergistic protocol: 100 µM)**	1µL miR (+ 2µL scr miR)	2µL miR (+ 4µL scr miR)	4µL miR (+ 8µL scr miR)
Diluted lipofectamine	50 µL	100 µL	200 µL
Diluted miRNA	50 µL	100 µL	200 µL
Incubate for 10min at room temperature in 1:1 ratio			
miRNA-lipofectamine mix/well	10 µL	50 µL	100 µL
Final miRNA concentration/well* **(for synergistic protocol)**	10-100 nM (300 nM)	10-100 nM (300 nM)	10-100 nM (300 nM)
Number of replicates	10	4	4
Final lipofectamine RNAiMAX/well	0.3 µL	1.5 µL	3 µL

Table 15: protocol used for transfection of miRNA mimics or inhibitors via lipofectamine RNAiMAX

*The miRNA stock solution concentration was 10-100 μM, such that depending on the stock concentration the final miRNA concentration/well was 10-100 nM, i.e. if the stock concentration was 50 μM, the final miRNA concentration/well was 50 nM etc.

For the synergistic protocol the stock solution of each miRNA was kept at 100 μM, such that the concentration of each functional miRNA was 100 nM/well and the final concentration of all three miRNAs was 300 nM/well. For the 'individual' miRNA conditions the respective miRNA was spiked with scramble miRNA to keep the total miRNA concentration/well at 300 nM.

4.8.3. Transfection of dy547 miR mimic into primary dermal fibroblasts

Nondiabetic fibroblasts at P4 were seeded at 18,000 cells or 22,000 cells/well in 24-well plates and at 5,000 cells or 8,000 cells/well in 96-well plates in full DMEM and left to adhere overnight. The following day the cells were washed twice with PBS prior to dy547-miR transfection and medium was replaced with antibiotic-free basal DMEM (supplemented with 2.5 mM L-glutamine). Dy547-miR was transfected at 10-30nM final concentration via lipofectamine RNAiMAX. The cells were returned to the incubator for another 24h at which point they were stained with Hoechst 33342 and fixed in 4% PFA. Images were taken with the Inverted Widefield Zeiss Axio Observer microscope in the DAPI and Cy3 channels.

4.8.4. Transfection of miR mimic positive control into primary dermal fibroblasts

Nondiabetic fibroblasts at P4 were seeded in 24-well plates at 25,000 cells/well in 450 μL antiobiotic-free DMEM (supplemented with 10% FBS, 2.5 mM L-glutamine) and left to adhere overnight. The next day miR mimic positive control (against GAPDH) was delivered at 100 nM via lipofectamine RNAiMAX. 48h post-transfection RNA was extracted via the Purelink RNA microscale kit and the amount and purity checked with Nanodrop 2000. RT was performed on 100 ng RNA using the nanoScript2 kit (Primerdesign). qPCR was run using Taqman primers (Primerdesign) and the TaqMan™ Fast Universal PCR Master Mix (2X), no AmpErase™ UNG (Thermofisher). 5 ng RT product in 10 μL/well was run on the ABI 7500 fast real-time machine using beta actin as the internal normalisation gene. The $2^{-\Delta\Delta CT}$ method

was used to determine the fold change in GAPDH expression compared to cells transfected with scramble miR mimic.

4.8.5. Transfection of siRNAs into primary dermal fibroblasts

Nondiabetic fibroblasts at P6 were seeded at 50,000 cells/well in 12-well plates in 900 μL antibiotic-free DMEM (supplemented with 10% FBS and 2.5 mM L-glutamine)/well and left to adhere overnight. The next day siRNAs against CAV1 or scramble miRNA mimic were delivered at 25 nM/well in triplicates via lipofectamine RNAiMAX. 24h later the medium was replaced with fresh DMEM and the cells were left to incubate for another 24h. The next day (48h after siRNA delivery) the cells were lysed and total RNA was extracted via the PureLink RNA MicroScale Kit. 300ng of total RNA was later reverse transcribed into cDNA using oligodT primers. qPCR was run with 5ng cDNA/well in 10 μL volume/well on the ABI 7500 fast machine using double-dye Taqman probes. Beta actin was used as the housekeeping gene and the 2-delta delta CT method was used to quantify the fold change in gene expression and the amount of gene knockdown.

4.8.6. Performing reverse transcription on mRNA

cDNA synthesis was done using the ProFlex PCR System (Applied Biosystems) in two steps – *annealing* step to anneal the oligodT primers and *extension* step to extend the newly synthesised cDNA:

a) Annealing step

For each RNA sample the following reagents were added to a 0.2mL PCR tube:

Component	1 reaction
RNA template (≤2 µg)	X µL
OligodT primer	1 µL
RNase/DNase free water	X µL
Final volume	**10 µL**

Table 16: first step in reverse transcription of mRNAs involves annealing the oligodT primers

The samples were heated to 65°C for 5 min followed by immediate cooling in ice.

b) Extension step

A mix was made up for all the reactions required according to the following:

Component	1 reaction
nanoScript2 4x buffer	5 µL
dNTP mix 10 mM	1 µL
RNAse/DNAse free water	3 µL
nanoScript2 enzyme	1 µL
Final volume	**10 µL**

Table 17: second step in reverse transcription of mRNAs involves synthesis of cDNA

10 µL of the RT mix was added to each sample on ice, followed by brief vortexing and a pulse spin. The samples were then incubated at 42°C for 20 min followed by heat inactivation at 75°C for 10 min. The resulting cDNA samples were stored at -20°C for long-term storage. Negative RT controls were also run to exclude genomic DNA amplification.

4.8.7. Running Taqman-qPCR on cDNA synthesised from mRNA

Double-dye Taqman probes (FAM/MGB) were used for qPCR. The following qPCR mix was made for each gene of interest (i.e. set of primers) for the total number of wells required:

Component	1 well
Primer (20x)*	0.5 µL
Taqman fast universal PCR mastermix (2x)	5 µL
RNase/DNase free water	3.5 µL
Final volume	**9 µL**

Table 18: the mix added to each well in the PCR plate includes primers, mastermix and water, followed by addition of cDNA later on

9 µL was added to each well, followed by addition of 1 µL of cDNA from each sample (2.5-10 ng RT product)/well in triplicates, i.e. three wells on the PCR plate. The qPCR plate was then sealed with an adhesive sheet and briefly centrifuged prior to amplification at the following conditions on the ABI 7500 fast real-time PCR machine:

Polymerase activation	PCR (40 cycles)	
Hold at 95°C	**Denature at 95°C**	**Anneal/extend at 60°C**
20 seconds	3 seconds	30 seconds

Table 19: qPCR on mRNA consists of three steps involving activation of the polymerase, followed by amplification over 40 cycles

The following settings were selected on the machine: Taqman reagents, fast run mode, standard curve, FAM and MGB probes, ROX present, 10 µL volume. After the 40 cycles of amplification a CT threshold was selected in the linear range of the amplification curves between 0.1-0.2 (Figure 78). Non-template controls were also run to exclude non-specific amplification, as well as negative RT controls to exclude genomic amplification.

Following amplification the average CT value was computed for each sample from the three technical replicates only if the range of their CT values was within 0.5, otherwise that sample was not be taken into consideration.

To determine the fold change in gene expression the $2^{-\Delta\Delta CT}$ method was used.

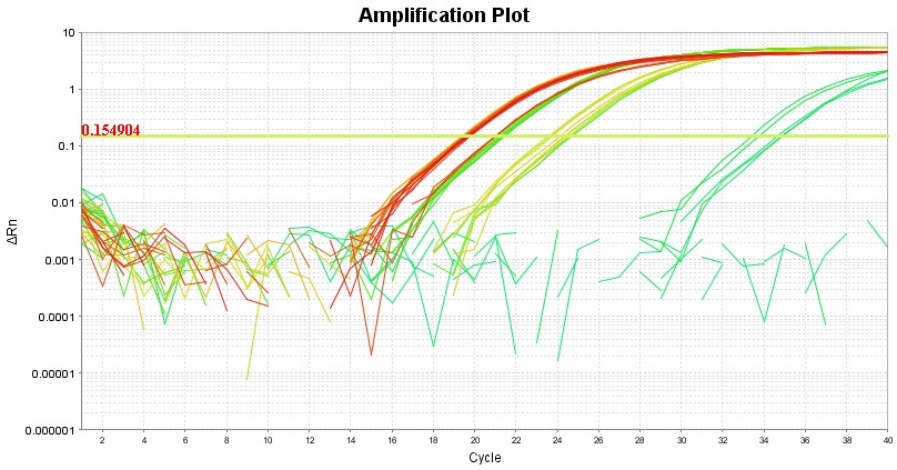


Figure 78: typical amplification curve observed after a qPCR run. The CT threshold for gene expression was chosen in the linear region of the amplification curve (note the log scale on the y-axis) between 0.1-0.2

*All primers were designed, validated and synthesised by Primerdesign.

4.8.8. Checking integrity of large RNA extracted via Purelink Microscale RNA kit or miRVana miRNA isolation kit on nondenaturing agarose gels

Briefly, 1% native agarose gels were made by dissolving 1g of agarose in 100 mL 1xTBE in the microwave and letting it cool down to room temperature. The agarose solution was poured into the tray containing combs and left to solidify for ~60 min at room temperature. The combs were gently removed and the gel moved into the electrophoresis tank which was covered with 1xTBE buffer. ~100ng RNA in 10 µL final volume containing 9 µL RNA and 1 µL of 10x gel loading solution (all purpose, native agarose) was carefully loaded into each well. The gel was run at 90V for ~80 min until the bromophenol blue has migrated 2/3 of the way down (Figure 79). The gel was then removed and stained with 1xSybr Gold in 1xTBE buffer for 30 min in the dark while being gently shaken. The RNA bands were visualised with a UV transilluminator.

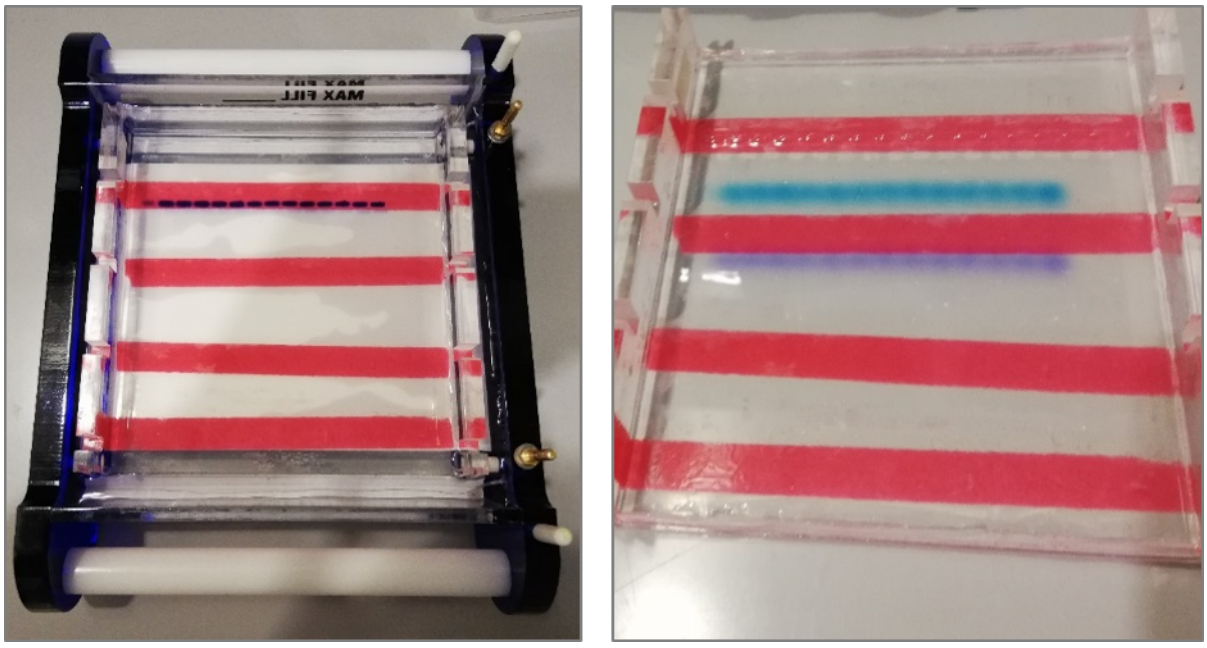


Figure 79: native 1% agarose gels with loaded RNA samples before the run started (left) and after it finished (right). Gel was run at 90V for 80 min.

4.8.9. Checking qPCR amplification efficiency of cDNA synthesised from mRNA or miRNAs

Total RNA extracted from a confluent T75 flask of nondiabetic fibroblasts via the miRVana miRNA isolation kit was serially diluted 1:2 in a range of 22.5-720 ng RNA/RT reaction and reverse transcribed using oligodT primers. qPCR was then run on the BETA ACTIN, KRAS, IRS1 and PTEN genes using double-dye Taqman probes to check the amplification efficiency of these genes. The same total RNA extracted via miRVana microRNA isolation kit was serially diluted 1:2 in a range of 0.625-10 ng/RT reaction and reverse transcribed using stem-loop miRNA primers for RNU44. qPCR was run using miRNA Taqman probes to check for amplification of efficiency.

Once amplification finished the average CT values vs $\log_{10}$ of (ng total RNA/RT reaction) was plotted and using linear regression analysis the equation for the line was obtained in the form y = mx+c, where m represents the gradient of the line. This value was then used to calculate the amplification efficiency, A using the formula $A = (10^{-1/m} -1)*100\%$, with amplification efficiency values between 90-110% being desirable.

4.8.10. Extracting total RNA via the miRVana miRNA isolation kit

This RNA extraction kit was used as it allows isolation of total RNA containing small RNAs (<200nt) as opposed to the PureLink RNA kit that extracts only large RNA.

Briefly, the cells were washed with PBS prior to lysis in cell lysis buffer on ice and being scraped into a microcentrifuge tube. The cell lysate was briefly vortexed followed by addition of miRNA homogenate additive (10min incubation on ice) and 1 volume of acid phenol-chloroform equal to the initial lysate. The mixture was vigorously vortexed for 1min and centrifuged at 10,000xg for 5 min at 12-14 °C to separate the organic phase (containing proteins and DNA at the interface) and the aqueous phase (containing the RNA). The aqueous (upper) layer was carefully removed, followed by addition of 1.25 volumes of 100% ethanol and passed through a filter cartridge. The filter cartridge was then washed three times with wash solutions and eluted in nuclease-free water pre-heated to 95°C. The eluate contained total RNA (i.e. small and large RNAs) which made it suitable for qPCR analysis on both

microRNAs and mRNAs from the same sample. The RNA samples were then treated with DNAse to remove any traces of genomic DNA contamination.

4.8.11. Running RT on microRNAs

microRNAs were reverse transcribed with a specific stem-loop primer unique to each miRNA (as opposed to the oligodT primers that reverse transcribe all mRNAs with a polyA tail) as part of Taqman microRNA assays*.

1-10 ng of total RNA (in 5 µL) extracted via the microRNA miRVana kit was added to 0.2 mL PCR tubes for each stem-loop miRNA primer of interest.

The following RT mix was prepared for all the reactions needed:

Component	1 reaction
100mM dNTPs (with dTTP)	0.15 µL
MultiScribe Reverse Transcriptase, 50 U/µL	1 µL
10x Reverse Transcription Buffer	1.50 µL
RNase inhibitor, 20 U/µL	0.19 µL
Nuclease-free water	4.16 µL
Total volume	**7 µL**

Table 20: the mastermix for running qPCR on microRNAs contains dNTPs, reverse transcriptase, reverse transcription buffer, RNAse inhibitor and water

7 µL of the mastermix was added to each PCR tube containing the RNA, followed by addition of 3 µL of 5xRT primer to the corresponding tubes to yield a 15 µL RT reaction.

The RT samples were incubated on ice for 5 min and briefly centrifuged prior being loaded on the ProFlex PCR System (Applied Biosystems) at the following conditions to synthesise cDNA:

Step	Time	Temperature
Hold	30 minutes	16°C
Hold	30 minutes	42°C
Hold	5 minutes	85°C
Hold	Infinite	4°C

Table 21: reverse transcription of microRNAs involves three holding steps at various temperatures for different periods of time

The cDNA samples were then incubated at -20°C for long-term storage. Negative RT controls were also run to exclude genomic DNA amplification.

*All Taqman microRNA assays were purchased from Applied Biosystems. Each assay contained a vial of miRNA-specific stem loop primer (5x) and a vial of Taqman probe/primer (20x).

4.8.12. Running qPCR on microRNAs

The following components were pipetted into microcentrifuge tubes for each RT sample:

Component	Volume for 3 replicates
Taqman small RNA assay (20x)	3.60 µL
Product from RT reaction	4.80 µL
Taqman fast advanced mastermix (2x)	36.00 µL
Nuclease-free water	27.61 µL
Total volume	**72.01 µL**

Table 22: the mastermix for running qPCR on microRNAs consists of Taqman probes, cDNA, mastermix and water

The tubes were mixed and briefly centrifuged followed by transferring 20 µL of the qPCR reaction mix into three wells in the 96-well PCR plate. The plate was briefly centrifuged and loaded into the ABI 7500 fast real-time PCR system at the following conditions:

Polymerase activation	PCR (40 cycles)	
Hold at 95°C	**Denature at 95°C**	**Anneal/extend at 60°C**
20 seconds	3 seconds	30 seconds

Table 23: qPCR runs on microRNAs consist of polymerase activation, followed by cDNA amplification over 40 cycles

The following settings were selected on the machine: Taqman reagents, fast run mode, standard curve, FAM and MGB probes, ROX present, 20 µL volume. After the 40 cycles of amplification the same threshold was selected for all microRNAs in the linear range of the amplification curves (between 0.1-0.2). Non-template controls were also run to exclude non-specific amplification, as well as negative RT controls to exclude genomic amplification.

Following amplification the average CT value was computed for each sample from the three technical replicates only if the range of their CT values was within 0.5, otherwise that sample would not be taken into consideration.

To determine the fold change in gene expression the $2^{-\Delta\Delta CT}$ method - a widely used technique for presenting relative gene expression [202] – was employed.

4.8.13. Over-expression of miRNAs after transfection of miR mimics (synergy protocol)

Nondiabetic fibroblasts were seeded at 40,000 cells/well in 900 μL antibiotic-free DMEM (supplemented with 10% FBS and 2.5 mM L-glutamine)/well in 12 -well plates and left to adhere overnight. The next day miRNA mimics were delivered via lipofectamine RNAiMAX at 300 nM final concentration/well according to the 'synergy protocol'. The next day the medium was replaced with fresh DMEM and the cells were left in culture for another 24h. The following day (48h after transfection) the cells were washed with PBS twice and trypsinised before RNA extraction via the microRNA miRVana kit. 20 ng of total RNA was reverse transcribed using stem-loop specific miRNA primers and qPCR was run on the ABI 7500 fast machine to check for miRNA over-expression. RNU44 served as the internal normalisation gene and the fold change in miRNA expression was determined relative to cells transfected with 300 nM scramble miR mimic.

4.8.14. Effect of scramble miR mimic on cell proliferation

Nondiabetic fibroblasts were seeded at 5,000 – 7,000 cells/well in 96-well plate in antibiotic-free DMEM (supplemented with 10% FBS and 2.5 mM L-glutamine) and left to adhere overnight. The following day scramble miR mimic was transfected at 10-300 nM via lipofectamine RNAiMAX or left untreated. Proliferation was measured 5 days later via Presto Blue (1h incubation at 37°C) and the fold change in cell viability was calculated relative to untreated cells.

4.8.15. Testing synergy of miRNAs at functional level (proliferation assays)

Nondiabetic fibroblasts from 3 donors were seeded at 5,000 cells/well in 90 μL of antibiotic-free DMEM (supplemented with 10% FBS and 2.5 mM L-glutamine) in 96-well plates and left to adhere overnight. The next day miRNAs were delivered individually, pairwise and in triple combinations via lipof RNAiMAX at 300 nM final concentration/well. The following day the medium on the cells was replaced with fresh medium and the cells returned to the incubator for another 4 days. Proliferation was measured on day 5 (post miR transfection) via Presto

Blue (1h incubation at 37°C) and the fold change calculated relative to cells transfected with 300nM scramble miR mimic.

4.8.16. Testing synergy of miRNAs at gene level

Nondiabetic fibroblasts from 2 donors were seeded at 40,000 cells/well in 900 μL of antibiotic-free DMEM (supplemented with 10% FBS and 2.5 mM L-glutamine) in 12-well plates and left to adhere overnight. The next day miRNAs were transfected at 300 nM final concentration/well via lipofectamine RNAiMAX. 24h later after transfection the medium was replaced with fresh DMEM and the cells were left in the incubator for another 24h. The following day (48h after transfection) the cells were washed with PBS twice and trypsinised following by lysis of the cell pellet. Total RNA was extracted using the miRVana miRNA isolation kit and treated with DNAse prior to being reverse transcribed (100ng) into cDNA using oligodT primers. qPCR was run on the ABI 7500 fast machine using 5 ng RT product in 10 μL final volume/well. Beta actin was used as the internal normalisation gene.

4.8.17. Dual behaviour of miR-181a on proliferative ability of fibroblast populations

Nondiabetic, diabetic ulcerated and diabetic nonulcerated fibroblasts (3 donors/condition) were seeded at 5,000 cells in 96-well plates in 90 μL of antibiotic-free DMEM (supplemented with 10% FBS and 2.5 mM L-glutamine) and left to adhere overnight. The following day miR-181a mimic or miR-27a mimic were transfected at 100 nM via lipofectamine RNAiMAX. The medium was replaced 24h later with fresh DMEM and proliferation was measured 4 days later, i.e. 5 days post miRNA transfection via Presto Blue (1h incubation at 37°C). The fold change in proliferation were determined relative to fibroblasts transfected with 100 nM scramble miR mimic.

4.8.18. Effect on fibroblast proliferation after transfection of miRNA inhibitors

Nondiabetic fibroblasts (3 donors) were seeded at 25,000 cells/well in a 24-well plate in 450 μL of antibiotic-free DMEM (supplemented with 10% FBS and 2.5 mM L-glutamine) and left to adhere overnight. The following day miR-181a inhibitor or miR-27a inhibitor were transfected at 100 nM via lipofectamine RNAiMAX. Proliferation was measured 5 days later via Presto

Blue (1h incubation at 37°C) after transferring the supernatant from the 24-well plate into a 96-well plate suitable for the Varioskan Flash plate reader. The fold change in proliferation were determined relative to fibroblasts transfected with 100 nM scramble miR inhibitor.

4.8.19. Expression of miRs-181a & -27a and KRAS & PTEN following transfection of miRNA inhibitors

Nondiabetic fibroblasts were seeded at 25,000 cells/well in a 24-well plate in 450 μL of antibiotic-free DMEM (supplemented with 10% FBS and 2.5 mM L-glutamine) and left to adhere overnight. The following day miR-181a inhibitor or miR-27a inhibitor were transfected at 100 nM via lipofectamine RNAiMAX. Two days later the cells were washed once with PBS and total RNA was extracted using the microRNA miRVana isolation kit. Reverse transcription was performed on 10 ng of total RNA using Taqman-miRNA probes and qPCR was run on the ABI 7500 fast machine. RNU44 served as the internal normalisation gene and the fold change in miRNA expression was determined relative to fibroblasts transfected with 100 nM scramble miRNA inhibitor. 50 ng of the same total RNA extracted was used to run RT at the mRNA level using oligodT primers to check for KRAS and PTEN and qPCR was run on the ABI 7500 fast machine. ACTB served as the internal normalisation gene and the fold change in gene expression was determined relative to fibroblasts transfected with 100 nM scramble miR inhibitor.

4.8.20. Testing the effect of Ly294002 on fibroblast proliferation

Nondiabetic fibroblasts were seeded at 7,000 cells/well in 100 μL antibiotic-free DMEM (supplemented with 10% FBS and 2.5 mM L-glutamine) and left to adhere overnight. The next day the cells were treated with 50 μM of Ly294002 (100 μL/well), DMSO diluted in DMEM 1:1000 (same ratio as for Ly294002 dilution) or just fresh DMEM for 24h and 72h, respectively. For the 24h treatment the medium was replaced with fresh DMEM the following day. Proliferation was measured via Presto Blue (1h incubation at 37°C) on day 3 after Ly294002 treatment to check whether this PI3K inhibitor had any effect on slowing down cell proliferation. Given that the Ly294002 powder had to be dissolved in DMSO prior to dilution in DMEM, DMSO diluted 1:1000 was used as one of the controls to rule out the effect of DMSO

alone (which is usually toxic) on cell proliferation. The fold change in proliferation was compared to untreated cells.

4.8.21. Effect of miR-181a mimic and Ly294002 treatment on fibroblast proliferation

Nondiabetic fibroblasts were seeded at 7,000 cells/well in a 96-well plate in 100 μL of antibiotic-free DMEM (supplemented with 10% FBS and 2.5 mM L-glutamine) and left to adhere overnight. The following day the medium was replaced with 90 μL of 50 μM Ly294002 or 90 μL of DMEM containing DMSO diluted 1:1000. 1h later miR-181a mimic or scramble miR mimic were transfected into the cells at 100 nM via lipofectamine RNAiMAX. Proliferation was measured 5 days later via Presto Blue (1h incubation at 37°C). The fold change in proliferation was compared to cells transfected with 100 nM scramble miR mimic kept in DMEM containing DMSO.

4.8.22. PTEN and RPS6KB1 expression after miR-181a mimic transfection

Nondiabetic fibroblasts were seeded at 24,000 cells/450 μL of antibiotic-free DMEM (supplemented with 10% FBS and 2.5 mM L-glutamine) in a 24-well plate and left to adhere overnight. The following day miR-181a mimic or scramble miR mimic were transfected at 100 nM via lipofectamine RNAiMAX. 48h post-transfection total RNA was extracted using the miRVana miRNA isolation kit and 100 ng of total RNA was used for reverse transcription using oligodT primers. Taqman-qPCR was run on the ABI 7500 fast machine (2.5 ng RT product/10 μL volume) and the fold change in PTEN and RPS6KB1 was determined relative to cells transfected with 100nM scramble miR mimic. ACTB served as the internal normalisation gene.

4.8.23. Preparation of cell lysate for RPPA (6-well format)

Step 1: Fibroblasts were seeded in a 6-well plate at 150,000 cells in 2250 μL of antibiotic-free DMEM (supplemented with 10% FBS and 2.5 mM L-glutamine)/well and left to adhere overnight. The following day cells were transfected with miR-181a mimic or scramble miR mimic at 100 nM via lipofectamine RNAiMAX or left untreated.

Step 2: 24h post transfection of miRNA mimics 1mL of the medium was replaced in each well with fresh DMEM to dilute the effects of the lipofectamine.

Step 3: 72h post-transfection the cells were washed twice with PBS and lysed in lysis buffer (120 μL/well) for 20 min on ice with occasional shaking every 5 min.

Step 4: The cells were scraped off the plates and collected into 1.5 mL microcentrifuge tubes. The cell lysates were spun at 14,0000 rpm for 10 min at 4°C.

Step 5: The supernantant was carefully collected (90 μL) and transferred into a fresh tube.

Step 6: The cell lysate was mixed with 4xSDS (containing Be-Mercaptoethanol 1/10) in a 3:1 ratio, i.e. 75 μL of cell lysate with 25 μL of 4xSDS

Step 7: The samples were denatured at 95°C on a hotplate for 5 min and stored at -80°C until sample submission.

Step 8: The protein concentration in the cell lysate (before adding Be-Mercaptoethanol) was measured using Pierce BCA Protein Assay.

- A standard curve of BSA protein was created by diluting the stock BSA concentration (2000 μg/mL).
- 25 μL of the standard or test sample was pipetted in a 96-well plate (the test samples were first diluted 1:5, i.e. 5 μL of cell lysate + 20 μL water)
- Working reagent was prepared by mixing Reagent A with Reagent B in a 50:1 ratio, i.e. 8 mL reagent A with 160 μL reagent B.
- 200 μL of working reagent was added/well using a multichannel pipette and mixed several times.
- The well plate was incubated at 37°C for 30 min.
- The plate was cooled to room temperature and absorbance was measured at 562 nm using the Varioskan Flash plate reader.

The lysis buffer and 4xSDS buffer were provided by the RPPA Core Facility at MD Anderson Cancer Centre.

Lysis Buffer: 1% Triton X-100, 50mM HEPES, pH 7.4, 150mM NaCl, 1.5mM MgCl2, 1mM EGTA, 100mM NaF, 10mM Na pyrophosphate, 1mM Na3VO4, 10% glycerol, containing

freshly added protease and phosphatase inhibitors from Roche Applied Science Cat. # 05056489001 and 04906837001, respectively

4XSDS Sample Buffer: 40% Glycerol, 8% SDS, 0.25M Tris-HCL, pH 6.8. Before use, add Beta-mercaptoethanol (B-Me) at 1/10 of the volume.

4.8.24. Expression of miR-181a and KRAS &PTEN after transfection of miR-181a mimic at 10-100nM

Nondiabetic fibroblasts were seeded at 24,000 cells/well in 450 μL of antibiotic-free DMEM (supplemented with 10% FBS and 2.5 mM L-glutamine) in 24-well plates and left to adhere overnight. The next day miR-181a and scramble miR, respectively were delivered at 10-100 nM via lipofectamine RNAiMAX. 48h after miR delivery the cells were washed four times with PBS and trypsinised followed by lysis of the cell pellet and extraction of total RNA using the microRNA miRVana kit. 10 ng of total RNA was reverse transcribed into cDNA using specific stem-loop RT primers and qPCR was run on the ABI 7500 fast machine. RNU44 served as the internal normalisation gene. 100 ng of the same total RNA extracted was also reverse transcribed using oligodT primers to check for KRAS and PTEN expression and qPCR was run on the ABI 7500 fast machine. ACTB served as the internal normalisation gene. The fold change in miR-181a expression or KRAS/PTEN was calculated relative to fibroblasts transfected with scramble miR mimic.

4.8.25. Effect of miR-181a or miR-27a mimic on fibroblast proliferation at 10-100nM

Nondiabetic fibroblasts were seeded at 5,000 cells/well in 90 μL of antibiotic-free DMEM (supplemented with 10% FBS and 2.5 mM L-glutamine) in 96-well plates and left to adhere overnight. The next day miR-181a mimic or miR-27a mimic were transfected at 10-100 nM via lipofectamine RNAiMAX. The next day the medium was replaced with fresh DMEM and the cells returned to the incubator for another 4 days. 5 days after miR transfection proliferation was measured via Presto Blue (1h incubation at 37°C) by adding 100 μL of 1x pre-mixed Presto Blue /well. The fold change in proliferation was determined relative to cells transfected with 10-100 nM scramble miR mimic.

4.8.26. Effect of miR-181a mimic on HUVEC proliferation at 10-100nM

HUVEC (2 cell lines) were seeded at 8,000 cells or 6,000 cells/well, respectively in 90 μL of antibiotic-free basal medium (supplemented with 10% FBS) and left to adhere overnight. The following day miR-181a mimic or scramble miR mimic was transfected at 10-100 nM via lipofectamine RNAiMAX folowed by fresh medium replacement after 6h. The next day the medium was replaced with the usual cell culture medium. Proliferation was measured on day 3 post transfection via Presto Blue (1h incubation time at 37°C) and the fold change in proliferation was determined relative to HUVEC transfected with 10-100 nM scramble miR mimic.

4.9. Supplementary data

4.9.1. Effect of cell density on transfection efficiency of dy547-miR mimic via lipofectamine RNAiMAX

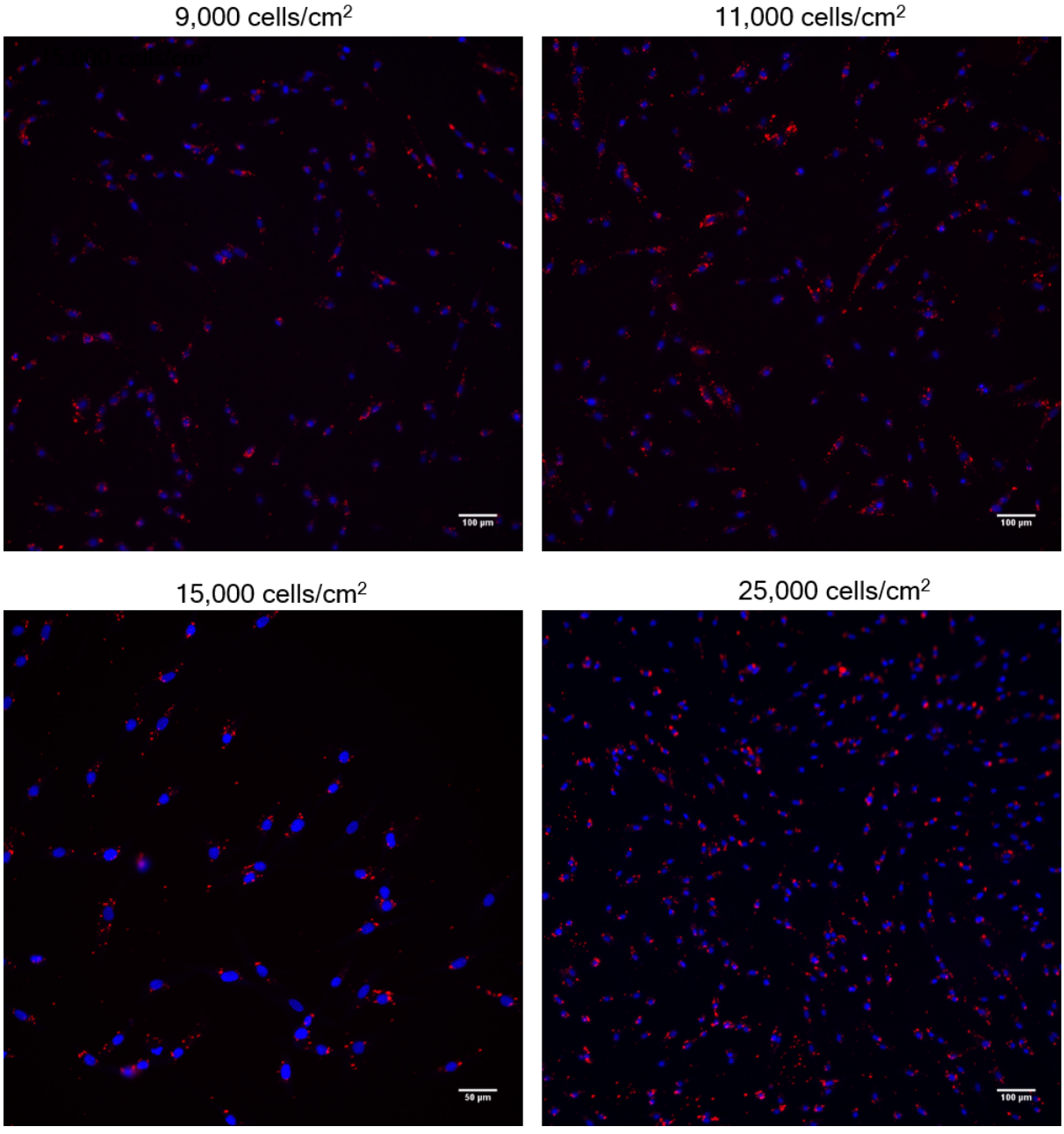


Figure 80: transfection of dy547-labelled scramble miRNA (red) into primary dermal fibroblasts occurs across all densities of cells tested. No notable difference in transfection efficiency is observed, showing that cells can be seeded at any of these densities for experiments. The scramble miRNA was transfected at 10-30 nM via lipofectamine RNAiMAX and cells were visualised 24h post transfection. Blue denotes the nuclear stain Hoechst 33342.

4.9.2. Checking integrity of large total RNA extracted via Purelink microscale RNA kit or miRVana miRNA isolation kit on nondenaturing agarose gels

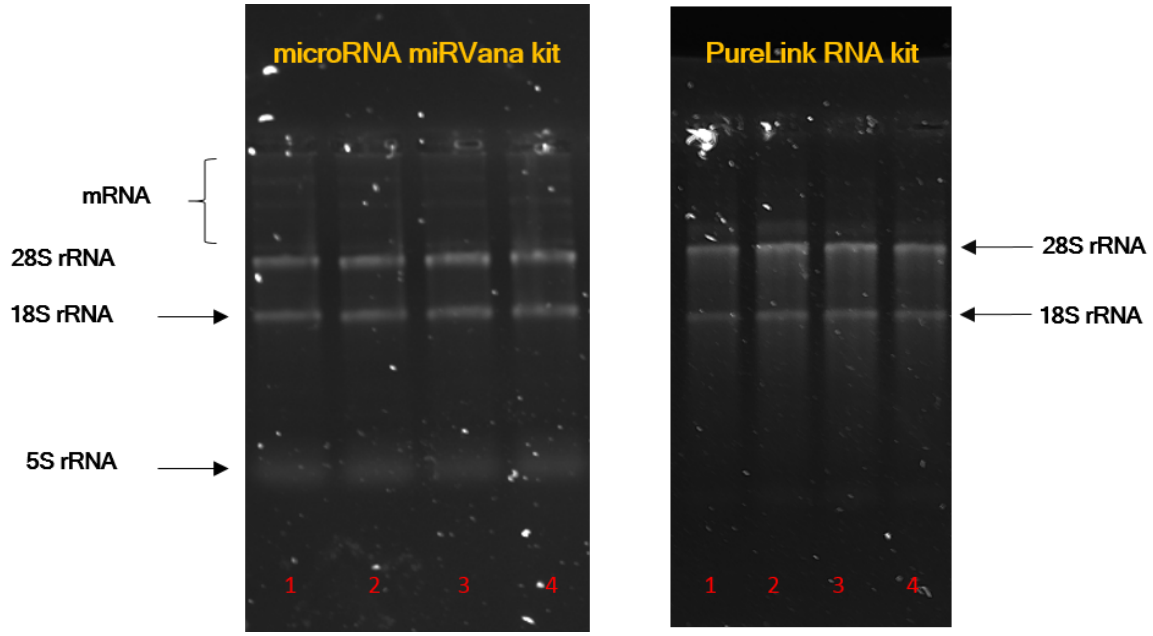
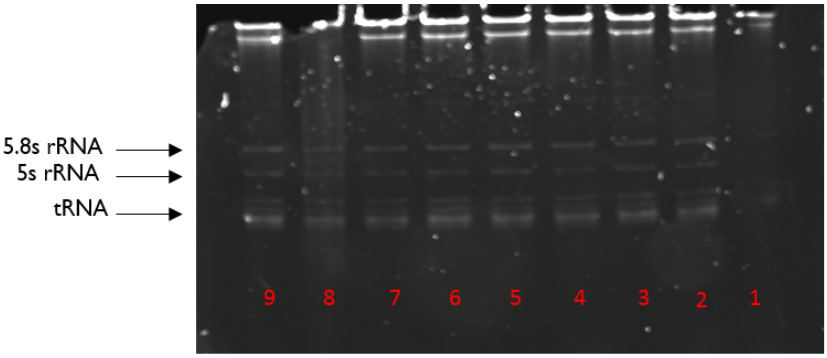
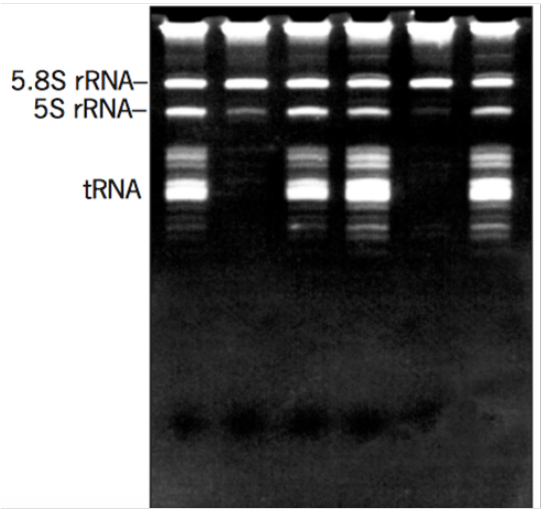


Figure 81: both RNA extraction methods yield good quality of total RNA as seen by the presence of the 28S rRNA band (5.0 kb) and 18S rRNA band (1.9 kb) on 1% native agarose gels. The microRNA miRVana kit displays a further band 5S rRNA (120nt) as it allows for extraction of small RNAs <200nt as opposed to the Purelink RNA kit which extracts only large RNA. The bands are not very sharp and the ratio of 28S:18S doesn't seem to be 2:1, but this might have been caused by the fact that the RNA samples were run on a native (non-denaturing) agarose gel which is known to cause less sharp bands.

4.9.3. Checking integrity of small RNA extracted via miRVana miRNA isolation kit on 15% polyacrylamide urea gels



Expected bands:



From the miRVana microRNA isolation kit instruction manual

Observed bands:

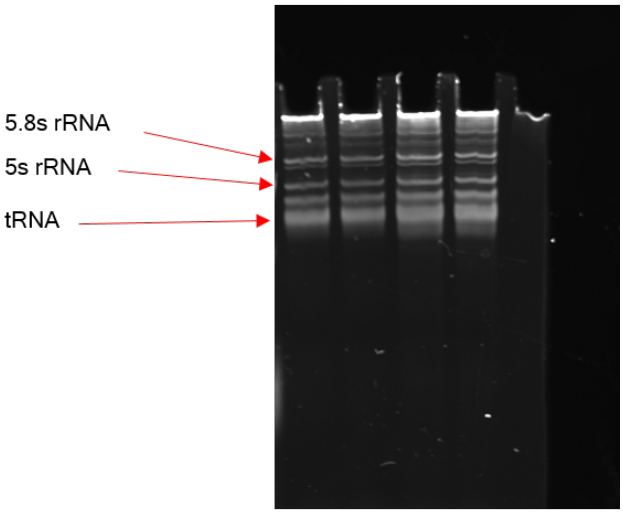
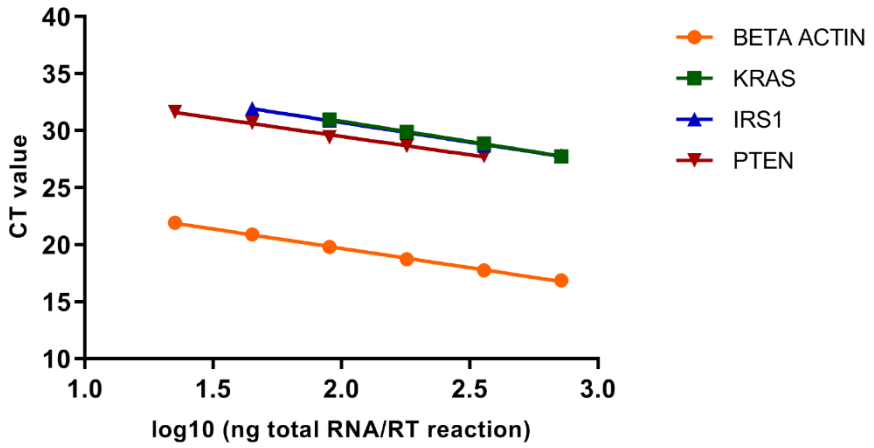


Figure 82: the observed RNA bands on 15% polyacrylamide urea gels from the test samples correspond to the expected bands of 5.8s rRNA, 5s rRNA and tRNA, confirming that the miRVana miRNA isolation kit extracts small RNA successfully. There is no sign of band smearing in any of the samples, signifying that the extracted small RNA is intact and not degraded

4.9.4. Checking qPCR amplification efficiency of cDNA synthesised from mRNA



	BETA ACTIN	KRAS	IRS1	PTEN
Equation	Y = -3.393*X + 26.48	Y = -3.566*X + 37.97	Y = -3.464*X + 37.66	Y = -3.231*X + 35.97

	BETA ACTIN	KRAS	IRS1	PTEN
R square	0.9988	0.9998	0.9984	0.9936

Amplification factor = 1.971
Amplification efficiency = 97.1%

Amplification factor = 1.907
Amplification efficiency = 90.7%

Amplification factor = 1.943
Amplification efficiency = 94.4%

Amplification factor = 2.039
Amplification efficiency = 103.9%

Figure 83: amplification efficiency of all genes tested is ~100%, which means that reverse transcription of large RNA and PCR amplification work adequately. This further implies that the $2^{-\Delta\Delta CT}$ method can be reliably used to determine changes in gene expression following transfection of miRNAs. To obtain the amplification curves total RNA extracted from a confluent T75 flask of nondiabetic fibroblasts was serially diluted 1:2 in a range of 22.5-720 ng RNA/RT reaction and reverse transcribed into cDNA. Following qPCR with the various primers of interest the average CT values vs $\log_{10}$ of (ng total RNA/RT reaction) was plotted and linear regression analysis was used to obtain the value of the gradient. This, in turn, was used to determine the amplification efficiency.

4.9.5. Checking amplification efficiency of cDNA synthesised from miRNAs

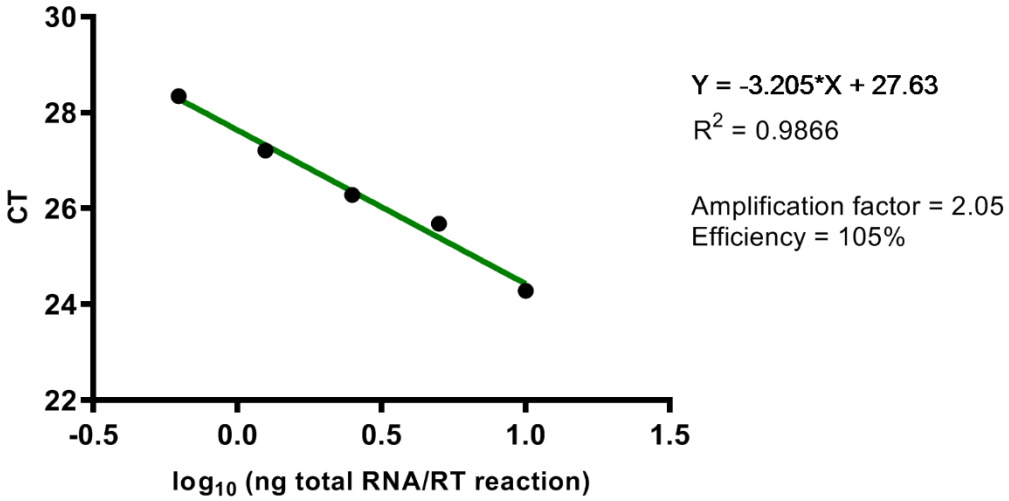


Figure 84: amplification efficiency of RNU44 is ~100%, indicating that reverse transcription and amplification of cDNA from miRNAs is adequate. This means this protocol can be reliably used for qPCR experiments involving changes in miRNA expression.

4.9.6. Transfection of siRNAs into primary dermal fibroblasts

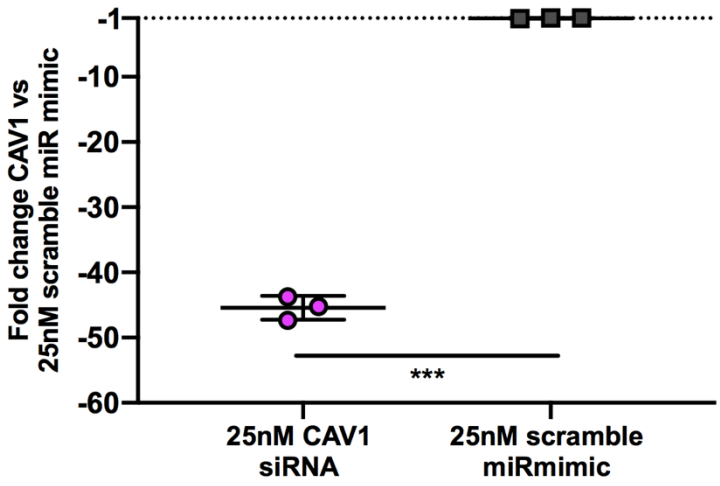


Figure 85: transfection of 25 nM siRNA against CAV1 into primary dermal fibroblasts via lipofectamine RNAiMAX yields a significant gene knockdown 48h post transfection with similar suppression values to the miRNA mimic positive control against GAPDH. This confirms that this transfection method works very well at delivering miRNAs into primary fibroblasts. Data points denote mean ± SD. Analysis of statistical significance was performed via unpaired two-tailed t-test. $p<0.001$, $n=3$

4.9.7. RNU44 is a suitable normalisation gene for miRNAs

	100nM miR-181a mimic + 200nM scramble miR	100nM miR-27a mimic + 200nM scramble miR	100nM miR-30a mimic + 200nM scramble miR	all 3 miRNAs (100nM each)	300nM scramble miR mimic
2^{-CT} (RNU44)	1.717E-08	1.49E-08	1.81E-08	1.64637E-08	1.49694E-08
2^{-CT} (RNU44)	1.514E-08	1.79E-08	1.35E-08	1.59E-08	1.38E-08
2^{-CT} (RNU44)	1.484E-08	9.44E-09	1.12E-08	1.64E-08	1.57E-08
Average	1.57167E-08	1.408E-08	1.42667E-08	1.62546E-08	1.48231E-08
FC to 300nM scramble miR	**1.060279653**	**0.94986665**	**0.962459579**	**1.096567527**	**1**

Table 24: RNU44 is a suitable normalisation gene for qPCR on miRNAs as expression of RNU44 does not change significantly following transfection of functional miRNA mimics compared to fibroblasts containing scramble miR mimic only (FC ~1). The fold changes were calculated by computing the average of the 2^{-CT} values of RNU44 across 3 samples from each condition (i.e. column in table) and dividing it by the average value of the samples containing 300nM scramble miR mimic.

4.9.8. ACTB is a suitable normalisation gene for mRNAs

Donor #1	100nM miR-181a mimic + 200nM scramble miR	100nM miR-27a mimic + 200nM scramble miR	100nM miR-30a mimic + 200nM scramble miR	all 3 miRNAs (100nM each)	300nM scramble miR mimic
2^{-CT} (ACTB)	0.000005635	0.0000054	0.00000436	0.00000494	0.00000547
2^{-CT} (ACTB)	0.000005955	0.00000531	0.0000061	4.6439E-06	0.00000525
2^{-CT} (ACTB)	0.000006319	0.00000489	0.00000642	0.000004797	0.00000477
Average	5.96967E-06	0.0000052	5.62667E-06	4.79363E-06	5.16333E-06
FC to 300nM scramble miR	**1.156165268**	**1.007101356**	**1.089735313**	**0.928398967**	**1**

Table 25: ACTB is a suitable normalisation gene for qPCR on mRNAs as expression of ACTB does not change significantly following transfection of functional miRNA mimics compared to fibroblasts containing scramble miR mimic only (FC~1). The fold changes were calculated by computing the average of the 2^{-CT} values of ACTB across 3 samples from each condition (i.e. column in table) and dividing it by the average value of the samples containing 300nM scramble miR mimic

4.9.9. Effect of scramble miR mimic on cell proliferation

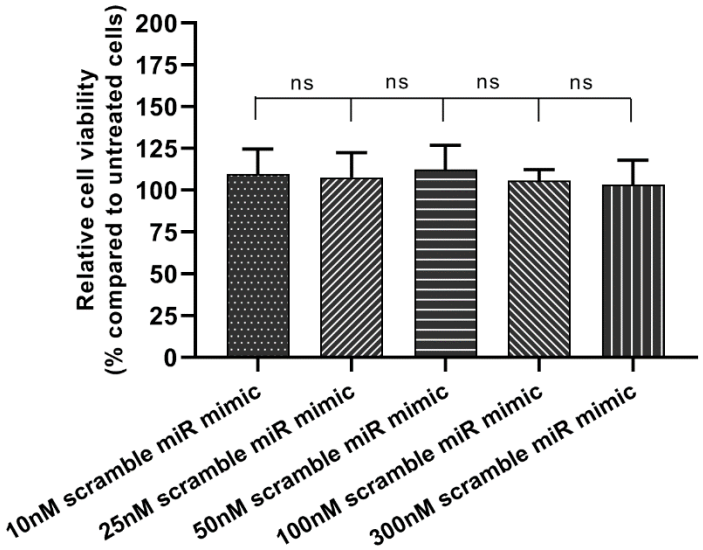


Figure 86: transfection of scramble miRNA mimic at 10-300 nM via lipofectamine RNAiMAX does not seem to have any effect on the proliferation of primary dermal nondiabetic fibroblasts when compared to untreated cells. This implies the scramble miRNA is neither toxic for fibroblasts nor has a biological effect on fibroblast behaviour and as such it is suitable to be used as a control miRNA mimic. Proliferation was measured 5 days post transfection via Presto Blue and compared to untreated fibroblasts. Statistical analysis to determine significance was calculated via one-way ANOVA, p=0.2107. N=2, n=9/donor

4.9.10. Primer sequences for genes used for qPCR on mRNAs

All Taqman double-dye probes used for qPCR on mRNAs were designed and synthesised by Primerdesign.

Gene name	Accession number	Sense primer	Anti-sense primer
PTEN	NM_000314	GTTCACATCCTACCCCTTTGC	ATTCCCTCCATTCCCCTAACC
KRAS	NM_004985.4	CACCTTGGCCTCATAAACCTG	CGGGATTATGTCTCTTGTTTGGG
IRS1	NM_005544	GTGGCATCAAACTACCGATTTAA	GGGAACTGAACACAAGGACTC
CAV1	NM_001753	GCGACCCTAAACACCTCAAC	GCCTTCCAAATGCCGTCAA
RPS6KB1	NM_00127204	GCAAGCTGGACAAACTATCACA	CCACTGAGATAATACTTGTGCTATAATG

Table 26: gene name, accession number, sense and anti-sense primers for the genes that were used for qPCR in the PhD project

Gene name	Accession number	Anchor nucleotide
ACTB	NM_001101	1195
GAPDH	NM_002046	1087

Table 27: gene name, accession number and anchor nucleotide for the housekeeping genes that were used for qPCR in the PhD project. As the sense and anti-sense primer sequences are proprietary information of Primerdesign only the anchor nucleotide can be published

5. Nanostraw-electroporation platform for delivery of microRNAs into primary dermal fibroblasts

One way to get round the limitation posed by the stochastic liposomal-based transfection is to use engineering-based approaches for miRNA delivery and no longer having to rely on biology. One such approach consists of a novel nanostraw-electroporation delivery platform that decouples delivery of cargo from biological machinery by allowing direct intracellular access to deliver the miRNAs. This platform is an innovative *in vitro* delivery system developed by Professor Nicholas Melosh at Stanford University. It combines nanotechnology with the widely used delivery method of electroporation to achieve safer, faster and more precise delivery of biomolecules across the cell membrane.

5.1. Mechanism of delivery

Nanostraw (NS) platforms consist of a track-etched polycarbonate membrane with protruding hollow alumina nanostraws that connect to an underlying fluidic environment. Cells cultured onto the membrane 'wrap' themselves tightly around the extended NS, allowing the plasma membrane to come in tight contact with them. When an electric field is applied across the NS membrane, the electric field passes through each of the NS - due to the insulating properties of the polycarbonate membrane – and becomes localised at the tips of the NS where the nanostraw-cell interface is tight (Figure 87). The concentrated electric field induces nondamaging local pore formation in the cell membrane and concurrently electrophoretically pulls up cargo from the underlying fluidic channel through the NS into the cells [203]. This allows fast uptake of biomolecules through the newly open pores, enhancing the diffusive process which otherwise would be very slow. Studies done with cell impermeant dyes further showed that the pores close ~10 min after the electric field is switched off, allowing the cell membrane to reseal very quickly [203]. In this way, the electric field acts as a valve to open the cell membrane and drive cargo into the cytoplasm on-demand with minimal disruption.

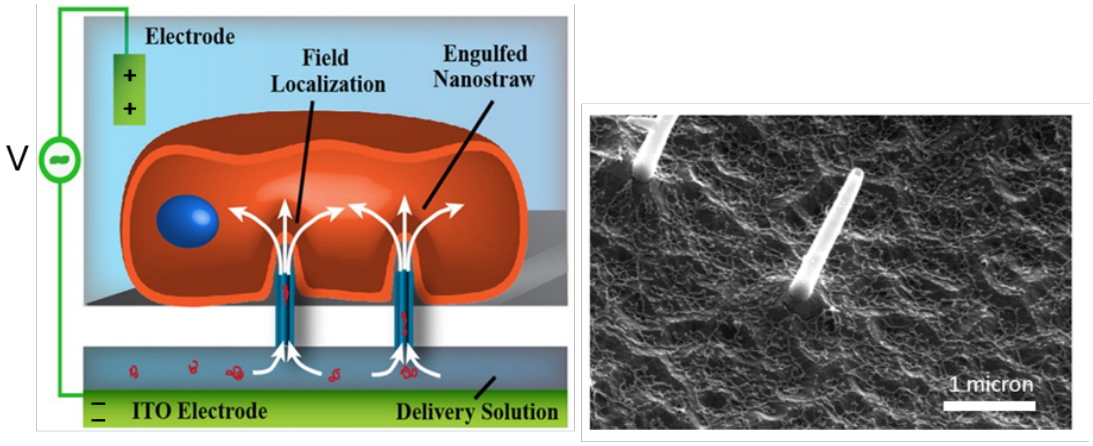


Figure 87: (Left) schematic representation of field localisation at the tip of the NS due to the tight interface between the cells and the NS. Image reprinted with permission from [203]. Copyright 2013 American Chemical Society; (Right) Scanning electron microscope image of the NS membrane with protruding NS - courtesy of Mr Ryan Swoboda, NAVAN

The intimate nanostraw-plasma membrane interface is crucial to this delivery system. First, it allows the electroporation voltage to be significantly reduced to 10-20V - as opposed to the bulk electroporation that requires much higher voltages of 150-200V – resulting in less damaging effects. Second, it reduces the variability of the local voltage 'felt' by the cells, ensuring more uniform delivery of cargo than bulk electroporation, which can cause inhomogeneities of the electric field across each particular cell [204]. This, in turn, furthermore results in higher cell viability as a larger fraction of cells become porated at a particular voltage.

In the past this system has further been shown to allow spatial, temporal and dose control for delivery for DNA and protein [205], and allow co – and sequential transfection of plasmid DNA [203]. Recently, the NS platforms were also revealed to allow non-destructive longitudinal sampling of proteins and mRNA from the interior of the cells [206]. However, they have not been used for delivery of miRNAs into cells - either primary or cell lines.

5.2. Protocol for microRNA delivery

To deliver miRNAs into the isolated dermal fibroblasts a prototype nanostraw-electroporation system was used that was devised and manufactured by the start-up company NAVAN (San Francisco, California). The system entailed NS wells, cell caps, an electroporation device, a power supply and a picoscope/oscilloscope. The NS wells consisted of plastic wells (6.5mm inner diameter) with the NS membrane glued to one end and nanostraws facing upwards. Typical nanostraws had a diameter of 80-100nm, 1.2-1.5 μm height and a density of 10^7-10^8 straws/cm^2, which corresponded to roughly 0.1 -1 straws/μm^2. This NS density was found to be suitable for delivery of biomolecules as higher densities (>10^9) caused cells to merely rest on top of the NS (the 'nail bed' effect), unable to come in close contact with the NS [207].

The protocol for miRNA delivery started with seeding fibroblasts in NS wells placed in 24-well plates at 30,000 – 50,000 cells/350 μL full DMEM medium (Figure 88). After leaving the cells to adhere for 2-3h, the 24-well plate was centrifuged at 1400 rpm for 4 min to ensure the cells were in close contact with the NS.

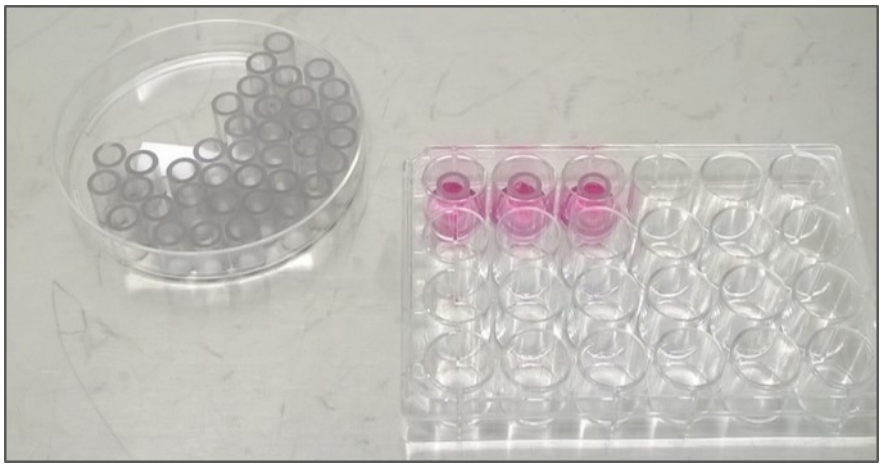


Figure 88: NS wells before seeding cells (in Petri dish) and after seeding cells (in 24-well plate). The NS wells fit in a 24-well plate that can be placed in the incubator or centrifuged. Pink colour denotes DMEM medium

Following centrifugation of the 24-well plate, 65μL of 0.0001x – 0.1x PBS containing miRNAs was placed on the bottom electrode of the cell cap into which the NS well was carefully inserted, followed by closing the lid of the cell cap containing the top electrode (Figure 89 top). The cell cap was placed into the electroporation device (NAV100) which contained a function

generator that allowed to adjust the duration (pulse width) and frequency of the electroporation signal (Figure 89 bottom).

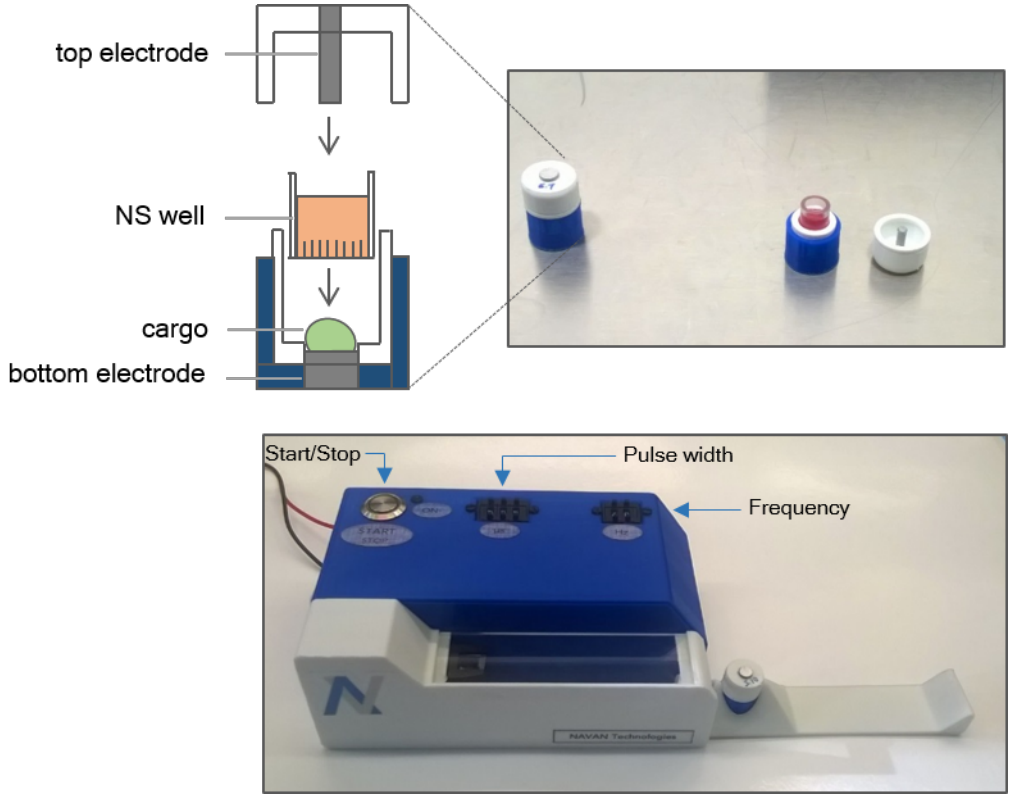


Figure 89: (top) schematic representation of the cell cap containing the NS well and the cargo droplet; (bottom) the cell cap is placed in the NAV100 device for electroporation. The NAV100 allows adjustment of parameters including pulse width and frequency

The electroporation device was further connected to the power supply to generate the voltage (15-25V) and a picoscope or oscilloscope to record the electrical current passing through the cell cap during electroporation (Figure 90). Electroporation was initiated when the NAV100 device was switched on by pressing 'Start'.

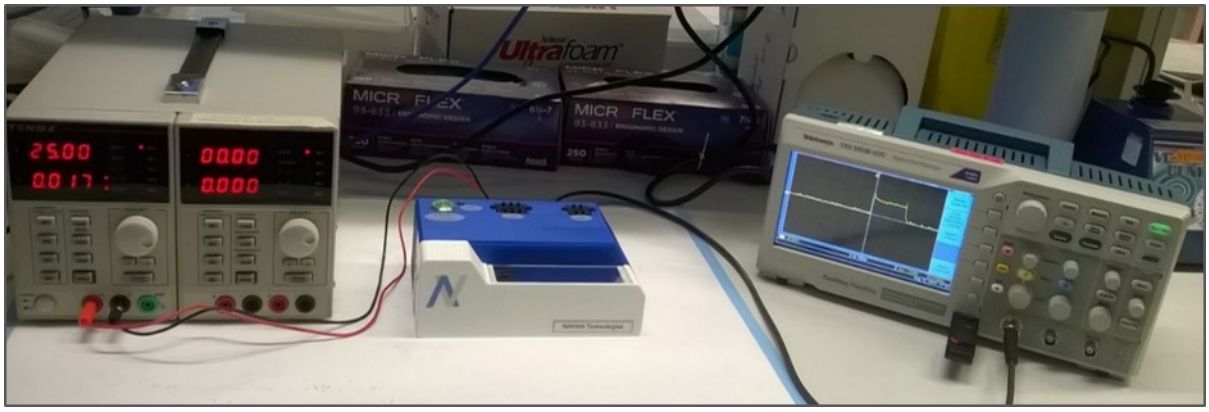


Figure 90: set-up of the nanostraw-electroporation system showing the NAV100 device connected to the power supply and the oscilloscope/picoscope

As the NS membrane is porous due to the nanostraws being hollow, when the NS well is inserted into the cell cap electrical continuity occurs as the cargo droplet comes in contact with the bottom of the NS well and the top electrode inserts into the DMEM medium in the NS well. As such, when the electric field is generated across the NS membrane electrical current passes through the cell cap that can be recorded by the picoscope. Setting 40Hz and 200µs pulse width for 40 seconds as the electroporation parameters – according to the manufacturer's recommendations - the following signal was typically observed during electroporation (Figure 91):

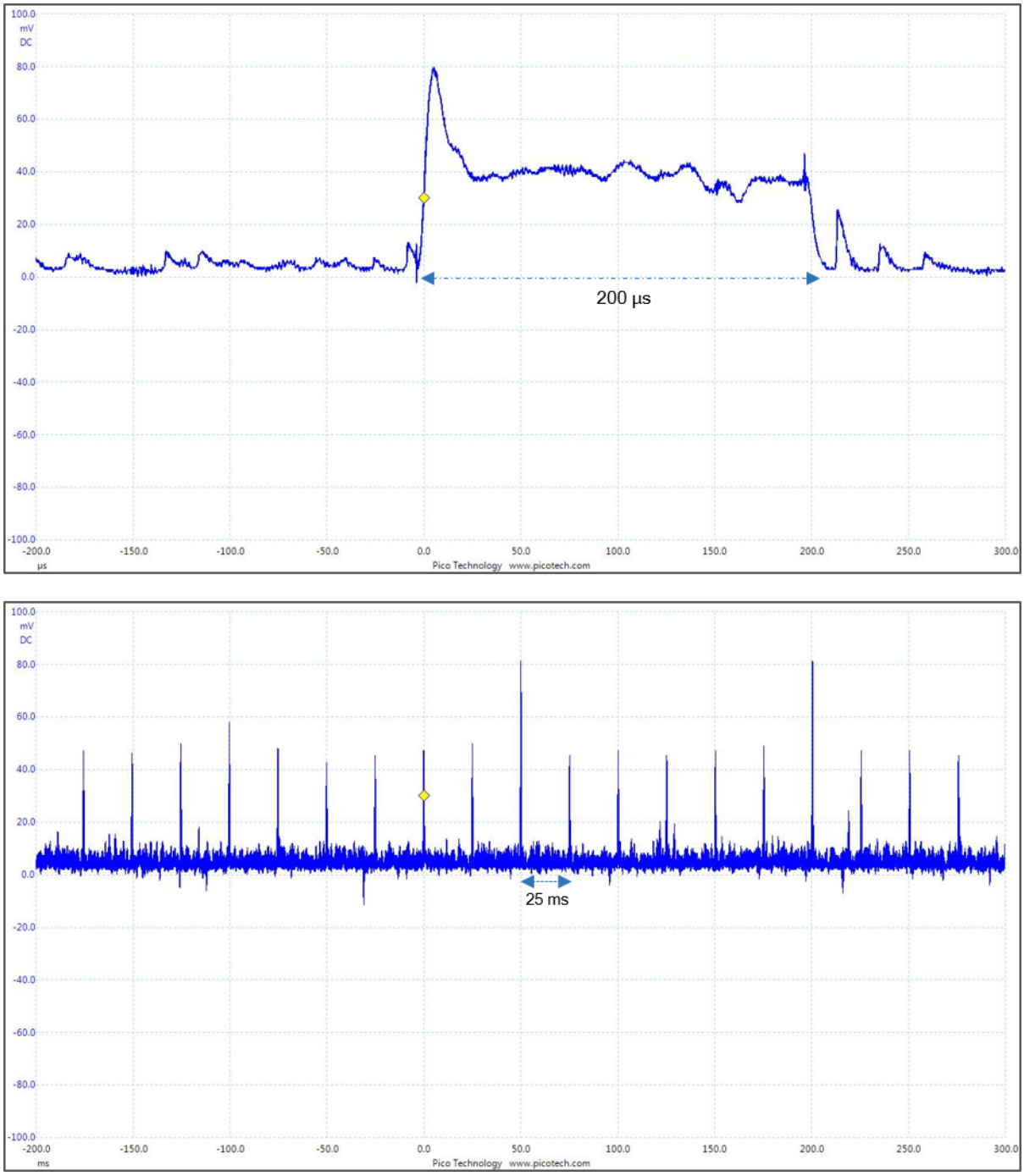


Figure 91: typical electrical signal recorded on the picoscope during electroporation. The signal displayed a square wave of 200 µs duration (top) occurring at intervals of 25 ms

The signal recorded had a square waveform of 200 µs pulse width and an amplitude ~40mV that was repeated every 25 ms (equivalent to a frequency of 40 Hz), resembling the parameters selected on the NAV100 device. The amplitude of 40 mV corresponded to an electrical current

of 40 mA flowing through the cell cap (1V = 1A) due to the layout of the electrical circuit (Figure 92) - although sometimes this value might fluctuate between 20-40 mA [k].

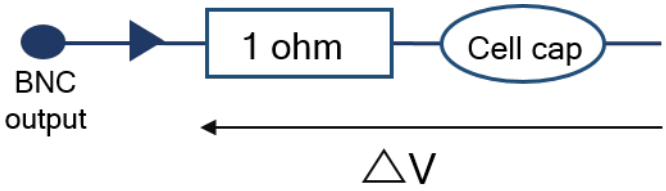


Figure 92: the picoscope records the voltage across the cell cap (ΔV). Due to a 1 ohm resistor placed in series with the cell cap the voltage drop across the cell cap corresponds to the electrical current passing through the cell cap. BNC output represents the output of the NAV100 device.

The electrical current passing through the cell cap was recorded every time electroporation was performed to ensure there was electrical contact between the cargo droplet and the bottom of the NS well. This was done to rule out the presence of any big air bubbles in the cargo droplet that could create an air gap between the cargo and the NS well, hindering the uptake of biomolecules. If this was the case the amplitude of the signal would be 0 mV at which point the NS well would be moved to a new cell cap with fresh cargo and electroporation would be repeated.

After electroporation was completed the NS wells were returned to the incubator for ~1h to allow the fibroblasts to 'recover', followed by detaching them from the NS membrane using trypsin and re-seeding the cells into multi-well plates for further studies.

Prior to using the nanostraw-electroporation system for delivery of miRNAs into fibroblasts the platform was extensively characterised for cell viability, suitable electroporation parameters and efficiency of delivery.

[k] Although the amplitude of the electrical current fluctuated between 20-40mA in between different electroporation events, no correlation was observed between the magnitude of the current and the efficiency of delivery.

5.3. Testing fibroblasts viability on the NS membrane

First, I confirmed that the NS membrane did not affect fibroblast viability. Nondiabetic fibroblasts were seeded in NS wells according to the protocol and left to adhere overnight. The following day some of the NS wells were stained with a Live/Dead assay [1] to check cell viability on the NS membrane. In the remaining NS wells, the cells were trypsinised and re-seeded into a 96-well plate for another 24h before being stained with the same assay.

Representative microscopy images showing viable cells (green) and dead cells (red) revealed that fibroblasts had a high cell viability and displayed normal cell morphology without obvious signs of increased cellular stress. This was the case both when the cells were kept on the NS membrane (Figure 93 - left) and following detachment from the NS membrane (Figure 93 – right), indicating that the NS membrane was neither toxic to the fibroblasts nor detrimentally impacting cell viability or behaviour.

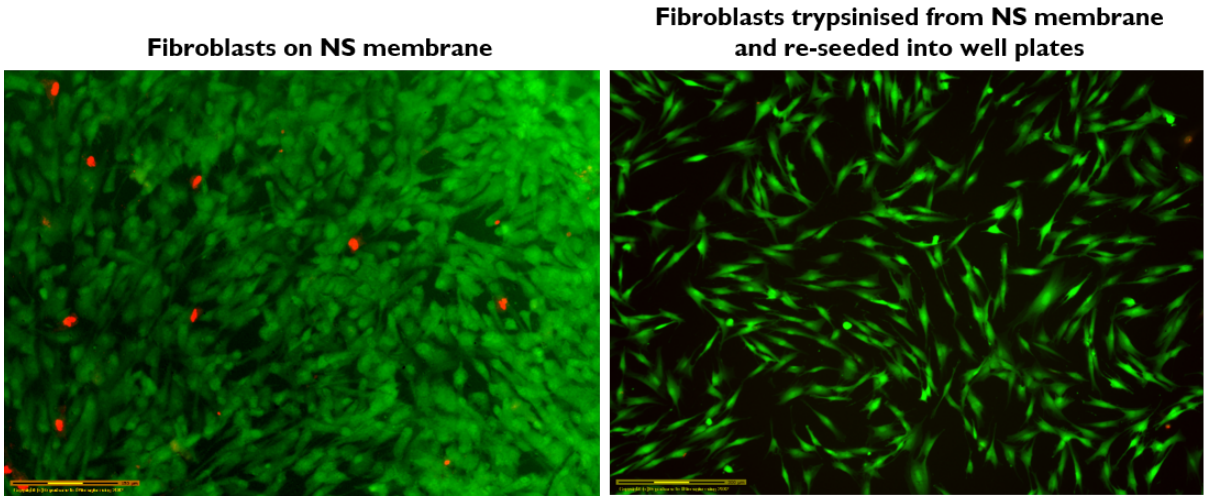


Figure 93: (left) fibroblasts seeded on the NS membrane overnight show high cell viability; (right) fibroblasts seeded on the NS membrane overnight, trypsinised and re-seeded into well plates display high cell viability and normal cell morphology the following day, thus confirming the NS membrane is not toxic to the cells. Green denotes viable cells, red denotes dead cells

[1] The Live/Dead assay consists of two dyes that identify live and dead cells, respectively. Live cells that are metabolically active are capable of hydrolysing the cell permeant 'live dye' to make it fluorescence green, while dead cells are unable to do so. Instead, these cells fluoresce red once the 'dead dye' - which is cell impermeant to healthy cells with an intact cell membrane - crosses the broken down cell membrane and binds to intracellular DNA/RNA.

5.4. Testing fibroblasts viability on the NS membrane after electroporation

After confirming that the NS membrane alone did not affect fibroblast viability, the next step was to determine what electroporation parameters were suitable for maintaining high cell viability. Nondiabetic fibroblasts were seeded on the NS membrane at 30,000-50,000 cells/ 350 μL full DMEM and left to adhere overnight. The following day cells were electroporated using a dummy cargo (i.e. 65 μL 0.1xPBS) at 15V, 20V and 25V [m] for one electroporation (40 seconds) or three electroporations (40 seconds each at 3 min intervals). The NS wells were then returned to the incubator and 3h later the cells were stained with a Live/Dead assay to assess how cell viability changed during this time window.

Representative microscopy images revealed that the fibroblasts remained viable at all conditions tested except 25V, three electroporations, which killed most of the cells (Figure 94). This suggested that 25V was borderline for ensuring cell survival, allowing high cell viability only when cells were exposed to this voltage for short periods (40 sec vs 120 sec).

Previously, delivery efficiency of DNA was shown to depend linearly with time of electroporation, but only quadratically with voltage [205], which meant that small increases in the duration of delivery (Δt) had more significant impact on cargo uptake than small increases in the voltage applied (ΔV). As such, I chose 20V, three electroporations (of 40 sec each at 3 min intervals) rather than 25V, one electroporation (40 sec long) for all subsequent miRNA deliveries (Figure 95).

[m] The voltage range tested started at 15V as this was the recommended starting value by the manufacturers

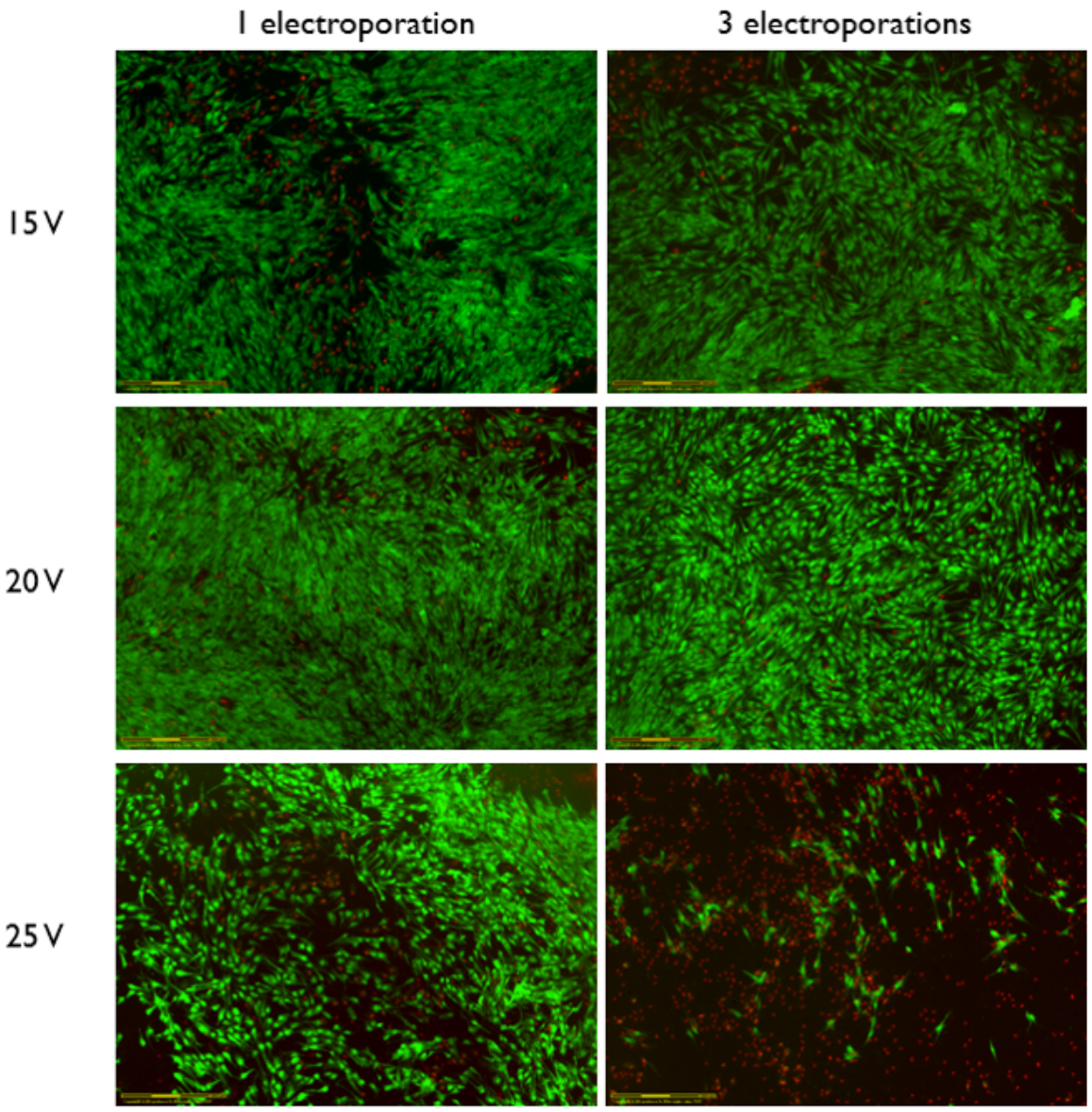


Figure 94: electroporation of fibroblasts at various voltages (15-25V) and durations (1 electroporation of 40 sec and 3 electroporations of 40 sec each at 3 min intervals) shows that 25V, three electroporations kills the cells. Cells were stained on the NS membrane with Live/Dead stain 3h post electroporation. Green denotes live cells, red denotes dead cells. All scale bars denote 300 µm

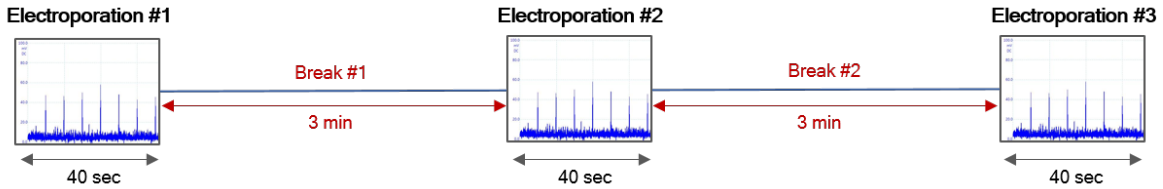


Figure 95: set-up used for all deliveries of biomolecules into primary dermal fibroblasts involved 3 electroporations of 40 sec each at 3 min intervals

5.5. Testing cell membrane permeabilisation following electroporation

Although 20V was confirmed to ensure high cell viability, it was still unknown whether this voltage was strong enough to cause nanostraw – mediated electroporation. To test that pores were indeed forming in the cell membranes at 20V, propidium iodide (PI) – a cell impermeable fluorescent DNA intercalator – was used as cargo.

Nondiabetic fibroblasts were seeded in NS wells and left to adhere overnight, followed by staining them with Cell Tracker Green – a cell permeable dye that stains viable cells green – and delivery of PI (0.1 mg/mL) in 0.0001xPBS at 20V. Fibroblasts cultured on the NS membrane with PI present in the cargo droplet underneath the NS well, but no electroporation were used as a negative control to account for passive diffusion. Similarly, fibroblasts kept in cell culture well plates and stained with PI (0.1 mg/mL) for the same amount of time served as a negative control to confirm that PI was not permeable at this concentration. Following PI delivery all outer NS membranes were rinsed with PBS to remove any adsorbed PI dye that might cause false positives and the cells were imaged with the fluorescent microscope.

Representative microscopy images showed that during electroporation PI from the underlying cargo droplet was being uptaken into viable fibroblasts (Figure 96). In the absence of electric field, i.e. passive diffusion very little PI entered the cells (due to spontaneous penetration of plasma membrane by the nanostraws), while in viable cells kept in cell culture well plates no PI entered the cells. This confirmed that PI was indeed impermeable to cells with intact plasma membrane and that nanostraw-mediated electroporation at 20V was able to open transient pores in the cell membrane, enabling a cell impermeable dye to enter the cytoplasm.

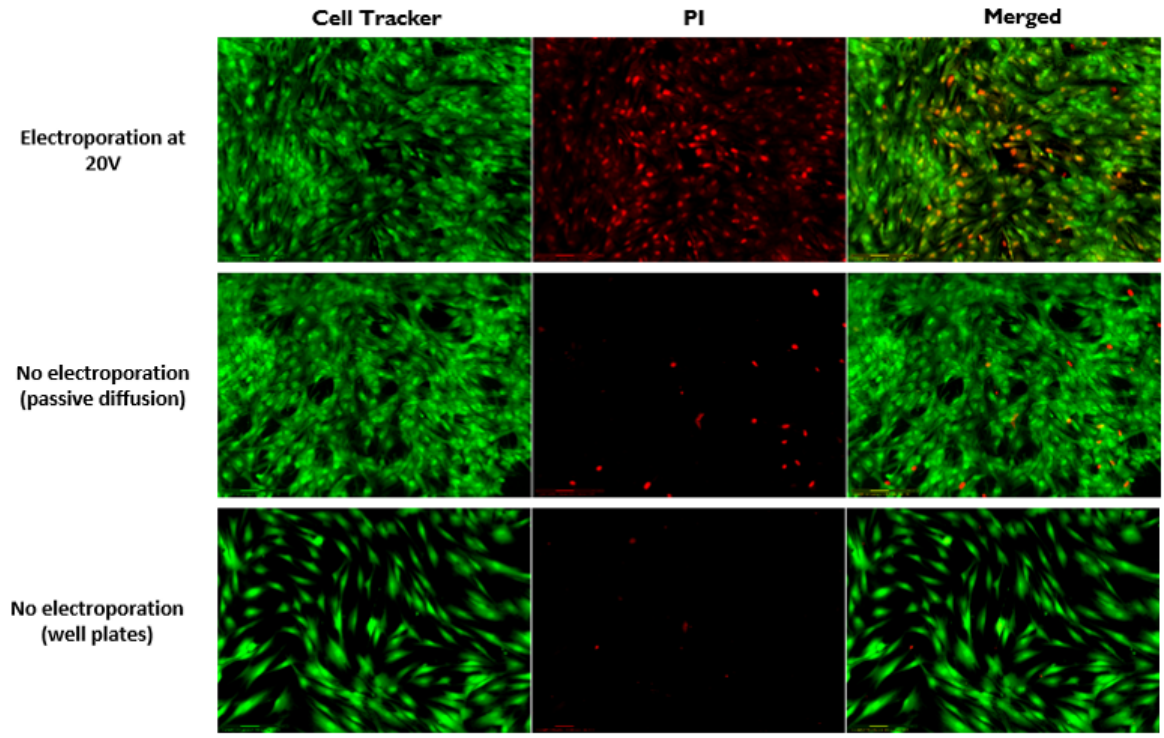


Figure 96: uptake of propidium iodide (PI, red) - a cell impermeant fluorescent DNA intercalator - into fibroblasts confirms cell membrane poration is taking place during electroporation at 20V. The minimal uptake of propidium iodide in the absence of electroporation further confirms that the presence of the electric field is necessary for efficient delivery. PI (0.1 mg/mL) was present in the cargo droplet in the cells cap. Cells were stained with Cell Tracker Green – a cell permeable dye that stains viable cells green – on the NS membrane. All scale bars denote 150 µm

5.6. Delivering fluorescently-tagged miRNAs into fibroblasts

Encouraged by the positive results with PI the next step involved delivery of fluorescently-tagged miRNA into fibroblasts to check its distribution throughout the cytoplasm. 2 µg of Cy3-tagged scramble miR was delivered at 20V, three electroporations at 3 min intervals in 0.0001xPBS, followed by re-seeding the fibroblasts into 96-well plates for further 24h. Representative fluorescence microscopy images revealed that delivery of Cy3-tagged scramble miR into the fibroblasts was highly efficient and the miRNA distribution was homogenous, i.e. dispersed across the entire cytoplasm (Figure 97) as opposed to the punctate delivery observed via lipofectamine RNAiMAX (Figure 51).

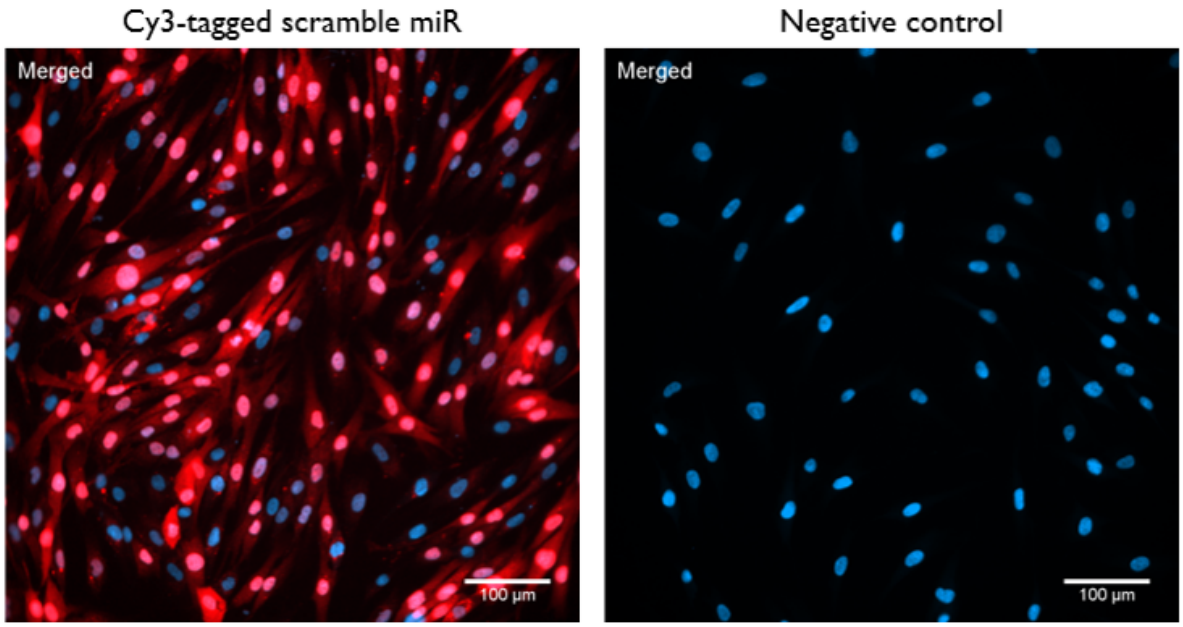


Figure 97: NS-mediated delivery of Cy3-tagged scramble miRNA (red) into primary dermal fibroblasts revealed efficient uptake and homogenous distribution of miRNA throughout the cytoplasm 24h post delivery. This confirmed the nanostraw-electroporation system enables direct intracellular access without relying on endosomal pathways for cargo uptake. The negative control denotes fibroblast cells in culture without Cy3-tagged scramble miRNA delivered and shows there is no autofluorescence in the Cy3 channel. Blue denotes the nuclear stain Hoechst 33342.

Such uniform distribution confirmed the nanostraw-electroporation system enabled direct intracellular delivery of miRNAs, overcoming the limitation of the miRNAs getting trapped in various entities along the way. Direct intracellular access furthermore meant that the majority of miRNA molecules delivered should be 'ready' to be loaded into RISC and become functional. In turn, this allows much better control over the amount of miRNA delivered as opposed to liposomal-based delivery, where it is unclear what proportion of trapped miRNA escapes to become functional.

5.7. Delivering functional miRNAs/siRNAs into fibroblasts

To check that the miRNAs delivered via the nanostraw-electroporation system become indeed functional I delivered a miRNA mimic positive control against GAPDH at 1-4 µg/NS well into nondiabetic fibroblasts. This dose range served as a starting point to determine what concentration of miRNA was needed for efficient gene knockdown. Taqman-qPCR revealed that 48h post-delivery, all doses of miRNA mimic positive control yielded efficient gene

knockdown (~75%), showing that 1 µg of miRNA was enough to suppress gene expression (Figure 98).

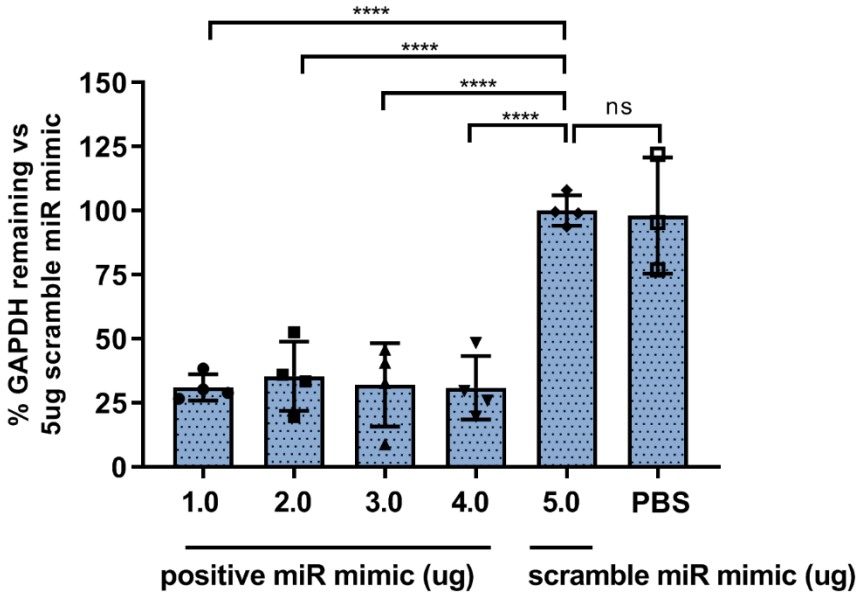


Figure 98: NS-mediated delivery of miRNA mimic positive control against GAPDH at 1-4 µg/NS well shows efficient suppression of GAPDH at all concentrations tested (75% gene suppression) 48h post delivery. This confirms that NS-mediated delivery of miRNAs into primary dermal fibroblasts is highly efficient. Bars denote mean ± SD. Statistical analysis to determine significance was done via one-way ANOVA, followed by posthoc Tukey's multiple comparisons test. ****p<0.0001. n=4

These findings were further corroborated by NS-mediated delivery of siRNA against CAV1 – an essential gene for normal tissue repair and fibroblast activity [208] - which showed that 1 µg of siRNA caused similar levels of gene knockdown (Figure 99). This suggested that the miRNA mimic positive control has most likely been altered by the manufacturers to behave like a siRNA. In turn, this meant that given the fine-tuning effects of miRNAs, perhaps 1 µg of miRNA may not be enough. Nevertheless, collectively these findings confirmed that NS-mediated delivery of small RNAs into fibroblasts was highly efficient.

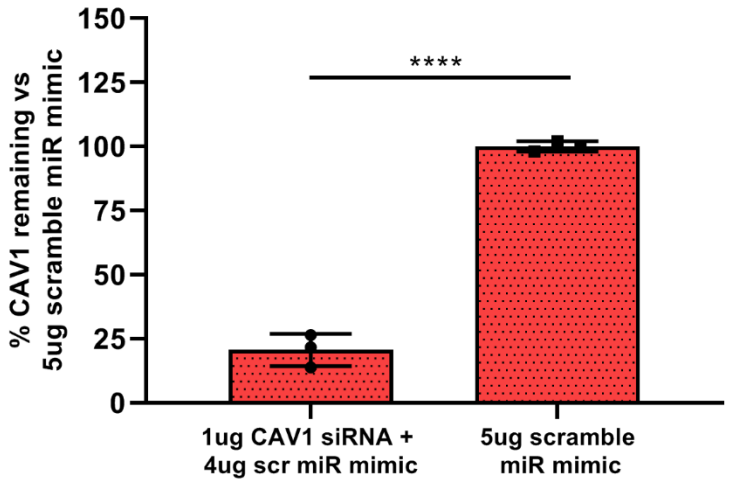


Figure 99: NS-mediated delivery of 1µg of siRNA against CAV1 into nondiabetic fibroblasts shows efficient gene knockdown (75% gene suppression) 48h post delivery, confirming the nanostraw-electroporation delivery system works efficiently at delivering small RNAs into fibroblasts. Bars denote mean ± SD. Statistical analysis was performed via two-tailed unpaired t-test, ****p<0.0001. n=3

5.8. Ratiometric delivery of miRNA mimics at increasing concentrations into fibroblasts

Encouraged by the promising results showing effective functional uptake of small RNAs, I focused on the two miRNAs of interest from the original miRNA combination, miR-181a and miR-27a. Using the nanostraw-electroporation system I delivered miR-181a and miR-27a mimics into fibroblasts in a ratiometric and symmetrical manner at 5 µg total miRNA/NS well. MiRNA expression was measured 48h later via Taqman-qPCR, which revealed a linear increase in both miR-181a and miR-27a expression (Figure 100). This pattern was a striking difference to liposomal-based delivery of miRNAs, illustrating that NS-mediated delivery could precisely control the miRNA dosage. In contrast, lipofectamine RNAiMAX could not achieve this, causing the same level of miR-181a over-expression at all concentrations of miR-181a mimic tested (Figure 69).

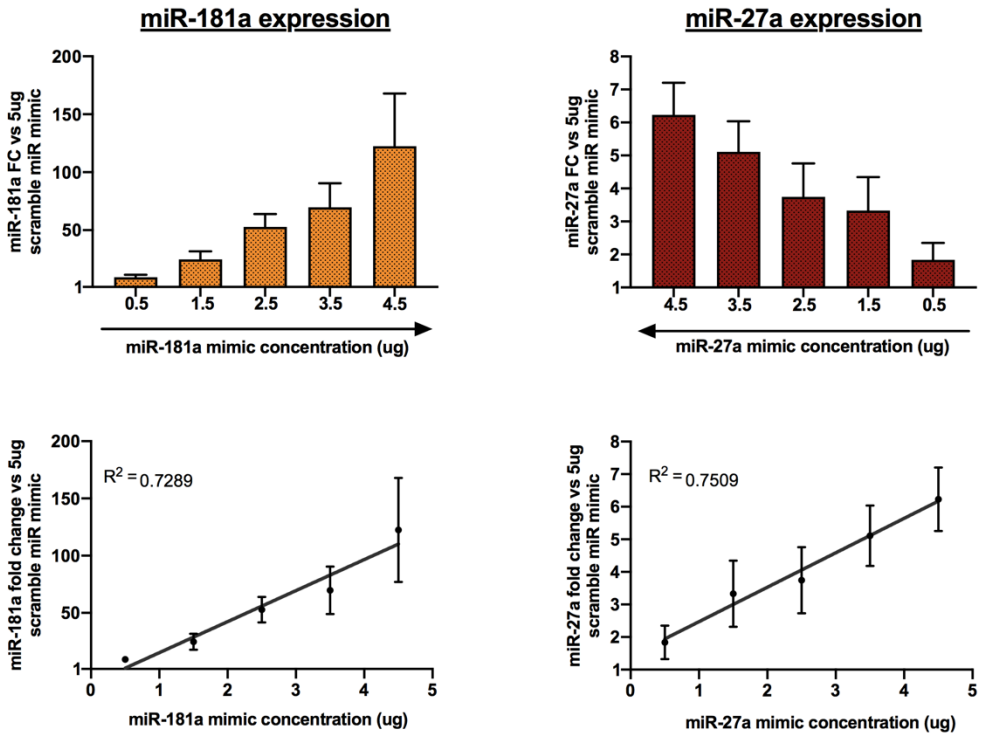


Figure 100: NS-mediated ratiometric delivery of miR-181a and miR-27a mimics at 5 µg final concentration into primary nondiabetic fibroblasts reveals a linear increase in miRNA over-expression with increasing miRNA mimic concentrations 48h post delivery, confirming the nanostraw-electroporation platform can deliver miRNAs in a dosage-controlled manner. R^2 values were obtained by linear regression analysis. N=2, n=4/donor

The ratiometric delivery of miR-181a and miR-27a mimics via NS revealed several notable aspects. First, the miRNAs became over-expressed to different extents with miR-181a showing fold changes of an order of magnitude higher than miR-27a. This, most likely, was due to the different endogenous expression levels of these two miRNAs in fibroblasts (Figure 54). Second, the magnitude of over-expression measured was very different to that caused by liposomal-based delivery. Using lipofectamine RNAiMAX, the fold changes observed were as high as several thousands, whereas via NS-mediated delivery the fold changes were much smaller. This could be a consequence of the chosen dose range, which might not necessarily be equivalent to the 10-100 nM used during lipofectamine delivery. However, the lower fold changes might also be attributed to the miRNA mimics detected being most likely functional miRNAs. Third, the miRNA over-expression levels induced via NS-mediated delivery may be more physiologically relevant than liposomal-based delivery. Even in the case of miR-27a that displayed very low fold changes (<10), these might be sufficient to cause differential behaviour in cells. In fact, studies have shown that miRNA fold changes as low as 3-4 were

enough to drive development of disease in transgenic mice [209]. As such, the nanostraw-electroporation system enables a novel way to study cellular effects following small changes in miRNA expression.

5.9. Exploring dosage effects of miR-181a on fibroblast behaviour

After confirming the NS-electroporation system could titrate miRNA doses, I chose miR-181a to investigate any dosage effects it might have on fibroblasts.

First, I studied any effects at the mRNA level. MiR-181a mimic was delivered at 0.5 - 4.5 µg/NS well into nondiabetic fibroblasts and Taqman-qPCR was used to quantify KRAS expression 48h later. KRAS was a good target gene to study as it was previously shown to respond well to miR-181a over-expression (Figure 56). Results indicated that KRAS was suppressed at all three concentrations of miR-181a mimic delivered, reaching a plateau at 4.5 µg miR-181a mimic (Figure 101).

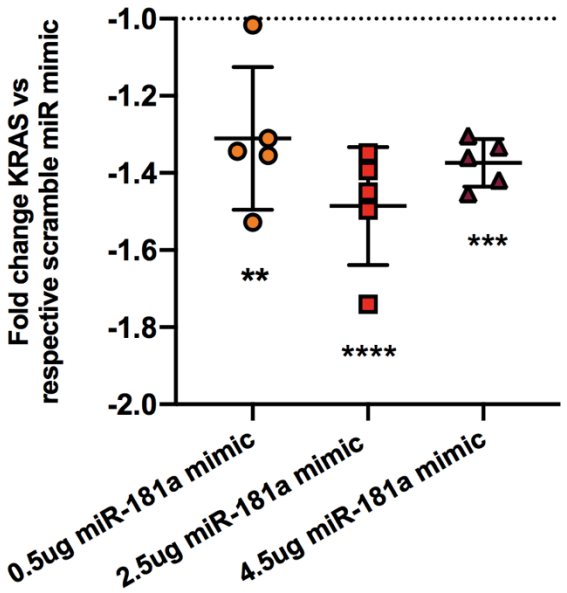


Figure 101: NS-mediated delivery of miR-181a mimic at increasing concentrations (0.5-4.5 µg/NS well) causes knockdown of KRAS at all three concentrations 48h post delivery. The level of suppression reaches a plateau at 4.5 µg of miR-181a mimic, showing no signs of dosage-dependent suppression in the tested range. Data points denote mean ± SD. Statistical analysis was performed via one-way ANOVA, followed by posthoc Sidak's multiple comparisons test. **p=0.0015, ***p=0.0002, ****p<0.0001. N=2, n=2-3/donor

No trend of increasing gene suppression was observed with increasing miR-181a mimic dosage in that range. This could have been because of positive feedback loops causing KRAS expression to go up at the higher concentrations. Interestingly, the level of suppression measured (~1.5-fold change) was milder than that caused by lipofectamine RNAiMAX (~2-fold), reinforcing that the NS platforms allow studying effects of incremental changes in gene expression.

Seeing that miR-181a mimic caused changes at the mRNA level, I next studied the effects of increasing miR-181a mimic concentrations on fibroblast proliferation. MiR-181a mimic, spiked with scramble miR mimic, was delivered into nondiabetic fibroblasts at 5 µg final concentration according to the usual protocol. Following delivery the cells were re-seeded into 96-well plates and the fold change in proliferation over 4 days was quantified using Presto Blue.

It was revealed that miR-181a mimic had a proliferative effect on cell proliferation at all concentrations delivered, albeit no statistical significance was reached at 0.5 µg (Figure 102). There seemed to be an increasing trend in cell proliferation with increasing miR-181a mimic concentration, however no statistically significant difference was reached amongst the three concentrations (p=0.2049).

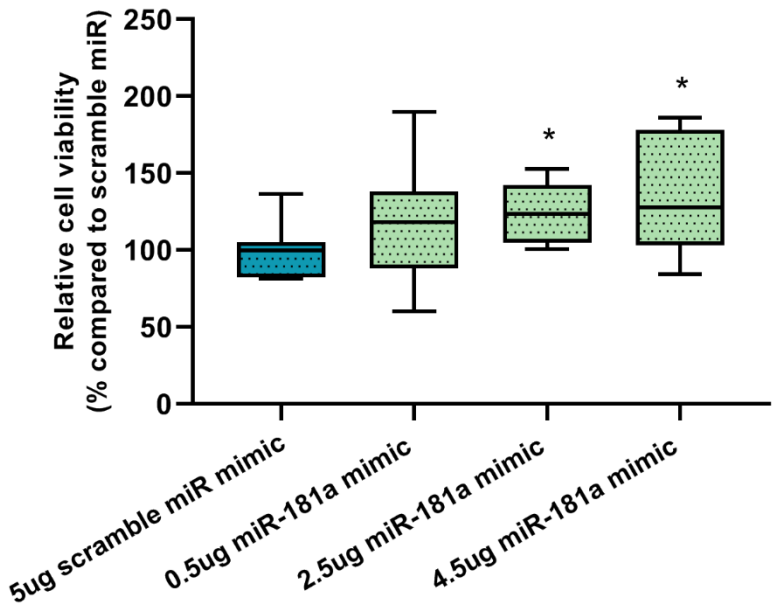


Figure 102: NS-mediated delivery of miR-181a mimic at increasing concentrations (0.5-4.5 µg/NS well) into primary nondiabetic fibroblasts shows a trend of increasing proliferation with increasing concentration of miR-181a mimic. Graph shows the fold change in proliferation over 4 days post delivery normalised to fibroblasts to which 5 µg of scramble miR mimic was delivered. Box and whisker plots span min to max. Statistical analysis to determine significance was done via pairwise two-tailed unpaired t-tests vs scramble miR samples. *p<0.05. N=3, n=2-3/donor

The fact that miR-181a did not exert a dosage-dependent effect on cell proliferation at 0.5 – 4.5 µg mimic, did nonetheless not exclude the possibility that might still occur at doses outside of that concentration range. This however, was not tested.

5.10. Delivering miRNA inhibitors into fibroblasts

The promising results achieved with the miRNA mimics encouraged further characterisation of the nanostraw-electroporation system. This included delivery of miRNA inhibitors to explore ratiometric dosage control and dosage-dependent functional effects.

First, I delivered antimiRs-181a and -27a in a ratiometric and symmetrical manner at 5 µg total miRNA/NS well into nondiabetic fibroblasts according to the usual protocol. Expression of miRs-181a and -27a was measured via Taqman-qPCR 48h later and the fold changes in miRNA expression were determined relative to fibroblasts containing 5µg of scramble miRNA inhibitor. Results from this testing revealed a trend of increasing suppression of miR-181a with increasing concentrations of miR-181a inhibitor, but surprisingly not for miR-27a (Figure 103).

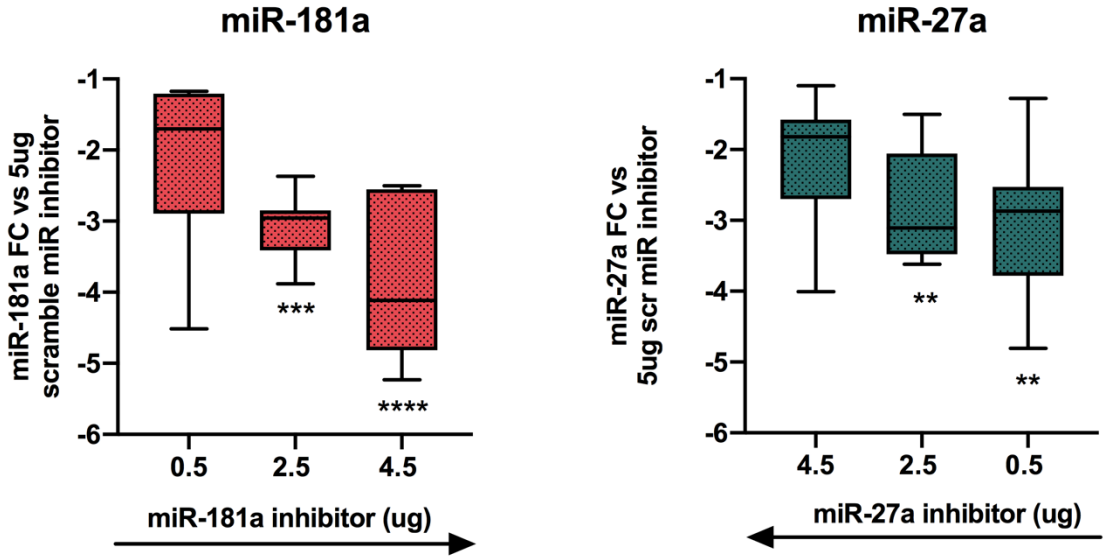


Figure 103: NS-mediated ratiometric delivery of miR-181a and miR-27a inhibitors at 5 µg final concentration into nondiabetic fibroblasts shows a trend of increasing miR-181a suppression with increasing antimiR-181a concentrations, but not for miR-27a 48h post delivery. Box plots span min to max. Statistical analysis was performed via one-way ANOVA, followed by posthoc Tukey's multiple comparisons test. **p<0.01, ***p<0.001, ****p<0.0001. N=2, n=3-4/donor

Regarding miR-181a the trend of suppression was not linear, like in the case of ratiometric miR-181a mimic delivery. Reasons for this may be the low endogenous expression of miR-181a in dermal fibroblasts, which caused inhibited miR-181a expression levels to be pushed to the borderline of detection by microRNA Taqman probes (CT ~33-34). Regarding miR-27a

no trend of increasing suppression was observed with increasing concentrations of miR-27a inhibitor. This unexpected result was unlikely caused by inefficient cargo uptake as the electrical current passing through the cell caps was monitored for all electroporations. However, this might have been due to the high endogenous expression of miR-27a in dermal fibroblasts, which meant even low concentrations of antimiR-27a were enough to strongly suppress miR-27a (i.e. similar to the effects of a siRNA). Though the exact reason as to why delivery of higher concentrations of inhibitor followed a trend of lower inhibition of miR-27a remains unknown. This behaviour also suggested it may be useful to do additional testing to confirm this trend.

Interestingly, once again the degree of suppression of miR-181a and miR-27a was milder compared to liposomal-based delivery of the same miRNA inhibitors. For example, miR-27a displayed a ~3-fold suppression following NS-mediated delivery, but ~12-fold suppression following transfection with lipofectamine RNAiMAX (Figure 62). This reinforced the idea that the nanostraw-electroporation system enables studying the effects of small changes in miRNA expression.

To test if NS-mediated delivery of miRNA inhibitors had a functional effect in fibroblasts, an elegant assay involving miR-29 inhibitor was used (Figure 104). This assay was developed, and kindly gifted to us, by Dr Svitlana Kurinna (University of Manchester). The assay consisted of a plasmid (tarmiR29) that harboured binding sites for miR-29 and coded for two luciferases, Firefly (serving as control) and Renilla (serving as reporter). In the presence of endogenous miR-29 Renilla expression is suppressed, leading to very little Renilla expression (Scenario A). However, when antimiR-29 is transfected into fibroblasts, it binds and sequesters endogenous miR-29, allowing de-repression of Renilla expression (Scenario B). A scramble miR unable to bind to miR-29 and hence de-repress Renilla, served as a negative control for the assay.

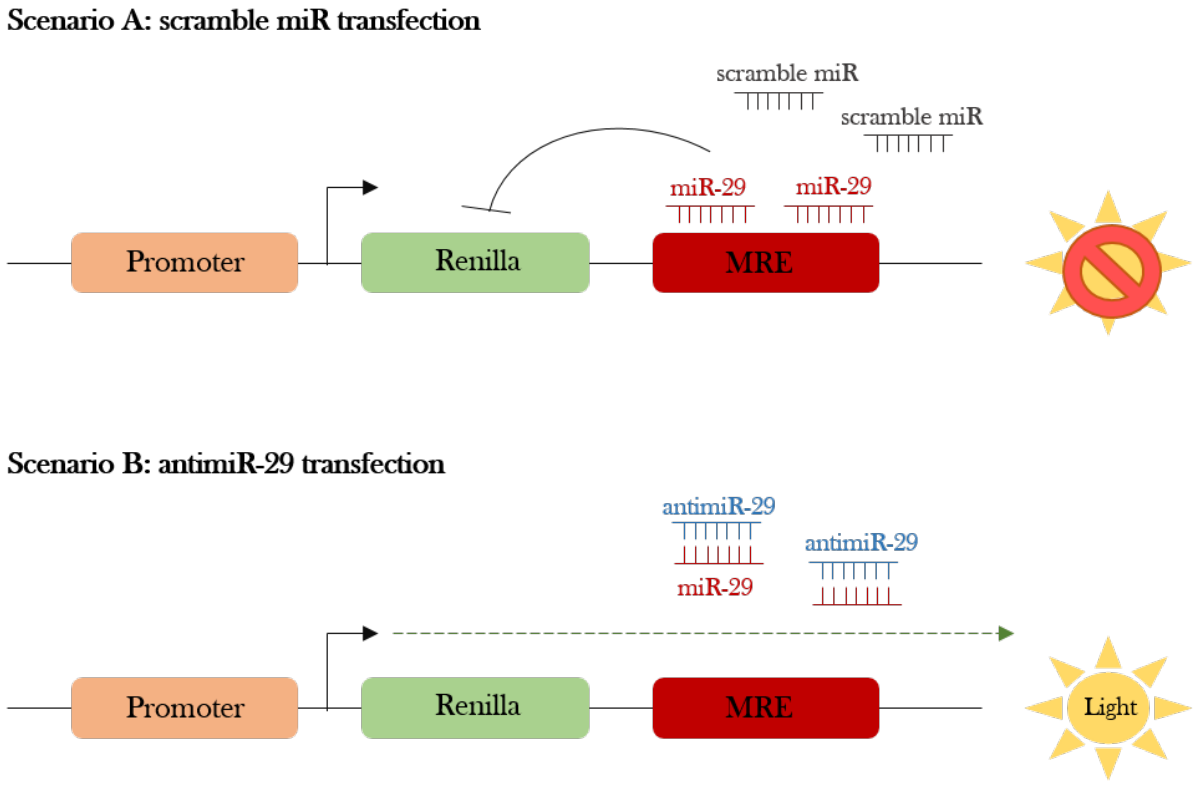


Figure 104: representation of the workings of tarmiR29 plasmid - in the presence of scramble miR endogenous miR-29 can suppress Renilla activity (top), but this gets sequestered by presence of antimiR-29, causing de-repression of Renilla activity (bottom). Abbreviations: MRE stands for miRNA response element.

Using the nanostraw-electroporation system antimiR-29 was delivered at 1-5 μg/NS well into nondiabetic fibroblasts, followed by re-seeding the fibroblasts into 96-well plates. 24h later tarmiR29 plasmid was transfected into fibroblasts via lipofectamine 2000 and Firefly and Renilla activity was quantified 48h later via the Dual-Glo luciferase assay [n]. Fibroblasts containing scramble miRNA - delivered via NS - and transfected with tarmiR29 plasmid via lipofectamine 2000 served as negative control for *bona fide* Renilla de-repression, while fibroblasts not transfected with plasmid served as control for the transfection procedure.

Prior to delivering antimiR-29, I confirmed that uptake of the miRNA via NS-mediated electroporation was successful, that Firefly expression remained roughly similar across conditions and that tarmiR29 transfection was effective (supplementary data 5.12.2). Lipofectamine 2000 was used for tarmiR29 plasmid transfection into fibroblasts as I noticed

[n] Dual-Glo luciferase assay allows to determine luminescence produced by Firefly and Renilla luciferases from the same sample. It contains a reagent that induces cell lysis and acts as a substrate for Firefly luciferase and another reagent that quenches the luminescence from the Firefly reaction and provides a substrate for Renilla luciferase. Luminescence signals produced by both luciferases have a half-life of ~2h, making it possible to use a luminometer without on-board injectors to measure luminescence.

the NS membrane geometry used throughout for small RNA delivery (80-100nm diameter, 1.2-1.5 μm height) was much less effective at delivering plasmids (supplementary data 5.12.3).

Luminescence measurements showed that antimiR-29 delivery into fibroblasts caused a derepression of Renilla across all concentrations of Cy3-anti29-294 delivered, with the strongest response occurring at 5 μg Cy3-anti29-294 (Figure 105). There seemed to be a dosage dependency, with 3 μg of Cy3-anti29-294 being the threshold dosage needed to cause significant Renilla de-repression. Although no miRNA dosage - controlled luciferase activity was observed in the dose range tested, this may still exist at concentrations higher than 5 μg of Cy3-anti29-294. However, due to limitations of the available reagents, additional concentrations were not able to be tested.

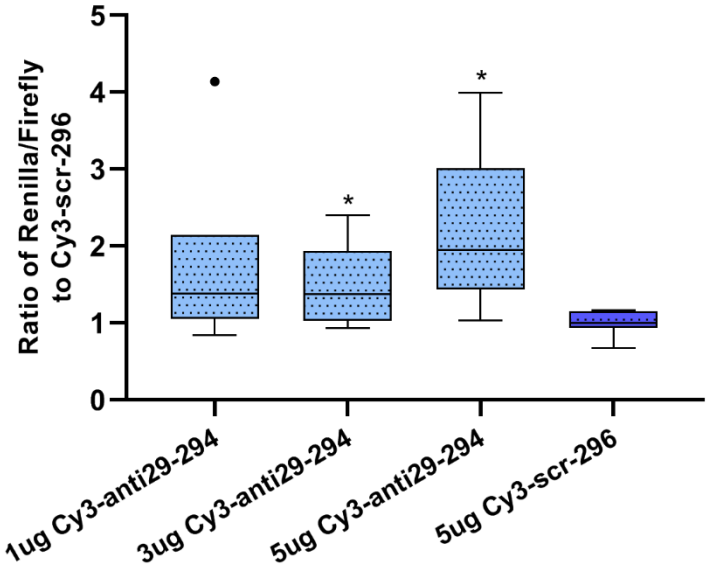


Figure 105: NS-mediated delivery of antimiR-29 at increasing concentrations into primary nondiabetic fibroblasts causes de-repression of Renilla activity 48h post transfection of the tarmiR29 plasmid at all concentrations of antimiR-29 tested, however no miRNA dosage-dependent de-repression of luciferase activity is observed. The tarmiR29 plasmid harbours binding sites for miR-29 and codes for the luciferases Firefly (control luciferase) and Renilla (reporter luciferase). In the presence of scramble miR endogenous miR-29 can suppress Renilla activity, but this gets sequestered by presence of antimiR-29, causing derepression of Renilla activity. Box and whisker plots span min to max. Statistical analysis was performed via pairwise two-tailed unpaired t-tests. $p<0.05$. N=3, n=2-3/donor

Collectively, these preliminary results indicated that NS-mediated delivery of antimiRNAs into fibroblasts, ratiometric or individually, was successful and leading to functional effects. This ability to precisely titrate miRNA levels up or down opens new opportunities to control relative levels of different miRNAs over time. This could be particularly useful for

manipulating signalling pathways or miRNA-gene regulatory networks to drive cellular processes important for tissue repair.

In addition to allowing dosage-controlled delivery of miRNAs, the nanostraw-electroporation system offered another great advantage. Due to its primarily physical mechanism of delivery, the system was less cell type specific than other transfection techniques. This ability to avoid cell type specificity meant that common hard-to-transfect cells, such as primary keratinocytes may now be efficiently transfected with biomolecules.

5.11. Methods

5.11.1. Testing fibroblast viability on the NS membrane

Nondiabetic fibroblasts were seeded at 40,000 cells/350 μL full DMEM in NS wells and left to adhere overnight. The following day the NS wells were processed in two different ways: some of the wells were stained with 5 μM Cell Tracker Green (40 min at 37°C), Hoechst 33342 at 1:2000 (10 min at room temperature) and 5x Live/Dead assay (10 min at room temperature), followed by imaging them with the PALM fluorescent microscope for viable and dead cells. For the remaining NS wells the cells were detached from the wells using trypsin and re-seeded into 96-wells overnight. The following day the cells were stained with 5 μM Cell Tracker Green (30 min at 37°C) and 5x Live/Dead assay (15 min at room temperature) and imaged with the PALM fluorescent microscope for viable and dead cells.

5.11.2. Testing the cell viability of fibroblasts on the NS membrane after electroporation

Nondiabetic fibroblasts were seeded at 40,000 cells/well in NS wells in full DMEM medium and left to adhere overnight. The next day the cell viability was checked by delivering 0.1xPBS into the cells at different voltages and pulse sequences: 15V 1 electroporation, 15V 3 electroporations, 20V 1 electroporation, 20V 3 electroporation, 25V 1 electroporation, 25V 3 electroporations with 1 electroporation being 40 sec long and 3 electroporations being three 40 sec long electroporations at intervals of 3 min. The NS wells were then returned to the incubator for 2-3h after which Cell tracker was added at 5 μM for 30 min according to the protocol, followed by addition of Live/Dead assay for >10 min. Images were then taken with the PALM microscope using 12-well plates with glass bottom.

5.11.3. Testing the cell membrane permeabilisation on the NS membrane

Nondiabetic fibroblasts were seeded at 30,000 cells/well in NS wells in 350 μL full DMEM/well and left to adhere overnight. The next day the cells were stained with 5 μM Cell Tracker for 30 min and then PI (1mg/mL) diluted 1:10 in 0.0001xPBS was delivered into the cells at 20V, 3 electroporations at 3 min intervals. The NS wells were then returned to the incubator until the last delivery was finished (10-20min). A negative control to check for passive diffusion was

also done – the NS well was left in the TC hood in the cell cap containing 65 μL of 1:10 diluted PI and then the NS well was put in the incubator for 10 min (together with the last delivery). After this the cells in the NS wells were washed with PBS once and the outer membrane was also rinsed with 0.0001xPBS before imaging with the PALM microscope. Cells seeded in well plates were also stained with 5 μM Cell Tracker for 60 min and then PI diluted 1:10 was added for 10 min in the incubator. All these negative controls were done to check whether PI is indeed cell impermeable at these concentrations.

5.11.4. Delivering fluorescently-tagged miRNAs into the fibroblasts

Nondiabetic fibroblasts were seeded at 50,000 cells/well in 350 μL full DMEM and left to adhere for 2h followed by centrifugation of the NS wells at 1400rpm for 4 min. 2 μg of Cy3-tagged scramble miRNA was delivered at 20V, 40Hz, 200μs (3 electroporations at 3 min intervals) in 0.0001xPBS. After the delivery the cells were washed twice with PBS on the inside and the NS membrane rinsed on the outside, followed by detachment via trypsinisation and re-seeding into 96-well plates. 24h later the cells were stained with Hoechst 33342 (7 min at room temperature) and fixed in 4% PFA (10 min at room temperature) and imaged with the Inverted Widefield Zeiss Axio Observer microscope.

5.11.5. Delivering functional miRNAs into fibroblasts

Nondiabetic fibroblasts were seeded at 50,000 cells/well in 350 μL of full DMEM and left to adhere for 1h. The NS wells were then centrifuged at 1400rpm for 4 min. Positive miR control against GAPDH was delivered in a concentration range of 1-4 μg/NS well after being spiked with scramble miR for a total amount of 5 μg miR/NS well. This was done to allow comparison to the same negative control samples. Deliveries were done at 20V, 3 electroporations at 3 min intervals in 0.0001xPBS. After delivery the cells were trypsinised and re-seeded into 24-well plates for 48h until RNA extraction via the PureLink microscale RNA kit. 100 ng of RNA was then reverse transcribed into cDNA using oligodT primers from the nanoScript2 kit and qPCR was run on the ABI 7500 fast machine (5 ng RT product in 10 μL/well) using double-dye Taqman probes. Beta actin was used as the internal normalisation (housekeeping) gene.

5.11.6. Delivering siRNAs into fibroblasts

Nondiabetic fibroblasts were seeded at 50,000 cells/NS well in 350 μL full DMEM and left to adhere for ~2h followed by centrifugation of the NS wells at 1400rpm for 4 min. 1 μg of CAV1 siRNA (spiked with 4 μg of scramble miR mimic) or 5 μg scramble miR mimic were delivered in n=3 at 20V, 40Hz, 200 μs (3 electroporations at 3 min intervals) in 0.0001xPBS. After the last delivery the cells were left in the incubator for ~1h, followed by detachment via trypsinisation and re-seeding into 24-well plates. 48h post siRNA delivery the cells were lysed and total RNA was extracted using the microRNA miRVana kit. 100 ng of total RNA was then reverse transcribed using oligodT primers and qPCR was run on the ABI 7500 fast machine using Taqman probes. Beta actin was used as the internal normalisation gene and the fold change of CAV1 expression was calculated relative to cells to which scramble miR mimic was delivered.

5.11.7. Ratiometric delivery of miRNA mimics into fibroblasts at increasing concentrations

Nondiabetic fibroblasts (N=2) were seeded at 50,000 cells/well in 350 μL full DMEM and left to adhere for 2h. The NS wells were then centrifuged at 1400rpm for 4 min and miR-181a and miR-27a mimics were delivered in n=4 replicates in a symmetric ratiometric manner at 5 μg total miRNA/NS well at 20V, 3 electroporations at 3 min interval in 0.0001xPBS. Following delivery the cells were trypsined and re-seeded in 24-well plates in full DMEM for 2 days. At this point total RNA was extracted via the miRNA miRVana kit and 10 ng of total RNA was reverse transcribed using microRNA specific stem-loop primers. qPCR was then run on the ABI 7500 fast machine using Taqman microRNA assays. RNU44 was used as the housekeeping gene and the fold changes in miRNA expression were compared to fibroblasts to which 5 μg scramble miR was delivered.

5.11.8. Delivering miR-181a mimic at increasing concentrations for KRAS qPCR

Nondiabetic fibroblasts (N=2) were seeded at 50,000 cells/350 μL full DMEM and left to adhere for 2-3h, followed by centrifugation of the NS wells at 1400rpm for 4 min. Next miR-181a mimic or scramble miR mimic was delivered at 0.5-4.5 μg miRNA/NS well at 20V, 3

electroporations at 3 min intervals in 0.0001xPBS. After delivery the cells were washed with PBS twice and the NS membrane was rinsed on the outside and the cells were re-seeded into 24-well plates in full DMEM. 48h later the cells were lysed and total RNA was extracted via the miRVana miRNA isolation kit. 50-60 ng of total RNA was used for reverse transcription using oligodT primers and qPCR was run on the ABI 7500 fast machine (2.5-3 ng cDNA/well in 10 μL/well). ACTB served as the internal normalisation gene. The fold change in KRAS expression was calculated relative to fibroblasts containing scramble miR mimic.

5.11.9. Delivering miR-181a mimic into fibroblasts for proliferation assays

Nondiabetic fibroblasts (N=3) were seeded at 50,000 cells/350 μL full DMEM and left to adhere for 2-3h, followed by centrifugation of the NS wells at 1400rpm for 4 min. Next miR-181a mimic, spiked with scramble miR mimic, was delivered at 5 μg total miRNA/NS well at 20V, 3 electroporations at 3 min intervals in 0.0001xPBS. After delivery the cells were washed with PBS twice and the NS membrane was rinsed on the outside and the cells were re-seeded into black 96-well plates (n=6-10/NS well) in full DMEM. Proliferation was measured on day 1 and day 5 via Presto Blue (1h incubation at 37 °C) and the fold change in proliferation over 4 days was determined and compared to cells to which 5 μg of scramble miR was delivered.

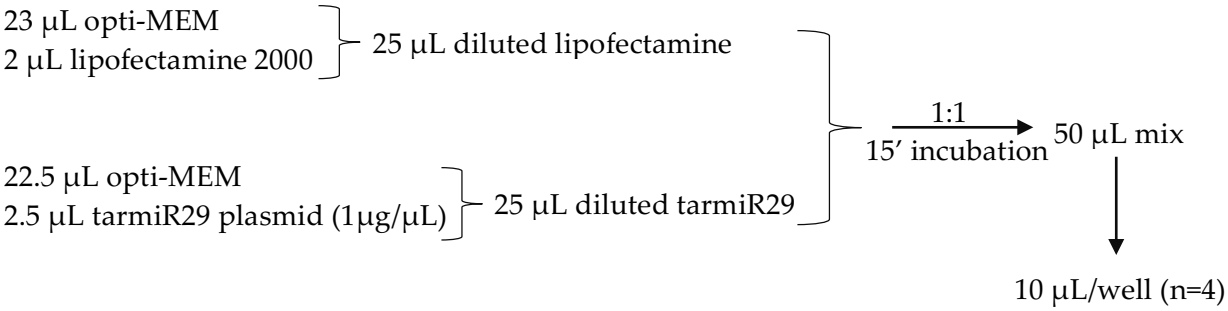
5.11.10. Ratiometric delivery of miRNA inhibitors into fibroblasts via NS

Nondiabetic fibroblasts (N=2) were seeded at 50,000 cells/well in 350 μL full DMEM and left to adhere for 2h. The NS wells were then centrifuged at 1400rpm for 4 min and antimiR-181a and antimiR-27a were delivered in n=3-4 replicates in a symmetric ratiometric manner at 5 μg total miRNA/NS well at 20V, 3 electroporations at 3 min interval in 0.0001xPBS. Following delivery the cells were trypsined and re-seeded in 24-well plates in full DMEM for 2 days. Total RNA was extracted via the miRVana miRNA isolation kit and 10 ng of total RNA was reverse transcribed using microRNA specific stem-loop primers. qPCR was then run on the ABI 7500 fast machine using Taqman microRNA assays. RNU44 was used as the internal normalisation gene and the fold changes in miR-181a or miR-27a expression were calculated relative to cells containing to 5 μg scramble miR inhibitor.

5.11.11. Delivering antimiR-29 into fibroblasts via NS

Nondiabetic fibroblasts (N=3) were seeded at 50,000 cells/350 μL full DMEM and left to adhere for 2-3h, followed by centrifugation of the NS wells at 1400rpm for 4 min. Cy3-anti29-294 was delivered at 1 μg, 3 μg or 5 μg/NS well or Cy3-scr-296 at 5 μg/NS well at 20V, 3 electroporations at 3 min intervals in 0.0001xPBS. After delivery the cells were washed with PBS twice and the NS membrane was rinsed on the outside and the cells were re-seeded into white 96-well plates (n=3/NS well) in antibiotic-free medium. 24h later tarmiR29 plasmid was delivered via lipofectamine 2000 and luminescence was measured 48h later via the Dual-Glo luciferase assay on the Varioskan Flash reader. The ratio of Renilla/Firefly of Cy3-anti29-294 vs that of Cy3-scr-296 was determined for each NS well to check for Renilla derepression following antimiR-29 delivery.

The following protocol was used for tarmiR29 transfection via lipofectamine 2000:



To measure the luminescence produced by Firefly and Renilla via the Dual-Glo luciferase assay the following protocol was used:

Step 1: The 96-well plate containing the samples was removed from the incubator and 75 μL of room temperature antibiotic-free DMEM (supplemented with 10% FBS and 2.5 mM L-glutamine) was added to each well. Three empty wells without cells served as negative control to measure background luminescence.

Step 2: Dual-Glo Luciferase Assay Reagent was added to each plate well using a multichannel pipette at 75 μL/well. This reagent induced cell lysis and provided a substrate for Firefly luciferase.

Step 3: The plate was left to incubate at room temperature for 30 min, followed by measuring Firefly luminescence with the Varioskan flash plate reader.

Step 4: Dual-Glo Stop&Glo Reagent was immediately added to each plate well using a multichannel pipette at 75 μL/well. This reagent quenched the luminescence from the Firefly reaction by at least 10,000 fold and provided a substrate for Renilla luciferase.

Step 5: The plate was left to incubate at room temperature for 30 min, followed by measuring Renilla luminescence with the Varioskan Flash plate reader.

Step 6: The Firefly or Renilla background luminescence values were subtracted from all respective readings and the ratio of Renilla/Firefly was calculated for each well.

5.11.12. Delivering GFP plasmid into primary fibroblasts via NS

Nondiabetic primary fibroblasts were seeded at 50,000 cells/350 μL full DMEM and left to adhere for 2-3h, followed by centrifugation of the NS wells at 1400rpm for 4 min. Next pmaxGFP plasmid was delivered at 2 μg /NS well at 20V, 3 electroporations at 3 min intervals in 0.0001xPBS or 1xPBS. After delivery the cells were washed with PBS twice and the NS membrane was rinsed on the outside and the cells were re-seeded into 24-well plates in full DMEM. 72h later the fibroblasts were stained with Hoechst 33342, fixed in 4% PFA and imaged with the Inverted Widefield Zeiss Axio Observer microscope. Fibroblasts without pmaxGFP plasmid, i.e. from cell culture served as negative control to account for autofluorescence of fibroblasts.

5.12. Supplementary data

5.12.1. Fabrication of nanostraw membrane

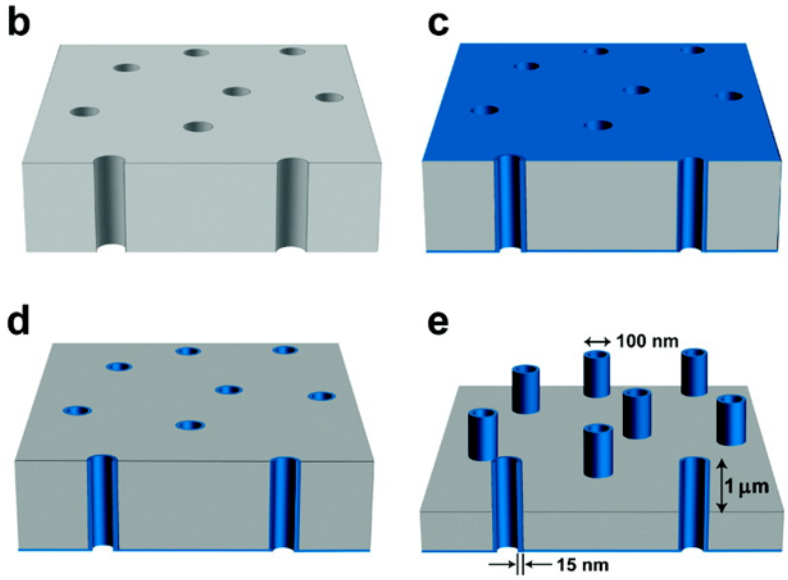


Figure 106: Fabrication starts with commercially available track-etched polycarbonate membranes (shown in grey) that are in a range of pore sizes. First, an alumina coating of 10-30nm thickness (shown in blue) is deposited on all surfaces of the membrane (top, bottom and inside of pores) using atomic layer deposition to create a uniform coating. The deposited alumina creates the nanostraw bodies within the interiors of the pores. Next, the alumina on the top surface is removed using reactive ion etching (RIE) to expose the polymer underneath. Finally, oxygen RIE is used to expose the nanostraws by selectively etching the polymer until the desired height of nanostraws is obtained (1-2 µm). Image reprinted with permission from [210]. Copyright 2012 American Chemical Society.

5.12.2. Delivering miR-29 inhibitor into fibroblasts via NS

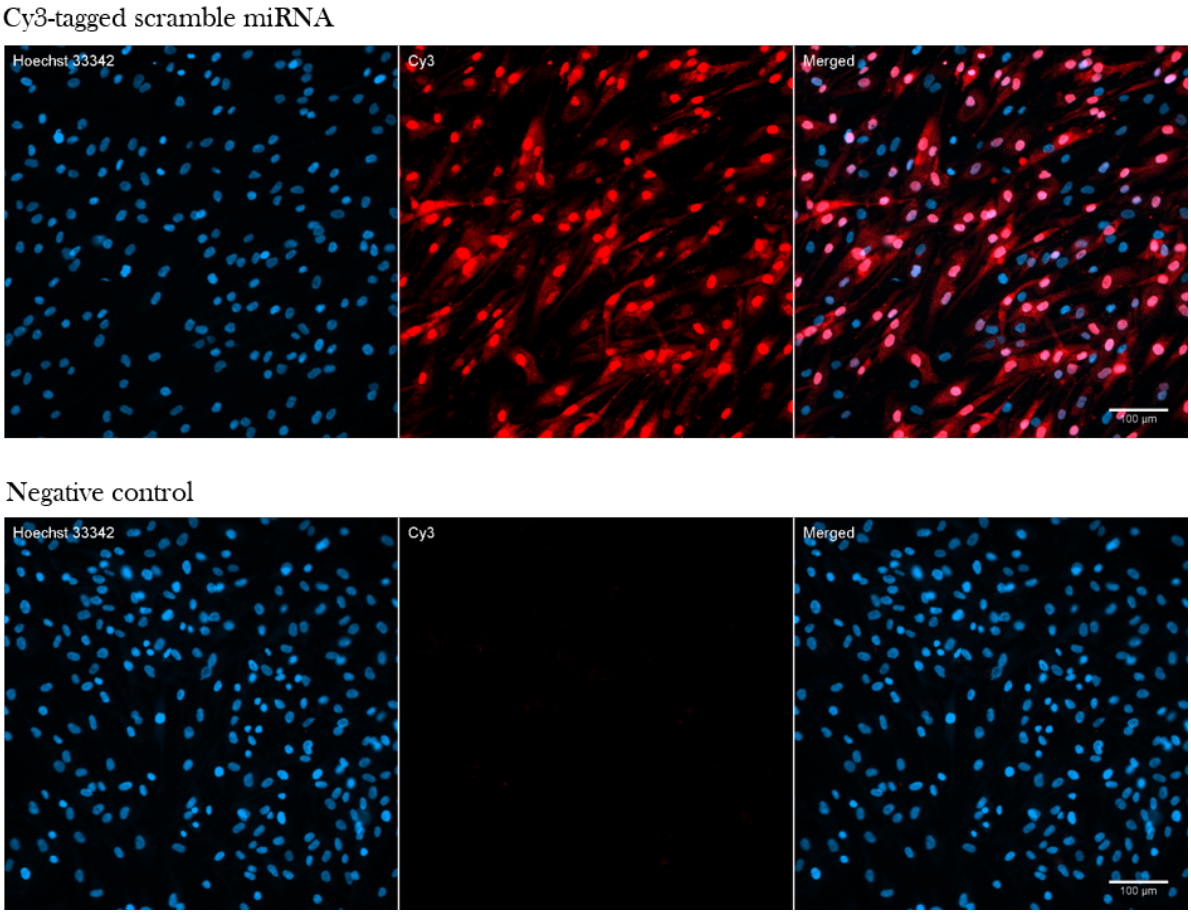


Figure 107: NS-mediated delivery of Cy3-tagged scramble miRNA (red) into primary nondiabetic fibroblasts is successful as measured 24h post delivery, confirming that delivery of Cy3-anti29-294 is most likely efficient as well. Blue denotes the nuclear stain Hoechst 33342

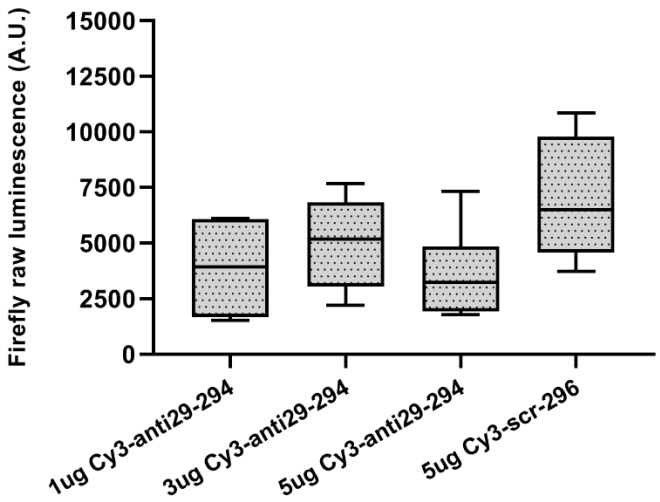


Figure 108: Firefly raw luminescence values in primary nondiabetic fibroblasts remain similar across all experimental conditions (p=0.0806) following delivery of antimiR-29 or scramble miR, confirming that Firefly is a reliable control. Statistical analysis was performed via one-way ANOVA. N=3, n=2-3/donor

Furthermore, transfection of tarmiR29 into primary fibroblasts via lipofectamine 2000 was efficient as Firefly raw luminescence values for transfected fibroblasts were ~100-fold higher than those of fibroblasts not transfected with the plasmid, i.e. 4684 ± 2530 vs 46 ± 30, respectively. This confirmed lipofectamine 2000 was able to successfully transfect the tarmiR29 plasmid into primary dermal fibroblasts.

5.12.3. pmaxGFP plasmid delivery into primary fibroblasts via NS-mediated electroporation

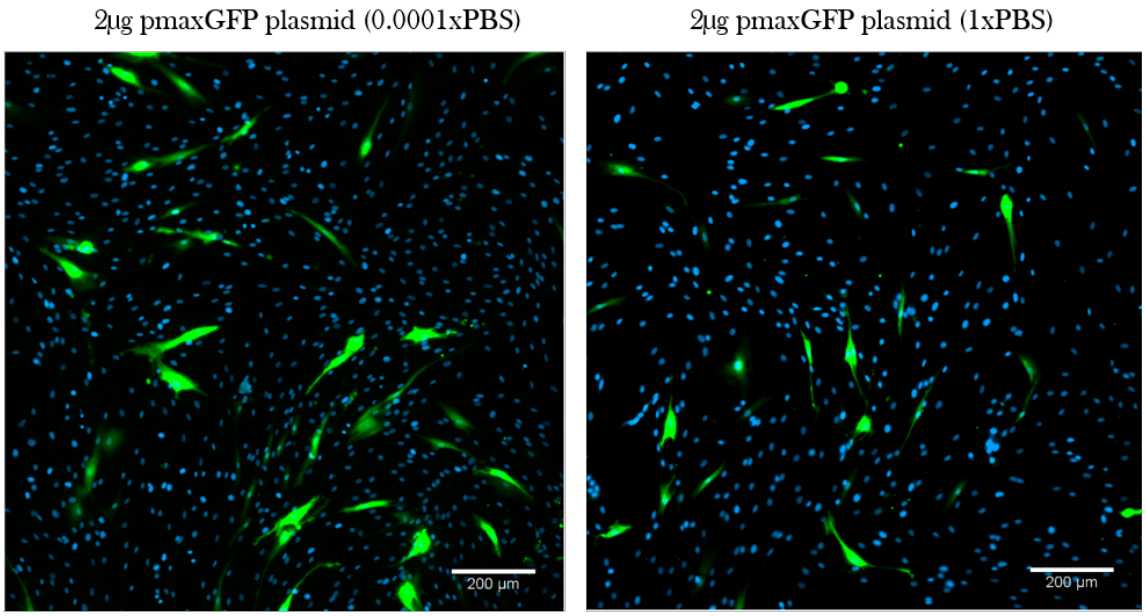


Figure 109: NS-mediated delivery of pmaxGFP plasmid (green) into primary nondiabetic fibroblasts shows poor expression of GFP 72h later, confirming that the NS geometry used for delivery of small RNAs (1.2-1.5 µm height and 100 nm diameter) may perhaps not be adequate for delivery of large cargos. Blue denotes the nuclear stain Hoechst 33342

6. Nanostraw-mediated delivery of microRNAs into primary keratinocytes

The nanostraw-electroporation system offers a significant advantage by relying on its physical mechanism of delivery involving transfer of cargo directly into the cytoplasm with no additional biological steps necessary. This lack of need to rely on any biological machinery for delivery means the system is less sensitive to cell types and cell-specific characteristics such as cell source and origin (primary vs cell line), cell density, passage number and age or cell cycle than other transfection techniques, such as viral-based or biochemical. In turn, this has made this system universal and suitable for intracellular cargo delivery into a variety of cells that are otherwise difficult to transfect using standard techniques. For instance, in the past the nanostraw-electroporation system has been shown to deliver mRNA successfully into hard-to-transfect cell types, such as human embryonic stem cells, mouse primary glia and mouse primary neuron cells [205]. However, it has not been used for transfection of cargo into primary keratinocytes, a type of skin cell that is challenging to transfect.

Keratinocytes (KC) constitute over 90% of the cells found in the epidermis, the outermost layer of the skin. Their primary function is to form a protective barrier against outside factors, such as pathogens, heat or UV and regulate water loss from the body. This protective role in providing the first line of defence has led to their nickname 'guardians of the skin'. Keratinocytes originate in a layer of the epidermis called the stratum basale (Figure 110). Anchored to the dermis, this layer is the first of five layers of the epidermis[o] and contains epidermal stem cells. Here, basal keratinocytes divide and proliferate to yield more stem cells, some of which migrate into the upper layers of the epidermis. As keratinocytes travel towards the surface of the skin they commit to terminal differentiation, changing their morphology, cellular composition and function throughout each layer. For instance, by the time keratinocytes reach the stratum corneum they will have lost their nucleus and have the sole purpose of providing a tight, protective barrier of keratin.

[o] The stratum lucidum is found only in the skin of the palms and soles, contributing to the thicker skin typically found in these areas

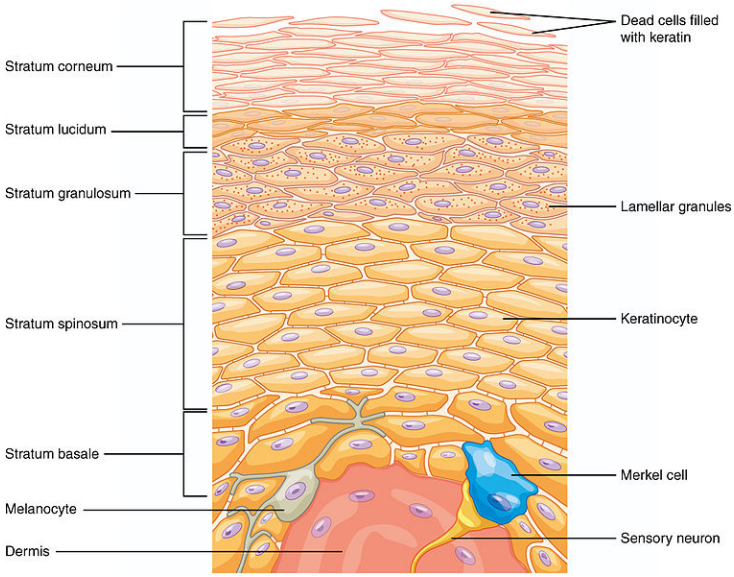


Figure 110: the epidermis consists of 4-5 different layers depending on the skin region, starting from the stratum basale closest to the dermis to stratum corneum at the skin surface. Each of the layers contains keratinocytes with different morphology, cellular composition and function. Other cell types, such as melanocytes or Merkel cells are also present in the epidermis.

6.1. Primary keratinocytes are hard-to-transfect cells

Primary keratinocytes are generally one of the hardest cell type to transfect with many common transfection methods, such as liposomal-, electroporation- or viral-based having limited success [211]. Low transfection efficiency may partly be attributed to poorer endocytotic properties of KC and high sensitivity to any sort of physical manipulation during treatments. To overcome these limitations, many studies use immortalised HaCaT cells – a widely employed model of keratinocytes - due to their increased resilience, ease of propagation in culture and improved efficiency of transfection [212]. However, as with every cell line these cells are not truly representative of their *in vivo* environment and cannot account for donor variability, especially important for understanding naturally occurring biological variations in human skin. As such, a method is required that can transfect primary keratinocytes in a reproducible and efficient manner. Given the successful NS-mediated delivery of miRNAs into fibroblasts (chapter 5), I decided to test this platform with primary keratinocytes.

Basal keratinocytes isolated from human breast tissue (Figure 111) were used for testing the nanostraw-electroporation platform. These cells were a gift from Mr Patel Sharad (technician in Dr Claire Higgins' lab, Department of Bioengineering). KC were subcultured according to the recommended protocol. Briefly, cells were grown in Epilife medium (supplemented with EDGS) in pre-coated flasks with coating matrix (CM) [p]. TryplE, a gentle non-enzymatic dissociation agent, was used to detach the KC during routine splitting and experiments. KC were used throughout experiments from P3-P9 as they displayed high proliferative capacity up to this passage.

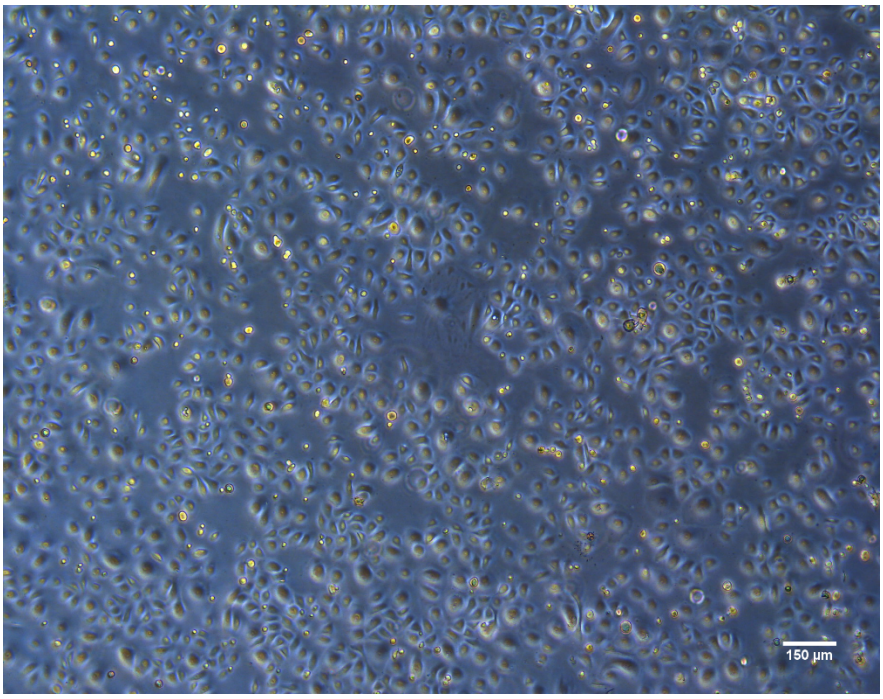


Figure 111: basal primary keratinocytes from human breast tissue in culture imaged with the light microscope. Small eye-shaped keratinocytes denote proliferating cells, large fried egg-shaped denote differentiated keratinocytes. These cells were used for characterising the nanostraw-electroporation platform for miRNA delivery into this hard-to-transfect cell type.

[p] Unlike fibroblasts KC cannot produce their own ECM. To facilitate increased cell adhesion and growth during routine subculture flasks are commonly coated with ECM components, such as collagen prior to seeding the KC. In this project T75 cell culture flasks were pre-coated with CM containing collagen I. Pre-coating was done by adding 5 mL of CM (1:100) for 30 min at room temperature, followed by aspirating the CM before seeding the KC.

6.2. NS-mediated delivery of miRNAs into keratinocytes in suspension (3 centrifugation protocol)

To deliver miRNAs into primary keratinocytes I initially used the same protocol as for fibroblasts (chapter 5). This involved seeding the KC from culture flasks into the NS wells, centrifuging the NS wells, delivering the miRNAs, followed by re-seeding the KC into well plates for further culturing (Figure 112). However, this procedure involved extensive manipulation of the cells over a relatively short period of time (i.e. 3 centrifugations and two treatments with TryplE), leading to the concern that the KC might not survive the protocol. Unlike fibroblasts - which are robust and resilient cells - KC are very sensitive cells that require gentle and minimal handling.

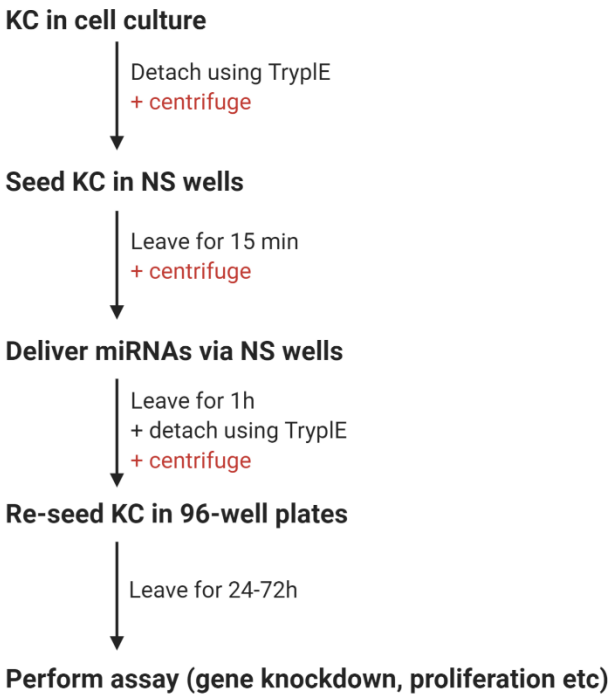


Figure 112: set-up of the '3 centrifugation' protocol for miRNA delivery into primary KC in suspension. First, KC are detached from the cell culture flasks and seeded into NS wells placed in a 24-well plate. Next, the NS wells are centrifuged to ensure the cells come in close contact with the nanostraws and the miRNAs are delivered via NS-mediated electroporation. After delivery the NS wells are returned to the incubator briefly to allow the cells to recover, followed by detaching the KC from the NS membrane and re-seeding them into 96-well plates for functional assays. Image created in BioRender.com and exported under a paid subscription.

As such, before delivering miRNAs using the nanostraw-electroporation system, I first tested KC cell viability at every step of the procedure by mimicking it in 96-well plates [q]. KC from cell culture were seeded in uncoated 96-well plates (30,000 cells/200 μL Epilife per well), followed by centrifuging the well plates (300xg for 4 min) and waiting 1-2h. Next the KC were detached using TryplE and centrifuged again, followed by seeding them into pre-coated 96-well plates overnight (15,000 cells/200 μL Epilife per well). The following day the KC were stained with nuclear dye Hoechst 33342 and Cell Tracker Green to monitor cell viability. Representative light and fluorescence microscopy images revealed high cell viability and healthy morphology, confirming that that the KC survived three centrifugations and two treatments with TryplE (Figure 113). This suggested the '3 centrifugation' protocol should be suitable for NS-mediated miRNA delivery.

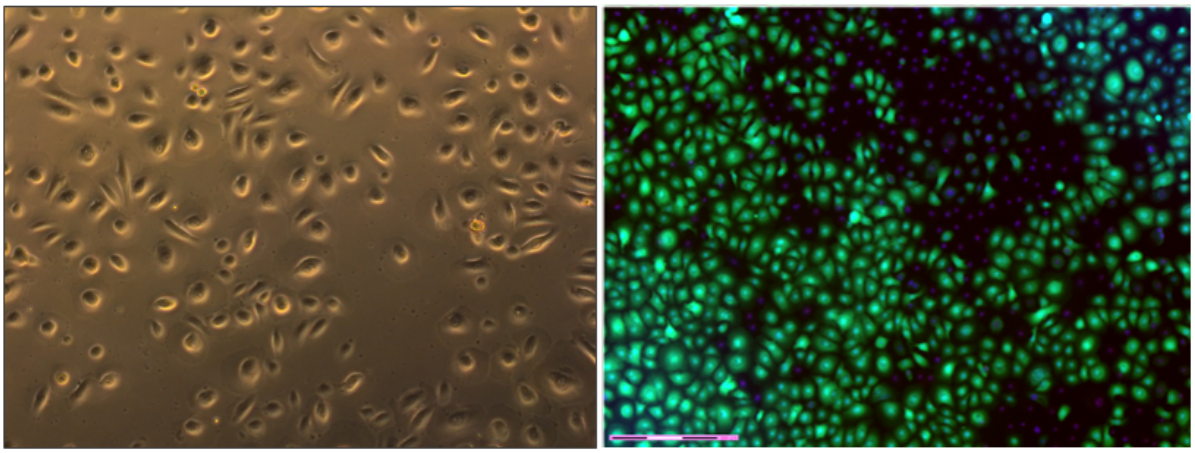


Figure 113: KC display healthy morphology (left) and high cell viability (right) 24h after extensive manipulation that involved two treatments with TryplE and three centrifugations over short periods of time, confirming the '3-centrifugation' protocol should be suitable for NS-mediated miRNA delivery. Green denotes viable cells, red denotes dead cells

The effect of electroporation on KC viability, however was still unknown. As such, I next tested what electroporation parameters were suitable during NS-mediated electroporation to ensure high cell viability. KC were seeded in uncoated NS wells (70,000 cells/350 μL Epilife), centrifuged at 300xg for 4 min and electroporated in 0.0001xPBS at 15V or 20V (40Hz, one 40 sec long electroporation). Following electroporation the NS wells were returned to the incubator for 30-60min, followed by re-seeding the KC into 96-well plates overnight. The

[q] 96-well plates were used because the area of the plate well was similar to the area of a NS well (~0.35 cm^2).

following day KC were stained with Hoechst 33342 and Cell Tracker Green to monitor cell viability.

Representative microscopy images revealed that both voltages ensured good cell viability, with 15V displaying slightly higher cell viability (Figure 114). This, perhaps was expected as 20V was used for electroporation of fibroblasts, which are more robust than KC. As such, I decided to use 15V, 40Hz, one electroporation (40 sec long) as the parameters for NS-mediated delivery of miRNAs into KC.

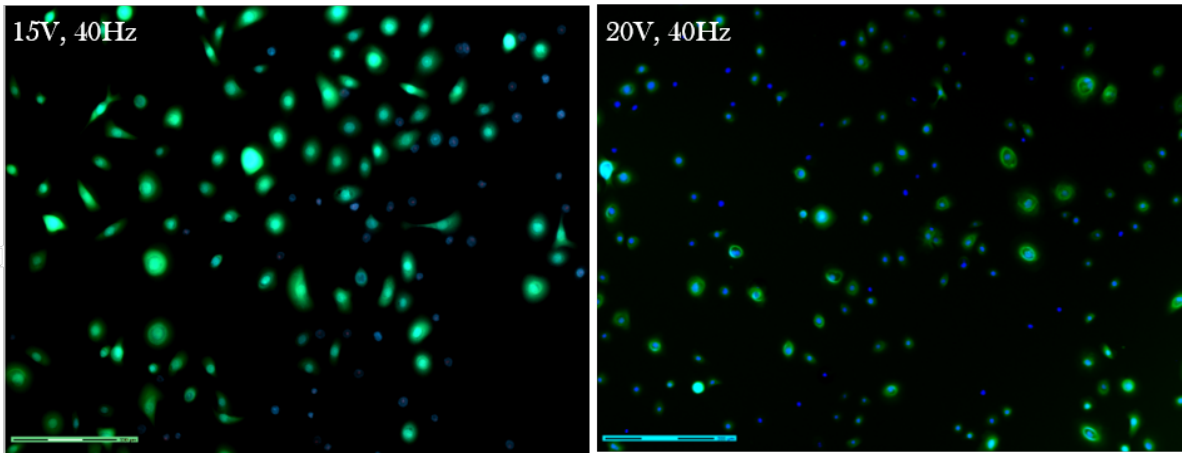


Figure 114: representative microscopy images of KC the day after NS-mediated electroporation at 15V and 20V reveals higher KC viability is maintained at 15V, suggesting 15V should be used for NS-mediated delivery of miRNAs into primary KC. Green denotes viable cells, blue denotes cell nuclei. Scale bars denote 150 μm

Having chosen the electroporation parameters I lastly tested if NS-mediated delivery of miRNAs into KC was successful. For this 2 μg of Cy3-tagged scramble miRNA was delivered at 15V, 40Hz for 40 sec in 0.0001xPBS according to the '3-centrifugation protocol'. Following delivery the bottom of the NS membranes were rinsed with PBS and the KC detached and re-seeded into pre-coated 96-well plates. KC were imaged the following day with the PALM fluorescent microscope to check uptake of miRNA. Surprisingly, however there was no sign of uptake of fluorescently-tagged miRNA into the KC (Figure 115).

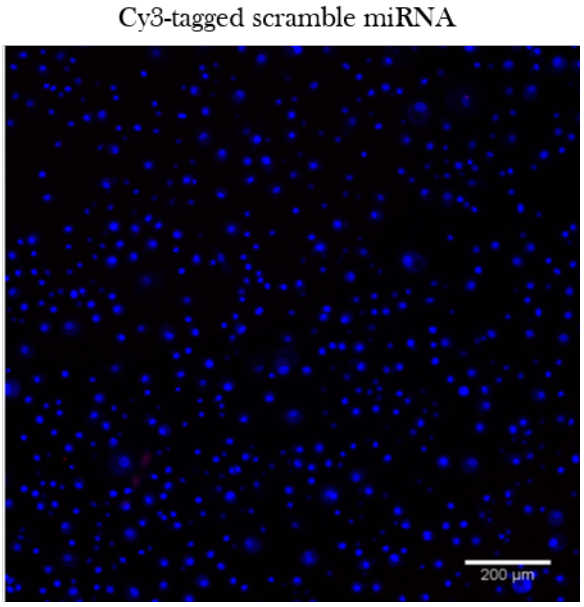


Figure 115: NS-mediated delivery of Cy3-tagged scramble miRNA (red) into primary KC via the '3 centrifugation' protocol shows no sign of cargo uptake 24h later, suggesting pore formation in the plasma membrane is not successful using this protocol. Blue denotes the nuclear stain Hoechst 33342

These findings were startling, as this protocol set-up worked very well for fibroblasts (chapter 5). This inability of the KC to uptake any small RNA could have been either because of the lower voltage used (15V instead of 20V as for fibroblasts), however this was unlikely as pore formation was previously shown to occur at voltages as low as 6V for other cell types [203]. Alternative explanations could have been that the KC did not remain in contact with the nanostraws following centrifugation of the NS wells. Usually some time would pass (15-20min) in between centrifugation and electroporation, which might have caused the KC to start floating again. Alternatively, it could have been that the adhesion molecules on the KC were disrupted after exposure to TryplE, unable to form a contact point with the nanostraws (even after centrifugation of the NS wells). This hypothesis seemed less likely as TryplE is a gentle dissociation agent that - according to the manufacturer - maintains integrity of cell-surface membrane proteins, such as epitopes. However, after seeking advice from the NAVAN team regarding this mystery, they mentioned an interesting observation that seemed to support this hypothesis. With certain cell types, they would observe efficient delivery if the cells were left to adhere onto the NS membrane for 12-24h before electroporation, but inefficient delivery if the cells were trypsinised and centrifuged in the NS wells shortly before electroporation. As such, moving forward I decided to deliver miRNAs into KC when they

were fully adherent onto the NS membrane. This involved seeding the KC in the NS wells the day before miRNA delivery.

6.3. NS-mediated delivery of miRNAs into adherent KC

Seeding KC in the NS wells the day before meant the cells would now be on the NS membrane for a much longer period (~24h) than in the '3 centrifugation' protocol. This, in turn, posed the question whether the NS membrane had to be pre-coated with coating matrix (CM) to ensure the KC adhered to it. However, the CM layer may cover the tips of the NS, preventing KC from coming in close contact with them which is required for pore formation. As an easy way to overcome this problem, I tested whether KC could adhere and proliferate without CM to begin with.

To verify this KC were seeded into uncoated 96-well plates at various cell densities (4,000 – 27,000 cells/well) and monitored over a period of 6 days. Fluorescence microscopy images, taken 24h after seeding, revealed that the KC adhered to the uncoated plastic surface and were viable (Figure 116 top). In fact, the KC remained viable for the next five days and successfully proliferated throughout this time (Figure 116 bottom). This confirmed that culturing KC on the NS membrane without CM should be fine short- and long-term.

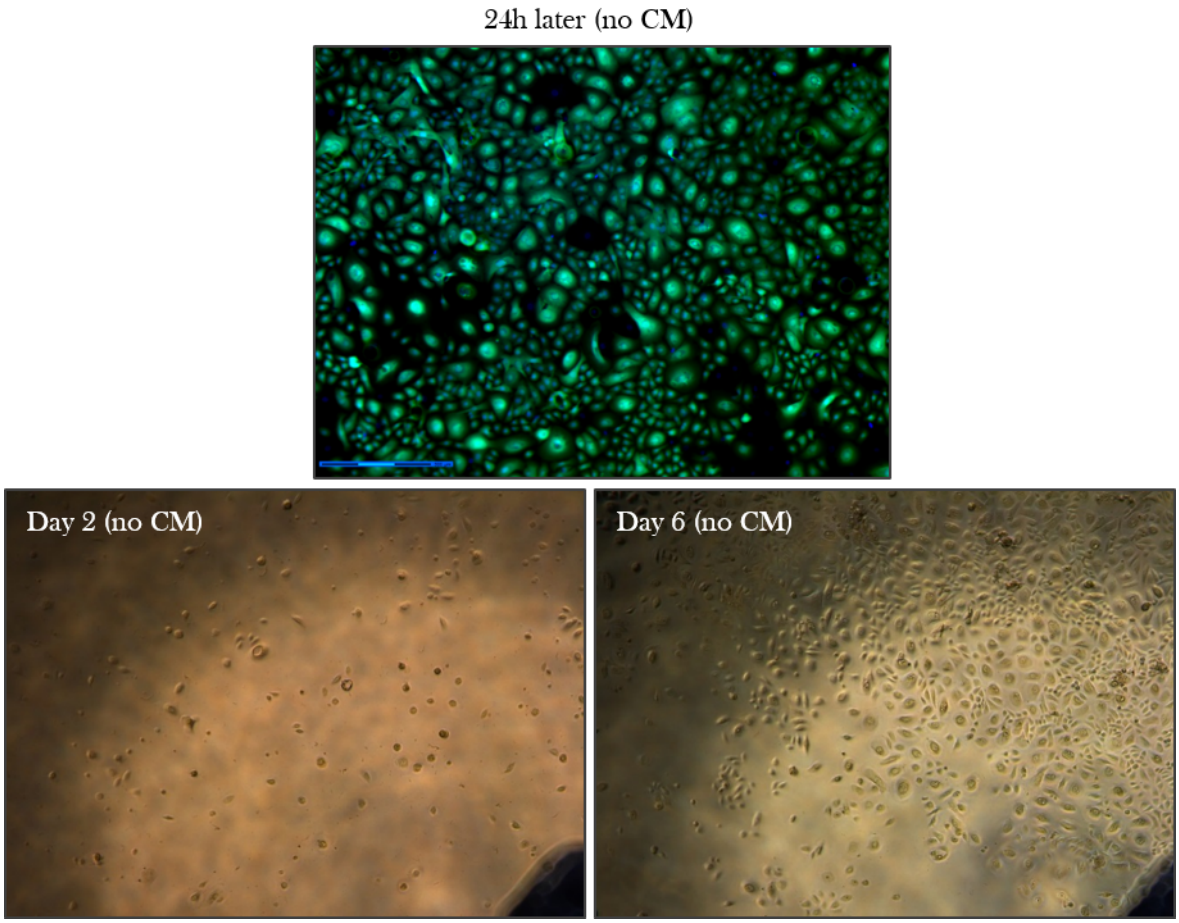


Figure 116: (top) primary KC cultured in uncoated 96-well plates are still able to adhere to the plastic surface and display high cell viability (green) 24h after seeding; (bottom) furthermore the cells are also able to proliferate well over 4 days, suggesting primary KC should be able to survive on the uncoated NS membrane. Uncoated denotes lack of coating matrix, normally used during routine subculture of KC. Bottom images were taken at 5x magnification.

However, when the KC were seeded onto uncoated NS membrane and left overnight, I discovered that cell viability was very low 24h post seeding (Figure 117). This suggested that the KC were not able to adhere to the NS membrane overnight and were dying as a result. Toxicity of the NS membrane was previously ruled out as fibroblasts were perfectly viable on the NS membrane 24h post seeding (Figure 93).

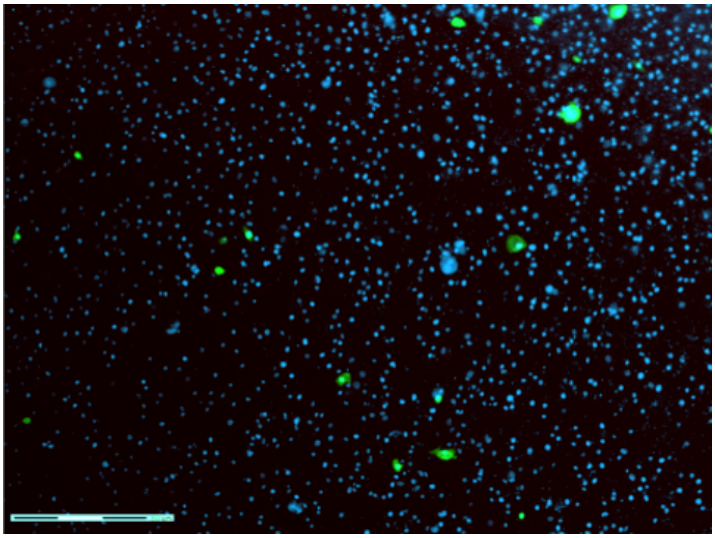


Figure 117: primary KC seeded on uncoated NS membrane display very low cell viability 24h after seeding, suggesting the NS membrane is unable to allow KC to adhere to it. Blue denotes KC nuclei, green denotes viable cells. Scale bar denotes 300 µm

This large difference in KC viability between the 96-well plate and the NS membrane may have been caused by a difference in chemical modification of the two surfaces. Namely, the plastic surface of the plate wells was 'TC-treated', whereas the NS membrane was not. The term 'TC-treated' refers to the technique of plasma treating hydrophobic polystyrene surfaces with oxygen to make them hydrophilic. This principle is widely employed by manufacturers of cell culture plates and flasks to improve cell adhesion. Plasma treatment introduces oxygen-containing functional groups, such as hydroxyl and carboxyl groups (C=O, -COOH, -OH etc) onto a hydrophobic surface. These chemical modifications give the surface a net negative charge, making it hydrophilic and 'wettable', i.e. water spreads over the plasma treated surface more easily due to the interactions with the newly formed functional groups (Figure 118). This change in the shape of the water droplet is often used to test if plasma treatment of a surface was successful (i.e. lower contact angle).

Following the 'TC-treated' principle, I postulated KC cell adhesion to the NS membrane may improve by plasma treating the NS wells with oxygen prior to seeding the cells. In fact, several studies previously showed that oxygen plasma treatment of various surfaces could improve adhesion and growth of HaCaT cells [213] and, more importantly, that polycarbonate surfaces - the material that the NS membrane is made out of - could be successfully plasma treated with oxygen [214].

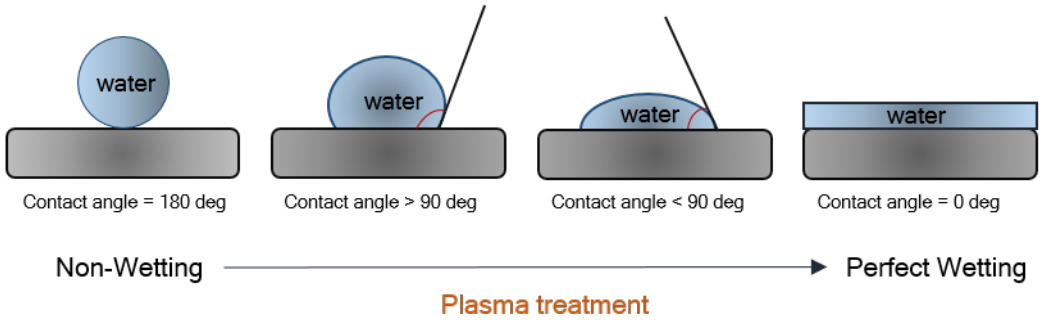


Figure 118: plasma treated surfaces display more 'wetting', as indicated by a lower contact angle of the water droplet relative to the surface. Plasma membrane introduces oxygen-containing functional groups onto surfaces, turning hydrophobic surfaces into hydrophilic ones.

To confirm the NS membrane could be effectively plasma treated too, I plasma treated a small square (7mm x 7mm) of NS membrane for 5 min at 0.3 mbar and medium power. Shortly after, I added a 1.5 µL droplet of water onto the untreated and plasma treated NS membrane to check if it changed shape. Indeed, the droplet shape revealed drastic differences between the plasma treated and untreated NS membrane. Namely, the plasma treated NS membrane had perfect wetting (i.e. the water droplet spread uniformly over the NS membrane), whereas the droplet on the untreated membrane retained its dome-like shape (Figure 119). This confirmed that oxygen plasma treatment was introducing functional groups onto the surface of the NS membrane, making it hydrophilic.

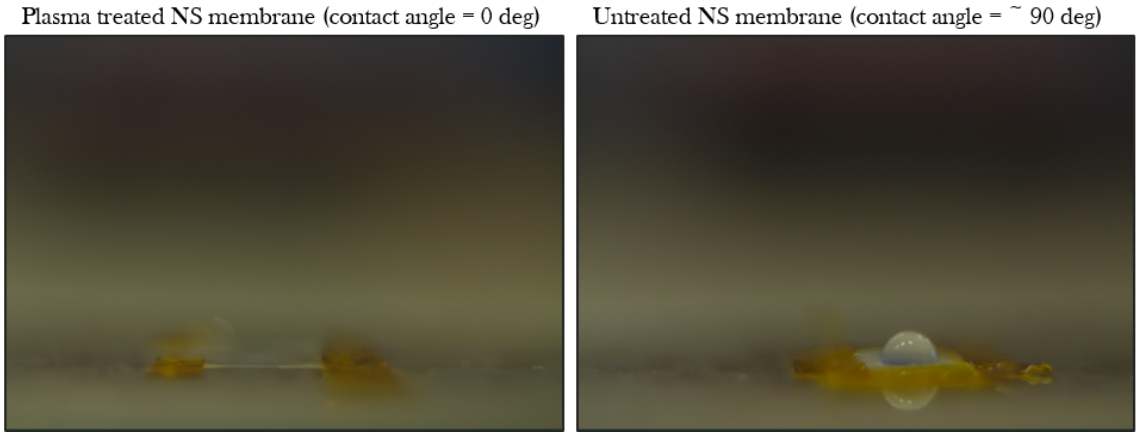


Figure 119: plasma treating the NS membrane with oxygen makes the membrane more hydrophilic as confirmed by the perfect wetting of the water droplet (left) compared to the dome-shaped water droplet on the untreated NS membrane (right)

Encouraged by these findings, I started plasma treating the NS wells for 5 min at 0.3-0.6 mbar prior to seeding KC in them [r]. Cell viability was monitored 24h post-seeding by staining the cells with Hoechst 33342 and Cell Tracker Green and imaging with the fluorescence microscope. Representative microscopy images revealed significant improvement in viability over seeding KC on untreated NS membrane (Figure 120).

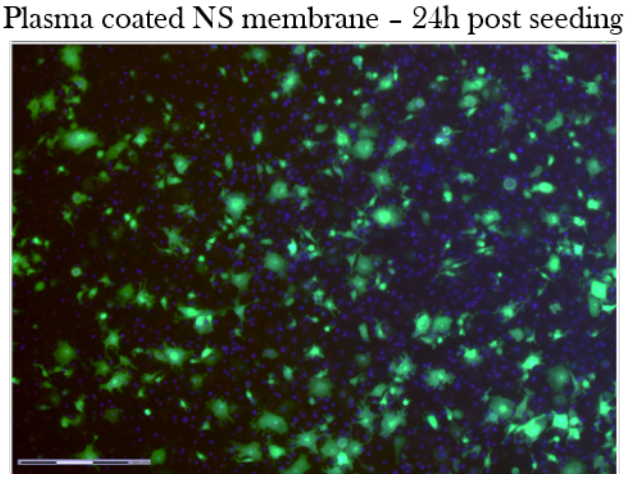


Figure 120: primary KC seeded on plasma treated NS membrane display significantly higher cell viability 24h later than on untreated NS membrane. Blue denotes KC nuclei, green denotes viable cells. Scale bar denotes 300 μm

Following the positive improvement of cell viability on plasma treated NS membrane, I next delivered fluorescently-tagged miRNA into KC using the nanostraw-electroporation system. Delivery of 2 μg of Cy3-tagged scramble miRNA according to the chosen parameters (15V, 40 Hz for 40 sec) in 0.0001xPBS revealed highly efficient (>95%) and homogenous cytoplasmic uptake of Cy3-tagged miRNA into the KC 24h later (Figure 121 left). In contrast, liposomal-based delivery of Cy3-tagged scramble miRNA into the same KC displayed significantly poorer cargo uptake, in accordance with the widely known difficulty of transfecting primary KC (Figure 121 right). Interestingly, the cargo that managed to be uptaken into the KC via lipofectamine transfection was confined to the nucleus rather than the cytoplasm (unknown reason). Overall, these results showed that NS-mediated delivery of small RNAs into KC represented a significant improvement over liposomal-based delivery.

[r] A plasma treated surface retains its hydrophilic chemical modifications for some time (~15 min). If the KC weren't ready to be seeded in this time window, I added deionised nuclease-free water to the plasma treated NS wells to keep the membrane in its hydrophilic state (for up to one hour).

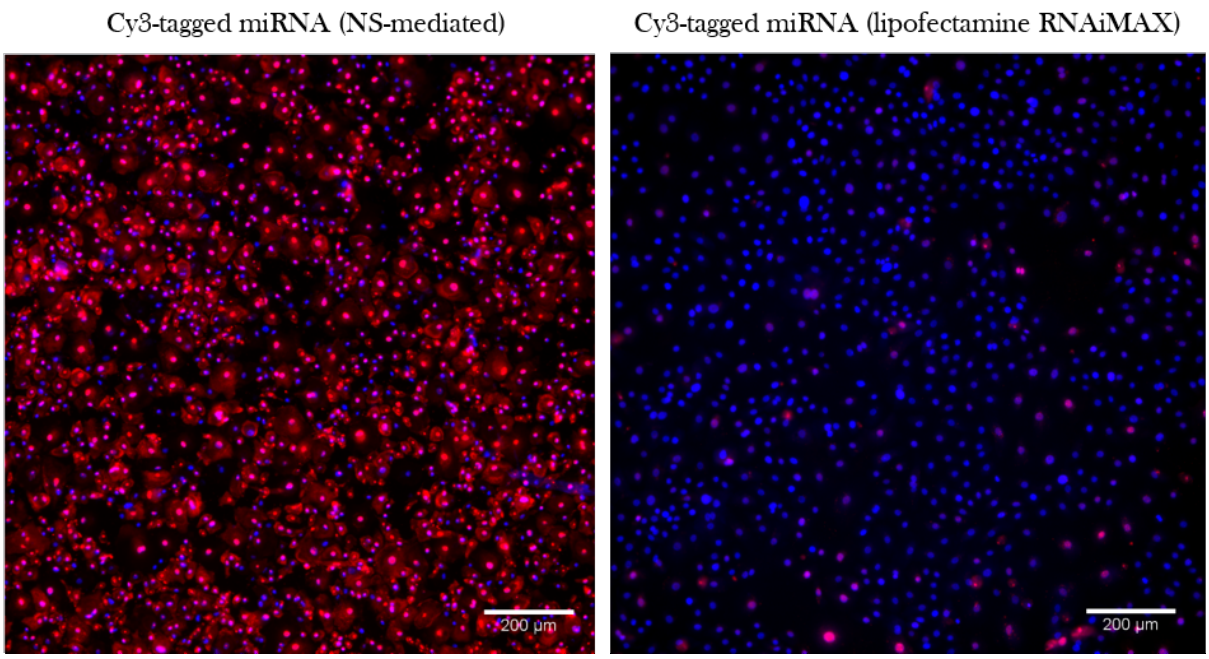


Figure 121: (left) NS-mediated delivery of Cy3-tagged scramble miRNA (red) into primary KC shows highly efficient and homogenous uptake of miRNA 24h after delivery; (right) in contrast liposomal-based delivery of the same miRNA into primary KC leads to much poorer uptake confined to the nuclei, reinforcing the known difficulty of transfecting primary KC with liposomal-based methods. Blue denotes KC nuclei following staining with Hoechst 33342

6.4. Improving KC viability on the NS membrane

Following the promising results observed with the fluorescently-tagged miRNA, I continued to explore new methods for refining KC survival.

Given that KC viability on the NS membrane was still relatively poor despite plasma treatment, I hypothesised that the KC must be affected by the nanostraw surface itself and the fact that it's not smooth (as the tissue culture flask). To verify this, I seeded the KC on a NS membrane with expanded pores, i.e. flat membrane that lacked the extended nanostraws, but still underwent the same chemical surface modification as the usual NS membranes (Figure 122).

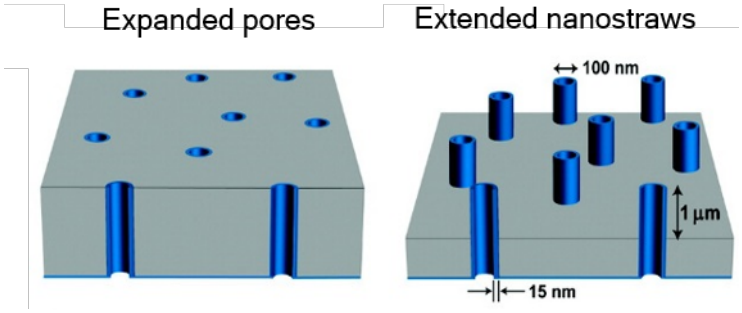


Figure 122: NS membranes with 'expanded pores' reveal a flat surface containing pores (left) that are not extending outwards (right), but have the same chemical surface modification. Nanostraws are depicted in blue, etched polycarbonate surface is depicted in grey. Image reprinted with permission from [210]. Copyright 2012 American Chemical Society.

KC were seeded on either a hydrophobic or plasma treated expanded pores NS membrane and the cell viability was checked the following day according to the usual protocol. Representative microscopy images revealed that KC viability was ~100%, similar to that observed in cell culture (Figure 123), confirming that the uneven surface created by the protruding NS was the reason for the low KC viability.

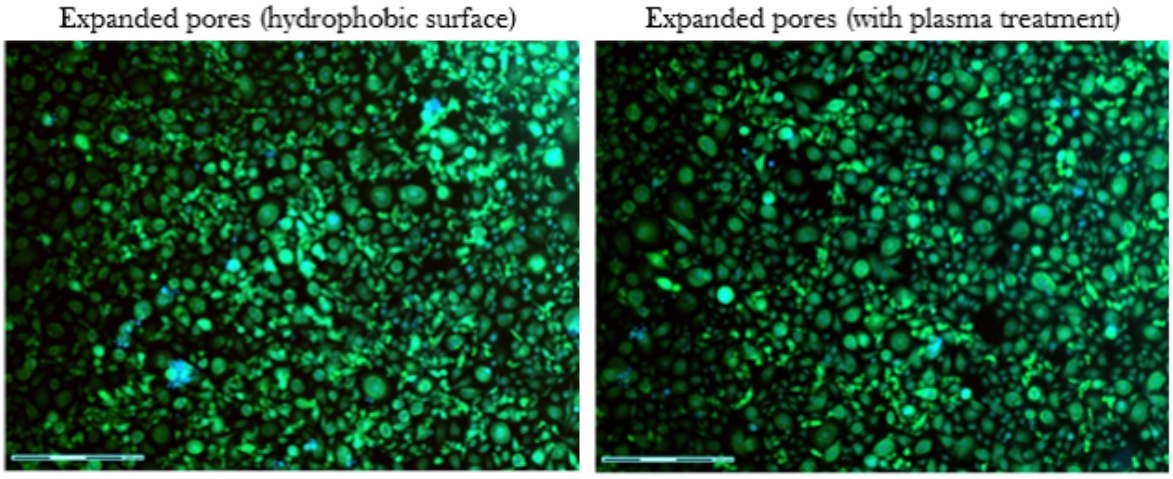


Figure 123: primary KC seeded on NS membrane with expanded pores exhibit ~100% cell viability 24h after seeding, both on the hydrophobic membrane (left) or hydrophilic membrane that was pre-treated with oxygen plasma (right). The NS membrane with expanded pores lacks the extended NS, but has still undergone the same chemical surface modification as the usual NS membrane. Green denotes viable KC. Scale bars denote 300 µm

These findings were curious as fibroblast viability was unaffected by the uneven surface of the NS membrane (chapter 5) and previous studies showed that the NS membrane perturbed cells minimally [210]. However, my results suggested a different response, namely that KC can sense the extended nanostraws underneath them despite their nanoscale dimensions. This

also, once again, reinforced how fragile primary keratinocytes are and how easily they can become stressed by small changes in the surrounding environment.

Going forward, it meant the only way to keep the KC alive in the NS wells was to 'mask' the nanostraws from the cells. One potential way to achieve this could be coating the NS membrane with CM prior to seeding the KC – despite the original fears of the CM potentially covering the NS tips to prevent pore formation. As such, I coated the plasma treated NS membrane with CM according to the manufacturer's instructions (1:100, 30min at room temperature) before seeding the KC in the NS wells. The following day the KC were stained with Cell Tracker Green and imaged with the fluorescence microscope to monitor cell viability.

Representative microscopy images of the NS wells showed cell viability was still fairly low and that the KC were still dying (Figure 124). Reasons for this could be that the CM didn't stick to the plasma treated NS membrane, possibly because it was a different material to the cell culture plastic ware, namely polycarbonate vs polystyrene.

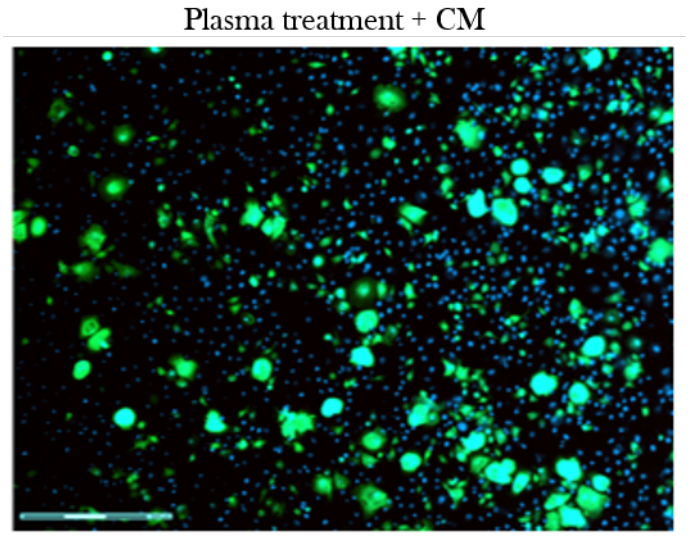


Figure 124: coating the NS membrane with CM after plasma treatment does not seem to improve KC viability over uncoated membrane, possibly due to the inability of the CM to stick to the NS membrane. Image was taken 24h after KC were seeded into the NS wells. Green denotes viable KC, blue denotes KC nuclei. Scale bar denotes 300 µm

Another way to 'mask' the nanostraws from the KC was to coat the NS membrane with 10% FBS. FBS contains a cocktail of sticky proteins that help with cell adhesion [215] and is usually used as a supplement in many cell culture media, including DMEM for fibroblasts. However,

KC differentiate in the presence of serum [216], such that supplementing Epilife with FBS was not an option. Instead, I coated the NS membrane with 10% FBS in PBS for 1-3h and washed it several times with PBS prior to seeding the KC in the NS wells. Similarly, cell viability was monitored the following day by staining the KC with Cell Tracker Green and imaging with the fluorescent microscope. Representative microscopy images revealed >95% cell viability on the NS membrane, a surprisingly high rate of KC survival (Figure 125 top). This confirmed that FBS was able to 'mask' the nanostraws enough from the KC to allow them to survive and as such, was the key to refining KC viability on the NS membrane. However, long-term monitoring of KC survival on the pre-coated NS membrane showed that cell viability started to decline by 48h, reaching very low survival rates by 72h post KC seeding (Figure 125 bottom). This meant that the coating effect of FBS was beneficial only short-term, i.e. 1 day and that the KC should not be kept in the NS wells for longer periods than that. In terms of the delivery protocol into adherent KC this restriction might not necessarily pose an issue as the KC would normally be electroporated for miRNA delivery 24h after seeding – at which point cell viability is high. However, the declining viability of KC after 24h on the pre-coated NS membrane, does mean that following miRNA delivery the KC should be detached from the NS membrane and re-seeded into well plates for future assays.

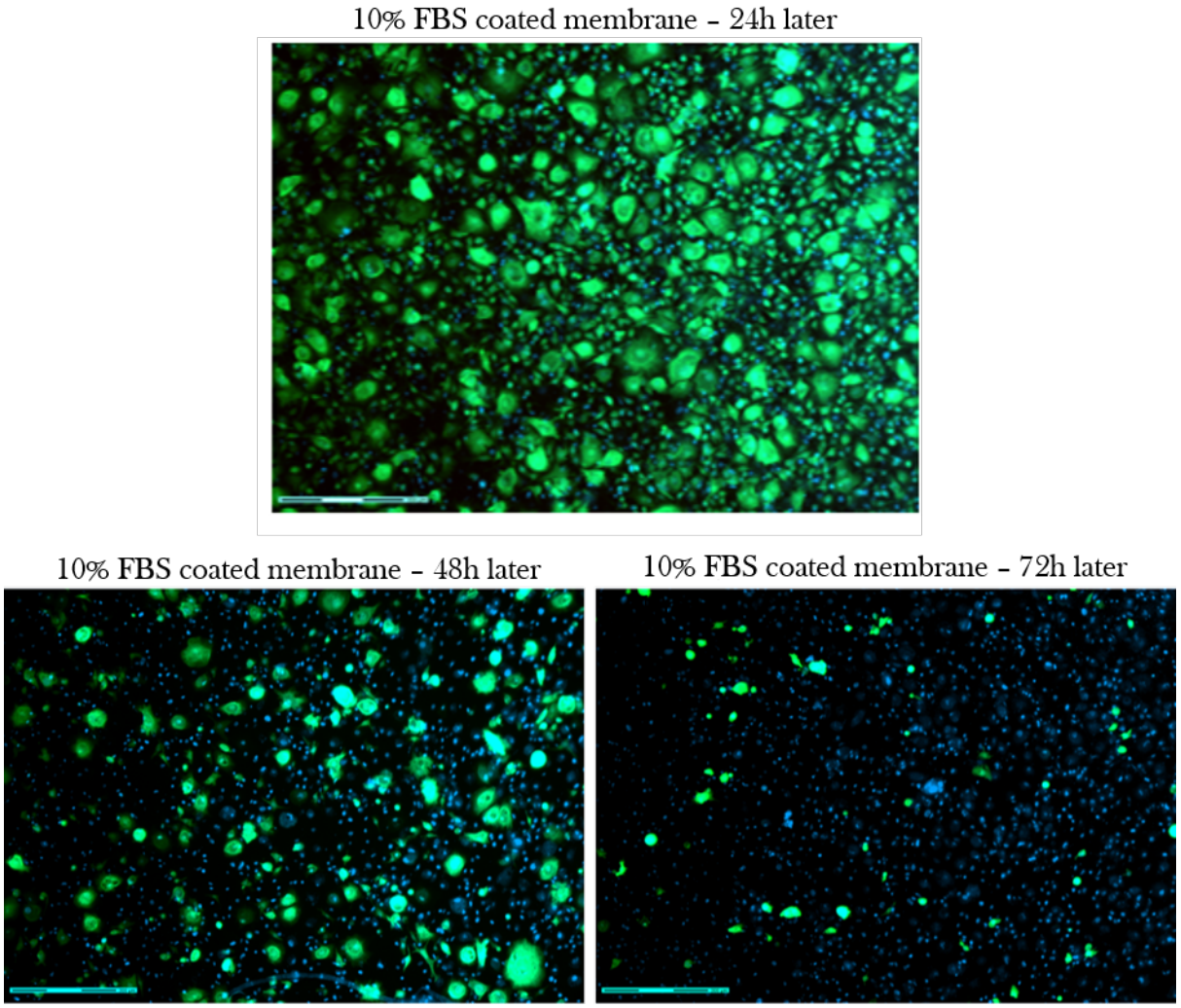


Figure 125: pre-coating the NS membrane with 10% FBS for 1-3h prior to seeding the primary KC improves cell viability dramatically the following day (top). However, this is not sustainable long-term as cell viability starts declining over the next several days (bottom), suggesting that coating the NS membrane with FBS is beneficial only short term. Green denotes viable KC, blue denotes KC nuclei. Images represent different NS wells. All scale bars denote 300 µm

Collectively, these findings showed the nanostraw-electroporation system enabled highly efficient uptake of small RNAs into primary KC, unlike liposomal-based delivery. Furthermore, the homogenous cytoplasmic distribution of the fluorescently-tagged miRNA beautifully matched the results observed with the primary fibroblasts (chapter 5). This confirmed that NS-mediated delivery of small RNAs was independent of cell type. Although additional future studies are needed with functional miRNAs and over longer periods of time, these preliminary findings open new opportunities for biomolecule delivery into this hard-to-transfect cell type.

6.5. Methods

6.5.1. KC subculture protocol

Primary KC were grown in Epilife medium (supplemented with EDGS) on pre-coated flasks with coating matrix (1:100, 30 min at room temperature). KC were detached from the flasks via 1x TryplE (10 min at 37°C), followed by diluting it with 7 mL Epilife medium. The cell suspension was centrifuged at 300xg for 4 min and the cells re-seeded at 5,000-6,000 cells/cm^2. For experiments involving NS-mediated delivery of cargo into adherent cells the Epilife medium (containing EDGS) was further supplemented by FGF-7 (10 ng/ml), a potent mitogen for KC proliferation and migration. This was done to minimise the stress the KC were encountering when seeded on the NS membrane overnight. The chosen concentration of FGF-7 (10 ng/mL) was based on the fact that was enough to cause a mitogenic effect on KC proliferation (~50% increase after 2 days of stimulation – supplementary data 6.6.1).

6.5.2. Staining protocol for monitoring cell viability and checking uptake of fluorescently–tagged miRNA into KC

Primary KC were stained with Cell Tracker Green in Epilife (5 μM) for 15-20 min at 37°C, followed by staining with Hoechst 33342 in PBS (1:2000) for 5 min at room temperature and fixing in 4% PFA (10 min at room temperature) prior to imaging. Exception: when checking uptake of Cy3-tagged miRNA into the primary KC the cells were not stained with Cell Tracker Green as the fluorescence spectra of these two dyes overlap.

6.5.3. Monitoring cell viability of adherent KC on NS membrane

KC were seeded at 50,000 cells/350 μL Epilife in NS wells that were either uncoated, plasma treated, coated with 10% FBS, plasma treated & coated with CM or contained expanded pores membranes and left to adhere overnight. The following day the cells were stained according to the usual protocol to monitor cell viability in the NS wells. When monitoring long-term KC viability on the FBS-coated NS membrane the cells were stained and imaged two and three days, respectively post KC seeding. All cells were imaged with the PALM microscope.

6.5.4. Delivering Cy3-tagged miRNA into adherent primary KC via NS

KC were seeded at 50,000 cells/NS well in 350 μL Epilife following plasma treatment at power 5, 0.5mbar for 5' and left to adhere to the NS membrane overnight. The next day 2 μg of Cy3-scr miRNA was delivered at 15V, 40Hz, 40sec (1 electroporation) in 0.0001XPBS (n=3). After the miRNA delivery the medium was replaced on the cells and the bottom of the membrane was rinsed with 1mL PBS on the outside to remove any cargo 'stuck' to it. The NS wells were returned to the incubator and 24h later the KC were stained according to the usual protocol and imaged with the Inverted Widefield Zeiss Axio Observer microscope in the NS wells.

6.5.5. Delivering Cy3-tagged miRNA into primary KC via lipofectamine RNAiMAX

KC were seeded in 96-well plates (pre-coated with CM) at 7,000/10,000/15,000 cells/well in 90 μL Epilife and left to adhere overnight. The following day Cy3-scr miRNA was transfected into the cells at 25 nM via lipofectamine RNAiMAX according to the usual protocol (methods 4.8.2). 24h later the cells were washed with PBS twice, stained according to the usual protocol and imaged with the Inverted Widefield Zeiss Axio Observer microscope.

6.5.6. Plasma treatment protocol

To plasma treat the NS membrane the Plasma Prep 5 machine (Gala Instrumente) was used according to the following protocol:

a. Turn machine on and use alan key to open gas flow from the cylinder by rotating the valve anticlockwise three times.
b. Press 'ventilation' to release the negative pressure and wait until door can be opened.
c. Put the NS membrane or NS wells inside the machine, put door back on. Turn off 'ventilation' and press 'pump'. This causes the pressure the decrease. At 1.0 mbar the timer comes on automatically. Select 5 min.
d. When pressure is 0.4 mbar, click 'gas 1' to fill the chamber with O_2. Wait 1 min. Set the power strength to 5. This causes the pressure to rise and decrease again.
e. When pressure is ~0.5 mbar press 'generator'. A white/bluish colour should appear representing the plasma.

f. When finished click ‘gas 1’, followed by ‘pump’ and ‘ventilation’. This releases the door.

g. Remove the NS wells from the machine, put door back on and press ‘pump’ to build up the negative pressure inside again. Once the door sticks to the machine, turn off the machine and close the gas flow from the cylinder by rotating the valve clockwise three times.

6.6. Supplementary data

6.6.1. Stimulation of primary keratinocytes with FGF-7

KC were seeded at 30,000 cells/well in Epilife + EDGS in a pre-coated 24-well plate and left to adhere overnight. The following day FGF-7 was added to the Epilife + EDGS in a concentration range of 5-80 ng/mL by doing 1:2 serial dilutions from the stock aliquots of FGF-7 (500 ng in 1 µL) at 500 µL medium/well. Proliferation was measured on day 2 post stimulation via PB (320 µL PB/well in 24-well plate for 1h that got transferred into 100 µL/well in 96-well plates) and the fold change compared to KC kept in Epilife + EDGS only.

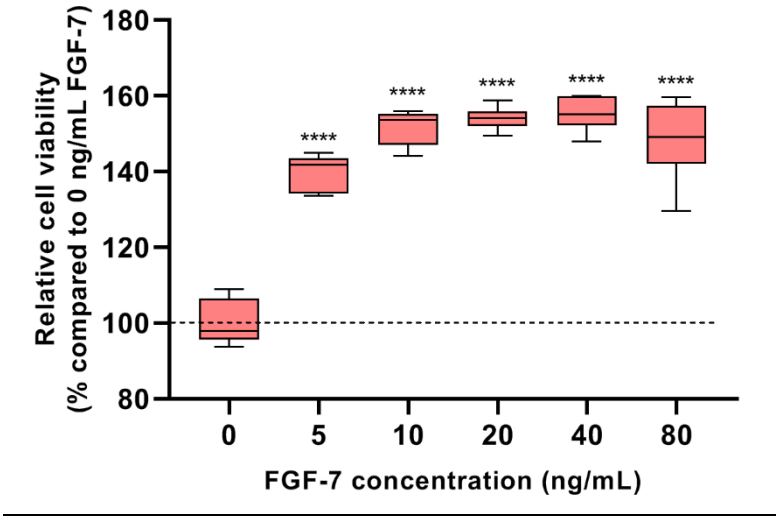


Figure 126: FGF-7 has a large stimulatory effect on basal primary KC that leads to ~50% increase in proliferation after 2 days of stimulation with FGF-7 compared to unstimulated cells. Box and whisker plots span min to max. Statistical analysis was performed via one-way ANOVA, followed by posthoc Tukey's multiple comparisons. ****p<0.0001, n=9

7. Main thesis conclusions and general discussion

MiRNAs are epigenetic modifications involved in regulating gene expression at the post-transcriptional level. These short noncoding RNA molecules become expressed in a spatiotemporal pattern to fine-tune a myriad of signalling pathways driving cellular processes, including proliferation, migration, differentiation and apoptosis, processes important for wound healing as well. Normal levels of miRNAs are essential for maintaining homeostasis, such that miRNA dysregulation has been implicated in a variety of diseases, including development and progression of chronic wounds.

In this PhD project it was hypothesised that dysregulated miRNAs in DFU-derived fibroblasts may cooperate to disrupt signalling pathways important for wound healing, in turn, impairing tissue repair. As such, the project aimed to i) use bioinformatics analysis to explore the biological impact miRNA dysregulation has on signalling pathways and ii) investigate *in vitro* whether temporarily manipulating dysregulated miRNA networks can serve as a combinatorial miRNA-based therapy to restore the scrambled signalling pathways and drive wound resolution. As the project progressed, some thought-provoking key findings emerged that helped shed light on this matter and uncover more about the mechanism of action of miRNAs.

Chapter 2 explored miRNA dysregulation in DFU-derived fibroblasts vs healthy nondiabetic fibroblasts. Using NanoStringDiff, a method specifically designed for analysing nanoString nCounter data, 39 DE miRNAs were identified in DFU-derived fibroblasts vs healthy fibroblasts (38 upregulated and one downregulated). Subsequent bioinformatics analysis of their biological impact revealed these miRNAs were mainly involved in affecting signal transduction in response to stimuli and were enriched in key cellular processes important for wound healing, including cellular movement and proliferation. These findings were consistent with the known impairment of DFU-derived fibroblasts to respond to growth factor stimulation. Amongst the dataset, seven of DE miRNAs clustered on the Dlk1-Dio3 genomic region, a chromosomal region with a tumour suppressive role that holds the largest cluster of miRNAs in humans. This result, together with the fact that the majority of the 39 DE miRNAs from the NanoStringDiff dataset were upregulated in DFU-derived fibroblasts suggested they have a suppressive role on impairing cellular signalling in these cells, potentially contributing

to the phenotype of DFU-derived fibroblasts. Lastly, this chapter investigated how the dysregulated miRNAs could potentially work together at the pathway level to cooperatively impair signal transduction in DFU-derived fibroblasts. Amongst these, bioinformatics analysis predicted miRs-181a, -27a and -30a jointly targeted key signalling pathways important for wound healing, such as the PI3K/AKT and MAPK/ERK signalling pathways. These miRNAs were ultimately selected for experimental validation *in vitro* and in detail investigation of their biological impact on fibroblast behaviour in the context of diabetic wound healing.

Chapter 3 described the isolation of primary skin cells from amputated human limbs that were nondiabetic non-ulcerated, diabetic ulcerated or diabetic non-ulcerated. Using these three categories of tissues ensured a comprehensive study could be done to explore differences attributed to ulceration or diabetes alone. Following enzymatic digestion of skin tissue site-matched primary fibroblasts and keratinocytes were extracted from multiple donors and expanded *in vitro*. The behaviour of the extracted fibroblasts was subsequently extensively characterised and the cells were shown to display a doubling time of 2-3 days, express collagen I and vimentin – markers of fibroblasts – and respond to PDGF-BB stimulation – a mitogenic growth factor for mesenchymal cells. Overall, these results confirmed they were *bona fide* fibroblasts suitable as an *in vitro* model to test the biological impact of the DE miRNAs.

Chapter 4 comprised testing of miRs-181a, -27a and -30a for synergy at the pathway level by over-expressing them in nondiabetic fibroblasts. No sign of synergy was observed as some of the miRNAs had opposing roles, i.e. miR-181a mimic had a proliferative effect on fibroblasts, whereas miR-27a mimic had a suppressive effect on fibroblast proliferation. The individual roles of miR-181a and miR-27a were further tested in diabetic fibroblasts, which revealed that over-expression of miR-181a drove a differential behaviour in non-diabetic vs diabetic fibroblasts, suppressing proliferation in diabetic - ulcerated and non-ulcerated – fibroblasts, whereas over-expression of miR-27a exerted a suppressive effect on all fibroblast populations. This intricate finding, in turn, posed the question as to the mechanism and the signalling pathways that were involved in driving the differential behaviour of miR-181a in diabetic vs non-diabetic fibroblasts. It was hypothesised that one of the potential reasons for the

divergent behaviour of this miRNA could be the activation status of the PI3K/AKT signalling pathway – a pathway that is known to be impaired in diabetes. This was because treatment of nondiabetic fibroblasts with Ly294002, a potent blocker of this pathway, not only abolished the stimulatory effect over-expression of miR-181a had on these cells, but suppressed proliferation even further – a similar effect to that observed in the diabetic fibroblasts. Additionally, for an in depth and comprehensive study on the changes in signalling proteins that occur following transfection of miR-181a mimic into nondiabetic vs diabetic fibroblasts, lysates from these cell populations were sent for RPPA analysis. Lastly, this chapter examined the mechanics of liposomal-based delivery in more detail and revealed that a major limitation of this delivery approach is its inability to control the miRNA dosage delivered. In turn, this precluded the ability to study dosage-dependent effects of miRNA combinations on cellular signalling.

Chapter 5 introduced a novel engineering-based platform for delivery of biomolecules that was based on a nanostraw-electroporation system. This system combined nanotechnology with low voltage electroporation to ensure efficient, localised and non-damaging delivery of miRNAs into primary fibroblasts. By bypassing the biological endosomal pathway this platform could overcome the stochasticity of the liposomal-based delivery, leading to homogenous and controlled uptake of miRNAs, while maintaining high cell viability. This was demonstrated by the ability of the nanostraw-electroporation system to deliver mimics of miR-181a and miR-27a into primary fibroblasts with precise linear dosage control. Ultimately, this chapter revealed the nanostraw-electroporation system led to functional effects in nondiabetic fibroblasts following delivery of miR-181a mimic or miR-29 inhibitor, confirming this innovative delivery approach can be used for studying dosage-dependent effects of relative concentrations of miRNAs.

Chapter 6 investigated how the nanostraw-electroporation system could be used for delivery of miRNAs into primary keratinocytes, a sensitive cell type that is considered difficult to transfect using conventional delivery methods. Relying on a physical mechanism of delivery that involves direct intracellular access into the cytoplasm, this system is less cell-type specific than other transfection methods and therefore it was hypothesised primary keratinocytes might be appropriate candidates for this novel delivery approach. Interestingly, it was

revealed that despite the nanoscale features of the nanostraws primary keratinocytes were still perturbed by the uneven surface beneath them, with many cells dying as a result. As such, various methods were employed to improve cell viability on the NS membrane, including oxygen plasma treatment, coating with collagen I or 10% FBS, with the latter proving to be the most promising at maintaining high cell viability. Lastly, following these improvements it was shown that the nanostraw-electroporation system delivered fluorescently-tagged miRNA into primary keratinocytes in a highly efficient and homogenous manner, representing a significant progress over liposomal-based delivery of the same miRNA. Overall, these findings demonstrated the universality of the nanostraw-electroporation system, paving the way for NS-mediated delivery of miRNAs into primary keratinocytes.

Some of the key findings obtained in this thesis were consistent with the original hypothesis of the project and the known literature on DFUs. For instance, bioinformatics analysis on the biological impact of the 39 DE miRNAs predicted the upregulated DE miRNAs impaired cellular processes significant for wound repair, such as cell proliferation and response to GF stimulation. This prediction was reinforced *in vitro* when over-expression of miR-181a or miR-27a in diabetic fibroblasts (ulcerated and non-ulcerated) resulted in decreased cell proliferation. This finding not only supported the original hypothesis but also confirmed that the list of DE miRNAs identified by NanoStringDiff analysis was biologically relevant in the context of diabetes and diabetic foot ulceration in fibroblasts. Furthermore, per the original aim, inhibiting the levels of some of these miRNAs, such as miR-181a or miR-27a, might be a promising miRNA-based therapy for the treatment of DFUs.

Interestingly, miR-181a and miR-27a have been already implicated in diabetes. For instance, upregulated levels of these two miRNAs were found in the serum of children with newly diagnosed type I diabetes compared to age-matched healthy controls [148]. Conversely, myocardial expression of miR-181a was significantly decreased in diabetic patients suffering from cardiomyopathy compared to healthy patients, and together with decreased levels of miR-30c it was found to synergistically contribute to increased apoptosis of cardiomyocytes [217]. Furthermore, another study revealed that in a diabetic rat model of bone fracture healing expression levels of miR-181a-1-3p were elevated in the newly forming callus at day 5 post-fracture compared to nondiabetic rats, contributing to a dysregulated inflammatory response

and impaired fracture healing [218]. Although different tissues to the one studied in this project, these findings collectively suggest a strong involvement of miR-181a in diabetes and diabetic wound healing and possibly, an important role in diabetic cutaneous wound healing as well.

Other key findings in this project, however, were unexpected. For instance, overexpression of miR-181a caused increased proliferation of nondiabetic fibroblasts, despite causing downregulation of the oncogene KRAS and upregulation of the tumour suppressor PTEN. Subsequent treatment with Ly294002 revealed this miRNA might exert its proliferative effects via activating the PI3K/Akt signalling pathway, in contrast to my original prediction in IPA that overexpression of miR-181a – together with miR-27a and miR-30a - might suppress this pathway. This surprising outcome, nevertheless, reinforced the idea of how difficult it is to predict the effects a miRNA will have *in vitro*. The multitude of target genes of each miRNA, non-linear regulation of protein levels of targets, miRNA dosage-dependent effects, as well as cooperation with and redundancy amongst different miRNAs significantly increase the complexity of trying to experimentally ascertain a full picture of the influences a miRNA may have. Furthermore, current methods for predicting targeting efficacy, such as seed complementarity and energy of miRNA-mRNA binding may not be sufficient as miRNAs might still not necessarily suppress the target gene despite being predicted to do so. Collectively, these complexities can cause selective downregulation of target genes of a miRNA, potentially leading to diverging results, which means that a) new, improved ways of predicting repression efficacy more accurately are urgently needed, and b) a miRNA needs to be always experimentally tested to conclude what particular effects it will exert in that specific context.

Another surprising key finding was the differential behaviour miR-181a caused in diabetic vs nondiabetic fibroblasts, suggesting that the disease state may cause a miRNA to have different effects. This, however, may apply only to specific miRNAs, as miR-27a had the same suppressive effect on proliferation in all fibroblast populations regardless of the disease state. Also, the fact that miR-181a overexpression led to impaired cell proliferation in diabetic fibroblasts further indicated that miRNA synergy might be dependent on the disease state of cells. In other words, a miRNA might show synergistic behaviour with other miRNAs in a healthy cell population, but not diseased and vice versa. Reasons for this could be different

expression levels of other (dysregulated) miRNAs or target genes that might cause the miRNAs to cooperate in one situation vs the other. In fact, a large scale study looking at functional miRNA synergism at a system-wide level showed that miRNAs in diseases exhibited stronger synergism than miRNAs in healthy cells, with disease miRNAs having more synergistic partners than non-disease miRNAs [134]. This suggested that, perhaps, miRs-181a, -27a and -30a might still cooperate at the pathway level when over-expressing them in diabetic ulcerated fibroblasts. This, however remains an open question that would be interesting to investigate in future studies.

Nevertheless, regardless of the disease state, synergy amongst different miRNAs may still heavily depend on the concentrations of the miRNAs of interest, such that synergy might occur at specific relative doses of miRNAs, but not others. This is because different doses of miRNAs are like pressing different keys on a piano, where each key can produce a diverse sound. This phenomenon becomes particularly significant when multiple miRNAs are taken into account. This is because different combinations of miRNAs at different relative concentrations can elicit different cellular processes, similar to how pressing different keys on the piano in a jointly manner can produce a completely different song. Yet, despite their crucial importance, dosage-dependent effects of miRNAs are vastly overlooked and unexplored, with the majority of studies done at one concentration of miRNA only. Reasons for this might be that current delivery methods are unable to control miRNA dosages as they rely on biological mechanisms for delivery, such as endocytosis which is primarily a stochastic process. Such mechanisms further depend on a multitude of other factors including cell type, origin of cells (primary vs cell line), age and state of the cell (dividing vs non-dividing), which can sometimes make delivery of miRNAs difficult to start with, like in primary keratinocytes.

The nanostraw-electroporation platform described in chapter 5 can overcome these limitations by gaining direct access into the cell cytoplasm for localised delivery. Its primarily physical mechanism of delivery and the high practicality of the platform itself enable this system to precisely control and manipulate dosages of miRNAs in a straight forward, effective and cell-type independent manner. In turn, this allows us to start investigating dosage-dependent effects of individual miRNAs, and in various combinations at different relative doses to explore how signalling pathways change in response to incremental changes of

miRNAs. Through this, we can gain a more in-depth understanding of the relative doses of miRNAs needed for a combinatorial miRNA-based therapy - for the treatment of DFUs, for instance - although a different delivery system will be required for *in vivo* research. Ultimately, this will allow the fundamental study of how signalling changes arise in disease states due to changing concentrations of miRNAs.

In addition to cotransfection of miRNAs, the nanostraw-electroporation system might also allow sequential delivery of miRNAs at specific doses. This is particularly important as synergy amongst miRNAs might also occur temporally, where miRNAs cooperate at the pathway level over time, rather than simultaneously. This type of synergy might be especially prevalent in dynamic cellular processes, such as tissue repair, where miRNAs become expressed in different amounts at different time points to coordinate specific events. One such example includes miRs-661, -612 and -940 that were shown to jointly regulate cell motility in retinal epithelial cells by phosphorylating myosin II over time in an antagonistic manner [219]. For example, ectopic expression of miR-661 strongly induced phosphorylation of myosin II increasing cell invasion, while in contrast, expression of either miR-612 or miR-940 inhibited phosphorylation of myosin II impairing cell invasion in a transwell assay. These miRNAs, however were not expressed at the same time in a tissue, confirming that these three miRNAs co-regulate cell motility in a temporal fashion, becoming expressed at different time points. This finding reinforces the importance of also taking into account temporal synergism when investigating cooperation of miRNAs at the gene or pathway level.

Overall, this PhD project advanced the field of miRNA research and DFU-related miRNA knowledge by a) identifying a new list of DE miRNAs in DFU-derived fibroblasts vs healthy fibroblasts that proposes how miRNA dysregulation can contribute to the DFU phenotype; b) illustrating a differential behaviour of miR-181a in diabetic vs non-diabetic primary dermal fibroblasts; c) showing ratiometric linear dosage control of miRNA mimics into primary dermal fibroblasts that has not been demonstrated using other existing methods; d) revealing highly effective uptake of small RNAs into primary keratinocytes that opens opportunities for manipulating miRNA levels in a hard-to-transfect cell type. On a broader scale, and perhaps more importantly, this project illustrated how a novel engineering-based delivery system can serve as a valuable tool to help us better understand the mechanism of action of miRNAs.

7.1. Future studies

Going forward, the biological role of additional DE miRNAs from the NanoStringDiff list can be explored. For instance, it would be interesting to explore more about the miRNAs belonging to the Dlk1-Dio3 chromosomal region and check if they show synergy based on clustering together and what role they might have in contributing to the DFU phenotype of fibroblasts.

Another motivating aspect to explore in more detail in the future is the differential role of miR-181a in diabetic vs non-diabetic cells. It would be very interesting to find out if miR-181a shows differential behaviour in diabetic cell types other than fibroblasts, or whether this occurrence is confined to this specific cell type. For instance, in chapter 4 it was shown that over-expression of miR-181a in HUVEC increases proliferation. A stimulating question to ask at this point is what happens when this miRNA becomes over-expressed in dermal microvascular endothelial cells that are diabetic. Does proliferation become suppressed similarly to the behaviour observed in diabetic fibroblasts? If so, this will point to miR-181a being a disease specific miRNA.

The NS-mediated delivery of small RNAs into primary keratinocytes needs to be developed and optimised even further. While coating the NS membrane with FBS was proven to be beneficial short-term, different methods will be required for maintaining long-term KC viability on the NS membrane. One such method that may prove beneficial involves functionalising the NS membrane with cell-adhesion peptides [220] that are specific for the integrins of basal KC [221]. Improving cell adhesion and survival of KC on the NS membrane will pave the way for delivery of functional miRNAs. In turn, this will allow us to start uncovering relevant miRNAs that are involved in re-epithelialisation and start exploring dosage-dependent effects of miRNAs in this hard-to-transfect cell type.

The nanostraw delivery platform can furthermore be used as a tool for longitudinal studies of miRNAs to track their biological effects over time. An interesting question to ask in this regard - when investigating two potentially cooperating miRNAs, for instance – is what happens if the delivered dose of one miRNA is kept constant, while the other miRNA is co-delivered at increasing/decreasing concentrations? In this way, a cell's behaviour can be guided towards a desired phenotype. Cell lysate, collected at several time points for each condition, can serve

as input for RPPA analysis to trace and follow how the signalling pathways alter in response to changing concentrations of miRNA.

Ultimately, the cell lysate samples that have been submitted for RPPA analysis (to investigate the signalling proteins that change in diabetic vs non-diabetic fibroblasts following over-expression of miR-181a) will open further questions. Once the results from the Core Facility come back, GO ontology and pathway enrichment analysis will need to be done to investigate what proteins, signalling pathways and cellular functions are different between i) samples containing miR-181a mimic vs scramble miR mimic or untreated, ii) the diabetic vs nondiabetic fibroblasts following over-expression of miR-181a mimic. Following bioinformatics analysis *in vitro* validation will further be required to confirm the RPPA results. This will involve confirming both the levels of specific DE proteins - via Western Blots or ELISA – or specific differentially activated signalling pathways – via chemical modulators. Altogether this will elucidate the reason behind the differential behaviour of miR-181a in diabetic vs non-diabetic fibroblasts.

Combined, these future studies will help advance the knowledge of how manipulation of DFU-specific miRNAs can be used for re-designing therapies to rewire cell signalling in diabetic wound healing.

8. References

1. Boulton, A. J., Vileikyte, L., Ragnarson-Tennvall, G. & Apelqvist, J. The global burden of diabetic foot disease. *Lancet* vol. 366 1719–1724 (2005).

2. Mekkes, J. R., Loots, M. A. M., Van Der Wal, A. C. & Bos, J. D. Causes, investigation and treatment of leg ulceration. *British Journal of Dermatology* vol. 148 388–401 (2003).

3. Kerr, M. Foot Care for People with Diabetes: The Economic Case for Change. *NHS Diabetes* 1–72 (2012).

4. Jones, J. E., Robinson, J., Barr, W. & Carlisle, C. Impact of exudate and odour from chronic venous leg ulceration. *Nurs. Stand.* **22**, 53–61 (2008).

5. Armstrong, D. G. *et al.* Mind the gap: Disparity between research funding and costs of care for diabetic foot ulcers. *Diabetes Care* **36**, 1815–1817 (2013).

6. Mekkes, J. R., Loots, M. A. M., Van Der Wal, A. C. & Bos, J. D. Causes, investigation and treatment of leg ulceration. *Br. J. Dermatol.* **148**, 388–401 (2003).

7. Armstrong, D. G. *et al.* Mind the gap: Disparity between research funding and costs of care for diabetic foot ulcers. *Diabetes Care* **36**, 1815–1817 (2013).

8. Sen, C. K. *et al.* Human skin wounds: A major and snowballing threat to public health and the economy: PERSPECTIVE ARTICLE. *Wound Repair Regen.* **17**, 763–771 (2009).

9. Fonder, M. A. *et al.* Treating the chronic wound: A practical approach to the care of nonhealing wounds and wound care dressings. *Journal of the American Academy of Dermatology* (2008) doi:10.1016/j.jaad.2007.08.048.

10. Singer, A. J. & Clark, R. Mechanisms of Disease - Cutaneous Wound Healing. *N. Engl. J. Med.* (1999).

11. DesJardins-Park, H. E., Mascharak, S., Chinta, M. S., Wan, D. C. & Longaker, M. T. The spectrum of scarring in craniofacial wound repair. *Front. Physiol.* (2019) doi:10.3389/fphys.2019.00322.

12. Singer, A. J. & Clark, R. A. F. Cutaneous Wound Healing. *N. Engl. J. Med.* **341**, 738–746

(1999).

13. Schmidt, B. a & Horsley, V. Intradermal adipocytes mediate fibroblast recruitment during skin wound healing. *Development* **140**, 1517–27 (2013).

14. Pastar, I. *et al.* Epithelialization in Wound Healing: A Comprehensive Review. *Adv. Wound Care* **3**, 445–464 (2014).

15. Ito, M. *et al.* Stem cells in the hair follicle bulge contribute to wound repair but not to homeostasis of the epidermis. *Nat. Med.* **11**, 1351–1354 (2005).

16. Jun, J. Il & Lau, L. F. Cellular senescence controls fibrosis in wound healing. *Aging (Albany. NY).* **2**, 627–631 (2010).

17. Larson, B. J., Longaker, M. T. & Lorenz, H. P. Scarless fetal wound healing: A basic science review. *Plastic and Reconstructive Surgery* 1172–80 (2010) doi:10.1097/PRS.0b013e3181eae781.

18. Jimenez, F., Poblet, E. & Izeta, A. Reflections on how wound healing-promoting effects of the hair follicle can be translated into clinical practice. *Exp. Dermatol.* **24**, 91–4 (2015).

19. DesJardins-Park, H. E., Mascharak, S., Chinta, M. S., Wan, D. C. & Longaker, M. T. The spectrum of scarring in craniofacial wound repair. *Front. Physiol.* **10**, (2019).

20. Martin, P. & Nunan, R. Cellular and molecular mechanisms of repair in acute and chronic wound healing. *British Journal of Dermatology* vol. 173 370–378 (2015).

21. Demidova-Rice, T. N., Hamblin, M. R. & Herman, I. M. Acute and impaired wound healing: Pathophysiology and current methods for drug delivery, part 1: Normal and chronic wounds: Biology, causes, and approaches to care. *Advances in Skin and Wound Care* (2012) doi:10.1097/01.ASW.0000416006.55218.d0.

22. Stojadinovic, A., Carlson, J. W., Schultz, G. S., Davis, T. A. & Elster, E. A. Topical advances in wound care. *Gynecol. Oncol.* **111**, S70–S80 (2008).

23. Loots, M. A. M. *et al.* Differences in cellular infiltrate and extracellular matrix of chronic diabetic and venous ulcers versus acute wounds. *J. Invest. Dermatol.* **111**, 850–

857 (1998).

24. Stojadinovic, O. *et al.* Deregulation of keratinocyte differentiation and activation: A hallmark of venous ulcers. *J. Cell. Mol. Med.* (2008) doi:10.1111/j.1582-4934.2008.00321.x.

25. Stojadinovic, O. *et al.* Molecular pathogenesis of chronic wounds: the role of beta-catenin and c-myc in the inhibition of epithelialization and wound healing. *Am. J. Pathol.* **167**, 59–69 (2005).

26. Harding, K. G., Moore, K. & Phillips, T. J. Wound chronicity and fibroblast senescence - Implications for treatment. *Int. Wound J.* (2005) doi:10.1111/j.1742-4801.2005.00149.x.

27. Trengove, N. J. *et al.* Analysis of the acute and chronic wound environments: The role of proteases and their inhibitors. *Wound Repair and Regeneration* (1999) doi:10.1046/j.1524-475X.1999.00442.x.

28. Barrientos, S., Stojadinovic, O., Golinko, M. S., Brem, H. & Tomic-Canic, M. PERSPECTIVE ARTICLE: Growth factors and cytokines in wound healing. *Wound Repair Regen.* **16**, 585–601 (2008).

29. Loot, M. a M. *et al.* Fibroblasts derived from chronic diabetic ulcers differ in their response to stimulation with EGF, IGF-I, bFGF and PDGF-AB compared to controls. *Eur. J. Cell Biol.* **81**, 153–160 (2002).

30. Pastar, I. *et al.* Attenuation of the transforming growth factor beta-signaling pathway in chronic venous ulcers. *Mol. Med.* **16**, 92–101 (2010).

31. Rafehi, H., El-Osta, A. & Karagiannis, T. C. Genetic and epigenetic events in diabetic wound healing. *International Wound Journal* vol. 8 12–21 (2011).

32. Charles, C. a *et al.* A gene signature of nonhealing venous ulcers: potential diagnostic markers. *J. Am. Acad. Dermatol.* **59**, 758–71 (2008).

33. Brem, H. *et al.* Molecular Markers in Patients with Chronic Wounds Guide to Surgical Debridement. *Mol. Med. Cambridge Mass* **13**, 30–39 (2007).

34. Maione, A. G. *et al.* Three-Dimensional Human Tissue Models That Incorporate

Diabetic Foot Ulcer-Derived Fibroblasts Mimic In Vivo Features of Chronic Wounds. *Tissue Eng. Part C Methods* **21**, 499–508 (2015).

35. Giacco, F. & Brownlee, M. Oxidative stress and diabetic complications. *Circulation Research* (2010) doi:10.1161/CIRCRESAHA.110.223545.

36. Lerman, O. Z., Galiano, R. D., Armour, M., Levine, J. P. & Gurtner, G. C. Cellular dysfunction in the diabetic fibroblast: Impairment in migration, vascular endothelial growth factor production, and response to hypoxia. *Am. J. Pathol.* (2003) doi:10.1016/S0002-9440(10)63821-7.

37. Khamaisi, M. *et al.* PKC inhibition normalizes the wound-healing capacity of diabetic human fibroblasts. *J. Clin. Invest.* (2016) doi:10.1172/JCI82788.

38. Blakytny, R., Jude, E. B., Martin Gibson, J., Boulton, A. J. M. & Ferguson, M. W. J. Lack of insulin-like growth factor I (IGF1) in the basal keratinocyte layer of diabetic skin and diabetic foot ulcers. *J. Pathol.* (2000) doi:10.1002/(SICI)1096-9896(200004)190:5<589::AID-PATH553>3.0.CO;2-T.

39. Khanna, S. *et al.* Macrophage dysfunction impairs resolution of inflammation in the wounds of diabetic mice. *PLoS One* (2010) doi:10.1371/journal.pone.0009539.

40. Jones, J. D., Ramser, H. E., Woessner, A. E. & Quinn, K. P. In vivo multiphoton microscopy detects longitudinal metabolic changes associated with delayed skin wound healing. *Commun. Biol.* (2018) doi:10.1038/s42003-018-0206-4.

41. Quinn, K. P. *et al.* Diabetic wounds exhibit distinct microstructural and metabolic heterogeneity through label-free multiphoton microscopy. *J. Invest. Dermatol.* (2016) doi:10.1038/JID.2015.371.

42. Wilkinson, H. N. *et al.* Tissue Iron Promotes Wound Repair via M2 Macrophage Polarization and the Chemokine (C-C Motif) Ligands 17 and 22. *Am. J. Pathol.* **189**, 2196–2208 (2019).

43. Wilkinson, H. N. *et al.* Reduced Iron in Diabetic Wounds: An Oxidative Stress-Dependent Role for STEAP3 in Extracellular Matrix Deposition and Remodeling. *J. Invest. Dermatol.* **139**, 2368–2377 (2019).

44. Gardiner, M. *et al.* A longitudinal study of the diabetic skin and wound microbiome. *PeerJ* **5**, e3543 (2017).

45. Gottrup, F. & Apelqvist, J. Present and new techniques and devices in the treatment of DFU: A critical review of evidence. *Diabetes/Metabolism Research and Reviews* (2012) doi:10.1002/dmrr.2242.

46. Goldman, R. Growth factors and chronic wound healing: past, present, and future. *Adv.Skin Wound.Care* **17**, 24–35 (2004).

47. Gainza, G., Villullas, S., Pedraz, J. L., Hernandez, R. M. & Igartua, M. Advances in drug delivery systems (DDSs) to release growth factors for wound healing and skin regeneration. *Nanomedicine: Nanotechnology, Biology, and Medicine* vol. 11 1551–1573 (2015).

48. Wieman, T. J. Clinical efficacy of becaplermin (rhPDGF-BB) gel. Becaplermin Gel Studies Group. *Am. J. Surg.* **176**, 74S-79S (1998).

49. Loots, M. A. M. *et al.* Fibroblasts derived from chronic diabetic ulcers differ in their response to stimulation with EGF, IGF-I, bFGF and PDGF-AB compared to controls. *Eur. J. Cell Biol.* **81**, 153–160 (2002).

50. No Title. https://www.fda.gov/downloads/Drugs/DrugSafety/PostmarketDrugSafetyInformationforPatientsandProviders/UCM142821.pdf.

51. Guo, W. & Giancotti, F. G. Integrin signalling during tumour progression. *Nat. Rev. Mol. Cell Biol.* **5**, 816–826 (2004).

52. Yi, R., Poy, M. N., Stoffel, M. & Fuchs, E. A skin microRNA promotes differentiation by repressing 'stemness'. *Nature* (2008) doi:10.1038/nature06642.

53. Sluijter, J. P. G. *et al.* MicroRNA-1 and-499 regulate differentiation and proliferation in human-derived cardiomyocyte progenitor cells. *Arterioscler. Thromb. Vasc. Biol.* **30**, 859–868 (2010).

54. Cimmino, A. *et al.* miR-15 and miR-16 induce apoptosis by targeting BCL2. *Proc. Natl. Acad. Sci.* **102**, 13944–13949 (2005).

55. Li, X., Cassidy, J. J., Reinke, C. A., Fischboeck, S. & Carthew, R. W. A MicroRNA Imparts Robustness against Environmental Fluctuation during Development. *Cell* (2009) doi:10.1016/j.cell.2009.01.058.

56. Lagos-Quintana, M., Rauhut, R., Meyer, J., Borkhardt, A. & Tuschl, T. New microRNAs from mouse and human. *RNA* **9**, 175–179 (2003).

57. Lim, L. P. *et al.* The microRNAs of Caenorhabditis elegans. *Genes Dev.* **17**, 991–1008 (2003).

58. Lewis, B. P., Burge, C. B. & Bartel, D. P. Conserved seed pairing, often flanked by adenosines, indicates that thousands of human genes are microRNA targets. *Cell* **120**, 15–20 (2005).

59. Banerjee, J., Chan, Y. C. & Sen, C. K. MicroRNAs in skin and wound healing. *Physiol. Genomics* **43**, 543–556 (2011).

60. Lai, W. F. & Siu, P. M. MicroRNAs as regulators of cutaneous wound healing. *J. Biosci.* **39**, 519–524 (2014).

61. Pastar, I. *et al.* Micro-RNAs: New Regulators of Wound Healing. *Surg. Technol. Int.* **XXI**, 51–60 (2011).

62. Andl, T. *et al.* The miRNA-Processing Enzyme Dicer Is Essential for the Morphogenesis and Maintenance of Hair Follicles. *Curr. Biol.* (2006) doi:10.1016/j.cub.2006.04.005.

63. Yi, R. *et al.* DGCR8-dependent microRNA biogenesis is essential for skin development. *Proc. Natl. Acad. Sci.* (2009) doi:10.1073/pnas.0810766105.

64. Yi, R. *et al.* Morphogenesis in skin is governed by discrete sets of differentially expressed microRNAs. *Nat. Genet.* (2006) doi:10.1038/ng1744.

65. Yi, R., Poy, M. N., Stoffel, M. & Fuchs, E. A skin microRNA promotes differentiation by repressing 'stemness'. *Nature* **452**, 225–229 (2008).

66. Pastar, I. *et al.* Induction of specific microRNAs inhibits cutaneous wound healing. *J. Biol. Chem.* **287**, 29324–29335 (2012).

67. Li, D. *et al.* MicroRNA-31 Promotes Skin Wound Healing by Enhancing Keratinocyte Proliferation and Migration. *J. Invest. Dermatol.* **135**, (2015).

68. Sundaram, G. M. *et al.* 'See-saw' expression of microRNA-198 and FSTL1 from a single transcript in wound healing. *Nature* **495**, 103–6 (2013).

69. Wang, T. *et al.* miR-21 regulates skin wound healing by targeting multiple aspects of the healing process. *Am. J. Pathol.* **181**, 1911–20 (2012).

70. Yang, X. *et al.* miR-21 promotes keratinocyte migration and re-epithelialization during wound healing. *International Journal of Biological Sciences* vol. 7 685–690 (2011).

71. Pastar, I. *et al.* Induction of specific microRNAs inhibits cutaneous wound healing. *J. Biol. Chem.* **287**, 29324–29335 (2012).

72. Yang, W. J. *et al.* Dicer is required for embryonic angiogenesis during mouse development. *J. Biol. Chem.* **280**, 9330–9335 (2005).

73. Suárez, Y., Fernández-Hernando, C., Pober, J. S. & Sessa, W. C. Dicer dependent microRNAs regulate gene expression and functions in human endothelial cells. *Circ. Res.* **100**, 1164–1173 (2007).

74. Wang, S. *et al.* The Endothelial-Specific MicroRNA miR-126 Governs Vascular Integrity and Angiogenesis. *Dev. Cell* **15**, 261–271 (2008).

75. Bonauer, A. *et al.* MicroRNA-92a controls angiogenesis and functional recovery of ischemic tissues in mice. *Science* **324**, 1710–1713 (2009).

76. Caporali, A. *et al.* Deregulation of microRNA-503 contributes to diabetes mellitus-induced impairment of endothelial function and reparative angiogenesis after Limb Ischemia. *Circulation* (2011) doi:10.1161/CIRCULATIONAHA.110.952325.

77. den Dekker, A., Davis, F. M., Kunkel, S. L. & Gallagher, K. A. Targeting epigenetic mechanisms in diabetic wound healing. *Transl. Res.* **204**, 39–50 (2019).

78. Peschansky, V. J. & Wahlestedt, C. Non-coding RNAs as direct and indirect modulators of epigenetic regulation. *Epigenetics* vol. 9 3–12 (2014).

79. Liu, G., Mattick, J. S. & Taft, R. J. A meta-analysis of the genomic and transcriptomic

composition of complex life. *Cell Cycle* **12**, 2061–2072 (2013).

80. Hannon, G. J. RNA interference. *Nature* **418**, 244–251 (2002).

81. Derrien, T. *et al.* The GENCODE v7 catalog of human long noncoding RNAs: Analysis of their gene structure, evolution, and expression. *Genome Res.* **22**, 1775–1789 (2012).

82. Ma, L., Bajic, V. B. & Zhang, Z. On the classification of long non-coding RNAs. *RNA Biol.* **10**, 924–933 (2013).

83. Wilusz, J. E., Sunwoo, H. & Spector, D. L. Long noncoding RNAs: Functional surprises from the RNA world. *Genes and Development* vol. 23 1494–1504 (2009).

84. Starke, S. *et al.* Exon circularization requires canonical splice signals. *Cell Rep.* **10**, 103–111 (2015).

85. Memczak, S. *et al.* Circular RNAs are a large class of animal RNAs with regulatory potency. *Nature* **495**, 333–338 (2013).

86. Salzman, J., Chen, R. E., Olsen, M. N., Wang, P. L. & Brown, P. O. Cell-Type Specific Features of Circular RNA Expression. *PLoS Genet.* **9**, (2013).

87. Szabo, L. *et al.* Statistically based splicing detection reveals neural enrichment and tissue-specific induction of circular RNA during human fetal development. *Genome Biol.* **16**, 126 (2015).

88. Jeck, W. R. *et al.* Circular RNAs are abundant, conserved, and associated with ALU repeats. *RNA* **19**, 141–157 (2013).

89. Hansen, T. B. *et al.* MiRNA-dependent gene silencing involving Ago2-mediated cleavage of a circular antisense RNA. *EMBO J.* **30**, 4414–4422 (2011).

90. Elbashir, S. M., Lendeckel, W. & Tuschl, T. RNA interference is mediated by 21- and 22-nucleotide RNAs. *Genes Dev.* (2001) doi:10.1101/gad.862301.

91. Rodriguez, A., Griffiths-Jones, S., Ashurst, J. L. & Bradley, A. Identification of mammalian microRNA host genes and transcription units. *Genome Res.* (2004) doi:10.1101/gr.2722704.

92. Kim, Y. K. & Kim, V. N. Processing of intronic microRNAs. *EMBO J.* (2007)

doi:10.1038/sj.emboj.7601512.

93. Baskerville, S. & Bartel, D. P. Microarray profiling of microRNAs reveals frequent coexpression with neighboring miRNAs and host genes. *RNA* (2005) doi:10.1261/rna.7240905.

94. Monteys, A. M. *et al.* Structure and activity of putative intronic miRNA promoters. *RNA* (2010) doi:10.1261/rna.1731910.

95. Lee, Y., Jeon, K., Lee, J. T., Kim, S. & Kim, V. N. MicroRNA maturation: Stepwise processing and subcellular localization. *EMBO J.* (2002) doi:10.1093/emboj/cdf476.

96. Wang, Y., Luo, J., Zhang, H. & Lu, J. MicroRNAs in the Same Clusters Evolve to Coordinately Regulate Functionally Related Genes. *Mol. Biol. Evol.* (2016) doi:10.1093/molbev/msw089.

97. Bentwich, I. *et al.* Identification of hundreds of conserved and nonconserved human microRNAs. *Nat. Genet.* (2005) doi:10.1038/ng1590.

98. Donker, R. B. *et al.* The expression profile of C19MC microRNAs in primary human trophoblast cells and exosomes. *Mol. Hum. Reprod.* (2012) doi:10.1093/molehr/gas013.

99. Khvorova, A., Reynolds, A. & Jayasena, S. D. Functional siRNAs and miRNAs exhibit strand bias. *Cell* **115**, 209–16 (2003).

100. Schwarz, D. S. *et al.* Asymmetry in the assembly of the RNAi enzyme complex. *Cell* (2003) doi:10.1016/S0092-8674(03)00759-1.

101. Hu, H. Y. *et al.* Sequence features associated with microRNA strand selection in humans and flies. *BMC Genomics* (2009) doi:10.1186/1471-2164-10-413.

102. Matoulkova, E., Michalova, E., Vojtesek, B. & Hrstka, R. The role of the 3′ untranslated region in post-transcriptional regulation of protein expression in mammalian cells. *RNA Biol.* **9**, 563–76 (2012).

103. Bartel, D. P. MicroRNAs: Target Recognition and Regulatory Functions. *Cell* vol. 136 215–233 (2009).

104. Ha, M. & Kim, V. N. Regulation of microRNA biogenesis. *Nat. Rev. Mol. Cell Biol.* **15**,

509–24 (2014).

105. Berezikov, E., Chung, W. J., Willis, J., Cuppen, E. & Lai, E. C. Mammalian Mirtron Genes. *Mol. Cell* (2007) doi:10.1016/j.molcel.2007.09.028.

106. Iorio, M. V. & Croce, C. M. Causes and consequences of MicroRNA dysregulation. *Cancer Journal (United States)* (2012) doi:10.1097/PPO.0b013e318250c001.

107. Calin, G. A. *et al.* Human microRNA genes are frequently located at fragile sites and genomic regions involved in cancers. *Proc. Natl. Acad. Sci.* (2004) doi:10.1073/pnas.0307323101.

108. Mahdipour, E. & Hasanzadeh, L. Dicer expression is impaired in diabetic cutaneous wound healing. *Int. J. Diabetes Dev. Ctries.* **38**, 173–178 (2018).

109. Weber, B., Stresemann, C., Brueckner, B. & Lyko, F. Methylation of human MicroRNA genes in normal and neoplastic cells. *Cell Cycle* **6**, 1001–5 (2007).

110. Singh, K. *et al.* Epigenetic Modification of MicroRNA-200b Contributes to Diabetic Vasculopathy. *Mol. Ther.* **25**, 2689–2704 (2017).

111. Chan, Y. C., Khanna, S., Roy, S. & Sen, C. K. MiR-200b targets Ets-1 and is down-regulated by hypoxia to induce angiogenic response of endothelial cells. *J. Biol. Chem.* **286**, 2047–56 (2011).

112. Iorio, M. V., Piovan, C. & Croce, C. M. Interplay between microRNAs and the epigenetic machinery: An intricate network. *Biochimica et Biophysica Acta - Gene Regulatory Mechanisms* vol. 1799 694–701 (2010).

113. Lewis, B. P., Shih, I. H., Jones-Rhoades, M. W., Bartel, D. P. & Burge, C. B. Prediction of Mammalian MicroRNA Targets. *Cell* (2003) doi:10.1016/S0092-8674(03)01018-3.

114. Brennecke, J., Stark, A., Russell, R. B. & Cohen, S. M. Principles of microRNA-target recognition. in *PLoS Biology* (2005). doi:10.1371/journal.pbio.0030085.

115. Grimson, A. *et al.* MicroRNA Targeting Specificity in Mammals: Determinants beyond Seed Pairing. *Mol. Cell* (2007) doi:10.1016/j.molcel.2007.06.017.

116. Piovesan, A., Caracausi, M., Antonaros, F., Pelleri, M. C. & Vitale, L. GeneBase 1.1: A

tool to summarize data from NCBI gene datasets and its application to an update of human gene statistics. *Database* (2016) doi:10.1093/database/baw153.

117. Majoros, W. H. & Ohler, U. Spatial preferences of microRNA targets in 3′ untranslated regions. *BMC Genomics* (2007) doi:10.1186/1471-2164-8-152.

118. Kertesz, M., Iovino, N., Unnerstall, U., Gaul, U. & Segal, E. The role of site accessibility in microRNA target recognition. *Nat. Genet.* (2007) doi:10.1038/ng2135.

119. Lim, L. P. *et al.* Microarray analysis shows that some microRNAs downregulate large numbers of-target mRNAs. *Nature* **433**, 769–73 (2005).

120. Selbach, M. *et al.* Widespread changes in protein synthesis induced by microRNAs. *Nature* (2008) doi:10.1038/nature07228.

121. Baek, D. *et al.* The impact of microRNAs on protein output. *Nature* **455**, 64–71 (2008).

122. Coller, J. & Parker, R. Eukaryotic mRNA Decapping. *Annu. Rev. Biochem.* **73**, 861–90 (2004).

123. Hu, W. & Coller, J. What comes first: Translational repression or mRNA degradation? the deepening mystery of microRNA function. *Cell Res.* (2012) doi:10.1038/cr.2012.80.

124. Guo, H., Ingolia, N. T., Weissman, J. S. & Bartel, D. P. Mammalian microRNAs predominantly act to decrease target mRNA levels. *Nature* (2010) doi:10.1038/nature09267.

125. Nam, J. W. *et al.* Global analyses of the effect of different cellular contexts on microRNA targeting. *Mol. Cell* (2014) doi:10.1016/j.molcel.2014.02.013.

126. Bartel, D. P. & Chen, C. Z. Micromanagers of gene expression: The potentially widespread influence of metazoan microRNAs. *Nature Reviews Genetics* (2004) doi:10.1038/nrg1328.

127. Friedman, R. C., Farh, K. K. H., Burge, C. B. & Bartel, D. P. Most mammalian mRNAs are conserved targets of microRNAs. *Genome Res.* **19**, 92–105 (2009).

128. Nielsen, C. B. *et al.* Determinants of targeting by endogenous and exogenous microRNAs and siRNAs. *RNA* (2007) doi:10.1261/rna.768207.

129. Wu, S. *et al.* Multiple microRNAs modulate p21Cip1/Waf1 expression by directly targeting its 3′ untranslated region. *Oncogene* **29**, 2302–2308 (2010).

130. Sætrom, P. *et al.* Distance constraints between microRNA target sites dictate efficacy and cooperativity. *Nucleic Acids Res.* **35**, 2333–2342 (2007).

131. Kulyté, A. *et al.* Additive effects of microRNAs and transcription factors on CCL2 production in human white adipose tissue. *Diabetes* (2014) doi:10.2337/db13-0702.

132. Forrest, a R. R. *et al.* Induction of microRNAs, mir-155, mir-222, mir-424 and mir-503, promotes monocytic differentiation through combinatorial regulation. *Leukemia* **24**, 460–466 (2010).

133. Inui, M., Martello, G. & Piccolo, S. MicroRNA control of signal transduction. *Nat. Rev. Mol. Cell Biol.* **11**, 264–275 (2010).

134. Xu, J. *et al.* MiRNA-miRNA synergistic network: construction via co-regulating functional modules and disease miRNA topological features. *Nucleic Acids Res.* **39**, 825–36 (2011).

135. Lal, A. *et al.* Capture of microRNA-bound mRNAs identifies the tumor suppressor miR-34a as a regulator of growth factor signaling. *PLoS Genet.* **7**, (2011).

136. Lal, A. *et al.* Capture of microRNA-bound mRNAs identifies the tumor suppressor miR-34a as a regulator of growth factor signaling. *PLoS Genet.* (2011) doi:10.1371/journal.pgen.1002363.

137. Mukherji, S. *et al.* MicroRNAs can generate thresholds in target gene expression. *Nat. Genet.* **43**, 854–9 (2011).

138. Mukherji, S. *et al.* MicroRNAs can generate thresholds in target gene expression. *Nat. Genet.* **43**, 854–9 (2011).

139. Liang, L. *et al.* Integrative analysis of miRNA and mRNA paired expression profiling of primary fibroblast derived from diabetic foot ulcers reveals multiple impaired cellular functions. *Wound Repair Regen.* **24**, 943–953 (2016).

140. Ramirez, H. A. *et al.* Comparative genomic, microRNA, and tissue analyses reveal

subtle differences between non-diabetic and diabetic foot skin. *PLoS One* (2015) doi:10.1371/journal.pone.0137133.

141. Liang, L. *et al.* Integrative analysis of miRNA and mRNA paired expression profiling of primary fibroblast derived from diabetic foot ulcers reveals multiple impaired cellular functions. *Wound Repair Regen.* (2016) doi:10.1111/wrr.12470.

142. Wang, H. *et al.* NanoStringDiff: A novel statistical method for differential expression analysis based on NanoString nCounter data. *Nucleic Acids Res.* (2016) doi:10.1093/nar/gkw677.

143. Mancini, M. *et al.* MicroRNAs in human skin ageing. *Ageing Research Reviews* (2014) doi:10.1016/j.arr.2014.04.003.

144. Rivetti di Val Cervo, P. *et al.* p63-microRNA feedback in keratinocyte senescence. *Proc. Natl. Acad. Sci.* (2012) doi:10.1073/pnas.1112257109.

145. Martinez, I., Cazalla, D., Almstead, L. L., Steitz, J. A. & DiMaio, D. miR-29 and miR-30 regulate B-Myb expression during cellular senescence. *Proc. Natl. Acad. Sci.* **108**, 522–7 (2011).

146. Mancini, M. *et al.* MicroRNA-152 and -181a participate in human dermal fibroblasts senescence acting on cell adhesion and remodeling of the extracellular matrix. *Aging (Albany. NY).* **4**, 843–853 (2012).

147. Li, T., Yan, X., Jiang, M. & Xiang, L. The comparison of microRNA profile of the dermis between the young and elderly. *J. Dermatol. Sci.* **82**, 75–83 (2016).

148. Nielsen, L. B. *et al.* Circulating levels of MicroRNA from children with newly diagnosed type 1 diabetes and healthy controls: Evidence that miR-25 associates to residual beta-cell function and glycaemic control during disease progression. *Exp. Diabetes Res.* **2012**, 896362 (2012).

149. Griffiths-Jones, S., Saini, H. K., van Dongen, S. & Enright, A. J. miRBase: tools for microRNA genomics. *Nucleic Acids Res.* **36**, D154-8 (2008).

150. Woods, K., Thomson, J. M. & Hammond, S. M. Direct regulation of an oncogenic micro-RNA cluster by E2F transcription factors. *J. Biol. Chem.* **282**, 2130–4 (2007).

151. Zhang, X., Azhar, G. & Wei, J. Y. The expression of microRNA and microRNA clusters in the aging heart. *PLoS One* **7**, e34688 (2012).

152. Chhabra, R., Dubey, R. & Saini, N. Cooperative and individualistic functions of the microRNAs in the miR-23a~27a~24-2 cluster and its implication in human diseases. *Mol. Cancer* **9**, 232 (2010).

153. Kim, Y. K. *et al.* Functional links between clustered microRNAs: Suppression of cell-cycle inhibitors by microRNA clusters in gastric cancer. *Nucleic Acids Res.* **37**, 1672–81 (2009).

154. Williams, A. E. Functional aspects of animal microRNAs. *Cell. Mol. Life Sci.* **65**, 545–62 (2008).

155. Benetatos, L. *et al.* The microRNAs within the DLK1-DIO3 genomic region: Involvement in disease pathogenesis. *Cell. Mol. Life Sci.* **70**, 795–814 (2013).

156. Welten, S. M. J. *et al.* Inhibition of 14q32 MicroRNAs miR-329, miR-487b, miR-494, and miR-495 increases neovascularization and blood flow recovery after ischemia. *Circ. Res.* **115**, 696–708 (2014).

157. Haga, C. L. & Phinney, D. G. MicroRNAs in the imprinted DLK1-DIO3 region repress the epithelial-to-mesenchymal transition by targeting the TWIST1 protein signaling network. *J. Biol. Chem.* **287**, 42695–707 (2012).

158. Dai, R., Lu, R. & Ansar Ahmed, S. The upregulation of genomic imprinted DLK1-Dio3 miRNAs in murine lupus is associated with global DNA hypomethylation. *PLoS One* **11**, e0153509 (2016).

159. Park, L. K. *et al.* Genome-wide DNA methylation analysis identifies a metabolic memory profile in patient-derived diabetic foot ulcer fibroblasts. *Epigenetics* **9**, 1339–49 (2014).

160. Lima, M. H. M. *et al.* Topical insulin accelerates wound healing in diabetes by enhancing the AKT and ERK pathways: A double-blind placebo-controlled clinical trial. *PLoS One* **7**, e36974 (2012).

161. Matsubayashi, Y., Ebisuya, M., Honjoh, S. & Nishida, E. ERK Activation Propagates in

Epithelial Cell Sheets and Regulates Their Migration during Wound Healing. *Curr. Biol.* (2004) doi:10.1016/j.cub.2004.03.060.

162. Sepe, L., Ferrari, M. C., Cantarella, C., Fioretti, F. & Paolella, G. Ras activated ERK and PI3K pathways differentially affect directional movement of cultured fibroblasts. *Cell. Physiol. Biochem.* (2013) doi:10.1159/000343355.

163. Yang, H. L., Tsai, Y. C., Korivi, M., Chang, C. T. & Hseu, Y. C. Lucidone Promotes the Cutaneous Wound Healing Process via Activation of the PI3K/AKT, Wnt/β-catenin and NF-κB Signaling Pathways. *Biochim. Biophys. Acta - Mol. Cell Res.* (2017) doi:10.1016/j.bbamcr.2016.10.021.

164. Squarize, C. H., Castilho, R. M., Bugge, T. H. & Gutkind, J. S. Accelerated wound healing by mTOR activation in genetically defined mouse models. *PLoS One* (2010) doi:10.1371/journal.pone.0010643.

165. Shegogue, D. & Trojanowska, M. Mammalian target of rapamycin positively regulates collagen type I production via a phosphatidylinositol 3-kinase-independent pathway. *J. Biol. Chem.* (2004) doi:10.1074/jbc.M401238200.

166. Goren, I. *et al.* Akt1 controls insulin-driven VEGF biosynthesis from keratinocytes: Implications for normal and diabetes-impaired skin repair in mice. *J. Invest. Dermatol.* (2009) doi:10.1038/jid.2008.230.

167. Castilho, R., Squarize, C. & Gutkind, J. Exploiting PI3K/mTOR signaling to accelerate epithelial wound healing. *Oral Diseases* (2013) doi:10.1111/odi.12070.

168. Jere, S. W., Houreld, N. N. & Abrahamse, H. Role of the PI3K/AKT (mTOR and GSK3β) signalling pathway and photobiomodulation in diabetic wound healing. *Cytokine and Growth Factor Reviews* (2019) doi:10.1016/j.cytogfr.2019.03.001.

169. Huang, H. *et al.* Impaired wound healing results from the dysfunction of the Akt/mTOR pathway in diabetic rats. *J. Dermatol. Sci.* (2015) doi:10.1016/j.jdermsci.2015.06.002.

170. Ledford, H. Cancer: The Ras renaissance. *Nature* (2015) doi:10.1038/520278a.

171. Chang, H. Y. *et al.* Diversity, topographic differentiation, and positional memory in

human fibroblasts. *Proc. Natl. Acad. Sci.* (2002) doi:10.1073/pnas.162488599.

172. Rinn, J. L., Bondre, C., Gladstone, H. B., Brown, P. O. & Chang, H. Y. Anatomic demarcation by positional variation in fibroblast gene expression programs. *PLoS Genet.* (2006) doi:10.1371/journal.pgen.0020119.

173. Rognoni, E. & Watt, F. M. Skin Cell Heterogeneity in Development, Wound Healing, and Cancer. *Trends in Cell Biology* (2018) doi:10.1016/j.tcb.2018.05.002.

174. Sriram, G., Bigliardi, P. L. & Bigliardi-Qi, M. Fibroblast heterogeneity and its implications for engineering organotypic skin models in vitro. *Eur. J. Cell Biol.* **94**, 483–512 (2015).

175. Topouzi, H., Boyle, C. J., Williams, G. & Higgins, C. A. Harnessing the Secretome of Hair Follicle Fibroblasts to Accelerate Ex Vivo Healing of Human Skin Wounds. *J. Invest. Dermatol.* **140**, 1075–1084 (2020).

176. Rognoni, E. & Watt, F. M. Skin Cell Heterogeneity in Development, Wound Healing, and Cancer. *Trends Cell Biol.* **28**, 709–722 (2018).

177. Grimm, D. *et al.* Fatality in mice due to oversaturation of cellular microRNA/short hairpin RNA pathways. *Nature* **441**, 537–41 (2006).

178. Zabner, J., Fasbender, A. J., Moninger, T., Poellinger, K. A. & Welsh, M. J. Cellular and molecular barriers to gene transfer by a cationic lipid. *J. Biol. Chem.* **270**, 18997–9007 (1995).

179. Dominska, M. & Dykxhoorn, D. M. Breaking down the barriers: siRNA delivery and endosome escape. *J. Cell Sci.* **123**, 1183–9 (2010).

180. Nabzdyk, C. S., Chun, M., Pradhan, L. & LoGerfo, F. W. High throughput RNAi assay optimization using adherent cell cytometry. *J. Transl. Med.* **9**, 48 (2011).

181. Thomson, D. W., Bracken, C. P., Szubert, J. M. & Goodall, G. J. On Measuring miRNAs after Transient Transfection of Mimics or Antisense Inhibitors. *PLoS One* (2013) doi:10.1371/journal.pone.0055214.

182. Verduci, L. *et al.* MicroRNA-181a enhances cell proliferation in acute lymphoblastic

leukemia by targeting EGR1. *Leuk. Res.* (2015) doi:10.1016/j.leukres.2015.01.010.

183. Zhu, Z. J. *et al.* MicroRNA-181a promotes proliferation and inhibits apoptosis by suppressing CFIm25 in osteosarcoma. *Mol. Med. Rep.* **14**, 4271–4278 (2016).

184. Zhu, D. *et al.* MicroRNA-181a inhibits activated B-Cell-Like diffuse large B-Cell lymphoma progression by repressing CARD11. *J. Oncol.* **2019**, (2019).

185. Ma, Z. *et al.* MiR-181a-5p inhibits cell proliferation and migration by targeting Kras in non-small cell lung cancer A549 cells. *Acta Biochim. Biophys. Sin. (Shanghai).* (2015) doi:10.1093/abbs/gmv054.

186. Tian, Y. *et al.* MicroRNA-27a promotes proliferation and suppresses apoptosis by targeting PLK2 in laryngeal carcinoma. *BMC Cancer* (2014) doi:10.1186/1471-2407-14-678.

187. Pan, W., Wang, H., Jianwei, R. & Ye, Z. MicroRNA-27a promotes proliferation, migration and invasion by targeting MAP2K4 in human osteosarcoma cells. *Cell. Physiol. Biochem.* (2014) doi:10.1159/000356679.

188. Li, Y. *et al.* MicroRNA-27a functions as a tumor suppressor in renal cell carcinoma by targeting epidermal growth factor receptor. *Oncol. Lett.* (2016) doi:10.3892/ol.2016.4500.

189. Zhu, L., Wang, Z., Fan, Q., Wang, R. & Sun, Y. MicroRNA-27a functions as a tumor suppressor in esophageal squamous cell carcinoma by targeting KRAS. *Oncol. Rep.* (2014) doi:10.3892/or.2013.2807.

190. Jiang, Y., Duan, Y. & Zhou, H. Microrna-27a directly targets KRAS to inhibit cell proliferation in esophageal squamous cell carcinoma. *Oncol. Lett.* (2015) doi:10.3892/ol.2014.2701.

191. Shen, H. *et al.* MicroRNA-30a attenuates mutant KRAS-driven colorectal tumorigenesis via direct suppression of ME1. *Cell Death Differ.* **24**, 1253–1262 (2017).

192. Zheng, J. *et al.* Hepatic stellate cell is activated by microRNA-181b via PTEN/Akt pathway. *Mol. Cell. Biochem.* **398**, 1–9 (2015).

193. Mendoza, M. C., Er, E. E. & Blenis, J. The Ras-ERK and PI3K-mTOR pathways: Cross-talk and compensation. *Trends Biochem. Sci.* **36**, 320–8 (2011).

194. Vlahos, C. J., Matter, W. F., Hui, K. Y. & Brown, R. F. A specific inhibitor of phosphatidylinositol 3-kinase, 2-(4-morpholinyl)- 8-phenyl-4H-1-benzopyran-4-one (LY294002). *J. Biol. Chem.* (1994).

195. Collado, M. *et al.* Inhibition of the phosphoinositide 3-kinase pathway induces a senescence-like arrest mediated by p27(kip)1. *J. Biol. Chem.* (2000) doi:10.1074/jbc.M000759200.

196. Rang, Z. *et al.* MIR-181a Targets PHLPP2 to Augment AKT Signaling and Regulate Proliferation and Apoptosis in Human Keloid Fibroblasts. *Cell. Physiol. Biochem.* (2016) doi:10.1159/000453139.

197. Boellner, S. & Becker, K.-F. Reverse Phase Protein Arrays—Quantitative Assessment of Multiple Biomarkers in Biopsies for Clinical Use. *Microarrays* (2015) doi:10.3390/microarrays4020098.

198. Hoke, G. D. *et al.* Atypical Diabetic Foot Ulcer Keratinocyte Protein Signaling Correlates with Impaired Wound Healing. *J. Diabetes Res.* (2016) doi:10.1155/2016/1586927.

199. Wachter, A., Bernhardt, S., Beissbarth, T. & Korf, U. Analysis of Reverse Phase Protein Array Data: From Experimental Design towards Targeted Biomarker Discovery. *Microarrays* (2015) doi:10.3390/microarrays4040520.

200. Shu, J. *et al.* Dose-dependent differential mRNA target selection and regulation by let-7a-7f and miR-17-92 cluster microRNAs. *RNA Biol.* **9**, 1275–87 (2012).

201. Oberprieler, N. G. & Taskén, K. Analysing phosphorylation-based signalling networks by phospho flow cytometry. *Cell. Signal.* **23**, 14–8 (2011).

202. Schmittgen, T. D. & Livak, K. J. Analyzing real-time PCR data by the comparative CT method. *Nat. Protoc.* **3**, 1101–8 (2008).

203. Xie, X. *et al.* Nanostraw-electroporation system for highly efficient intracellular delivery and transfection. *ACS Nano* **7**, 4351–4358 (2013).

204. Canatella, P. J., Karr, J. F., Petros, J. A. & Prausnitz, M. R. Quantitative study of electroporation-mediated molecular uptake and cell viability. *Biophys. J.* (2001) doi:10.1016/S0006-3495(01)76055-9.

205. Cao, Y. *et al.* Universal intracellular biomolecule delivery with precise dosage control. *Sci. Adv.* (2018) doi:10.1126/sciadv.aat8131.

206. Cao, Y. *et al.* Nondestructive nanostraw intracellular sampling for longitudinal cell monitoring. *Proc. Natl. Acad. Sci. U. S. A.* (2017) doi:10.1073/pnas.1615375114.

207. Vandersarl, J. J., Xu, A. M. & Melosh, N. A. Nanostraws for direct fluidic intracellular access. *Nano Lett.* **12**, 3881–3886 (2012).

208. Gvaramia, D., Blaauboer, M. E., Hanemaaijer, R. & Everts, V. Role of caveolin-1 in fibrotic diseases. *Matrix Biology* (2013) doi:10.1016/j.matbio.2013.03.005.

209. Jin, H. Y. *et al.* MicroRNA-17~92 plays a causative role in lymphomagenesis by coordinating multiple oncogenic pathways. *EMBO J.* (2013) doi:10.1038/emboj.2013.178.

210. Vandersarl, J. J., Xu, A. M. & Melosh, N. A. Nanostraws for direct fluidic intracellular access. *Nano Lett.* **12**, 3881–6 (2012).

211. Distler, J. H. W. *et al.* Nucleofection: A new, highly efficient transfection method for primary human keratinocytes. *Exp. Dermatol.* **14**, 315–320 (2005).

212. Deyrieux, A. F. & Wilson, V. G. In vitro culture conditions to study keratinocyte differentiation using the HaCaT cell line. *Cytotechnology* (2007) doi:10.1007/s10616-007-9076-1.

213. Bacakova, M. *et al.* Effects of fiber density and plasma modification of nanofibrous membranes on the adhesion and growth of HaCaT keratinocytes. *J. Biomater. Appl.* (2015) doi:10.1177/0885328214546647.

214. Muir, B. W. *et al.* Effects of oxygen plasma treatment on the surface of bisphenol A polycarbonate: A study using SIMS, principal component analysis, ellipsometry, XPS and AFM nanoindentation. *Surf. Interface Anal.* (2006) doi:10.1002/sia.2363.

215. Hayman, E. G., Pierschbacher, M. D., Suzuki, S. & Ruoslahti, E. Vitronectin-A major cell attachment-promoting protein in fetal bovine serum. *Exp. Cell Res.* (1985) doi:10.1016/0014-4827(85)90173-9.

216. Bertolero, F., Kaighn, M. E., Camalier, R. F. & Saffiotti, U. Effects of serum and serum-derived factors on growth and differentiation of mouse keratinocytes. *Vitr. Cell. Dev. Biol.* (1986) doi:10.1007/BF02623533.

217. Raut, S. K. *et al.* miR-30c and miR-181a synergistically modulate p53–p21 pathway in diabetes induced cardiac hypertrophy. *Mol. Cell. Biochem.* (2016) doi:10.1007/s11010-016-2729-7.

218. Takahara, S. *et al.* Altered expression of microRNA during fracture healing in diabetic rats. *Bone Jt. Res.* (2018) doi:10.1302/2046-3758.72.BJR-2017-0082.R1.

219. Bhajun, R. *et al.* A statistically inferred microRNA network identifies breast cancer target miR-940 as an actin cytoskeleton regulator. *Sci. Rep.* **5**, 8336 (2015).

220. Huettner, N., Dargaville, T. R. & Forget, A. Discovering Cell-Adhesion Peptides in Tissue Engineering: Beyond RGD. *Trends in Biotechnology* (2018) doi:10.1016/j.tibtech.2018.01.008.

221. Kligys, K. R. *et al.* α6β4 integrin, a master regulator of expression of integrins in human keratinocytes. *J. Biol. Chem.* (2012) doi:10.1074/jbc.M111.310458.

222. Su, Z., Xia, J. & Zhao, Z. Functional complementation between transcriptional methylation regulation and post-transcriptional microRNA regulation in the human genome. *BMC Genomics* **12**, S15 (2011).

223. Vaissière, T., Sawan, C. & Herceg, Z. Epigenetic interplay between histone modifications and DNA methylation in gene silencing. *Mutation Research - Reviews in Mutation Research* vol. 659 40–48 (2008).

224. Liu, X. *et al.* Regulation of microRNAs by epigenetics and their interplay involved in cancer. *Journal of Experimental and Clinical Cancer Research* (2013) doi:10.1186/1756-9966-32-96.

225. Cheng, C., Bhardwaj, N. & Gerstein, M. The relationship between the evolution of

microRNA targets and the length of their UTRs. *BMC Genomics* **10**, 431 (2009).

226. Yamaguchi, T. *et al.* Visualization of specific collagen-producing cells by Col1-GFP transgenic mice revealed novel type I collagen-producing cells other than fibroblasts in systemic organs/tissues. *Biochem. Biophys. Res. Commun.* **505**, 267–273 (2018).

9. Appendix

9.1. List of chemicals and materials used

Fibroblast cell culture

- Dulbecco's Modified Eagle's Medium – high glucose (Sigma Aldrich, D5671-500ML)
- Fetal Bovine Serum, qualified, Brazil (Gibco, 10270106)
- L-glutamine (200mM) (Thermofisher, 25030024)
- Penicillin-Streptomycin (Sigma Aldrich, P4333-100ML)
- Antibiotic Antimycotic Solution (100x), Stabilised (Sigma Aldrich, A5955-100ML)
- Trypsin-EDTA solution (Sigma Aldrich, T4049-100ML)
- Dulbecco's Phosphate Buffered Saline (Sigma Aldrich, D8537-500ML)
- Dimethyl sulfoxide (Sigma Aldrich, D8418-100ML)
- Dispase (5U/mL) (Stem Cell Technologies, 07913)
- Collagenase, Type I, Powder (Gibco, 17100017)
- EASYstrainer Cell Sieve for 50 ml tubes, 70µm mesh (Greiner Bio-One, 542070)
- EASYstrainer Cell Sieve for 50 ml tubes, 40µm mesh (Greiner Bio-One, 542040)

Keratinocyte cell culture

- Epilife Medium, with 60 µM calcium (Cascade Biologics, MEPI500CA)
- Epilife Defined Growth Supplement (EDGS) (Cascade Biologics, S0125)
- Coating Matrix Kit Protein (Cascade Biologics, R011K)
- Defined Trypsin Inhibitor (Cascade Biologics, R007100)
- TryplE Express Enzyme (1x), no phenol red (Gibco, 12604013)
- Synth-a-Freeze Cryopreservation Medium (Gibco, A1254201)
- Cryovial with Internal Thread, Silicone Seal Cap, 1.8 ml (Starlab, E3110-6122)

HUVEC cell culture

- HUVEC, pre-screened single donor, cryo-preserved (PromoCell, C-12205)
- Endothelial Cell Growth Medium, Basal Medium (PromoCell, C-22210)

- Endothelial Cell Growth Medium, Growth Medium Kit (PromoCell, C-22110)

Mycoplasma testing

- PCR Mycoplasma test kit II (ITW Reagents, A8894,0025)
- PCR Mycoplasma test kit II (PromoCell, PK-CA20-700-20)
- Low Molecular Weight DNA Ladder (New England BioLabs, N3233L)

Growth factor stimulation

- Recombinant Human PDGF-BB (carrier-free) (BioLegend, 577304)
- Recombinant Human KGF (FGF-7) (Animal-Free) (BioLegend, 711702)

MicroRNA mimics and inhibitors (Dharmacon)

- miRIDIAN microRNA Human hsa-miR-181a-5p – Mimic (C-300552-05-0010)
- miRIDIAN microRNA Human hsa-miR-27a-3p – Mimic (C- 300502-03-0010)
- miRIDIAN microRNA Human hsa-miR-30a-5p – Mimic (C-300505-03-0010)
- miRIDIAN microRNA Mimic Negative Control #1 (CN-001000-01-20)
- miRIDIAN microRNA Mimic Transfection Control with Dy547 (CP-004500-01-05)
- miRIDIAN microRNA Mimic Housekeeping Positive Control #2 (GAPD)-Human (CP-001000-02-05)
- miRIDIAN microRNA Human hsa-miR-181a-5p – Hairpin Inhibitor (IH-300552-07-0010)
- miRIDIAN microRNA Human hsa-miR-27a-3p – Hairpin Inhibitor (IH-300502-05-0010)
- miRIDIAN microRNA Hairpin Inhibitor Negative Control #1 (IN-001005-01-20)

MicroRNA transfection via liposomal-based delivery

- Lipofectamine RNAiMAX Transfection Reagent (Invitrogen, 13778075)
- Opti-MEM I Reduced Serum Medium (Gibco, 31985062)
- 5x siRNA buffer 100mL (Dharmacon, B-002000-UB-100)
- Water, nuclease-free (Thermofisher Scientific, R0581)

- Nonstick, RNase-free Microcentrifuge tubes, 0.5 mL (Ambion, AM12350)

LY294002 (Cell Signalling Technology, 9901S)

RNA extraction

- PureLink RNA Micro Scale Kit (Invitrogen, 12183016)
- QIAshredder (50) (Qiagen, 79654)
- 2-Mercaptoethanol (Sigma-Aldrich, M6250-10ML)
- mirVana miRNA Isolation Kit, with phenol (Ambion, AM1560)
- Ethanol absolute (200 Proof), Molecular Biology Grade (Fisher Scientific, 10644795)
- RNAseZap RNase Decontaminating Solution (Ambion, AM9780)
- DNA-free DNA removal kit (Ambion, AM1906)
- 1.5 ml TubeOne Microcentrifuge tubes, Natural (Starlab, S1615-5550)

RT-qPCR (on microRNAs and mRNAs)

- Taqman MicroRNA Reverse Transcription kit (Applied Biosystems, 4366596)
- Taqman Fast Advanced Mastermix (Applied Biosystems, 4444557)
- Hsa-miR-181a-5p Taqman microRNA assay (ID: 000480) (Thermofisher Scientific, 4427975)
- Hsa-miR-27a-3p Taqman microRNA assay (ID: 000408) (Thermofisher Scientific, 4427975)
- Hsa-miR-30a-5p Taqman microRNA assay (ID: 000417) (Thermofisher Scientific, 4427975)
- RNU44 Human Taqman microRNA assay control miRNA (ID: 001094) (Thermofisher Scientific, 4427975)
- Precision nanoScript2 Reverse Transcription Kit (Primerdesign, RT-NanoScript2)
- Taqman Fast Universal PCR Master Mix (2x), no AmpErase UNG (Applied Biosystems, 4366072)
- Reference gene assays with Double-dye (Taqman-style) probe for human ACTB and GAPDH genes (Primerdesign, HK-DD-hu-600)

- Custom human real-time PCR assays with double dye probe (Taqman style) 300rxn for CAV1, KRAS, IRS1, PTEN (Primerdesign, DD-hu-300)
- RT-PCR grade water (Ambion, AM9935)
- 8-Strip PCR Tubes With Individual Attached Caps, 0.2 ml (natural) (Starlab, I1402-2900)
- MicroAmp Fast Optical 96-Well Reaction Plate with Barcode, 0.1 mL (Applied Biosystems, 4346906)
- MicroAmp Optical Adhesive Film (Applied Biosystems, 4360954)
- DNAZap PCR DNA Degradation Solutions (Ambion, AM9890)

Testing RNA integrity & visualising DNA bands

- TopVision Low Melting Point Agarose (Thermofisher Scientific, R0801)
- Gel Loading Solution (All-Purpose, Native Agarose) (Ambion, AM8556)
- Novex TBE Running buffer (5x) (Thermofisher Scientific, LC6675)
- Novex TBE-Urea Gels, 15%, 10 Well (Thermofisher Scientific, EC6885BOX)
- Gel Loading Buffer II (Denaturing PAGE) (Ambion, AM8546G)
- 10/60 ladder (Integrated DNA Technologies, 51-05-15-01)
- SYBR Gold Nucleic Acid Gel Stain (10,000x Concentrate in DMSO) (Thermofisher Scientific, S11494)

Proliferation assays

- Prestoblue Cell Viability Reagent (Invitrogen, A13262)
- 96 Well Advanced TC treated plate with lid, black (Greiner Bio-One, 655986)

Luminescence assays

- Dual-Glo Luciferase Assay System (Promega, E2920)
- 96 well tissue culture treated plate, white (Greiner Bio-One, 655088)
- Microplate lid with condensation rings, sterile (Greiner Bio-One, 656171)
- Lipofectamine 2000 Transfection Reagent (Invitrogen, 11668030)

Protein measurement assays

- Pierce BCA Protein Assay Kit (Thermofisher Scientific, 23227)

- Falcon 96-well Clear Flat Bottom TC-treated Culture Microplate (Scientific Laboratory Supplies, 353072)

Staining

- Hoechst 33342, Trihydrochloride, Trigydrate (Invitrogen, H3570)
- CellTracker Green CMFDA Dye (Invitrogen, C7025)
- Propidium Iodide – 1.0 mg/ml Solution in Water (Invitrogen, P3566)
- Vectashield mounting medium for fluorescence (Vector Laboratories, H-1000)
- Pierce 16% Formaldehyde (w/v), Methanol-free (Thermofisher Scientific, 28908)
- Live and Dead Cell Assay (Abcam, ab115347)

NS-mediated delivery of miRNAs

- PBS – Phosphate-Buffered Saline (10x) pH 7.4, RNase-free (Ambion, AM9625)
- Nuclease-Free Water (not DEPC-Treated) (Ambion, AM9932)

Immunostaining

- Triton X-100 (Sigma Aldrich, T8787-250ML)
- Chicken Anti-Vimentin primary antibody (Abcam, ab24525)
- Rabbit Anti-Collagen I antibody (Abcam, ab34710)
- Normal Goat Serum Blocking Solution (Vector Laboratories, S-1000)

Cryosectioning

- O.C.T compound for embedding, for cryotomy (VWR, 361603E)
- Simport Base Mould 15x15x5mm (Scientific Laboratory Supplies, HIS0221)
- Adhesion Slides SuperFrost Plus (VWR, 631-0108)

General Plasticware

- Corning T25 flasks (Scientific Laboratory Supplies, 430639)
- Corning T75 flasks (Scientific Laboratory Supplies, 430641U)
- 24-Well CytoOne Plate, TC-Treated (Starlab, CC7682-7524)
- 6-Well CytoOne Plate, TC-Treated (Starlab, CC7682-7506)

9.2. Permission to re-publish or modify images from third parties

Figure number	Licensed Content Publisher	License number	License date	Permission to re-use
Figure 1	Elsevier	4747520385422	14-01-20	Yes
Figure 2	Springer Nature	4745301109078	10-01-20	Yes
Figure 4	Springer Nature	4745350311442	10-01-20	Yes
Figure 11	Elsevier	4745461076170	10-01-20	Yes
Figure 12	Elsevier	4745470973921	10-01-20	Yes
Figure 13	Elsevier	4745470973921	10-01-20	Yes
Figure 14	Springer Nature	4745480758998	10-01-20	Yes
Figure 15	Elsevier	4745481281126	10-01-20	Yes
Figure 17	Elsevier	4745470973921	10-01-20	Yes
Figure 18	Elsevier	4745470973921	10-01-20	Yes
Figure 19	Oxford University Press	4745850560060	11-01-20	Yes
Figure 20	Springer Nature	4745421483764	10-01-2020	Yes
Figure 22	Springer Nature	4745861014658	11-01-20	Yes
Figure 24	John Wiley and Sons	4744311246439	08-01-20	Yes
Figure 63	Elsevier	4744700256919	09-01-20	Yes
Figure 76	Elsevier	4744780398082	09-01-20	Yes

Table 28: permission to re-publish or modify figures from journals has been requested and granted

Note: Full documents showing permission has been granted are shown at the end of the appendix.

Permission for Figure 36

This file is licensed under the Creative Commons Attribution 4.0 International license (https://creativecommons.org/licenses/by/4.0/deed.en). Author: CNX OpenStax. Source: https://cnx.org/contents/5CvTdmJL@4.4 Only part b) from the original image was used.

Permission for Figure 50



SHOPPING CART Empty this cart

Cart Total: 0.00 GBP CHECKOUT

Currency GBP

1. Journal of cell science 0.00 GBP

Publisher Terms and Conditions

ISSN	1477-9137
Type of Use	Republish in a thesis/dissertation
Publisher	COMPANY OF BIOLOGISTS LTD.
Portion	Image/photo/illustration

LICENSED CONTENT

Publication Title	Journal of cell science	Country	United Kingdom of Great Britain and Northern Ireland
Author/Editor	Company of Biologists.	Rightsholder	The Company of Biologists Ltd.
Date	01/01/1966	Publication Type	e-Journal
Language	English	URL	http://jcs.biologists.org/

REQUEST DETAILS

Portion Type	Image/photo/illustration	Distribution	Worldwide
Number of images / photos / illustrations	1	Translation	Original language of publication
Format (select all that apply)	Print, Electronic	Copies for the disabled?	No
Who will republish the content?	Academic institution	Minor editing privileges?	Yes
Duration of Use	Life of current and all future editions	Incidental promotional use?	No
Lifetime Unit Quantity	Up to 4,999	Currency	GBP
Rights Requested	Main product		

NEW WORK DETAILS

Title	Miss	Institution name	Imperial College London
Instructor name	Mara Alexandra Pop	Expected presentation date	2020-03-20

ADDITIONAL DETAILS

1/8/2020 https://marketplace.copyright.com/rs-ui-web/mp/checkout/shopping-cart

Order reference number	N/A	The requesting person / organization to appear on the license	Mara A Pop

REUSE CONTENT DETAILS

Title, description or numeric reference of the portion(s)	Uptake and intracellular trafficking of a targeted siRNA delivery vehicle.	Title of the article/chapter the portion is from	Intracellular trafficking of siRNAs
		Author of portion(s)	The Company of Biologists Ltd
Editor of portion(s)	n/a		
Volume of serial or monograph	n/a	Issue, if republishing an article from a serial	N/A
Page or page range of portion	1185	Publication date of portion	2010-03-31

Remove

Total Items: 1

Figure 127: screenshot of permission to re-use figure in the thesis

Permission for Figure 75



Figure 128: screenshot of permission to re-use figure in the thesis

Permission for Figure 87

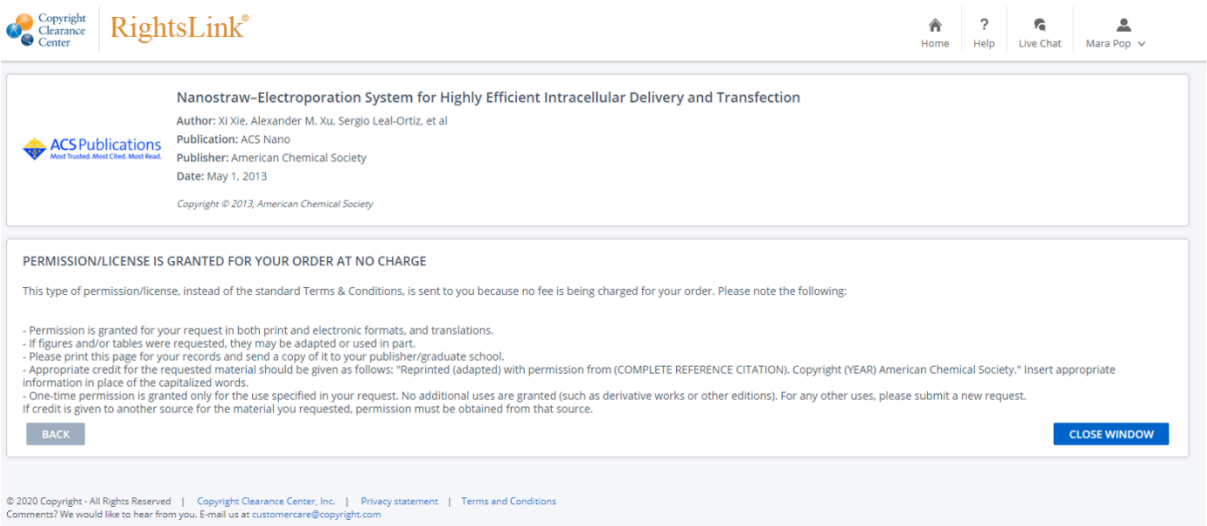


Figure 129: screenshot of permission to re-use figure in the thesis

Permission for Figure 106 and Figure 122

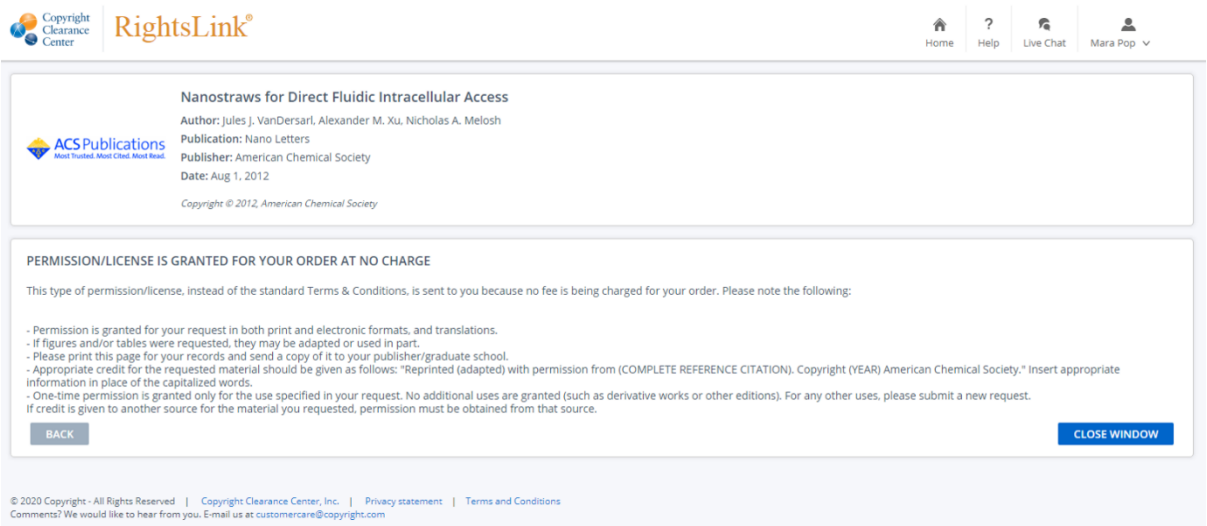


Figure 130: screenshot of permission to re-use image in the thesis

Permission for Figure 110

This file is licensed under the Creative Commons Attribution 3.0 Unported license (https://creativecommons.org/licenses/by/3.0/deed.en). Author: OpenStax College. Source: Anatomy & Physiology, Connexions Web site. http://cnx.org/content/col11496/1.6/, Jun 19, 2013.

ELSEVIER LICENSE
TERMS AND CONDITIONS
Jan 25, 2020

This Agreement between Mara A Pop ("You") and Elsevier ("Elsevier") consists of your license details and the terms and conditions provided by Elsevier and Copyright Clearance Center.

License Number	4747520385422
License date	Jan 14, 2020
Licensed Content Publisher	Elsevier
Licensed Content Publication	Journal of the American Academy of Dermatology
Licensed Content Title	Treating the chronic wound: A practical approach to the care of nonhealing wounds and wound care dressings
Licensed Content Author	Margaret A. Fonder,Gerald S. Lazarus,David A. Cowan,Barbara Aronson-Cook,Angela R. Kohli,Adam J. Mamelak
Licensed Content Date	Feb 1, 2008
Licensed Content Volume	58
Licensed Content Issue	2
Licensed Content Pages	22
Start Page	185
End Page	206
Type of Use	reuse in a thesis/dissertation
Portion	figures/tables/illustrations
Number of figures/tables/illustrations	1
Format	both print and electronic
Are you the author of this Elsevier article?	No
Will you be translating?	No
Title	Exploring combinatorial microRNA therapy for chronic wound healing
Institution name	Imperial College London
Expected presentation date	Jan 2020
Portions	Figure 2
Requestor Location	Mara A Pop Prince Consort Road Royal School of Mines

	London, London SW7 2BP United Kingdom Attn: Mara A Pop
Publisher Tax ID	GB 494 6272 12
Total	0.00 GBP

Terms and Conditions

INTRODUCTION

1. The publisher for this copyrighted material is Elsevier. By clicking "accept" in connection with completing this licensing transaction, you agree that the following terms and conditions apply to this transaction (along with the Billing and Payment terms and conditions established by Copyright Clearance Center, Inc. ("CCC"), at the time that you opened your Rightslink account and that are available at any time at http://myaccount.copyright.com).

GENERAL TERMS

2. Elsevier hereby grants you permission to reproduce the aforementioned material subject to the terms and conditions indicated.

3. Acknowledgement: If any part of the material to be used (for example, figures) has appeared in our publication with credit or acknowledgement to another source, permission must also be sought from that source. If such permission is not obtained then that material may not be included in your publication/copies. Suitable acknowledgement to the source must be made, either as a footnote or in a reference list at the end of your publication, as follows:

"Reprinted from Publication title, Vol /edition number, Author(s), Title of article / title of chapter, Pages No., Copyright (Year), with permission from Elsevier [OR APPLICABLE SOCIETY COPYRIGHT OWNER]." Also Lancet special credit - "Reprinted from The Lancet, Vol. number, Author(s), Title of article, Pages No., Copyright (Year), with permission from Elsevier."

4. Reproduction of this material is confined to the purpose and/or media for which permission is hereby given.

5. Altering/Modifying Material: Not Permitted. However figures and illustrations may be altered/adapted minimally to serve your work. Any other abbreviations, additions, deletions and/or any other alterations shall be made only with prior written authorization of Elsevier Ltd. (Please contact Elsevier at permissions@elsevier.com). No modifications can be made to any Lancet figures/tables and they must be reproduced in full.

6. If the permission fee for the requested use of our material is waived in this instance, please be advised that your future requests for Elsevier materials may attract a fee.

7. Reservation of Rights: Publisher reserves all rights not specifically granted in the combination of (i) the license details provided by you and accepted in the course of this licensing transaction, (ii) these terms and conditions and (iii) CCC's Billing and Payment terms and conditions.

8. License Contingent Upon Payment: While you may exercise the rights licensed immediately upon issuance of the license at the end of the licensing process for the transaction, provided that you have disclosed complete and accurate details of your proposed use, no license is finally effective unless and until full payment is received from you (either by publisher or by CCC) as provided in CCC's Billing and Payment terms and conditions. If full payment is not received on a timely basis, then any license preliminarily granted shall be deemed automatically revoked and shall be void as if never granted. Further, in the event that you breach any of these terms and conditions or any of CCC's Billing and Payment terms and conditions, the license is automatically revoked and shall be void as if never granted. Use of materials as described in a revoked license, as well as any use of the materials beyond the scope of an unrevoked license, may constitute copyright infringement and publisher reserves the right to take any and all action to protect its copyright in the materials.

9. Warranties: Publisher makes no representations or warranties with respect to the licensed material.

10. Indemnity: You hereby indemnify and agree to hold harmless publisher and CCC, and their respective officers, directors, employees and agents, from and against any and all claims arising out of your use of the licensed material other than as specifically authorized pursuant to this license.

11. No Transfer of License: This license is personal to you and may not be sublicensed, assigned, or transferred by you to any other person without publisher's written permission.

12. No Amendment Except in Writing: This license may not be amended except in a writing signed by both parties (or, in the case of publisher, by CCC on publisher's behalf).

13. Objection to Contrary Terms: Publisher hereby objects to any terms contained in any purchase order, acknowledgment, check endorsement or other writing prepared by you, which terms are inconsistent with these terms and conditions or CCC's Billing and Payment terms and conditions. These terms and conditions, together with CCC's Billing and Payment terms and conditions (which are incorporated herein), comprise the entire agreement between you and publisher (and CCC) concerning this licensing transaction. In the event of any conflict between your obligations established by these terms and conditions and those established by CCC's Billing and Payment terms and conditions, these terms and conditions shall control.

14. Revocation: Elsevier or Copyright Clearance Center may deny the permissions described in this License at their sole discretion, for any reason or no reason, with a full refund payable to you. Notice of such denial will be made using the contact information

provided by you. Failure to receive such notice will not alter or invalidate the denial. In no event will Elsevier or Copyright Clearance Center be responsible or liable for any costs, expenses or damage incurred by you as a result of a denial of your permission request, other than a refund of the amount(s) paid by you to Elsevier and/or Copyright Clearance Center for denied permissions.

LIMITED LICENSE

The following terms and conditions apply only to specific license types:

15. **Translation**: This permission is granted for non-exclusive world **English** rights only unless your license was granted for translation rights. If you licensed translation rights you may only translate this content into the languages you requested. A professional translator must perform all translations and reproduce the content word for word preserving the integrity of the article.

16. **Posting licensed content on any Website**: The following terms and conditions apply as follows: Licensing material from an Elsevier journal: All content posted to the web site must maintain the copyright information line on the bottom of each image; A hyper-text must be included to the Homepage of the journal from which you are licensing at http://www.sciencedirect.com/science/journal/xxxxx or the Elsevier homepage for books at http://www.elsevier.com; Central Storage: This license does not include permission for a scanned version of the material to be stored in a central repository such as that provided by Heron/XanEdu.

Licensing material from an Elsevier book: A hyper-text link must be included to the Elsevier homepage at http://www.elsevier.com . All content posted to the web site must maintain the copyright information line on the bottom of each image.

Posting licensed content on Electronic reserve: In addition to the above the following clauses are applicable: The web site must be password-protected and made available only to bona fide students registered on a relevant course. This permission is granted for 1 year only. You may obtain a new license for future website posting.

17. **For journal authors:** the following clauses are applicable in addition to the above:

Preprints:

A preprint is an author's own write-up of research results and analysis, it has not been peer-reviewed, nor has it had any other value added to it by a publisher (such as formatting, copyright, technical enhancement etc.).

Authors can share their preprints anywhere at any time. Preprints should not be added to or enhanced in any way in order to appear more like, or to substitute for, the final

versions of articles however authors can update their preprints on arXiv or RePEc with their Accepted Author Manuscript (see below).

If accepted for publication, we encourage authors to link from the preprint to their formal publication via its DOI. Millions of researchers have access to the formal publications on ScienceDirect, and so links will help users to find, access, cite and use the best available version. Please note that Cell Press, The Lancet and some society-owned have different preprint policies. Information on these policies is available on the journal homepage.

Accepted Author Manuscripts: An accepted author manuscript is the manuscript of an article that has been accepted for publication and which typically includes author-incorporated changes suggested during submission, peer review and editor-author communications.

Authors can share their accepted author manuscript:

- immediately
    - via their non-commercial person homepage or blog
    - by updating a preprint in arXiv or RePEc with the accepted manuscript
    - via their research institute or institutional repository for internal institutional uses or as part of an invitation-only research collaboration work-group
    - directly by providing copies to their students or to research collaborators for their personal use
    - for private scholarly sharing as part of an invitation-only work group on commercial sites with which Elsevier has an agreement
- After the embargo period
    - via non-commercial hosting platforms such as their institutional repository
    - via commercial sites with which Elsevier has an agreement

In all cases accepted manuscripts should:

- link to the formal publication via its DOI
- bear a CC-BY-NC-ND license - this is easy to do
- if aggregated with other manuscripts, for example in a repository or other site, be shared in alignment with our hosting policy not be added to or enhanced in any way to appear more like, or to substitute for, the published journal article.

Published journal article (JPA): A published journal article (PJA) is the definitive final record of published research that appears or will appear in the journal and embodies all value-adding publishing activities including peer review co-ordination, copy-editing, formatting, (if relevant) pagination and online enrichment.

Policies for sharing publishing journal articles differ for subscription and gold open access articles:

Subscription Articles: If you are an author, please share a link to your article rather than the full-text. Millions of researchers have access to the formal publications on ScienceDirect, and so links will help your users to find, access, cite, and use the best available version.

Theses and dissertations which contain embedded PJAs as part of the formal submission can be posted publicly by the awarding institution with DOI links back to the formal publications on ScienceDirect.

If you are affiliated with a library that subscribes to ScienceDirect you have additional private sharing rights for others' research accessed under that agreement. This includes use for classroom teaching and internal training at the institution (including use in course packs and courseware programs), and inclusion of the article for grant funding purposes.

Gold Open Access Articles: May be shared according to the author-selected end-user license and should contain a CrossMark logo, the end user license, and a DOI link to the formal publication on ScienceDirect.

Please refer to Elsevier's posting policy for further information.

18. **For book authors** the following clauses are applicable in addition to the above: Authors are permitted to place a brief summary of their work online only. You are not allowed to download and post the published electronic version of your chapter, nor may you scan the printed edition to create an electronic version. **Posting to a repository:** Authors are permitted to post a summary of their chapter only in their institution's repository.

19. **Thesis/Dissertation**: If your license is for use in a thesis/dissertation your thesis may be submitted to your institution in either print or electronic form. Should your thesis be published commercially, please reapply for permission. These requirements include permission for the Library and Archives of Canada to supply single copies, on demand, of the complete thesis and include permission for Proquest/UMI to supply single copies, on demand, of the complete thesis. Should your thesis be published commercially, please reapply for permission. Theses and dissertations which contain embedded PJAs as part of the formal submission can be posted publicly by the awarding institution with DOI links back to the formal publications on ScienceDirect.

Elsevier Open Access Terms and Conditions

You can publish open access with Elsevier in hundreds of open access journals or in nearly 2000 established subscription journals that support open access publishing. Permitted third party re-use of these open access articles is defined by the author's choice of Creative Commons user license. See our open access license policy for more information.

Terms & Conditions applicable to all Open Access articles published with Elsevier:

Any reuse of the article must not represent the author as endorsing the adaptation of the article nor should the article be modified in such a way as to damage the author's honour or reputation. If any changes have been made, such changes must be clearly indicated.

The author(s) must be appropriately credited and we ask that you include the end user license and a DOI link to the formal publication on ScienceDirect.

If any part of the material to be used (for example, figures) has appeared in our publication with credit or acknowledgement to another source it is the responsibility of the user to ensure their reuse complies with the terms and conditions determined by the rights holder.

Additional Terms & Conditions applicable to each Creative Commons user license:

CC BY: The CC-BY license allows users to copy, to create extracts, abstracts and new works from the Article, to alter and revise the Article and to make commercial use of the Article (including reuse and/or resale of the Article by commercial entities), provided the user gives appropriate credit (with a link to the formal publication through the relevant DOI), provides a link to the license, indicates if changes were made and the licensor is not represented as endorsing the use made of the work. The full details of the license are available at http://creativecommons.org/licenses/by/4.0.

CC BY NC SA: The CC BY-NC-SA license allows users to copy, to create extracts, abstracts and new works from the Article, to alter and revise the Article, provided this is not done for commercial purposes, and that the user gives appropriate credit (with a link to the formal publication through the relevant DOI), provides a link to the license, indicates if changes were made and the licensor is not represented as endorsing the use made of the work. Further, any new works must be made available on the same conditions. The full details of the license are available at http://creativecommons.org/licenses/by-nc-sa/4.0.

CC BY NC ND: The CC BY-NC-ND license allows users to copy and distribute the Article, provided this is not done for commercial purposes and further does not permit distribution of the Article if it is changed or edited in any way, and provided the user gives appropriate credit (with a link to the formal publication through the relevant DOI), provides a link to the license, and that the licensor is not represented as endorsing the use made of the work. The full details of the license are available at http://creativecommons.org/licenses/by-nc-nd/4.0. Any commercial reuse of Open Access articles published with a CC BY NC SA or CC BY NC ND license requires permission from Elsevier and will be subject to a fee.

Commercial reuse includes:

- Associating advertising with the full text of the Article
- Charging fees for document delivery or access

- Article aggregation
- Systematic distribution via e-mail lists or share buttons

Posting or linking by commercial companies for use by customers of those companies.

20. **Other Conditions**:

v1.9

Questions? customercare@copyright.com or +1-855-239-3415 (toll free in the US) or +1-978-646-2777.

SPRINGER NATURE LICENSE
TERMS AND CONDITIONS

Jan 25, 2020

This Agreement between Mara A Pop ("You") and Springer Nature ("Springer Nature") consists of your license details and the terms and conditions provided by Springer Nature and Copyright Clearance Center.

License Number	4745301109078
License date	Jan 10, 2020
Licensed Content Publisher	Springer Nature
Licensed Content Publication	Nature
Licensed Content Title	Wound repair and regeneration
Licensed Content Author	Geoffrey C. Gurtner et al
Licensed Content Date	May 14, 2008
Type of Use	Thesis/Dissertation
Requestor type	academic/university or research institute
Format	print and electronic
Portion	figures/tables/illustrations
Number of figures/tables/illustrations	1
High-res required	no
Will you be translating?	no
Circulation/distribution	500 - 999
Author of this Springer Nature content	no
Title	Exploring combinatorial microRNA therapy for chronic wound healing
Institution name	n/a
Expected presentation date	Jan 2020
Portions	Figure 1
Requestor Location	Mara A Pop Prince Consort Road Royal School of Mines London, London SW7 2BP United Kingdom Attn: Mara A Pop
Total	0.00 USD

Terms and Conditions

Springer Nature Customer Service Centre GmbH
Terms and Conditions

This agreement sets out the terms and conditions of the licence (the **Licence**) between you and **Springer Nature Customer Service Centre GmbH** (the **Licensor**). By clicking 'accept' and completing the transaction for the material (**Licensed Material**), you also confirm your acceptance of these terms and conditions.

1. **Grant of License**

    1. The Licensor grants you a personal, non-exclusive, non-transferable, world-wide licence to reproduce the Licensed Material for the purpose specified in your order only. Licences are granted for the specific use requested in the order and for no other use, subject to the conditions below.

    2. The Licensor warrants that it has, to the best of its knowledge, the rights to license reuse of the Licensed Material. However, you should ensure that the material you are requesting is original to the Licensor and does not carry the copyright of another entity (as credited in the published version).

    3. If the credit line on any part of the material you have requested indicates that it was reprinted or adapted with permission from another source, then you should also seek permission from that source to reuse the material.

2. **Scope of Licence**

    1. You may only use the Licensed Content in the manner and to the extent permitted by these Ts&Cs and any applicable laws.

    2. A separate licence may be required for any additional use of the Licensed Material, e.g. where a licence has been purchased for print only use, separate permission must be obtained for electronic re-use. Similarly, a licence is only valid in the language selected and does not apply for editions in other languages unless additional translation rights have been granted separately in the licence. Any content owned by third parties are expressly excluded from the licence.

    3. Similarly, rights for additional components such as custom editions and derivatives require additional permission and may be subject to an additional fee. Please apply to Journalpermissions@springernature.com/bookpermissions@springernature.com for these rights.

    4. Where permission has been granted **free of charge** for material in print, permission may also be granted for any electronic version of that work,

provided that the material is incidental to your work as a whole and that the electronic version is essentially equivalent to, or substitutes for, the print version.

5. An alternative scope of licence may apply to signatories of the STM Permissions Guidelines, as amended from time to time.

Duration of Licence

1. A licence for is valid from the date of purchase ('Licence Date') at the end of the relevant period in the below table:

Scope of Licence	Duration of Licence
Post on a website	12 months
Presentations	12 months
Books and journals	Lifetime of the edition in the language purchased

Acknowledgement

1. The Licensor's permission must be acknowledged next to the Licenced Material in print. In electronic form, this acknowledgement must be visible at the same time as the figures/tables/illustrations or abstract, and must be hyperlinked to the journal/book's homepage. Our required acknowledgement format is in the Appendix below.

Restrictions on use

1. Use of the Licensed Material may be permitted for incidental promotional use and minor editing privileges e.g. minor adaptations of single figures, changes of format, colour and/or style where the adaptation is credited as set out in Appendix 1 below. Any other changes including but not limited to, cropping, adapting, omitting material that affect the meaning, intention or moral rights of the author are strictly prohibited.

2. You must not use any Licensed Material as part of any design or trademark.

3. Licensed Material may be used in Open Access Publications (OAP) before publication by Springer Nature, but any Licensed Material must be removed from OAP sites prior to final publication.

Ownership of Rights

1. Licensed Material remains the property of either Licensor or the relevant third party and any rights not explicitly granted herein are expressly reserved.

Warranty

IN NO EVENT SHALL LICENSOR BE LIABLE TO YOU OR ANY OTHER PARTY OR ANY OTHER PERSON OR FOR ANY SPECIAL, CONSEQUENTIAL, INCIDENTAL OR INDIRECT DAMAGES, HOWEVER CAUSED, ARISING OUT OF OR IN CONNECTION WITH THE DOWNLOADING, VIEWING OR USE OF THE MATERIALS REGARDLESS OF THE FORM OF ACTION, WHETHER FOR BREACH OF CONTRACT, BREACH OF WARRANTY, TORT, NEGLIGENCE, INFRINGEMENT OR OTHERWISE (INCLUDING, WITHOUT LIMITATION, DAMAGES BASED ON LOSS OF PROFITS, DATA, FILES, USE, BUSINESS OPPORTUNITY OR CLAIMS OF THIRD PARTIES), AND
WHETHER OR NOT THE PARTY HAS BEEN ADVISED OF THE POSSIBILITY OF SUCH DAMAGES. THIS LIMITATION SHALL APPLY NOTWITHSTANDING ANY FAILURE OF ESSENTIAL PURPOSE OF ANY LIMITED REMEDY PROVIDED HEREIN.

Limitations

1. ***BOOKS ONLY:***Where '**reuse in a dissertation/thesis**' has been selected the following terms apply: Print rights of the final author's accepted manuscript (for clarity, NOT the published version) for up to 100 copies, electronic rights for use only on a personal website or institutional repository as defined by the Sherpa guideline (www.sherpa.ac.uk/romeo/).

Termination and Cancellation

1. Licences will expire after the period shown in Clause 3 (above).

2. Licensee reserves the right to terminate the Licence in the event that payment is not received in full or if there has been a breach of this agreement by you.

Appendix 1 — Acknowledgements:

For Journal Content:
Reprinted by permission from [**the Licensor**]: [**Journal Publisher** (e.g. Nature/Springer/Palgrave)] [**JOURNAL NAME**] [**REFERENCE CITATION** (Article name, Author(s) Name), [**COPYRIGHT**] (year of publication)
For **Advance Online Publication papers:**
Reprinted by permission from [**the Licensor**]: [**Journal Publisher** (e.g. Nature/Springer/Palgrave)] [**JOURNAL NAME**] [**REFERENCE CITATION** (Article name, Author(s) Name), [**COPYRIGHT**] (year of publication), advance online publication, day month year (doi: 10.1038/sj.[JOURNAL ACRONYM].)
For Adaptations/Translations:
Adapted/Translated by permission from [**the Licensor**]: [**Journal Publisher** (e.g. Nature/Springer/Palgrave)] [**JOURNAL NAME**] [**REFERENCE CITATION** (Article name, Author(s) Name), [**COPYRIGHT**] (year of publication)
Note: For any republication from the British Journal of Cancer, the following credit line style applies:
Reprinted/adapted/translated by permission from [**the Licensor**]: on behalf of Cancer Research UK: : [**Journal Publisher** (e.g. Nature/Springer/Palgrave)] [**JOURNAL NAME**] [**REFERENCE CITATION** (Article name, Author(s) Name), [**COPYRIGHT]** (year of publication)
For **Advance Online Publication** papers:
Reprinted by permission from The [**the Licensor**]: on behalf of Cancer Research UK: [**Journal Publisher** (e.g. Nature/Springer/Palgrave)] [**JOURNAL NAME**] [**REFERENCE CITATION** (Article name, Author(s) Name), [**COPYRIGHT**] (year of publication), advance online publication, day month year (doi: 10.1038/sj.[JOURNAL ACRONYM])
For Book content:
Reprinted/adapted by permission from [**the Licensor**]: [**Book Publisher** (e.g. Palgrave Macmillan, Springer etc) [**Book Title**] by [**Book author**(s)] [**COPYRIGHT**] (year of publication)

Other Conditions:

Version 1.2

Questions? customercare@copyright.com or +1-855-239-3415 (toll free in the US) or +1-978-646-2777.

SPRINGER NATURE LICENSE
TERMS AND CONDITIONS

Jan 25, 2020

This Agreement between Mara A Pop ("You") and Springer Nature ("Springer Nature") consists of your license details and the terms and conditions provided by Springer Nature and Copyright Clearance Center.

License Number	4745350311442
License date	Jan 10, 2020
Licensed Content Publisher	Springer Nature
Licensed Content Publication	Nature Reviews Molecular Cell Biology
Licensed Content Title	Integrin signalling during tumour progression
Licensed Content Author	Wenjun Guo et al
Licensed Content Date	Oct 1, 2004
Type of Use	Thesis/Dissertation
Requestor type	non-commercial (non-profit)
Format	print and electronic
Portion	figures/tables/illustrations
Number of figures/tables/illustrations	1
High-res required	no
Will you be translating?	no
Circulation/distribution	50000 or greater
Author of this Springer Nature content	no
Title	Exploring combinatorial microRNA therapy for chronic wound healing
Institution name	n/a
Expected presentation date	Jan 2020
Portions	Box 1
Requestor Location	Mara A Pop Prince Consort Road Royal School of Mines London, London SW7 2BP United Kingdom Attn: Mara A Pop
Total	0.00 GBP
Terms and Conditions	

Springer Nature Customer Service Centre GmbH
Terms and Conditions

This agreement sets out the terms and conditions of the licence (the **Licence**) between you and **Springer Nature Customer Service Centre GmbH** (the **Licensor**). By clicking 'accept' and completing the transaction for the material (**Licensed Material**), you also confirm your acceptance of these terms and conditions.

1. **Grant of License**

    1. The Licensor grants you a personal, non-exclusive, non-transferable, world-wide licence to reproduce the Licensed Material for the purpose specified in your order only. Licences are granted for the specific use requested in the order and for no other use, subject to the conditions below.

    2. The Licensor warrants that it has, to the best of its knowledge, the rights to license reuse of the Licensed Material. However, you should ensure that the material you are requesting is original to the Licensor and does not carry the copyright of another entity (as credited in the published version).

    3. If the credit line on any part of the material you have requested indicates that it was reprinted or adapted with permission from another source, then you should also seek permission from that source to reuse the material.

2. **Scope of Licence**

    1. You may only use the Licensed Content in the manner and to the extent permitted by these Ts&Cs and any applicable laws.

    2. A separate licence may be required for any additional use of the Licensed Material, e.g. where a licence has been purchased for print only use, separate permission must be obtained for electronic re-use. Similarly, a licence is only valid in the language selected and does not apply for editions in other languages unless additional translation rights have been granted separately in the licence. Any content owned by third parties are expressly excluded from the licence.

    3. Similarly, rights for additional components such as custom editions and derivatives require additional permission and may be subject to an additional fee. Please apply to Journalpermissions@springernature.com/bookpermissions@springernature.com for these rights.

    4. Where permission has been granted **free of charge** for material in print, permission may also be granted for any electronic version of that work,

provided that the material is incidental to your work as a whole and that the electronic version is essentially equivalent to, or substitutes for, the print version.

5. An alternative scope of licence may apply to signatories of the STM Permissions Guidelines, as amended from time to time.

Duration of Licence

1. A licence for is valid from the date of purchase ('Licence Date') at the end of the relevant period in the below table:

Scope of Licence	Duration of Licence
Post on a website	12 months
Presentations	12 months
Books and journals	Lifetime of the edition in the language purchased

Acknowledgement

1. The Licensor's permission must be acknowledged next to the Licenced Material in print. In electronic form, this acknowledgement must be visible at the same time as the figures/tables/illustrations or abstract, and must be hyperlinked to the journal/book's homepage. Our required acknowledgement format is in the Appendix below.

Restrictions on use

1. Use of the Licensed Material may be permitted for incidental promotional use and minor editing privileges e.g. minor adaptations of single figures, changes of format, colour and/or style where the adaptation is credited as set out in Appendix 1 below. Any other changes including but not limited to, cropping, adapting, omitting material that affect the meaning, intention or moral rights of the author are strictly prohibited.

2. You must not use any Licensed Material as part of any design or trademark.

3. Licensed Material may be used in Open Access Publications (OAP) before publication by Springer Nature, but any Licensed Material must be removed from OAP sites prior to final publication.

Ownership of Rights

1. Licensed Material remains the property of either Licensor or the relevant third party and any rights not explicitly granted herein are expressly reserved.

Warranty

IN NO EVENT SHALL LICENSOR BE LIABLE TO YOU OR ANY OTHER PARTY OR ANY OTHER PERSON OR FOR ANY SPECIAL, CONSEQUENTIAL, INCIDENTAL OR INDIRECT DAMAGES, HOWEVER CAUSED, ARISING OUT OF OR IN CONNECTION WITH THE DOWNLOADING, VIEWING OR USE OF THE MATERIALS REGARDLESS OF THE FORM OF ACTION, WHETHER FOR BREACH OF CONTRACT, BREACH OF WARRANTY, TORT, NEGLIGENCE, INFRINGEMENT OR OTHERWISE (INCLUDING, WITHOUT LIMITATION, DAMAGES BASED ON LOSS OF PROFITS, DATA, FILES, USE, BUSINESS OPPORTUNITY OR CLAIMS OF THIRD PARTIES), AND
WHETHER OR NOT THE PARTY HAS BEEN ADVISED OF THE POSSIBILITY OF SUCH DAMAGES. THIS LIMITATION SHALL APPLY NOTWITHSTANDING ANY FAILURE OF ESSENTIAL PURPOSE OF ANY LIMITED REMEDY PROVIDED HEREIN.

Limitations

1. ***BOOKS ONLY:***Where '**reuse in a dissertation/thesis**' has been selected the following terms apply: Print rights of the final author's accepted manuscript (for clarity, NOT the published version) for up to 100 copies, electronic rights for use only on a personal website or institutional repository as defined by the Sherpa guideline (www.sherpa.ac.uk/romeo/).

Termination and Cancellation

1. Licences will expire after the period shown in Clause 3 (above).

2. Licensee reserves the right to terminate the Licence in the event that payment is not received in full or if there has been a breach of this agreement by you.

Appendix 1 — Acknowledgements:

For Journal Content:
Reprinted by permission from [**the Licensor**]: [**Journal Publisher** (e.g. Nature/Springer/Palgrave)] [**JOURNAL NAME**] [**REFERENCE CITATION** (Article name, Author(s) Name), [**COPYRIGHT**] (year of publication)
For **Advance Online Publication papers:**
Reprinted by permission from [**the Licensor**]: [**Journal Publisher** (e.g. Nature/Springer/Palgrave)] [**JOURNAL NAME**] [**REFERENCE CITATION** (Article name, Author(s) Name), [**COPYRIGHT**] (year of publication), advance online publication, day month year (doi: 10.1038/sj.[JOURNAL ACRONYM].)
For Adaptations/Translations:
Adapted/Translated by permission from [**the Licensor**]: [**Journal Publisher** (e.g. Nature/Springer/Palgrave)] [**JOURNAL NAME**] [**REFERENCE CITATION** (Article name, Author(s) Name), [**COPYRIGHT**] (year of publication)
Note: For any republication from the British Journal of Cancer, the following credit line style applies:
Reprinted/adapted/translated by permission from [**the Licensor**]: on behalf of Cancer Research UK: : [**Journal Publisher** (e.g. Nature/Springer/Palgrave)] [**JOURNAL NAME**] [**REFERENCE CITATION** (Article name, Author(s) Name), [**COPYRIGHT]** (year of publication)
For **Advance Online Publication** papers:
Reprinted by permission from The [**the Licensor**]: on behalf of Cancer Research UK: [**Journal Publisher** (e.g. Nature/Springer/Palgrave)] [**JOURNAL NAME**] [**REFERENCE CITATION** (Article name, Author(s) Name), [**COPYRIGHT**] (year of publication), advance online publication, day month year (doi: 10.1038/sj.[JOURNAL ACRONYM])
For Book content:
Reprinted/adapted by permission from [**the Licensor**]: [**Book Publisher** (e.g. Palgrave Macmillan, Springer etc) [**Book Title**] by [**Book author**(s)] [**COPYRIGHT**] (year of publication)

Other Conditions:

Version 1.2

Questions? customercare@copyright.com or +1-855-239-3415 (toll free in the US) or +1-978-646-2777.

ELSEVIER LICENSE
TERMS AND CONDITIONS
Jan 25, 2020

This Agreement between Mara A Pop ("You") and Elsevier ("Elsevier") consists of your license details and the terms and conditions provided by Elsevier and Copyright Clearance Center.

License Number	4745461076170
License date	Jan 10, 2020
Licensed Content Publisher	Elsevier
Licensed Content Publication	Biochimica et Biophysica Acta (BBA) - Gene Regulatory Mechanisms
Licensed Content Title	Interplay between microRNAs and the epigenetic machinery: An intricate network
Licensed Content Author	Marilena V. Iorio,Claudia Piovan,Carlo M. Croce
Licensed Content Date	October–December 2010
Licensed Content Volume	1799
Licensed Content Issue	10-12
Licensed Content Pages	8
Start Page	694
End Page	701
Type of Use	reuse in a thesis/dissertation
Portion	figures/tables/illustrations
Number of figures/tables/illustrations	1
Format	both print and electronic
Are you the author of this Elsevier article?	No
Will you be translating?	No
Title	Exploring combinatorial microRNA therapy for chronic wound healing
Institution name	Imperial College London
Expected presentation date	Jan 2020
Portions	Figure 1
Requestor Location	Mara A Pop Prince Consort Road Royal School of Mines London, London SW7 2BP

	United Kingdom Attn: Mara A Pop
Publisher Tax ID	GB 494 6272 12
Total	0.00 GBP

Terms and Conditions

INTRODUCTION

1. The publisher for this copyrighted material is Elsevier. By clicking "accept" in connection with completing this licensing transaction, you agree that the following terms and conditions apply to this transaction (along with the Billing and Payment terms and conditions established by Copyright Clearance Center, Inc. ("CCC"), at the time that you opened your Rightslink account and that are available at any time at http://myaccount.copyright.com).

GENERAL TERMS

2. Elsevier hereby grants you permission to reproduce the aforementioned material subject to the terms and conditions indicated.

3. Acknowledgement: If any part of the material to be used (for example, figures) has appeared in our publication with credit or acknowledgement to another source, permission must also be sought from that source. If such permission is not obtained then that material may not be included in your publication/copies. Suitable acknowledgement to the source must be made, either as a footnote or in a reference list at the end of your publication, as follows:

"Reprinted from Publication title, Vol /edition number, Author(s), Title of article / title of chapter, Pages No., Copyright (Year), with permission from Elsevier [OR APPLICABLE SOCIETY COPYRIGHT OWNER]." Also Lancet special credit - "Reprinted from The Lancet, Vol. number, Author(s), Title of article, Pages No., Copyright (Year), with permission from Elsevier."

4. Reproduction of this material is confined to the purpose and/or media for which permission is hereby given.

5. Altering/Modifying Material: Not Permitted. However figures and illustrations may be altered/adapted minimally to serve your work. Any other abbreviations, additions, deletions and/or any other alterations shall be made only with prior written authorization of Elsevier Ltd. (Please contact Elsevier at permissions@elsevier.com). No modifications can be made to any Lancet figures/tables and they must be reproduced in full.

6. If the permission fee for the requested use of our material is waived in this instance, please be advised that your future requests for Elsevier materials may attract a fee.

7. Reservation of Rights: Publisher reserves all rights not specifically granted in the combination of (i) the license details provided by you and accepted in the course of this

licensing transaction, (ii) these terms and conditions and (iii) CCC's Billing and Payment terms and conditions.

8. License Contingent Upon Payment: While you may exercise the rights licensed immediately upon issuance of the license at the end of the licensing process for the transaction, provided that you have disclosed complete and accurate details of your proposed use, no license is finally effective unless and until full payment is received from you (either by publisher or by CCC) as provided in CCC's Billing and Payment terms and conditions. If full payment is not received on a timely basis, then any license preliminarily granted shall be deemed automatically revoked and shall be void as if never granted. Further, in the event that you breach any of these terms and conditions or any of CCC's Billing and Payment terms and conditions, the license is automatically revoked and shall be void as if never granted. Use of materials as described in a revoked license, as well as any use of the materials beyond the scope of an unrevoked license, may constitute copyright infringement and publisher reserves the right to take any and all action to protect its copyright in the materials.

9. Warranties: Publisher makes no representations or warranties with respect to the licensed material.

10. Indemnity: You hereby indemnify and agree to hold harmless publisher and CCC, and their respective officers, directors, employees and agents, from and against any and all claims arising out of your use of the licensed material other than as specifically authorized pursuant to this license.

11. No Transfer of License: This license is personal to you and may not be sublicensed, assigned, or transferred by you to any other person without publisher's written permission.

12. No Amendment Except in Writing: This license may not be amended except in a writing signed by both parties (or, in the case of publisher, by CCC on publisher's behalf).

13. Objection to Contrary Terms: Publisher hereby objects to any terms contained in any purchase order, acknowledgment, check endorsement or other writing prepared by you, which terms are inconsistent with these terms and conditions or CCC's Billing and Payment terms and conditions. These terms and conditions, together with CCC's Billing and Payment terms and conditions (which are incorporated herein), comprise the entire agreement between you and publisher (and CCC) concerning this licensing transaction. In the event of any conflict between your obligations established by these terms and conditions and those established by CCC's Billing and Payment terms and conditions, these terms and conditions shall control.

14. Revocation: Elsevier or Copyright Clearance Center may deny the permissions described in this License at their sole discretion, for any reason or no reason, with a full refund payable to you. Notice of such denial will be made using the contact information provided by you. Failure to receive such notice will not alter or invalidate the denial. In no event will Elsevier or Copyright Clearance Center be responsible or liable for any costs,

expenses or damage incurred by you as a result of a denial of your permission request, other than a refund of the amount(s) paid by you to Elsevier and/or Copyright Clearance Center for denied permissions.

LIMITED LICENSE

The following terms and conditions apply only to specific license types:

15. **Translation**: This permission is granted for non-exclusive world **English** rights only unless your license was granted for translation rights. If you licensed translation rights you may only translate this content into the languages you requested. A professional translator must perform all translations and reproduce the content word for word preserving the integrity of the article.

16. **Posting licensed content on any Website**: The following terms and conditions apply as follows: Licensing material from an Elsevier journal: All content posted to the web site must maintain the copyright information line on the bottom of each image; A hyper-text must be included to the Homepage of the journal from which you are licensing at http://www.sciencedirect.com/science/journal/xxxxx or the Elsevier homepage for books at http://www.elsevier.com; Central Storage: This license does not include permission for a scanned version of the material to be stored in a central repository such as that provided by Heron/XanEdu.

Licensing material from an Elsevier book: A hyper-text link must be included to the Elsevier homepage at http://www.elsevier.com . All content posted to the web site must maintain the copyright information line on the bottom of each image.

Posting licensed content on Electronic reserve: In addition to the above the following clauses are applicable: The web site must be password-protected and made available only to bona fide students registered on a relevant course. This permission is granted for 1 year only. You may obtain a new license for future website posting.

17. **For journal authors:** the following clauses are applicable in addition to the above:

Preprints:

A preprint is an author's own write-up of research results and analysis, it has not been peer-reviewed, nor has it had any other value added to it by a publisher (such as formatting, copyright, technical enhancement etc.).

Authors can share their preprints anywhere at any time. Preprints should not be added to or enhanced in any way in order to appear more like, or to substitute for, the final versions of articles however authors can update their preprints on arXiv or RePEc with their Accepted Author Manuscript (see below).

If accepted for publication, we encourage authors to link from the preprint to their formal publication via its DOI. Millions of researchers have access to the formal publications on ScienceDirect, and so links will help users to find, access, cite and use the best available version. Please note that Cell Press, The Lancet and some society-owned have different preprint policies. Information on these policies is available on the journal homepage.

Accepted Author Manuscripts: An accepted author manuscript is the manuscript of an article that has been accepted for publication and which typically includes author-incorporated changes suggested during submission, peer review and editor-author communications.

Authors can share their accepted author manuscript:

- immediately
    - via their non-commercial person homepage or blog
    - by updating a preprint in arXiv or RePEc with the accepted manuscript
    - via their research institute or institutional repository for internal institutional uses or as part of an invitation-only research collaboration work-group
    - directly by providing copies to their students or to research collaborators for their personal use
    - for private scholarly sharing as part of an invitation-only work group on commercial sites with which Elsevier has an agreement
- After the embargo period
    - via non-commercial hosting platforms such as their institutional repository
    - via commercial sites with which Elsevier has an agreement

In all cases accepted manuscripts should:

- link to the formal publication via its DOI
- bear a CC-BY-NC-ND license - this is easy to do
- if aggregated with other manuscripts, for example in a repository or other site, be shared in alignment with our hosting policy not be added to or enhanced in any way to appear more like, or to substitute for, the published journal article.

Published journal article (JPA): A published journal article (PJA) is the definitive final record of published research that appears or will appear in the journal and embodies all value-adding publishing activities including peer review co-ordination, copy-editing, formatting, (if relevant) pagination and online enrichment.

Policies for sharing publishing journal articles differ for subscription and gold open access articles:

Subscription Articles: If you are an author, please share a link to your article rather than the full-text. Millions of researchers have access to the formal publications on

ScienceDirect, and so links will help your users to find, access, cite, and use the best available version.

Theses and dissertations which contain embedded PJAs as part of the formal submission can be posted publicly by the awarding institution with DOI links back to the formal publications on ScienceDirect.

If you are affiliated with a library that subscribes to ScienceDirect you have additional private sharing rights for others' research accessed under that agreement. This includes use for classroom teaching and internal training at the institution (including use in course packs and courseware programs), and inclusion of the article for grant funding purposes.

Gold Open Access Articles: May be shared according to the author-selected end-user license and should contain a CrossMark logo, the end user license, and a DOI link to the formal publication on ScienceDirect.

Please refer to Elsevier's posting policy for further information.

18. **For book authors** the following clauses are applicable in addition to the above: Authors are permitted to place a brief summary of their work online only. You are not allowed to download and post the published electronic version of your chapter, nor may you scan the printed edition to create an electronic version. **Posting to a repository:** Authors are permitted to post a summary of their chapter only in their institution's repository.

19. **Thesis/Dissertation**: If your license is for use in a thesis/dissertation your thesis may be submitted to your institution in either print or electronic form. Should your thesis be published commercially, please reapply for permission. These requirements include permission for the Library and Archives of Canada to supply single copies, on demand, of the complete thesis and include permission for Proquest/UMI to supply single copies, on demand, of the complete thesis. Should your thesis be published commercially, please reapply for permission. Theses and dissertations which contain embedded PJAs as part of the formal submission can be posted publicly by the awarding institution with DOI links back to the formal publications on ScienceDirect.

Elsevier Open Access Terms and Conditions

You can publish open access with Elsevier in hundreds of open access journals or in nearly 2000 established subscription journals that support open access publishing. Permitted third party re-use of these open access articles is defined by the author's choice of Creative Commons user license. See our open access license policy for more information.

Terms & Conditions applicable to all Open Access articles published with Elsevier:

Any reuse of the article must not represent the author as endorsing the adaptation of the article nor should the article be modified in such a way as to damage the author's honour or reputation. If any changes have been made, such changes must be clearly indicated.

The author(s) must be appropriately credited and we ask that you include the end user license and a DOI link to the formal publication on ScienceDirect.

If any part of the material to be used (for example, figures) has appeared in our publication with credit or acknowledgement to another source it is the responsibility of the user to ensure their reuse complies with the terms and conditions determined by the rights holder.

Additional Terms & Conditions applicable to each Creative Commons user license:

CC BY: The CC-BY license allows users to copy, to create extracts, abstracts and new works from the Article, to alter and revise the Article and to make commercial use of the Article (including reuse and/or resale of the Article by commercial entities), provided the user gives appropriate credit (with a link to the formal publication through the relevant DOI), provides a link to the license, indicates if changes were made and the licensor is not represented as endorsing the use made of the work. The full details of the license are available at http://creativecommons.org/licenses/by/4.0.

CC BY NC SA: The CC BY-NC-SA license allows users to copy, to create extracts, abstracts and new works from the Article, to alter and revise the Article, provided this is not done for commercial purposes, and that the user gives appropriate credit (with a link to the formal publication through the relevant DOI), provides a link to the license, indicates if changes were made and the licensor is not represented as endorsing the use made of the work. Further, any new works must be made available on the same conditions. The full details of the license are available at http://creativecommons.org/licenses/by-nc-sa/4.0.

CC BY NC ND: The CC BY-NC-ND license allows users to copy and distribute the Article, provided this is not done for commercial purposes and further does not permit distribution of the Article if it is changed or edited in any way, and provided the user gives appropriate credit (with a link to the formal publication through the relevant DOI), provides a link to the license, and that the licensor is not represented as endorsing the use made of the work. The full details of the license are available at http://creativecommons.org/licenses/by-nc-nd/4.0. Any commercial reuse of Open Access articles published with a CC BY NC SA or CC BY NC ND license requires permission from Elsevier and will be subject to a fee.

Commercial reuse includes:

- Associating advertising with the full text of the Article
- Charging fees for document delivery or access
- Article aggregation

- Systematic distribution via e-mail lists or share buttons

Posting or linking by commercial companies for use by customers of those companies.

20. **Other Conditions**:

v1.9

Questions? customercare@copyright.com or +1-855-239-3415 (toll free in the US) or +1-978-646-2777.

ELSEVIER LICENSE
TERMS AND CONDITIONS
Jan 25, 2020

This Agreement between Mara A Pop ("You") and Elsevier ("Elsevier") consists of your license details and the terms and conditions provided by Elsevier and Copyright Clearance Center.

License Number	4745470973921
License date	Jan 10, 2020
Licensed Content Publisher	Elsevier
Licensed Content Publication	Molecular Cell
Licensed Content Title	MicroRNA Targeting Specificity in Mammals: Determinants beyond Seed Pairing
Licensed Content Author	Andrew Grimson,Kyle Kai-How Farh,Wendy K. Johnston,Philip Garrett-Engele,Lee P. Lim,David P. Bartel
Licensed Content Date	Jul 6, 2007
Licensed Content Volume	27
Licensed Content Issue	1
Licensed Content Pages	15
Start Page	91
End Page	105
Type of Use	reuse in a thesis/dissertation
Portion	figures/tables/illustrations
Number of figures/tables/illustrations	3
Format	both print and electronic
Are you the author of this Elsevier article?	No
Will you be translating?	No
Title	Exploring combinatorial microRNA therapy for chronic wound healing
Institution name	Imperial College London
Expected presentation date	Jan 2020
Portions	Figure 1, Figure 2, Figure 5
Requestor Location	Mara A Pop Prince Consort Road Royal School of Mines

	London, London SW7 2BP United Kingdom Attn: Mara A Pop
Publisher Tax ID	GB 494 6272 12
Total	0.00 GBP

Terms and Conditions

INTRODUCTION

1. The publisher for this copyrighted material is Elsevier. By clicking "accept" in connection with completing this licensing transaction, you agree that the following terms and conditions apply to this transaction (along with the Billing and Payment terms and conditions established by Copyright Clearance Center, Inc. ("CCC"), at the time that you opened your Rightslink account and that are available at any time at http://myaccount.copyright.com).

GENERAL TERMS

2. Elsevier hereby grants you permission to reproduce the aforementioned material subject to the terms and conditions indicated.

3. Acknowledgement: If any part of the material to be used (for example, figures) has appeared in our publication with credit or acknowledgement to another source, permission must also be sought from that source. If such permission is not obtained then that material may not be included in your publication/copies. Suitable acknowledgement to the source must be made, either as a footnote or in a reference list at the end of your publication, as follows:

"Reprinted from Publication title, Vol /edition number, Author(s), Title of article / title of chapter, Pages No., Copyright (Year), with permission from Elsevier [OR APPLICABLE SOCIETY COPYRIGHT OWNER]." Also Lancet special credit - "Reprinted from The Lancet, Vol. number, Author(s), Title of article, Pages No., Copyright (Year), with permission from Elsevier."

4. Reproduction of this material is confined to the purpose and/or media for which permission is hereby given.

5. Altering/Modifying Material: Not Permitted. However figures and illustrations may be altered/adapted minimally to serve your work. Any other abbreviations, additions, deletions and/or any other alterations shall be made only with prior written authorization of Elsevier Ltd. (Please contact Elsevier at permissions@elsevier.com). No modifications can be made to any Lancet figures/tables and they must be reproduced in full.

6. If the permission fee for the requested use of our material is waived in this instance, please be advised that your future requests for Elsevier materials may attract a fee.

7. Reservation of Rights: Publisher reserves all rights not specifically granted in the combination of (i) the license details provided by you and accepted in the course of this licensing transaction, (ii) these terms and conditions and (iii) CCC's Billing and Payment terms and conditions.

8. License Contingent Upon Payment: While you may exercise the rights licensed immediately upon issuance of the license at the end of the licensing process for the transaction, provided that you have disclosed complete and accurate details of your proposed use, no license is finally effective unless and until full payment is received from you (either by publisher or by CCC) as provided in CCC's Billing and Payment terms and conditions. If full payment is not received on a timely basis, then any license preliminarily granted shall be deemed automatically revoked and shall be void as if never granted. Further, in the event that you breach any of these terms and conditions or any of CCC's Billing and Payment terms and conditions, the license is automatically revoked and shall be void as if never granted. Use of materials as described in a revoked license, as well as any use of the materials beyond the scope of an unrevoked license, may constitute copyright infringement and publisher reserves the right to take any and all action to protect its copyright in the materials.

9. Warranties: Publisher makes no representations or warranties with respect to the licensed material.

10. Indemnity: You hereby indemnify and agree to hold harmless publisher and CCC, and their respective officers, directors, employees and agents, from and against any and all claims arising out of your use of the licensed material other than as specifically authorized pursuant to this license.

11. No Transfer of License: This license is personal to you and may not be sublicensed, assigned, or transferred by you to any other person without publisher's written permission.

12. No Amendment Except in Writing: This license may not be amended except in a writing signed by both parties (or, in the case of publisher, by CCC on publisher's behalf).

13. Objection to Contrary Terms: Publisher hereby objects to any terms contained in any purchase order, acknowledgment, check endorsement or other writing prepared by you, which terms are inconsistent with these terms and conditions or CCC's Billing and Payment terms and conditions. These terms and conditions, together with CCC's Billing and Payment terms and conditions (which are incorporated herein), comprise the entire agreement between you and publisher (and CCC) concerning this licensing transaction. In the event of any conflict between your obligations established by these terms and conditions and those established by CCC's Billing and Payment terms and conditions, these terms and conditions shall control.

14. Revocation: Elsevier or Copyright Clearance Center may deny the permissions described in this License at their sole discretion, for any reason or no reason, with a full refund payable to you. Notice of such denial will be made using the contact information

provided by you. Failure to receive such notice will not alter or invalidate the denial. In no event will Elsevier or Copyright Clearance Center be responsible or liable for any costs, expenses or damage incurred by you as a result of a denial of your permission request, other than a refund of the amount(s) paid by you to Elsevier and/or Copyright Clearance Center for denied permissions.

LIMITED LICENSE

The following terms and conditions apply only to specific license types:

15. **Translation**: This permission is granted for non-exclusive world **English** rights only unless your license was granted for translation rights. If you licensed translation rights you may only translate this content into the languages you requested. A professional translator must perform all translations and reproduce the content word for word preserving the integrity of the article.

16. **Posting licensed content on any Website**: The following terms and conditions apply as follows: Licensing material from an Elsevier journal: All content posted to the web site must maintain the copyright information line on the bottom of each image; A hyper-text must be included to the Homepage of the journal from which you are licensing at http://www.sciencedirect.com/science/journal/xxxxx or the Elsevier homepage for books at http://www.elsevier.com; Central Storage: This license does not include permission for a scanned version of the material to be stored in a central repository such as that provided by Heron/XanEdu.

Licensing material from an Elsevier book: A hyper-text link must be included to the Elsevier homepage at http://www.elsevier.com . All content posted to the web site must maintain the copyright information line on the bottom of each image.

Posting licensed content on Electronic reserve: In addition to the above the following clauses are applicable: The web site must be password-protected and made available only to bona fide students registered on a relevant course. This permission is granted for 1 year only. You may obtain a new license for future website posting.

17. **For journal authors:** the following clauses are applicable in addition to the above:

Preprints:

A preprint is an author's own write-up of research results and analysis, it has not been peer-reviewed, nor has it had any other value added to it by a publisher (such as formatting, copyright, technical enhancement etc.).

Authors can share their preprints anywhere at any time. Preprints should not be added to or enhanced in any way in order to appear more like, or to substitute for, the final

versions of articles however authors can update their preprints on arXiv or RePEc with their Accepted Author Manuscript (see below).

If accepted for publication, we encourage authors to link from the preprint to their formal publication via its DOI. Millions of researchers have access to the formal publications on ScienceDirect, and so links will help users to find, access, cite and use the best available version. Please note that Cell Press, The Lancet and some society-owned have different preprint policies. Information on these policies is available on the journal homepage.

Accepted Author Manuscripts: An accepted author manuscript is the manuscript of an article that has been accepted for publication and which typically includes author-incorporated changes suggested during submission, peer review and editor-author communications.

Authors can share their accepted author manuscript:

- immediately
    - via their non-commercial person homepage or blog
    - by updating a preprint in arXiv or RePEc with the accepted manuscript
    - via their research institute or institutional repository for internal institutional uses or as part of an invitation-only research collaboration work-group
    - directly by providing copies to their students or to research collaborators for their personal use
    - for private scholarly sharing as part of an invitation-only work group on commercial sites with which Elsevier has an agreement
- After the embargo period
    - via non-commercial hosting platforms such as their institutional repository
    - via commercial sites with which Elsevier has an agreement

In all cases accepted manuscripts should:

- link to the formal publication via its DOI
- bear a CC-BY-NC-ND license - this is easy to do
- if aggregated with other manuscripts, for example in a repository or other site, be shared in alignment with our hosting policy not be added to or enhanced in any way to appear more like, or to substitute for, the published journal article.

Published journal article (JPA): A published journal article (PJA) is the definitive final record of published research that appears or will appear in the journal and embodies all value-adding publishing activities including peer review co-ordination, copy-editing, formatting, (if relevant) pagination and online enrichment.

Policies for sharing publishing journal articles differ for subscription and gold open access articles:

Subscription Articles: If you are an author, please share a link to your article rather than the full-text. Millions of researchers have access to the formal publications on ScienceDirect, and so links will help your users to find, access, cite, and use the best available version.

Theses and dissertations which contain embedded PJAs as part of the formal submission can be posted publicly by the awarding institution with DOI links back to the formal publications on ScienceDirect.

If you are affiliated with a library that subscribes to ScienceDirect you have additional private sharing rights for others' research accessed under that agreement. This includes use for classroom teaching and internal training at the institution (including use in course packs and courseware programs), and inclusion of the article for grant funding purposes.

Gold Open Access Articles: May be shared according to the author-selected end-user license and should contain a CrossMark logo, the end user license, and a DOI link to the formal publication on ScienceDirect.

Please refer to Elsevier's posting policy for further information.

18. **For book authors** the following clauses are applicable in addition to the above: Authors are permitted to place a brief summary of their work online only. You are not allowed to download and post the published electronic version of your chapter, nor may you scan the printed edition to create an electronic version. **Posting to a repository:** Authors are permitted to post a summary of their chapter only in their institution's repository.

19. **Thesis/Dissertation**: If your license is for use in a thesis/dissertation your thesis may be submitted to your institution in either print or electronic form. Should your thesis be published commercially, please reapply for permission. These requirements include permission for the Library and Archives of Canada to supply single copies, on demand, of the complete thesis and include permission for Proquest/UMI to supply single copies, on demand, of the complete thesis. Should your thesis be published commercially, please reapply for permission. Theses and dissertations which contain embedded PJAs as part of the formal submission can be posted publicly by the awarding institution with DOI links back to the formal publications on ScienceDirect.

Elsevier Open Access Terms and Conditions

You can publish open access with Elsevier in hundreds of open access journals or in nearly 2000 established subscription journals that support open access publishing. Permitted third party re-use of these open access articles is defined by the author's choice of Creative Commons user license. See our open access license policy for more information.

Terms & Conditions applicable to all Open Access articles published with Elsevier:

Any reuse of the article must not represent the author as endorsing the adaptation of the article nor should the article be modified in such a way as to damage the author's honour or reputation. If any changes have been made, such changes must be clearly indicated.

The author(s) must be appropriately credited and we ask that you include the end user license and a DOI link to the formal publication on ScienceDirect.

If any part of the material to be used (for example, figures) has appeared in our publication with credit or acknowledgement to another source it is the responsibility of the user to ensure their reuse complies with the terms and conditions determined by the rights holder.

Additional Terms & Conditions applicable to each Creative Commons user license:

CC BY: The CC-BY license allows users to copy, to create extracts, abstracts and new works from the Article, to alter and revise the Article and to make commercial use of the Article (including reuse and/or resale of the Article by commercial entities), provided the user gives appropriate credit (with a link to the formal publication through the relevant DOI), provides a link to the license, indicates if changes were made and the licensor is not represented as endorsing the use made of the work. The full details of the license are available at http://creativecommons.org/licenses/by/4.0.

CC BY NC SA: The CC BY-NC-SA license allows users to copy, to create extracts, abstracts and new works from the Article, to alter and revise the Article, provided this is not done for commercial purposes, and that the user gives appropriate credit (with a link to the formal publication through the relevant DOI), provides a link to the license, indicates if changes were made and the licensor is not represented as endorsing the use made of the work. Further, any new works must be made available on the same conditions. The full details of the license are available at http://creativecommons.org/licenses/by-nc-sa/4.0.

CC BY NC ND: The CC BY-NC-ND license allows users to copy and distribute the Article, provided this is not done for commercial purposes and further does not permit distribution of the Article if it is changed or edited in any way, and provided the user gives appropriate credit (with a link to the formal publication through the relevant DOI), provides a link to the license, and that the licensor is not represented as endorsing the use made of the work. The full details of the license are available at http://creativecommons.org/licenses/by-nc-nd/4.0. Any commercial reuse of Open Access articles published with a CC BY NC SA or CC BY NC ND license requires permission from Elsevier and will be subject to a fee.

Commercial reuse includes:

- Associating advertising with the full text of the Article
- Charging fees for document delivery or access

- Article aggregation
- Systematic distribution via e-mail lists or share buttons

Posting or linking by commercial companies for use by customers of those companies.

20. **Other Conditions**:

v1.9

Questions? customercare@copyright.com or +1-855-239-3415 (toll free in the US) or +1-978-646-2777.

SPRINGER NATURE LICENSE
TERMS AND CONDITIONS

Jan 25, 2020

This Agreement between Mara A Pop ("You") and Springer Nature ("Springer Nature") consists of your license details and the terms and conditions provided by Springer Nature and Copyright Clearance Center.

License Number	4745480758998
License date	Jan 10, 2020
Licensed Content Publisher	Springer Nature
Licensed Content Publication	Nature
Licensed Content Title	Widespread changes in protein synthesis induced by microRNAs
Licensed Content Author	Matthias Selbach et al
Licensed Content Date	Jul 30, 2008
Type of Use	Thesis/Dissertation
Requestor type	academic/university or research institute
Format	print and electronic
Portion	figures/tables/illustrations
Number of figures/tables/illustrations	1
High-res required	no
Will you be translating?	no
Circulation/distribution	30 - 99
Author of this Springer Nature content	no
Title	Exploring combinatorial microRNA therapy for chronic wound healing
Institution name	Imperial College London
Expected presentation date	Jan 2020
Portions	Figure 4
Requestor Location	Mara A Pop Prince Consort Road Royal School of Mines London, London SW7 2BP United Kingdom Attn: Mara A Pop
Total	0.00 GBP

Terms and Conditions

Springer Nature Customer Service Centre GmbH
Terms and Conditions

This agreement sets out the terms and conditions of the licence (the **Licence**) between you and **Springer Nature Customer Service Centre GmbH** (the **Licensor**). By clicking 'accept' and completing the transaction for the material (**Licensed Material**), you also confirm your acceptance of these terms and conditions.

1. **Grant of License**

    1. The Licensor grants you a personal, non-exclusive, non-transferable, world-wide licence to reproduce the Licensed Material for the purpose specified in your order only. Licences are granted for the specific use requested in the order and for no other use, subject to the conditions below.

    2. The Licensor warrants that it has, to the best of its knowledge, the rights to license reuse of the Licensed Material. However, you should ensure that the material you are requesting is original to the Licensor and does not carry the copyright of another entity (as credited in the published version).

    3. If the credit line on any part of the material you have requested indicates that it was reprinted or adapted with permission from another source, then you should also seek permission from that source to reuse the material.

2. **Scope of Licence**

    1. You may only use the Licensed Content in the manner and to the extent permitted by these Ts&Cs and any applicable laws.

    2. A separate licence may be required for any additional use of the Licensed Material, e.g. where a licence has been purchased for print only use, separate permission must be obtained for electronic re-use. Similarly, a licence is only valid in the language selected and does not apply for editions in other languages unless additional translation rights have been granted separately in the licence. Any content owned by third parties are expressly excluded from the licence.

    3. Similarly, rights for additional components such as custom editions and derivatives require additional permission and may be subject to an additional fee. Please apply to Journalpermissions@springernature.com/bookpermissions@springernature.com for these rights.

    4. Where permission has been granted **free of charge** for material in print, permission may also be granted for any electronic version of that work,

provided that the material is incidental to your work as a whole and that the electronic version is essentially equivalent to, or substitutes for, the print version.

5. An alternative scope of licence may apply to signatories of the STM Permissions Guidelines, as amended from time to time.

Duration of Licence

1. A licence for is valid from the date of purchase ('Licence Date') at the end of the relevant period in the below table:

Scope of Licence	Duration of Licence
Post on a website	12 months
Presentations	12 months
Books and journals	Lifetime of the edition in the language purchased

Acknowledgement

1. The Licensor's permission must be acknowledged next to the Licenced Material in print. In electronic form, this acknowledgement must be visible at the same time as the figures/tables/illustrations or abstract, and must be hyperlinked to the journal/book's homepage. Our required acknowledgement format is in the Appendix below.

Restrictions on use

1. Use of the Licensed Material may be permitted for incidental promotional use and minor editing privileges e.g. minor adaptations of single figures, changes of format, colour and/or style where the adaptation is credited as set out in Appendix 1 below. Any other changes including but not limited to, cropping, adapting, omitting material that affect the meaning, intention or moral rights of the author are strictly prohibited.

2. You must not use any Licensed Material as part of any design or trademark.

3. Licensed Material may be used in Open Access Publications (OAP) before publication by Springer Nature, but any Licensed Material must be removed from OAP sites prior to final publication.

Ownership of Rights

1. Licensed Material remains the property of either Licensor or the relevant third party and any rights not explicitly granted herein are expressly reserved.

Warranty

IN NO EVENT SHALL LICENSOR BE LIABLE TO YOU OR ANY OTHER PARTY OR ANY OTHER PERSON OR FOR ANY SPECIAL, CONSEQUENTIAL, INCIDENTAL OR INDIRECT DAMAGES, HOWEVER CAUSED, ARISING OUT OF OR IN CONNECTION WITH THE DOWNLOADING, VIEWING OR USE OF THE MATERIALS REGARDLESS OF THE FORM OF ACTION, WHETHER FOR BREACH OF CONTRACT, BREACH OF WARRANTY, TORT, NEGLIGENCE, INFRINGEMENT OR OTHERWISE (INCLUDING, WITHOUT LIMITATION, DAMAGES BASED ON LOSS OF PROFITS, DATA, FILES, USE, BUSINESS OPPORTUNITY OR CLAIMS OF THIRD PARTIES), AND
WHETHER OR NOT THE PARTY HAS BEEN ADVISED OF THE POSSIBILITY OF SUCH DAMAGES. THIS LIMITATION SHALL APPLY NOTWITHSTANDING ANY FAILURE OF ESSENTIAL PURPOSE OF ANY LIMITED REMEDY PROVIDED HEREIN.

Limitations

1. ***BOOKS ONLY:***Where '**reuse in a dissertation/thesis**' has been selected the following terms apply: Print rights of the final author's accepted manuscript (for clarity, NOT the published version) for up to 100 copies, electronic rights for use only on a personal website or institutional repository as defined by the Sherpa guideline (www.sherpa.ac.uk/romeo/).

Termination and Cancellation

1. Licences will expire after the period shown in Clause 3 (above).

2. Licensee reserves the right to terminate the Licence in the event that payment is not received in full or if there has been a breach of this agreement by you.

Appendix 1 — Acknowledgements:

For Journal Content:
Reprinted by permission from [**the Licensor**]: [**Journal Publisher** (e.g. Nature/Springer/Palgrave)] [**JOURNAL NAME**] [**REFERENCE CITATION** (Article name, Author(s) Name), [**COPYRIGHT**] (year of publication)
For **Advance Online Publication papers:**
Reprinted by permission from [**the Licensor**]: [**Journal Publisher** (e.g. Nature/Springer/Palgrave)] [**JOURNAL NAME**] [**REFERENCE CITATION** (Article name, Author(s) Name), [**COPYRIGHT**] (year of publication), advance online publication, day month year (doi: 10.1038/sj.[JOURNAL ACRONYM].)
For Adaptations/Translations:
Adapted/Translated by permission from [**the Licensor**]: [**Journal Publisher** (e.g. Nature/Springer/Palgrave)] [**JOURNAL NAME**] [**REFERENCE CITATION** (Article name, Author(s) Name), [**COPYRIGHT**] (year of publication)
Note: For any republication from the British Journal of Cancer, the following credit line style applies:
Reprinted/adapted/translated by permission from [**the Licensor**]: on behalf of Cancer Research UK: : [**Journal Publisher** (e.g. Nature/Springer/Palgrave)] [**JOURNAL NAME**] [**REFERENCE CITATION** (Article name, Author(s) Name), [**COPYRIGHT]** (year of publication)
For **Advance Online Publication** papers:
Reprinted by permission from The [**the Licensor**]: on behalf of Cancer Research UK: [**Journal Publisher** (e.g. Nature/Springer/Palgrave)] [**JOURNAL NAME**] [**REFERENCE CITATION** (Article name, Author(s) Name), [**COPYRIGHT**] (year of publication), advance online publication, day month year (doi: 10.1038/sj.[JOURNAL ACRONYM])
For Book content:
Reprinted/adapted by permission from [**the Licensor**]: [**Book Publisher** (e.g. Palgrave Macmillan, Springer etc) [**Book Title**] by [**Book author**(s)] [**COPYRIGHT**] (year of publication)

Other Conditions:

Version 1.2

Questions? customercare@copyright.com or +1-855-239-3415 (toll free in the US) or +1-978-646-2777.

ELSEVIER LICENSE
TERMS AND CONDITIONS
Jan 25, 2020

This Agreement between Mara A Pop ("You") and Elsevier ("Elsevier") consists of your license details and the terms and conditions provided by Elsevier and Copyright Clearance Center.

License Number	4745481281126
License date	Jan 10, 2020
Licensed Content Publisher	Elsevier
Licensed Content Publication	Molecular Cell
Licensed Content Title	Global Analyses of the Effect of Different Cellular Contexts on MicroRNA Targeting
Licensed Content Author	Jin-Wu Nam,Olivia S. Rissland,David Koppstein,Cei Abreu-Goodger,Calvin H. Jan,Vikram Agarwal,Muhammed A. Yildirim,Antony Rodriguez,David P. Bartel
Licensed Content Date	Mar 20, 2014
Licensed Content Volume	53
Licensed Content Issue	6
Licensed Content Pages	13
Start Page	1031
End Page	1043
Type of Use	reuse in a thesis/dissertation
Portion	figures/tables/illustrations
Number of figures/tables/illustrations	1
Format	both print and electronic
Are you the author of this Elsevier article?	No
Will you be translating?	No
Title	Exploring combinatorial microRNA therapy for chronic wound healing
Institution name	Imperial College London
Expected presentation date	Jan 2020
Portions	Figure 1
Requestor Location	Mara A Pop Prince Consort Road Royal School of Mines

	London, London SW7 2BP United Kingdom Attn: Mara A Pop
Publisher Tax ID	GB 494 6272 12
Total	0.00 GBP

Terms and Conditions

INTRODUCTION

1. The publisher for this copyrighted material is Elsevier. By clicking "accept" in connection with completing this licensing transaction, you agree that the following terms and conditions apply to this transaction (along with the Billing and Payment terms and conditions established by Copyright Clearance Center, Inc. ("CCC"), at the time that you opened your Rightslink account and that are available at any time at http://myaccount.copyright.com).

GENERAL TERMS

2. Elsevier hereby grants you permission to reproduce the aforementioned material subject to the terms and conditions indicated.

3. Acknowledgement: If any part of the material to be used (for example, figures) has appeared in our publication with credit or acknowledgement to another source, permission must also be sought from that source. If such permission is not obtained then that material may not be included in your publication/copies. Suitable acknowledgement to the source must be made, either as a footnote or in a reference list at the end of your publication, as follows:

"Reprinted from Publication title, Vol /edition number, Author(s), Title of article / title of chapter, Pages No., Copyright (Year), with permission from Elsevier [OR APPLICABLE SOCIETY COPYRIGHT OWNER]." Also Lancet special credit - "Reprinted from The Lancet, Vol. number, Author(s), Title of article, Pages No., Copyright (Year), with permission from Elsevier."

4. Reproduction of this material is confined to the purpose and/or media for which permission is hereby given.

5. Altering/Modifying Material: Not Permitted. However figures and illustrations may be altered/adapted minimally to serve your work. Any other abbreviations, additions, deletions and/or any other alterations shall be made only with prior written authorization of Elsevier Ltd. (Please contact Elsevier at permissions@elsevier.com). No modifications can be made to any Lancet figures/tables and they must be reproduced in full.

6. If the permission fee for the requested use of our material is waived in this instance, please be advised that your future requests for Elsevier materials may attract a fee.

7. Reservation of Rights: Publisher reserves all rights not specifically granted in the combination of (i) the license details provided by you and accepted in the course of this licensing transaction, (ii) these terms and conditions and (iii) CCC's Billing and Payment terms and conditions.

8. License Contingent Upon Payment: While you may exercise the rights licensed immediately upon issuance of the license at the end of the licensing process for the transaction, provided that you have disclosed complete and accurate details of your proposed use, no license is finally effective unless and until full payment is received from you (either by publisher or by CCC) as provided in CCC's Billing and Payment terms and conditions. If full payment is not received on a timely basis, then any license preliminarily granted shall be deemed automatically revoked and shall be void as if never granted. Further, in the event that you breach any of these terms and conditions or any of CCC's Billing and Payment terms and conditions, the license is automatically revoked and shall be void as if never granted. Use of materials as described in a revoked license, as well as any use of the materials beyond the scope of an unrevoked license, may constitute copyright infringement and publisher reserves the right to take any and all action to protect its copyright in the materials.

9. Warranties: Publisher makes no representations or warranties with respect to the licensed material.

10. Indemnity: You hereby indemnify and agree to hold harmless publisher and CCC, and their respective officers, directors, employees and agents, from and against any and all claims arising out of your use of the licensed material other than as specifically authorized pursuant to this license.

11. No Transfer of License: This license is personal to you and may not be sublicensed, assigned, or transferred by you to any other person without publisher's written permission.

12. No Amendment Except in Writing: This license may not be amended except in a writing signed by both parties (or, in the case of publisher, by CCC on publisher's behalf).

13. Objection to Contrary Terms: Publisher hereby objects to any terms contained in any purchase order, acknowledgment, check endorsement or other writing prepared by you, which terms are inconsistent with these terms and conditions or CCC's Billing and Payment terms and conditions. These terms and conditions, together with CCC's Billing and Payment terms and conditions (which are incorporated herein), comprise the entire agreement between you and publisher (and CCC) concerning this licensing transaction. In the event of any conflict between your obligations established by these terms and conditions and those established by CCC's Billing and Payment terms and conditions, these terms and conditions shall control.

14. Revocation: Elsevier or Copyright Clearance Center may deny the permissions described in this License at their sole discretion, for any reason or no reason, with a full refund payable to you. Notice of such denial will be made using the contact information

provided by you. Failure to receive such notice will not alter or invalidate the denial. In no event will Elsevier or Copyright Clearance Center be responsible or liable for any costs, expenses or damage incurred by you as a result of a denial of your permission request, other than a refund of the amount(s) paid by you to Elsevier and/or Copyright Clearance Center for denied permissions.

LIMITED LICENSE

The following terms and conditions apply only to specific license types:

15. **Translation**: This permission is granted for non-exclusive world **English** rights only unless your license was granted for translation rights. If you licensed translation rights you may only translate this content into the languages you requested. A professional translator must perform all translations and reproduce the content word for word preserving the integrity of the article.

16. **Posting licensed content on any Website**: The following terms and conditions apply as follows: Licensing material from an Elsevier journal: All content posted to the web site must maintain the copyright information line on the bottom of each image; A hyper-text must be included to the Homepage of the journal from which you are licensing at http://www.sciencedirect.com/science/journal/xxxxx or the Elsevier homepage for books at http://www.elsevier.com; Central Storage: This license does not include permission for a scanned version of the material to be stored in a central repository such as that provided by Heron/XanEdu.

Licensing material from an Elsevier book: A hyper-text link must be included to the Elsevier homepage at http://www.elsevier.com . All content posted to the web site must maintain the copyright information line on the bottom of each image.

Posting licensed content on Electronic reserve: In addition to the above the following clauses are applicable: The web site must be password-protected and made available only to bona fide students registered on a relevant course. This permission is granted for 1 year only. You may obtain a new license for future website posting.

17. **For journal authors:** the following clauses are applicable in addition to the above:

Preprints:

A preprint is an author's own write-up of research results and analysis, it has not been peer-reviewed, nor has it had any other value added to it by a publisher (such as formatting, copyright, technical enhancement etc.).

Authors can share their preprints anywhere at any time. Preprints should not be added to or enhanced in any way in order to appear more like, or to substitute for, the final

versions of articles however authors can update their preprints on arXiv or RePEc with their Accepted Author Manuscript (see below).

If accepted for publication, we encourage authors to link from the preprint to their formal publication via its DOI. Millions of researchers have access to the formal publications on ScienceDirect, and so links will help users to find, access, cite and use the best available version. Please note that Cell Press, The Lancet and some society-owned have different preprint policies. Information on these policies is available on the journal homepage.

Accepted Author Manuscripts: An accepted author manuscript is the manuscript of an article that has been accepted for publication and which typically includes author-incorporated changes suggested during submission, peer review and editor-author communications.

Authors can share their accepted author manuscript:

- immediately
    - via their non-commercial person homepage or blog
    - by updating a preprint in arXiv or RePEc with the accepted manuscript
    - via their research institute or institutional repository for internal institutional uses or as part of an invitation-only research collaboration work-group
    - directly by providing copies to their students or to research collaborators for their personal use
    - for private scholarly sharing as part of an invitation-only work group on commercial sites with which Elsevier has an agreement
- After the embargo period
    - via non-commercial hosting platforms such as their institutional repository
    - via commercial sites with which Elsevier has an agreement

In all cases accepted manuscripts should:

- link to the formal publication via its DOI
- bear a CC-BY-NC-ND license - this is easy to do
- if aggregated with other manuscripts, for example in a repository or other site, be shared in alignment with our hosting policy not be added to or enhanced in any way to appear more like, or to substitute for, the published journal article.

Published journal article (JPA): A published journal article (PJA) is the definitive final record of published research that appears or will appear in the journal and embodies all value-adding publishing activities including peer review co-ordination, copy-editing, formatting, (if relevant) pagination and online enrichment.

Policies for sharing publishing journal articles differ for subscription and gold open access articles:

Subscription Articles: If you are an author, please share a link to your article rather than the full-text. Millions of researchers have access to the formal publications on ScienceDirect, and so links will help your users to find, access, cite, and use the best available version.

Theses and dissertations which contain embedded PJAs as part of the formal submission can be posted publicly by the awarding institution with DOI links back to the formal publications on ScienceDirect.

If you are affiliated with a library that subscribes to ScienceDirect you have additional private sharing rights for others' research accessed under that agreement. This includes use for classroom teaching and internal training at the institution (including use in course packs and courseware programs), and inclusion of the article for grant funding purposes.

Gold Open Access Articles: May be shared according to the author-selected end-user license and should contain a CrossMark logo, the end user license, and a DOI link to the formal publication on ScienceDirect.

Please refer to Elsevier's posting policy for further information.

18. **For book authors** the following clauses are applicable in addition to the above: Authors are permitted to place a brief summary of their work online only. You are not allowed to download and post the published electronic version of your chapter, nor may you scan the printed edition to create an electronic version. **Posting to a repository:** Authors are permitted to post a summary of their chapter only in their institution's repository.

19. **Thesis/Dissertation**: If your license is for use in a thesis/dissertation your thesis may be submitted to your institution in either print or electronic form. Should your thesis be published commercially, please reapply for permission. These requirements include permission for the Library and Archives of Canada to supply single copies, on demand, of the complete thesis and include permission for Proquest/UMI to supply single copies, on demand, of the complete thesis. Should your thesis be published commercially, please reapply for permission. Theses and dissertations which contain embedded PJAs as part of the formal submission can be posted publicly by the awarding institution with DOI links back to the formal publications on ScienceDirect.

Elsevier Open Access Terms and Conditions

You can publish open access with Elsevier in hundreds of open access journals or in nearly 2000 established subscription journals that support open access publishing. Permitted third party re-use of these open access articles is defined by the author's choice of Creative Commons user license. See our open access license policy for more information.

Terms & Conditions applicable to all Open Access articles published with Elsevier:

Any reuse of the article must not represent the author as endorsing the adaptation of the article nor should the article be modified in such a way as to damage the author's honour or reputation. If any changes have been made, such changes must be clearly indicated.

The author(s) must be appropriately credited and we ask that you include the end user license and a DOI link to the formal publication on ScienceDirect.

If any part of the material to be used (for example, figures) has appeared in our publication with credit or acknowledgement to another source it is the responsibility of the user to ensure their reuse complies with the terms and conditions determined by the rights holder.

Additional Terms & Conditions applicable to each Creative Commons user license:

CC BY: The CC-BY license allows users to copy, to create extracts, abstracts and new works from the Article, to alter and revise the Article and to make commercial use of the Article (including reuse and/or resale of the Article by commercial entities), provided the user gives appropriate credit (with a link to the formal publication through the relevant DOI), provides a link to the license, indicates if changes were made and the licensor is not represented as endorsing the use made of the work. The full details of the license are available at http://creativecommons.org/licenses/by/4.0.

CC BY NC SA: The CC BY-NC-SA license allows users to copy, to create extracts, abstracts and new works from the Article, to alter and revise the Article, provided this is not done for commercial purposes, and that the user gives appropriate credit (with a link to the formal publication through the relevant DOI), provides a link to the license, indicates if changes were made and the licensor is not represented as endorsing the use made of the work. Further, any new works must be made available on the same conditions. The full details of the license are available at http://creativecommons.org/licenses/by-nc-sa/4.0.

CC BY NC ND: The CC BY-NC-ND license allows users to copy and distribute the Article, provided this is not done for commercial purposes and further does not permit distribution of the Article if it is changed or edited in any way, and provided the user gives appropriate credit (with a link to the formal publication through the relevant DOI), provides a link to the license, and that the licensor is not represented as endorsing the use made of the work. The full details of the license are available at http://creativecommons.org/licenses/by-nc-nd/4.0. Any commercial reuse of Open Access articles published with a CC BY NC SA or CC BY NC ND license requires permission from Elsevier and will be subject to a fee.

Commercial reuse includes:

- Associating advertising with the full text of the Article
- Charging fees for document delivery or access

- Article aggregation
- Systematic distribution via e-mail lists or share buttons

Posting or linking by commercial companies for use by customers of those companies.

20. **Other Conditions**:

v1.9

Questions? customercare@copyright.com or +1-855-239-3415 (toll free in the US) or +1-978-646-2777.

OXFORD UNIVERSITY PRESS LICENSE
TERMS AND CONDITIONS
Jan 25, 2020

This Agreement between Mara A Pop ("You") and Oxford University Press ("Oxford University Press") consists of your license details and the terms and conditions provided by Oxford University Press and Copyright Clearance Center.

License Number	4745850560060
License date	Jan 11, 2020
Licensed content publisher	Oxford University Press
Licensed content publication	Nucleic Acids Research
Licensed content title	Distance constraints between microRNA target sites dictate efficacy and cooperativity
Licensed content author	Sætrom, Pål; Heale, Bret S.E.
Licensed content date	Mar 27, 2007
Type of Use	Thesis/Dissertation
Institution name	
Title of your work	Exploring combinatorial microRNA therapy for chronic wound healing
Publisher of your work	Imperial College London
Expected publication date	Jan 2020
Permissions cost	0.00 GBP
Value added tax	0.00 GBP
Total	0.00 GBP
Title	Exploring combinatorial microRNA therapy for chronic wound healing
Institution name	Imperial College London
Expected presentation date	Jan 2020
Portions	Figure 3
Requestor Location	Mara A Pop Prince Consort Road Royal School of Mines London, London SW7 2BP United Kingdom Attn: Mara A Pop
Publisher Tax ID	GB125506730
Total	0.00 GBP

Terms and Conditions

STANDARD TERMS AND CONDITIONS FOR REPRODUCTION OF MATERIAL FROM AN OXFORD UNIVERSITY PRESS JOURNAL

1. Use of the material is restricted to the type of use specified in your order details.

2. This permission covers the use of the material in the English language in the following territory: world. If you have requested additional permission to translate this material, the terms and conditions of this reuse will be set out in clause 12.

3. This permission is limited to the particular use authorized in (1) above and does not allow you to sanction its use elsewhere in any other format other than specified above, nor does it apply to quotations, images, artistic works etc that have been reproduced from other sources which may be part of the material to be used.

4. No alteration, omission or addition is made to the material without our written consent. Permission must be re-cleared with Oxford University Press if/when you decide to reprint.

5. The following credit line appears wherever the material is used: author, title, journal, year, volume, issue number, pagination, by permission of Oxford University Press or the sponsoring society if the journal is a society journal. Where a journal is being published on behalf of a learned society, the details of that society must be included in the credit line.

6. For the reproduction of a full article from an Oxford University Press journal for whatever purpose, the corresponding author of the material concerned should be informed of the proposed use. Contact details for the corresponding authors of all Oxford University Press journal contact can be found alongside either the abstract or full text of the article concerned, accessible from www.oxfordjournals.org Should there be a problem clearing these rights, please contact journals.permissions@oup.com

7. If the credit line or acknowledgement in our publication indicates that any of the figures, images or photos was reproduced, drawn or modified from an earlier source it will be necessary for you to clear this permission with the original publisher as well. If this permission has not been obtained, please note that this material cannot be included in your publication/photocopies.

8. While you may exercise the rights licensed immediately upon issuance of the license at the end of the licensing process for the transaction, provided that you have disclosed complete and accurate details of your proposed use, no license is finally effective unless and until full payment is received from you (either by Oxford University Press or by Copyright Clearance Center (CCC)) as provided in CCC's Billing and Payment terms and conditions. If full payment is not received on a timely basis, then any license preliminarily granted shall be deemed automatically revoked and shall be void as if never granted. Further, in the event that you breach any of these terms and conditions or any of CCC's

Billing and Payment terms and conditions, the license is automatically revoked and shall be void as if never granted. Use of materials as described in a revoked license, as well as any use of the materials beyond the scope of an unrevoked license, may constitute copyright infringement and Oxford University Press reserves the right to take any and all action to protect its copyright in the materials.

9. This license is personal to you and may not be sublicensed, assigned or transferred by you to any other person without Oxford University Press's written permission.

10. Oxford University Press reserves all rights not specifically granted in the combination of (i) the license details provided by you and accepted in the course of this licensing transaction, (ii) these terms and conditions and (iii) CCC's Billing and Payment terms and conditions.

11. You hereby indemnify and agree to hold harmless Oxford University Press and CCC, and their respective officers, directors, employs and agents, from and against any and all claims arising out of your use of the licensed material other than as specifically authorized pursuant to this license.

12. Other Terms and Conditions:

v1.4

Questions? customercare@copyright.com or +1-855-239-3415 (toll free in the US) or +1-978-646-2777.

SPRINGER NATURE LICENSE
TERMS AND CONDITIONS

Jan 25, 2020

This Agreement between Mara A Pop ("You") and Springer Nature ("Springer Nature") consists of your license details and the terms and conditions provided by Springer Nature and Copyright Clearance Center.

License Number	4745421483764
License date	Jan 10, 2020
Licensed Content Publisher	Springer Nature
Licensed Content Publication	Nature Reviews Molecular Cell Biology
Licensed Content Title	MicroRNA control of signal transduction
Licensed Content Author	Masafumi Inui et al
Licensed Content Date	Mar 10, 2010
Type of Use	Thesis/Dissertation
Requestor type	academic/university or research institute
Format	print and electronic
Portion	figures/tables/illustrations
Number of figures/tables/illustrations	3
High-res required	no
Will you be translating?	no
Circulation/distribution	50000 or greater
Author of this Springer Nature content	no
Title	Exploring combinatorial microRNA therapy for chronic wound healing
Institution name	n/a
Expected presentation date	Jan 2020
Portions	Figure 2e, Figure 3b, Figure 4b
Requestor Location	Mara A Pop Prince Consort Road Royal School of Mines London, London SW7 2BP United Kingdom Attn: Mara A Pop
Total	0.00 GBP

Terms and Conditions

Springer Nature Customer Service Centre GmbH
Terms and Conditions

This agreement sets out the terms and conditions of the licence (the **Licence**) between you and **Springer Nature Customer Service Centre GmbH** (the **Licensor**). By clicking 'accept' and completing the transaction for the material (**Licensed Material**), you also confirm your acceptance of these terms and conditions.

1. **Grant of License**

    1. The Licensor grants you a personal, non-exclusive, non-transferable, world-wide licence to reproduce the Licensed Material for the purpose specified in your order only. Licences are granted for the specific use requested in the order and for no other use, subject to the conditions below.

    2. The Licensor warrants that it has, to the best of its knowledge, the rights to license reuse of the Licensed Material. However, you should ensure that the material you are requesting is original to the Licensor and does not carry the copyright of another entity (as credited in the published version).

    3. If the credit line on any part of the material you have requested indicates that it was reprinted or adapted with permission from another source, then you should also seek permission from that source to reuse the material.

2. **Scope of Licence**

    1. You may only use the Licensed Content in the manner and to the extent permitted by these Ts&Cs and any applicable laws.

    2. A separate licence may be required for any additional use of the Licensed Material, e.g. where a licence has been purchased for print only use, separate permission must be obtained for electronic re-use. Similarly, a licence is only valid in the language selected and does not apply for editions in other languages unless additional translation rights have been granted separately in the licence. Any content owned by third parties are expressly excluded from the licence.

    3. Similarly, rights for additional components such as custom editions and derivatives require additional permission and may be subject to an additional fee. Please apply to Journalpermissions@springernature.com/bookpermissions@springernature.com for these rights.

    4. Where permission has been granted **free of charge** for material in print, permission may also be granted for any electronic version of that work,

provided that the material is incidental to your work as a whole and that the electronic version is essentially equivalent to, or substitutes for, the print version.

5. An alternative scope of licence may apply to signatories of the STM Permissions Guidelines, as amended from time to time.

Duration of Licence

1. A licence for is valid from the date of purchase ('Licence Date') at the end of the relevant period in the below table:

Scope of Licence	Duration of Licence
Post on a website	12 months
Presentations	12 months
Books and journals	Lifetime of the edition in the language purchased

Acknowledgement

1. The Licensor's permission must be acknowledged next to the Licenced Material in print. In electronic form, this acknowledgement must be visible at the same time as the figures/tables/illustrations or abstract, and must be hyperlinked to the journal/book's homepage. Our required acknowledgement format is in the Appendix below.

Restrictions on use

1. Use of the Licensed Material may be permitted for incidental promotional use and minor editing privileges e.g. minor adaptations of single figures, changes of format, colour and/or style where the adaptation is credited as set out in Appendix 1 below. Any other changes including but not limited to, cropping, adapting, omitting material that affect the meaning, intention or moral rights of the author are strictly prohibited.

2. You must not use any Licensed Material as part of any design or trademark.

3. Licensed Material may be used in Open Access Publications (OAP) before publication by Springer Nature, but any Licensed Material must be removed from OAP sites prior to final publication.

Ownership of Rights

1. Licensed Material remains the property of either Licensor or the relevant third party and any rights not explicitly granted herein are expressly reserved.

Warranty

IN NO EVENT SHALL LICENSOR BE LIABLE TO YOU OR ANY OTHER PARTY OR ANY OTHER PERSON OR FOR ANY SPECIAL, CONSEQUENTIAL, INCIDENTAL OR INDIRECT DAMAGES, HOWEVER CAUSED, ARISING OUT OF OR IN CONNECTION WITH THE DOWNLOADING, VIEWING OR USE OF THE MATERIALS REGARDLESS OF THE FORM OF ACTION, WHETHER FOR BREACH OF CONTRACT, BREACH OF WARRANTY, TORT, NEGLIGENCE, INFRINGEMENT OR OTHERWISE (INCLUDING, WITHOUT LIMITATION, DAMAGES BASED ON LOSS OF PROFITS, DATA, FILES, USE, BUSINESS OPPORTUNITY OR CLAIMS OF THIRD PARTIES), AND
WHETHER OR NOT THE PARTY HAS BEEN ADVISED OF THE POSSIBILITY OF SUCH DAMAGES. THIS LIMITATION SHALL APPLY NOTWITHSTANDING ANY FAILURE OF ESSENTIAL PURPOSE OF ANY LIMITED REMEDY PROVIDED HEREIN.

Limitations

1. ***BOOKS ONLY:***Where '**reuse in a dissertation/thesis**' has been selected the following terms apply: Print rights of the final author's accepted manuscript (for clarity, NOT the published version) for up to 100 copies, electronic rights for use only on a personal website or institutional repository as defined by the Sherpa guideline (www.sherpa.ac.uk/romeo/).

Termination and Cancellation

1. Licences will expire after the period shown in Clause 3 (above).

2. Licensee reserves the right to terminate the Licence in the event that payment is not received in full or if there has been a breach of this agreement by you.

Appendix 1 — Acknowledgements:

For Journal Content:
Reprinted by permission from [**the Licensor**]: [**Journal Publisher** (e.g. Nature/Springer/Palgrave)] [**JOURNAL NAME**] [**REFERENCE CITATION** (Article name, Author(s) Name), [**COPYRIGHT**] (year of publication)
For **Advance Online Publication papers:**
Reprinted by permission from [**the Licensor**]: [**Journal Publisher** (e.g. Nature/Springer/Palgrave)] [**JOURNAL NAME**] [**REFERENCE CITATION** (Article name, Author(s) Name), [**COPYRIGHT**] (year of publication), advance online publication, day month year (doi: 10.1038/sj.[JOURNAL ACRONYM].)
For Adaptations/Translations:
Adapted/Translated by permission from [**the Licensor**]: [**Journal Publisher** (e.g. Nature/Springer/Palgrave)] [**JOURNAL NAME**] [**REFERENCE CITATION** (Article name, Author(s) Name), [**COPYRIGHT**] (year of publication)
Note: For any republication from the British Journal of Cancer, the following credit line style applies:
Reprinted/adapted/translated by permission from [**the Licensor**]: on behalf of Cancer Research UK: : [**Journal Publisher** (e.g. Nature/Springer/Palgrave)] [**JOURNAL NAME**] [**REFERENCE CITATION** (Article name, Author(s) Name), [**COPYRIGHT]** (year of publication)
For **Advance Online Publication** papers:
Reprinted by permission from The [**the Licensor**]: on behalf of Cancer Research UK: [**Journal Publisher** (e.g. Nature/Springer/Palgrave)] [**JOURNAL NAME**] [**REFERENCE CITATION** (Article name, Author(s) Name), [**COPYRIGHT**] (year of publication), advance online publication, day month year (doi: 10.1038/sj.[JOURNAL ACRONYM])
For Book content:
Reprinted/adapted by permission from [**the Licensor**]: [**Book Publisher** (e.g. Palgrave Macmillan, Springer etc) [**Book Title**] by [**Book author**(s)] [**COPYRIGHT**] (year of publication)

Other Conditions:

Version 1.2

Questions? customercare@copyright.com or +1-855-239-3415 (toll free in the US) or +1-978-646-2777.

SPRINGER NATURE LICENSE
TERMS AND CONDITIONS

Jan 25, 2020

This Agreement between Mara A Pop ("You") and Springer Nature ("Springer Nature") consists of your license details and the terms and conditions provided by Springer Nature and Copyright Clearance Center.

License Number	4745861014658
License date	Jan 11, 2020
Licensed Content Publisher	Springer Nature
Licensed Content Publication	Nature Genetics
Licensed Content Title	MicroRNAs can generate thresholds in target gene expression
Licensed Content Author	Shankar Mukherji et al
Licensed Content Date	Aug 21, 2011
Type of Use	Thesis/Dissertation
Requestor type	academic/university or research institute
Format	print and electronic
Portion	figures/tables/illustrations
Number of figures/tables/illustrations	1
High-res required	no
Will you be translating?	no
Circulation/distribution	30 - 99
Author of this Springer Nature content	no
Title	Exploring combinatorial microRNA therapy for chronic wound healing
Institution name	Imperial College London
Expected presentation date	Jan 2020
Portions	Figure 2
Requestor Location	Mara A Pop Prince Consort Road Royal School of Mines London, London SW7 2BP United Kingdom Attn: Mara A Pop
Total	0.00 GBP

Terms and Conditions

Springer Nature Customer Service Centre GmbH
Terms and Conditions

This agreement sets out the terms and conditions of the licence (the **Licence**) between you and **Springer Nature Customer Service Centre GmbH** (the **Licensor**). By clicking 'accept' and completing the transaction for the material (**Licensed Material**), you also confirm your acceptance of these terms and conditions.

1. **Grant of License**

    1. The Licensor grants you a personal, non-exclusive, non-transferable, world-wide licence to reproduce the Licensed Material for the purpose specified in your order only. Licences are granted for the specific use requested in the order and for no other use, subject to the conditions below.

    2. The Licensor warrants that it has, to the best of its knowledge, the rights to license reuse of the Licensed Material. However, you should ensure that the material you are requesting is original to the Licensor and does not carry the copyright of another entity (as credited in the published version).

    3. If the credit line on any part of the material you have requested indicates that it was reprinted or adapted with permission from another source, then you should also seek permission from that source to reuse the material.

2. **Scope of Licence**

    1. You may only use the Licensed Content in the manner and to the extent permitted by these Ts&Cs and any applicable laws.

    2. A separate licence may be required for any additional use of the Licensed Material, e.g. where a licence has been purchased for print only use, separate permission must be obtained for electronic re-use. Similarly, a licence is only valid in the language selected and does not apply for editions in other languages unless additional translation rights have been granted separately in the licence. Any content owned by third parties are expressly excluded from the licence.

    3. Similarly, rights for additional components such as custom editions and derivatives require additional permission and may be subject to an additional fee. Please apply to Journalpermissions@springernature.com/bookpermissions@springernature.com for these rights.

    4. Where permission has been granted **free of charge** for material in print, permission may also be granted for any electronic version of that work,

provided that the material is incidental to your work as a whole and that the electronic version is essentially equivalent to, or substitutes for, the print version.

5. An alternative scope of licence may apply to signatories of the STM Permissions Guidelines, as amended from time to time.

Duration of Licence

1. A licence for is valid from the date of purchase ('Licence Date') at the end of the relevant period in the below table:

Scope of Licence	Duration of Licence
Post on a website	12 months
Presentations	12 months
Books and journals	Lifetime of the edition in the language purchased

Acknowledgement

1. The Licensor's permission must be acknowledged next to the Licenced Material in print. In electronic form, this acknowledgement must be visible at the same time as the figures/tables/illustrations or abstract, and must be hyperlinked to the journal/book's homepage. Our required acknowledgement format is in the Appendix below.

Restrictions on use

1. Use of the Licensed Material may be permitted for incidental promotional use and minor editing privileges e.g. minor adaptations of single figures, changes of format, colour and/or style where the adaptation is credited as set out in Appendix 1 below. Any other changes including but not limited to, cropping, adapting, omitting material that affect the meaning, intention or moral rights of the author are strictly prohibited.

2. You must not use any Licensed Material as part of any design or trademark.

3. Licensed Material may be used in Open Access Publications (OAP) before publication by Springer Nature, but any Licensed Material must be removed from OAP sites prior to final publication.

Ownership of Rights

1. Licensed Material remains the property of either Licensor or the relevant third party and any rights not explicitly granted herein are expressly reserved.

Warranty

IN NO EVENT SHALL LICENSOR BE LIABLE TO YOU OR ANY OTHER PARTY OR ANY OTHER PERSON OR FOR ANY SPECIAL, CONSEQUENTIAL, INCIDENTAL OR INDIRECT DAMAGES, HOWEVER CAUSED, ARISING OUT OF OR IN CONNECTION WITH THE DOWNLOADING, VIEWING OR USE OF THE MATERIALS REGARDLESS OF THE FORM OF ACTION, WHETHER FOR BREACH OF CONTRACT, BREACH OF WARRANTY, TORT, NEGLIGENCE, INFRINGEMENT OR OTHERWISE (INCLUDING, WITHOUT LIMITATION, DAMAGES BASED ON LOSS OF PROFITS, DATA, FILES, USE, BUSINESS OPPORTUNITY OR CLAIMS OF THIRD PARTIES), AND
WHETHER OR NOT THE PARTY HAS BEEN ADVISED OF THE POSSIBILITY OF SUCH DAMAGES. THIS LIMITATION SHALL APPLY NOTWITHSTANDING ANY FAILURE OF ESSENTIAL PURPOSE OF ANY LIMITED REMEDY PROVIDED HEREIN.

Limitations

1. ***BOOKS ONLY:***Where '**reuse in a dissertation/thesis**' has been selected the following terms apply: Print rights of the final author's accepted manuscript (for clarity, NOT the published version) for up to 100 copies, electronic rights for use only on a personal website or institutional repository as defined by the Sherpa guideline (www.sherpa.ac.uk/romeo/).

Termination and Cancellation

1. Licences will expire after the period shown in Clause 3 (above).

2. Licensee reserves the right to terminate the Licence in the event that payment is not received in full or if there has been a breach of this agreement by you.

Appendix 1 — Acknowledgements:

For Journal Content:
Reprinted by permission from [**the Licensor**]: [**Journal Publisher** (e.g. Nature/Springer/Palgrave)] [**JOURNAL NAME**] [**REFERENCE CITATION** (Article name, Author(s) Name), [**COPYRIGHT**] (year of publication)
For **Advance Online Publication papers:**
Reprinted by permission from [**the Licensor**]: [**Journal Publisher** (e.g. Nature/Springer/Palgrave)] [**JOURNAL NAME**] [**REFERENCE CITATION** (Article name, Author(s) Name), [**COPYRIGHT**] (year of publication), advance online publication, day month year (doi: 10.1038/sj.[JOURNAL ACRONYM].)
For Adaptations/Translations:
Adapted/Translated by permission from [**the Licensor**]: [**Journal Publisher** (e.g. Nature/Springer/Palgrave)] [**JOURNAL NAME**] [**REFERENCE CITATION** (Article name, Author(s) Name), [**COPYRIGHT**] (year of publication)
Note: For any republication from the British Journal of Cancer, the following credit line style applies:
Reprinted/adapted/translated by permission from [**the Licensor**]: on behalf of Cancer Research UK: : [**Journal Publisher** (e.g. Nature/Springer/Palgrave)] [**JOURNAL NAME**] [**REFERENCE CITATION** (Article name, Author(s) Name), [**COPYRIGHT]** (year of publication)
For **Advance Online Publication** papers:
Reprinted by permission from The [**the Licensor**]: on behalf of Cancer Research UK: [**Journal Publisher** (e.g. Nature/Springer/Palgrave)] [**JOURNAL NAME**] [**REFERENCE CITATION** (Article name, Author(s) Name), [**COPYRIGHT**] (year of publication), advance online publication, day month year (doi: 10.1038/sj.[JOURNAL ACRONYM])
For Book content:
Reprinted/adapted by permission from [**the Licensor**]: [**Book Publisher** (e.g. Palgrave Macmillan, Springer etc) [**Book Title**] by [**Book author**(s)] [**COPYRIGHT**] (year of publication)

Other Conditions:

Version 1.2

Questions? customercare@copyright.com or +1-855-239-3415 (toll free in the US) or +1-978-646-2777.

JOHN WILEY AND SONS LICENSE
TERMS AND CONDITIONS

Jan 25, 2020

This Agreement between Mara A Pop ("You") and John Wiley and Sons ("John Wiley and Sons") consists of your license details and the terms and conditions provided by John Wiley and Sons and Copyright Clearance Center.

License Number	4744311246439
License date	Jan 08, 2020
Licensed Content Publisher	John Wiley and Sons
Licensed Content Publication	Wound Repair and Regeneration
Licensed Content Title	Integrative analysis of miRNA and mRNA paired expression profiling of primary fibroblast derived from diabetic foot ulcers reveals multiple impaired cellular functions
Licensed Content Author	Marjana Tomic-Canic, Jonathan A. Garlick, Robert S. Kirsner, et al
Licensed Content Date	Oct 4, 2016
Licensed Content Volume	24
Licensed Content Issue	6
Licensed Content Pages	11
Type of use	Dissertation/Thesis
Requestor type	University/Academic
Format	Print and electronic
Portion	Figure/table
Number of figures/tables	1
Original Wiley figure/table number(s)	Figure 1
Will you be translating?	No
Title of your thesis / dissertation	Exploring combinatorial microRNA therapy for chronic wound healing
Expected completion date	Jan 2020
Expected size (number of pages)	200

Requestor Location	Mara A Pop Prince Consort Road Royal School of Mines London, London SW7 2BP United Kingdom Attn: Mara A Pop
Publisher Tax ID	EU826007151
Total	0.00 GBP

Terms and Conditions

TERMS AND CONDITIONS

This copyrighted material is owned by or exclusively licensed to John Wiley & Sons, Inc. or one of its group companies (each a"Wiley Company") or handled on behalf of a society with which a Wiley Company has exclusive publishing rights in relation to a particular work (collectively "WILEY"). By clicking "accept" in connection with completing this licensing transaction, you agree that the following terms and conditions apply to this transaction (along with the billing and payment terms and conditions established by the Copyright Clearance Center Inc., ("CCC's Billing and Payment terms and conditions"), at the time that you opened your RightsLink account (these are available at any time at http://myaccount.copyright.com).

Terms and Conditions

- The materials you have requested permission to reproduce or reuse (the "Wiley Materials") are protected by copyright.

- You are hereby granted a personal, non-exclusive, non-sub licensable (on a stand-alone basis), non-transferable, worldwide, limited license to reproduce the Wiley Materials for the purpose specified in the licensing process. This license, **and any CONTENT (PDF or image file) purchased as part of your order,** is for a one-time use only and limited to any maximum distribution number specified in the license. The first instance of republication or reuse granted by this license must be completed within two years of the date of the grant of this license (although copies prepared before the end date may be distributed thereafter). The Wiley Materials shall not be used in any other manner or for any other purpose, beyond what is granted in the license. Permission is granted subject to an appropriate acknowledgement given to the author, title of the material/book/journal and the publisher. You shall also duplicate the copyright notice that appears in the Wiley publication in your use of the Wiley Material. Permission is also granted on the understanding that nowhere in the text is a previously published source acknowledged for all or part of this Wiley Material. Any third party content is expressly excluded from this permission.

- With respect to the Wiley Materials, all rights are reserved. Except as expressly granted by the terms of the license, no part of the Wiley Materials may be copied, modified, adapted (except for minor reformatting required by the new Publication), translated, reproduced, transferred or distributed, in any form or by any means, and no derivative works may be made based on the Wiley Materials without the prior permission of the respective copyright owner.**For STM Signatory Publishers clearing permission under the terms of the STM Permissions Guidelines only, the terms of the license are extended to include subsequent editions and for editions in other languages, provided such editions are for the work as a whole in situ and does not involve the separate exploitation of the permitted figures or extracts,** You may not alter, remove or suppress in any manner any copyright, trademark or other notices displayed by the Wiley Materials. You may not license, rent, sell, loan, lease, pledge, offer as security, transfer or assign the Wiley Materials on a stand-alone basis, or any of the rights granted to you hereunder to any other person.

- The Wiley Materials and all of the intellectual property rights therein shall at all times remain the exclusive property of John Wiley & Sons Inc, the Wiley Companies, or their respective licensors, and your interest therein is only that of having possession of and the right to reproduce the Wiley Materials pursuant to Section 2 herein during the continuance of this Agreement. You agree that you own no right, title or interest in or to the Wiley Materials or any of the intellectual property rights therein. You shall have no rights hereunder other than the license as provided for above in Section 2. No right, license or interest to any trademark, trade name, service mark or other branding ("Marks") of WILEY or its licensors is granted hereunder, and you agree that you shall not assert any such right, license or interest with respect thereto

- NEITHER WILEY NOR ITS LICENSORS MAKES ANY WARRANTY OR REPRESENTATION OF ANY KIND TO YOU OR ANY THIRD PARTY, EXPRESS, IMPLIED OR STATUTORY, WITH RESPECT TO THE MATERIALS OR THE ACCURACY OF ANY INFORMATION CONTAINED IN THE MATERIALS, INCLUDING, WITHOUT LIMITATION, ANY IMPLIED WARRANTY OF MERCHANTABILITY, ACCURACY, SATISFACTORY QUALITY, FITNESS FOR A PARTICULAR PURPOSE, USABILITY, INTEGRATION OR NON-INFRINGEMENT AND ALL SUCH WARRANTIES ARE HEREBY EXCLUDED BY WILEY AND ITS LICENSORS AND WAIVED BY YOU.

- WILEY shall have the right to terminate this Agreement immediately upon breach of this Agreement by you.

- You shall indemnify, defend and hold harmless WILEY, its Licensors and their respective directors, officers, agents and employees, from and against any actual or threatened claims, demands, causes of action or proceedings arising from any breach of this Agreement by you.

- IN NO EVENT SHALL WILEY OR ITS LICENSORS BE LIABLE TO YOU OR ANY OTHER PARTY OR ANY OTHER PERSON OR ENTITY FOR ANY SPECIAL, CONSEQUENTIAL, INCIDENTAL, INDIRECT, EXEMPLARY OR PUNITIVE DAMAGES, HOWEVER CAUSED, ARISING OUT OF OR IN CONNECTION WITH THE DOWNLOADING, PROVISIONING, VIEWING OR USE OF THE MATERIALS REGARDLESS OF THE FORM OF ACTION, WHETHER FOR BREACH OF CONTRACT, BREACH OF WARRANTY, TORT, NEGLIGENCE, INFRINGEMENT OR OTHERWISE (INCLUDING, WITHOUT LIMITATION, DAMAGES BASED ON LOSS OF PROFITS, DATA, FILES, USE, BUSINESS OPPORTUNITY OR CLAIMS OF THIRD PARTIES), AND WHETHER OR NOT THE PARTY HAS BEEN ADVISED OF THE POSSIBILITY OF SUCH DAMAGES. THIS LIMITATION SHALL APPLY NOTWITHSTANDING ANY FAILURE OF ESSENTIAL PURPOSE OF ANY LIMITED REMEDY PROVIDED HEREIN.

- Should any provision of this Agreement be held by a court of competent jurisdiction to be illegal, invalid, or unenforceable, that provision shall be deemed amended to achieve as nearly as possible the same economic effect as the original provision, and the legality, validity and enforceability of the remaining provisions of this Agreement shall not be affected or impaired thereby.

- The failure of either party to enforce any term or condition of this Agreement shall not constitute a waiver of either party's right to enforce each and every term and condition of this Agreement. No breach under this agreement shall be deemed waived or excused by either party unless such waiver or consent is in writing signed by the party granting such waiver or consent. The waiver by or consent of a party to a breach of any provision of this Agreement shall not operate or be construed as a waiver of or consent to any other or subsequent breach by such other party.

- This Agreement may not be assigned (including by operation of law or otherwise) by you without WILEY's prior written consent.

- Any fee required for this permission shall be non-refundable after thirty (30) days from receipt by the CCC.

- These terms and conditions together with CCC's Billing and Payment terms and conditions (which are incorporated herein) form the entire agreement between you and WILEY concerning this licensing transaction and (in the absence of fraud) supersedes all prior agreements and representations of the parties, oral or written. This Agreement may not be amended except in writing signed by both parties. This Agreement shall be binding upon and inure to the benefit of the parties' successors, legal representatives, and authorized assigns.

- In the event of any conflict between your obligations established by these terms and conditions and those established by CCC's Billing and Payment terms and conditions, these terms and conditions shall prevail.

- WILEY expressly reserves all rights not specifically granted in the combination of (i) the license details provided by you and accepted in the course of this licensing transaction, (ii) these terms and conditions and (iii) CCC's Billing and Payment terms and conditions.

- This Agreement will be void if the Type of Use, Format, Circulation, or Requestor Type was misrepresented during the licensing process.

- This Agreement shall be governed by and construed in accordance with the laws of the State of New York, USA, without regards to such state's conflict of law rules. Any legal action, suit or proceeding arising out of or relating to these Terms and Conditions or the breach thereof shall be instituted in a court of competent jurisdiction in New York County in the State of New York in the United States of America and each party hereby consents and submits to the personal jurisdiction of such court, waives any objection to venue in such court and consents to service of process by registered or certified mail, return receipt requested, at the last known address of such party.

WILEY OPEN ACCESS TERMS AND CONDITIONS

Wiley Publishes Open Access Articles in fully Open Access Journals and in Subscription journals offering Online Open. Although most of the fully Open Access journals publish open access articles under the terms of the Creative Commons Attribution (CC BY) License only, the subscription journals and a few of the Open Access Journals offer a choice of Creative Commons Licenses. The license type is clearly identified on the article.

The Creative Commons Attribution License

The Creative Commons Attribution License (CC-BY) allows users to copy, distribute and transmit an article, adapt the article and make commercial use of the article. The CC-BY license permits commercial and non-

Creative Commons Attribution Non-Commercial License

The Creative Commons Attribution Non-Commercial (CC-BY-NC)License permits use, distribution and reproduction in any medium, provided the original work is properly cited and is not used for commercial purposes.(see below)

Creative Commons Attribution-Non-Commercial-NoDerivs License

The Creative Commons Attribution Non-Commercial-NoDerivs License (CC-BY-NC-ND) permits use, distribution and reproduction in any medium, provided the original work is properly cited, is not used for commercial purposes and no modifications or adaptations are made. (see below)

Use by commercial "for-profit" organizations

Use of Wiley Open Access articles for commercial, promotional, or marketing purposes requires further explicit permission from Wiley and will be subject to a fee.

Further details can be found on Wiley Online Library http://olabout.wiley.com/WileyCDA/Section/id-410895.html

Other Terms and Conditions:

v1.10 Last updated September 2015

Questions? customercare@copyright.com or +1-855-239-3415 (toll free in the US) or +1-978-646-2777.

ELSEVIER LICENSE
TERMS AND CONDITIONS
Jan 25, 2020

This Agreement between Mara A Pop ("You") and Elsevier ("Elsevier") consists of your license details and the terms and conditions provided by Elsevier and Copyright Clearance Center.

License Number	4744700256919
License date	Jan 09, 2020
Licensed Content Publisher	Elsevier
Licensed Content Publication	Trends in Biochemical Sciences
Licensed Content Title	The Ras-ERK and PI3K-mTOR pathways: cross-talk and compensation
Licensed Content Author	Michelle C. Mendoza,E. Emrah Er,John Blenis
Licensed Content Date	Jun 1, 2011
Licensed Content Volume	36
Licensed Content Issue	6
Licensed Content Pages	9
Start Page	320
End Page	328
Type of Use	reuse in a thesis/dissertation
Portion	figures/tables/illustrations
Number of figures/tables/illustrations	1
Format	both print and electronic
Are you the author of this Elsevier article?	No
Will you be translating?	No
Title	Exploring combinatorial microRNA therapy for chronic wound healing
Institution name	n/a
Expected presentation date	Jan 2020
Portions	Figure 1b)
Requestor Location	Mara A Pop Prince Consort Road Royal School of Mines London, London SW7 2BP United Kingdom Attn: Mara A Pop

Publisher Tax ID	GB 494 6272 12
Total	0.00 GBP

Terms and Conditions

INTRODUCTION

1. The publisher for this copyrighted material is Elsevier. By clicking "accept" in connection with completing this licensing transaction, you agree that the following terms and conditions apply to this transaction (along with the Billing and Payment terms and conditions established by Copyright Clearance Center, Inc. ("CCC"), at the time that you opened your Rightslink account and that are available at any time at http://myaccount.copyright.com).

GENERAL TERMS

2. Elsevier hereby grants you permission to reproduce the aforementioned material subject to the terms and conditions indicated.

3. Acknowledgement: If any part of the material to be used (for example, figures) has appeared in our publication with credit or acknowledgement to another source, permission must also be sought from that source. If such permission is not obtained then that material may not be included in your publication/copies. Suitable acknowledgement to the source must be made, either as a footnote or in a reference list at the end of your publication, as follows:

"Reprinted from Publication title, Vol /edition number, Author(s), Title of article / title of chapter, Pages No., Copyright (Year), with permission from Elsevier [OR APPLICABLE SOCIETY COPYRIGHT OWNER]." Also Lancet special credit - "Reprinted from The Lancet, Vol. number, Author(s), Title of article, Pages No., Copyright (Year), with permission from Elsevier."

4. Reproduction of this material is confined to the purpose and/or media for which permission is hereby given.

5. Altering/Modifying Material: Not Permitted. However figures and illustrations may be altered/adapted minimally to serve your work. Any other abbreviations, additions, deletions and/or any other alterations shall be made only with prior written authorization of Elsevier Ltd. (Please contact Elsevier at permissions@elsevier.com). No modifications can be made to any Lancet figures/tables and they must be reproduced in full.

6. If the permission fee for the requested use of our material is waived in this instance, please be advised that your future requests for Elsevier materials may attract a fee.

7. Reservation of Rights: Publisher reserves all rights not specifically granted in the combination of (i) the license details provided by you and accepted in the course of this

licensing transaction, (ii) these terms and conditions and (iii) CCC's Billing and Payment terms and conditions.

8. License Contingent Upon Payment: While you may exercise the rights licensed immediately upon issuance of the license at the end of the licensing process for the transaction, provided that you have disclosed complete and accurate details of your proposed use, no license is finally effective unless and until full payment is received from you (either by publisher or by CCC) as provided in CCC's Billing and Payment terms and conditions. If full payment is not received on a timely basis, then any license preliminarily granted shall be deemed automatically revoked and shall be void as if never granted. Further, in the event that you breach any of these terms and conditions or any of CCC's Billing and Payment terms and conditions, the license is automatically revoked and shall be void as if never granted. Use of materials as described in a revoked license, as well as any use of the materials beyond the scope of an unrevoked license, may constitute copyright infringement and publisher reserves the right to take any and all action to protect its copyright in the materials.

9. Warranties: Publisher makes no representations or warranties with respect to the licensed material.

10. Indemnity: You hereby indemnify and agree to hold harmless publisher and CCC, and their respective officers, directors, employees and agents, from and against any and all claims arising out of your use of the licensed material other than as specifically authorized pursuant to this license.

11. No Transfer of License: This license is personal to you and may not be sublicensed, assigned, or transferred by you to any other person without publisher's written permission.

12. No Amendment Except in Writing: This license may not be amended except in a writing signed by both parties (or, in the case of publisher, by CCC on publisher's behalf).

13. Objection to Contrary Terms: Publisher hereby objects to any terms contained in any purchase order, acknowledgment, check endorsement or other writing prepared by you, which terms are inconsistent with these terms and conditions or CCC's Billing and Payment terms and conditions. These terms and conditions, together with CCC's Billing and Payment terms and conditions (which are incorporated herein), comprise the entire agreement between you and publisher (and CCC) concerning this licensing transaction. In the event of any conflict between your obligations established by these terms and conditions and those established by CCC's Billing and Payment terms and conditions, these terms and conditions shall control.

14. Revocation: Elsevier or Copyright Clearance Center may deny the permissions described in this License at their sole discretion, for any reason or no reason, with a full refund payable to you. Notice of such denial will be made using the contact information provided by you. Failure to receive such notice will not alter or invalidate the denial. In no event will Elsevier or Copyright Clearance Center be responsible or liable for any costs,

expenses or damage incurred by you as a result of a denial of your permission request, other than a refund of the amount(s) paid by you to Elsevier and/or Copyright Clearance Center for denied permissions.

LIMITED LICENSE

The following terms and conditions apply only to specific license types:

15. **Translation**: This permission is granted for non-exclusive world **English** rights only unless your license was granted for translation rights. If you licensed translation rights you may only translate this content into the languages you requested. A professional translator must perform all translations and reproduce the content word for word preserving the integrity of the article.

16. **Posting licensed content on any Website**: The following terms and conditions apply as follows: Licensing material from an Elsevier journal: All content posted to the web site must maintain the copyright information line on the bottom of each image; A hyper-text must be included to the Homepage of the journal from which you are licensing at http://www.sciencedirect.com/science/journal/xxxxx or the Elsevier homepage for books at http://www.elsevier.com; Central Storage: This license does not include permission for a scanned version of the material to be stored in a central repository such as that provided by Heron/XanEdu.

Licensing material from an Elsevier book: A hyper-text link must be included to the Elsevier homepage at http://www.elsevier.com . All content posted to the web site must maintain the copyright information line on the bottom of each image.

Posting licensed content on Electronic reserve: In addition to the above the following clauses are applicable: The web site must be password-protected and made available only to bona fide students registered on a relevant course. This permission is granted for 1 year only. You may obtain a new license for future website posting.

17. **For journal authors:** the following clauses are applicable in addition to the above:

Preprints:

A preprint is an author's own write-up of research results and analysis, it has not been peer-reviewed, nor has it had any other value added to it by a publisher (such as formatting, copyright, technical enhancement etc.).

Authors can share their preprints anywhere at any time. Preprints should not be added to or enhanced in any way in order to appear more like, or to substitute for, the final versions of articles however authors can update their preprints on arXiv or RePEc with their Accepted Author Manuscript (see below).

If accepted for publication, we encourage authors to link from the preprint to their formal publication via its DOI. Millions of researchers have access to the formal publications on ScienceDirect, and so links will help users to find, access, cite and use the best available version. Please note that Cell Press, The Lancet and some society-owned have different preprint policies. Information on these policies is available on the journal homepage.

Accepted Author Manuscripts: An accepted author manuscript is the manuscript of an article that has been accepted for publication and which typically includes author-incorporated changes suggested during submission, peer review and editor-author communications.

Authors can share their accepted author manuscript:

- immediately
    - via their non-commercial person homepage or blog
    - by updating a preprint in arXiv or RePEc with the accepted manuscript
    - via their research institute or institutional repository for internal institutional uses or as part of an invitation-only research collaboration work-group
    - directly by providing copies to their students or to research collaborators for their personal use
    - for private scholarly sharing as part of an invitation-only work group on commercial sites with which Elsevier has an agreement
- After the embargo period
    - via non-commercial hosting platforms such as their institutional repository
    - via commercial sites with which Elsevier has an agreement

In all cases accepted manuscripts should:

- link to the formal publication via its DOI
- bear a CC-BY-NC-ND license - this is easy to do
- if aggregated with other manuscripts, for example in a repository or other site, be shared in alignment with our hosting policy not be added to or enhanced in any way to appear more like, or to substitute for, the published journal article.

Published journal article (JPA): A published journal article (PJA) is the definitive final record of published research that appears or will appear in the journal and embodies all value-adding publishing activities including peer review co-ordination, copy-editing, formatting, (if relevant) pagination and online enrichment.

Policies for sharing publishing journal articles differ for subscription and gold open access articles:

Subscription Articles: If you are an author, please share a link to your article rather than the full-text. Millions of researchers have access to the formal publications on

ScienceDirect, and so links will help your users to find, access, cite, and use the best available version.

Theses and dissertations which contain embedded PJAs as part of the formal submission can be posted publicly by the awarding institution with DOI links back to the formal publications on ScienceDirect.

If you are affiliated with a library that subscribes to ScienceDirect you have additional private sharing rights for others' research accessed under that agreement. This includes use for classroom teaching and internal training at the institution (including use in course packs and courseware programs), and inclusion of the article for grant funding purposes.

Gold Open Access Articles: May be shared according to the author-selected end-user license and should contain a CrossMark logo, the end user license, and a DOI link to the formal publication on ScienceDirect.

Please refer to Elsevier's posting policy for further information.

18. **For book authors** the following clauses are applicable in addition to the above: Authors are permitted to place a brief summary of their work online only. You are not allowed to download and post the published electronic version of your chapter, nor may you scan the printed edition to create an electronic version. **Posting to a repository:** Authors are permitted to post a summary of their chapter only in their institution's repository.

19. **Thesis/Dissertation**: If your license is for use in a thesis/dissertation your thesis may be submitted to your institution in either print or electronic form. Should your thesis be published commercially, please reapply for permission. These requirements include permission for the Library and Archives of Canada to supply single copies, on demand, of the complete thesis and include permission for Proquest/UMI to supply single copies, on demand, of the complete thesis. Should your thesis be published commercially, please reapply for permission. Theses and dissertations which contain embedded PJAs as part of the formal submission can be posted publicly by the awarding institution with DOI links back to the formal publications on ScienceDirect.

Elsevier Open Access Terms and Conditions

You can publish open access with Elsevier in hundreds of open access journals or in nearly 2000 established subscription journals that support open access publishing. Permitted third party re-use of these open access articles is defined by the author's choice of Creative Commons user license. See our open access license policy for more information.

Terms & Conditions applicable to all Open Access articles published with Elsevier:

Any reuse of the article must not represent the author as endorsing the adaptation of the article nor should the article be modified in such a way as to damage the author's honour or reputation. If any changes have been made, such changes must be clearly indicated.

The author(s) must be appropriately credited and we ask that you include the end user license and a DOI link to the formal publication on ScienceDirect.

If any part of the material to be used (for example, figures) has appeared in our publication with credit or acknowledgement to another source it is the responsibility of the user to ensure their reuse complies with the terms and conditions determined by the rights holder.

Additional Terms & Conditions applicable to each Creative Commons user license:

CC BY: The CC-BY license allows users to copy, to create extracts, abstracts and new works from the Article, to alter and revise the Article and to make commercial use of the Article (including reuse and/or resale of the Article by commercial entities), provided the user gives appropriate credit (with a link to the formal publication through the relevant DOI), provides a link to the license, indicates if changes were made and the licensor is not represented as endorsing the use made of the work. The full details of the license are available at http://creativecommons.org/licenses/by/4.0.

CC BY NC SA: The CC BY-NC-SA license allows users to copy, to create extracts, abstracts and new works from the Article, to alter and revise the Article, provided this is not done for commercial purposes, and that the user gives appropriate credit (with a link to the formal publication through the relevant DOI), provides a link to the license, indicates if changes were made and the licensor is not represented as endorsing the use made of the work. Further, any new works must be made available on the same conditions. The full details of the license are available at http://creativecommons.org/licenses/by-nc-sa/4.0.

CC BY NC ND: The CC BY-NC-ND license allows users to copy and distribute the Article, provided this is not done for commercial purposes and further does not permit distribution of the Article if it is changed or edited in any way, and provided the user gives appropriate credit (with a link to the formal publication through the relevant DOI), provides a link to the license, and that the licensor is not represented as endorsing the use made of the work. The full details of the license are available at http://creativecommons.org/licenses/by-nc-nd/4.0. Any commercial reuse of Open Access articles published with a CC BY NC SA or CC BY NC ND license requires permission from Elsevier and will be subject to a fee.

Commercial reuse includes:

- Associating advertising with the full text of the Article
- Charging fees for document delivery or access
- Article aggregation

- Systematic distribution via e-mail lists or share buttons

Posting or linking by commercial companies for use by customers of those companies.

20. **Other Conditions**:

v1.9

Questions? customercare@copyright.com or +1-855-239-3415 (toll free in the US) or +1-978-646-2777.

ELSEVIER LICENSE
TERMS AND CONDITIONS
Jan 25, 2020

This Agreement between Mara A Pop ("You") and Elsevier ("Elsevier") consists of your license details and the terms and conditions provided by Elsevier and Copyright Clearance Center.

License Number	4744780398082
License date	Jan 09, 2020
Licensed Content Publisher	Elsevier
Licensed Content Publication	Cellular Signalling
Licensed Content Title	Analysing phosphorylation-based signalling networks by phospho flow cytometry
Licensed Content Author	Nikolaus G. Oberprieler,Kjetil Taskén
Licensed Content Date	Jan 1, 2011
Licensed Content Volume	23
Licensed Content Issue	1
Licensed Content Pages	5
Start Page	14
End Page	18
Type of Use	reuse in a thesis/dissertation
Portion	figures/tables/illustrations
Number of figures/tables/illustrations	1
Format	both print and electronic
Are you the author of this Elsevier article?	No
Will you be translating?	No
Title	Exploring combinatorial microRNA therapy for chronic wound healing
Institution name	n/a
Expected presentation date	Jan 2020
Portions	Figure 2
Requestor Location	Mara A Pop Prince Consort Road Royal School of Mines London, London SW7 2BP United Kingdom Attn: Mara A Pop

Publisher Tax ID	GB 494 6272 12
Total	0.00 GBP

Terms and Conditions

INTRODUCTION

1. The publisher for this copyrighted material is Elsevier. By clicking "accept" in connection with completing this licensing transaction, you agree that the following terms and conditions apply to this transaction (along with the Billing and Payment terms and conditions established by Copyright Clearance Center, Inc. ("CCC"), at the time that you opened your Rightslink account and that are available at any time at http://myaccount.copyright.com).

GENERAL TERMS

2. Elsevier hereby grants you permission to reproduce the aforementioned material subject to the terms and conditions indicated.

3. Acknowledgement: If any part of the material to be used (for example, figures) has appeared in our publication with credit or acknowledgement to another source, permission must also be sought from that source. If such permission is not obtained then that material may not be included in your publication/copies. Suitable acknowledgement to the source must be made, either as a footnote or in a reference list at the end of your publication, as follows:

"Reprinted from Publication title, Vol /edition number, Author(s), Title of article / title of chapter, Pages No., Copyright (Year), with permission from Elsevier [OR APPLICABLE SOCIETY COPYRIGHT OWNER]." Also Lancet special credit - "Reprinted from The Lancet, Vol. number, Author(s), Title of article, Pages No., Copyright (Year), with permission from Elsevier."

4. Reproduction of this material is confined to the purpose and/or media for which permission is hereby given.

5. Altering/Modifying Material: Not Permitted. However figures and illustrations may be altered/adapted minimally to serve your work. Any other abbreviations, additions, deletions and/or any other alterations shall be made only with prior written authorization of Elsevier Ltd. (Please contact Elsevier at permissions@elsevier.com). No modifications can be made to any Lancet figures/tables and they must be reproduced in full.

6. If the permission fee for the requested use of our material is waived in this instance, please be advised that your future requests for Elsevier materials may attract a fee.

7. Reservation of Rights: Publisher reserves all rights not specifically granted in the combination of (i) the license details provided by you and accepted in the course of this

licensing transaction, (ii) these terms and conditions and (iii) CCC's Billing and Payment terms and conditions.

8. License Contingent Upon Payment: While you may exercise the rights licensed immediately upon issuance of the license at the end of the licensing process for the transaction, provided that you have disclosed complete and accurate details of your proposed use, no license is finally effective unless and until full payment is received from you (either by publisher or by CCC) as provided in CCC's Billing and Payment terms and conditions. If full payment is not received on a timely basis, then any license preliminarily granted shall be deemed automatically revoked and shall be void as if never granted. Further, in the event that you breach any of these terms and conditions or any of CCC's Billing and Payment terms and conditions, the license is automatically revoked and shall be void as if never granted. Use of materials as described in a revoked license, as well as any use of the materials beyond the scope of an unrevoked license, may constitute copyright infringement and publisher reserves the right to take any and all action to protect its copyright in the materials.

9. Warranties: Publisher makes no representations or warranties with respect to the licensed material.

10. Indemnity: You hereby indemnify and agree to hold harmless publisher and CCC, and their respective officers, directors, employees and agents, from and against any and all claims arising out of your use of the licensed material other than as specifically authorized pursuant to this license.

11. No Transfer of License: This license is personal to you and may not be sublicensed, assigned, or transferred by you to any other person without publisher's written permission.

12. No Amendment Except in Writing: This license may not be amended except in a writing signed by both parties (or, in the case of publisher, by CCC on publisher's behalf).

13. Objection to Contrary Terms: Publisher hereby objects to any terms contained in any purchase order, acknowledgment, check endorsement or other writing prepared by you, which terms are inconsistent with these terms and conditions or CCC's Billing and Payment terms and conditions. These terms and conditions, together with CCC's Billing and Payment terms and conditions (which are incorporated herein), comprise the entire agreement between you and publisher (and CCC) concerning this licensing transaction. In the event of any conflict between your obligations established by these terms and conditions and those established by CCC's Billing and Payment terms and conditions, these terms and conditions shall control.

14. Revocation: Elsevier or Copyright Clearance Center may deny the permissions described in this License at their sole discretion, for any reason or no reason, with a full refund payable to you. Notice of such denial will be made using the contact information provided by you. Failure to receive such notice will not alter or invalidate the denial. In no event will Elsevier or Copyright Clearance Center be responsible or liable for any costs,

expenses or damage incurred by you as a result of a denial of your permission request, other than a refund of the amount(s) paid by you to Elsevier and/or Copyright Clearance Center for denied permissions.

LIMITED LICENSE

The following terms and conditions apply only to specific license types:

15. **Translation**: This permission is granted for non-exclusive world **English** rights only unless your license was granted for translation rights. If you licensed translation rights you may only translate this content into the languages you requested. A professional translator must perform all translations and reproduce the content word for word preserving the integrity of the article.

16. **Posting licensed content on any Website**: The following terms and conditions apply as follows: Licensing material from an Elsevier journal: All content posted to the web site must maintain the copyright information line on the bottom of each image; A hyper-text must be included to the Homepage of the journal from which you are licensing at http://www.sciencedirect.com/science/journal/xxxxx or the Elsevier homepage for books at http://www.elsevier.com; Central Storage: This license does not include permission for a scanned version of the material to be stored in a central repository such as that provided by Heron/XanEdu.

Licensing material from an Elsevier book: A hyper-text link must be included to the Elsevier homepage at http://www.elsevier.com . All content posted to the web site must maintain the copyright information line on the bottom of each image.

Posting licensed content on Electronic reserve: In addition to the above the following clauses are applicable: The web site must be password-protected and made available only to bona fide students registered on a relevant course. This permission is granted for 1 year only. You may obtain a new license for future website posting.

17. **For journal authors:** the following clauses are applicable in addition to the above:

Preprints:

A preprint is an author's own write-up of research results and analysis, it has not been peer-reviewed, nor has it had any other value added to it by a publisher (such as formatting, copyright, technical enhancement etc.).

Authors can share their preprints anywhere at any time. Preprints should not be added to or enhanced in any way in order to appear more like, or to substitute for, the final versions of articles however authors can update their preprints on arXiv or RePEc with their Accepted Author Manuscript (see below).

If accepted for publication, we encourage authors to link from the preprint to their formal publication via its DOI. Millions of researchers have access to the formal publications on ScienceDirect, and so links will help users to find, access, cite and use the best available version. Please note that Cell Press, The Lancet and some society-owned have different preprint policies. Information on these policies is available on the journal homepage.

Accepted Author Manuscripts: An accepted author manuscript is the manuscript of an article that has been accepted for publication and which typically includes author-incorporated changes suggested during submission, peer review and editor-author communications.

Authors can share their accepted author manuscript:

- immediately
    - via their non-commercial person homepage or blog
    - by updating a preprint in arXiv or RePEc with the accepted manuscript
    - via their research institute or institutional repository for internal institutional uses or as part of an invitation-only research collaboration work-group
    - directly by providing copies to their students or to research collaborators for their personal use
    - for private scholarly sharing as part of an invitation-only work group on commercial sites with which Elsevier has an agreement
- After the embargo period
    - via non-commercial hosting platforms such as their institutional repository
    - via commercial sites with which Elsevier has an agreement

In all cases accepted manuscripts should:

- link to the formal publication via its DOI
- bear a CC-BY-NC-ND license - this is easy to do
- if aggregated with other manuscripts, for example in a repository or other site, be shared in alignment with our hosting policy not be added to or enhanced in any way to appear more like, or to substitute for, the published journal article.

Published journal article (JPA): A published journal article (PJA) is the definitive final record of published research that appears or will appear in the journal and embodies all value-adding publishing activities including peer review co-ordination, copy-editing, formatting, (if relevant) pagination and online enrichment.

Policies for sharing publishing journal articles differ for subscription and gold open access articles:

Subscription Articles: If you are an author, please share a link to your article rather than the full-text. Millions of researchers have access to the formal publications on

ScienceDirect, and so links will help your users to find, access, cite, and use the best available version.

Theses and dissertations which contain embedded PJAs as part of the formal submission can be posted publicly by the awarding institution with DOI links back to the formal publications on ScienceDirect.

If you are affiliated with a library that subscribes to ScienceDirect you have additional private sharing rights for others' research accessed under that agreement. This includes use for classroom teaching and internal training at the institution (including use in course packs and courseware programs), and inclusion of the article for grant funding purposes.

Gold Open Access Articles: May be shared according to the author-selected end-user license and should contain a CrossMark logo, the end user license, and a DOI link to the formal publication on ScienceDirect.

Please refer to Elsevier's posting policy for further information.

18. **For book authors** the following clauses are applicable in addition to the above: Authors are permitted to place a brief summary of their work online only. You are not allowed to download and post the published electronic version of your chapter, nor may you scan the printed edition to create an electronic version. **Posting to a repository:** Authors are permitted to post a summary of their chapter only in their institution's repository.

19. **Thesis/Dissertation**: If your license is for use in a thesis/dissertation your thesis may be submitted to your institution in either print or electronic form. Should your thesis be published commercially, please reapply for permission. These requirements include permission for the Library and Archives of Canada to supply single copies, on demand, of the complete thesis and include permission for Proquest/UMI to supply single copies, on demand, of the complete thesis. Should your thesis be published commercially, please reapply for permission. Theses and dissertations which contain embedded PJAs as part of the formal submission can be posted publicly by the awarding institution with DOI links back to the formal publications on ScienceDirect.

Elsevier Open Access Terms and Conditions

You can publish open access with Elsevier in hundreds of open access journals or in nearly 2000 established subscription journals that support open access publishing. Permitted third party re-use of these open access articles is defined by the author's choice of Creative Commons user license. See our open access license policy for more information.

Terms & Conditions applicable to all Open Access articles published with Elsevier:

Any reuse of the article must not represent the author as endorsing the adaptation of the article nor should the article be modified in such a way as to damage the author's honour or reputation. If any changes have been made, such changes must be clearly indicated.

The author(s) must be appropriately credited and we ask that you include the end user license and a DOI link to the formal publication on ScienceDirect.

If any part of the material to be used (for example, figures) has appeared in our publication with credit or acknowledgement to another source it is the responsibility of the user to ensure their reuse complies with the terms and conditions determined by the rights holder.

Additional Terms & Conditions applicable to each Creative Commons user license:

CC BY: The CC-BY license allows users to copy, to create extracts, abstracts and new works from the Article, to alter and revise the Article and to make commercial use of the Article (including reuse and/or resale of the Article by commercial entities), provided the user gives appropriate credit (with a link to the formal publication through the relevant DOI), provides a link to the license, indicates if changes were made and the licensor is not represented as endorsing the use made of the work. The full details of the license are available at http://creativecommons.org/licenses/by/4.0.

CC BY NC SA: The CC BY-NC-SA license allows users to copy, to create extracts, abstracts and new works from the Article, to alter and revise the Article, provided this is not done for commercial purposes, and that the user gives appropriate credit (with a link to the formal publication through the relevant DOI), provides a link to the license, indicates if changes were made and the licensor is not represented as endorsing the use made of the work. Further, any new works must be made available on the same conditions. The full details of the license are available at http://creativecommons.org/licenses/by-nc-sa/4.0.

CC BY NC ND: The CC BY-NC-ND license allows users to copy and distribute the Article, provided this is not done for commercial purposes and further does not permit distribution of the Article if it is changed or edited in any way, and provided the user gives appropriate credit (with a link to the formal publication through the relevant DOI), provides a link to the license, and that the licensor is not represented as endorsing the use made of the work. The full details of the license are available at http://creativecommons.org/licenses/by-nc-nd/4.0. Any commercial reuse of Open Access articles published with a CC BY NC SA or CC BY NC ND license requires permission from Elsevier and will be subject to a fee.

Commercial reuse includes:

- Associating advertising with the full text of the Article
- Charging fees for document delivery or access
- Article aggregation

- Systematic distribution via e-mail lists or share buttons

Posting or linking by commercial companies for use by customers of those companies.

20. **Other Conditions**:

v1.9

Questions? customercare@copyright.com or +1-855-239-3415 (toll free in the US) or +1-978-646-2777.